



This electronic thesis or dissertation has been downloaded from Explore Bristol Research, <http://research-information.bristol.ac.uk>

Author:
Bell, Oliver

Title:
Transcriptional plasticity of microglia during intraocular inflammation

General rights

Access to the thesis is subject to the Creative Commons Attribution - NonCommercial-No Derivatives 4.0 International Public License. A copy of this may be found at <https://creativecommons.org/licenses/by-nc-nd/4.0/legalcode>. This license sets out your rights and the restrictions that apply to your access to the thesis so it is important you read this before proceeding.

Take down policy

Some pages of this thesis may have been removed for copyright restrictions prior to having it been deposited in Explore Bristol Research. However, if you have discovered material within the thesis that you consider to be unlawful e.g. breaches of copyright (either yours or that of a third party) or any other law, including but not limited to those relating to patent, trademark, confidentiality, data protection, obscenity, defamation, libel, then please contact collections-metadata@bristol.ac.uk and include the following information in your message:

- Your contact details
- Bibliographic details for the item, including a URL
- An outline nature of the complaint

Your claim will be investigated and, where appropriate, the item in question will be removed from public view as soon as possible.

Transcriptional Plasticity of Microglia during Intraocular Inflammation



Oliver Hugh Bell

A dissertation submitted to the University of Bristol in accordance with the requirements for award of the degree of Doctor of Philosophy in the Faculty of Health Sciences.

Bristol Medical School: Translational Health Sciences

October 2020

Word Count: 59,853

Abstract Page

Microglia are a tissue-resident immune cell of the central nervous system known to possess functions involved in immune surveillance and tissue homeostasis. Transcriptomics has characterised microglia and enabled discovery of microglial heterogeneity in addition to core microglial transcriptional programmes. However, investigation of microglia during severe inflammatory contexts has been challenging because no markers reliably discriminate them from the monocyte populations that ingress during inflammation. Nonetheless, candidate markers have been identified; these show promise in specific microglial identification yet remain to be widely validated.

Within the literature, there are conflicting reports on how microglia regulate or promote inflammation depending on the tissue insult. However, it is well-recognised that the homeostatic state of microglia is altered yet it remains unknown if this state is restored post-resolution. Furthermore, understanding the plasticity of microglial responses to both acute and persistent inflammation within the eye will help to determine the extent to which different pathways are perturbed.

The purpose of this thesis was to investigate the transcriptional changes that occur in retinal microglia in response to inflammation and whether the homeostatic threshold remains perturbed after acute and/or chronic inflammation.

The data presented herein demonstrates how an ultra-low input mRNA-Seq approach was optimised and validated to permit transcriptomic assessment of low numbers of cells isolated from individual retinas. The *Cx3cr1^{CreER}:R26-tdTomato* mouse line was then validated as microglial-specific during inflammation. mRNA-Seq was utilised to profile the temporal kinetics of the microglial transcriptome in the acute endotoxin-induced uveitis (EIU) model. Restoration of the microglial homeostatic state was confirmed, and key marker changes were orthogonally validated. Furthermore, C5AR₁ was validated as a marker for differentiating microglial subsets during inflammation. The next steps have begun to examine microglial behaviour in experimental autoimmune uveitis (EAU), a model of chronic inflammation, and new approaches are being optimised to better understand tissue heterogeneity.

Dedication and Acknowledgements

This doctoral thesis is dedicated to my brother Harry David Bell who tragically died in the time during which I was entering the third year of my PhD.

--

First and foremost, I would like to thank the various people (mentioned below) involved in putting together the successful project and funding proposal that enabled me to undertake this PhD. It has truly been a life-changing experience and I am forever grateful for the opportunities and privilege this has afforded me. I hope this, and my continuing work, does them proud and represents a good investment in eye research.

Secondly, I would like to thank my funding body, the National Eye Research Centre (NERC), for not only providing funding for this PhD, but for additional funding on the side that has allowed me (and others) to perform further work and present at international conferences – particularly in advancement of expertise on and the acquisition of mRNA-Seq data. Furthermore, NERC have also very kindly agreed to fund a post-doctoral research project – another huge privilege and fantastic set of opportunities.

There are a multitude of people without whom this thesis may not have been written. At the forefront are my supervisors Dave Copland and Colin Chu: thank you both for countless instances of support, advice, and encouragement that have allowed me to develop and refine my scientific expertise, but also many other more general skills (including confidence) useful not only in the lab but beyond. To Andrew Dick, our group's director, thank you for a whole encyclopaedia of reasons too long to list but in particular for leading by example and demonstrating how to successfully run a research group – and how your humble, courteous approach creates parity that leads to mutual respect. To Lindsay Nicholson, thank you for both personal and scientific advice, but especially for all the insightful comments, questions, and suggestions in relation to the sequencing data that often aligned with (and validated) my own thoughts and ideas. I also want to thank all the aforementioned for incredibly quick turnaround on a variety of imminent deadlines – whether that be paper submissions, abstracts, or even to provide supporting evidence for applications!

To my fellow PhD students, Amy Ward and Louis Scott, thank you for all the good banter, comradery, and support throughout our PhD journeys together. Amy, I relish the opportunity to continue working with you in our post-docs and look forward to our future collaborations on imaging and sequencing – the extra pair of hands has made a lot of previously impossible work

feasible, and our chats (especially during the long imaging sessions) have certainly kept me far more sane! Louis, I wish you all the best for your travels but do hope you manage to stay out of trouble! Always game for a pint – whether that be after your travels, during your next career step, or both – that will hopefully materialise in the coming months.

I would also like to thank Emily Williams for providing an abundance of support and endless patience with me when I first started in Bristol and we worked on the ICG clinical study together – and to Richard Lee who has provided personal support, the infrastructure that enabled me to undertake the study, and for playing the role of publicist and showing me how to enhance how we sold our research and narrated the paper.

And to many other colleagues within the Ophthalmology research group (past and present), Madeleine Stimpson, Lydia Bradley, Kepeng Ou, Alison Young, Jiahui Wu, Philippa Lait, Jian Liu, Lauren Schewitz-Bowers, John Pooley, Alison Clare, and Alan Abraham, thank you for the chats and banter, support, and for being part of such a great team to work within!

There are many other people who I would like to thank: Andrew Herman and Lorena Ballesteros (Flow Cytometry Facility), Christy Waterfall and Jane Coghill (Genomics Facility), Tom Batstone and Alex Paterson (Bioinformatics arm of the Genomics Facility), and Dominic Alibhai, Stephen Cross, and Katy Jepson (Wolfson Bioimaging Facility) for technical assistance. I would also like to thank Clemens Lange (University of Freiburg, Germany) for kindly providing the *Cx3cr1^{CreER}:R26-tdTomato* mouse line that has been vital to my work.

To my family, Mum, Dad, and my brothers Tom and Jack, thank you for all the constant support and help behind the scenes, for always being there for me, and for encouraging me to pursue my interests once I finally realised what they were.

Lastly, but most importantly, I want to thank my partner Amy. She has been my rock throughout, cherishing the good times and providing enormous support to help me through the tough; she is forever patient with and understanding of me, always proud and encouraging of my achievements, and has always been by my side – especially when I have needed it most. Without her, I honestly do not know how I would have made it through what has been my toughest period for a whole host of reasons. I earnestly look forward to our future together.

Author's Declaration

I declare that the work in this dissertation was carried out in accordance with the requirements of the University's Regulations and Code of Practice for Research Degree Programmes and that it has not been submitted for any other academic award. Except where indicated by specific reference in the text, the work is the candidate's own work. Work done in collaboration with, or with the assistance of, others, is indicated as such. Any views expressed in the dissertation are those of the author.

SIGNED: DATE:

Research Outputs and Plagiarism

In concordance with the Faculty of Health Sciences policy on Turnitin submission and plagiarism, all publications arising from this research will be listed below to include all contributions using CRediT taxonomy. The First and Last Author's signature (where available) will be provided to indicate agreement.

Bell OH, Carreño E, Williams EL, Wu J, Copland DA, Fruttiger M, Sim DA, Lee RWJ, Dick AD, Chu CJ. Intravenous Indocyanine Green Dye is Insufficient for Robust Human Immune Cell Labelling in the Retina. *PLoS One* 15 (2): e0226311; 2020. **Author role:** Data curation, Formal analysis, Investigation, Project administration, Validation, Visualisation, Writing – original draft, Writing – review & editing.

C. Chu

Wu J, **Bell OH**, Copland DA, Young A, Pooley J, Maswood R, Evans R, Khaw PT, Ali RR, Dick AD, Chu CJ. Gene therapy for Glaucoma by Ciliary Body Aquaporin 1 disruption using CRISPR-Cas9. *Molecular Therapy*; 2020. **Author role:** Methodology, Formal analysis, Investigation, Writing – original draft preparation, Writing – review & editing.

C. Chu

Bell OH, Copland DA, Ward A, Chu CJ, Lange CAK, Dick AD. Single eye mRNA-Seq Reveals Normalisation of the Retinal Microglial Transcriptome following Acute Inflammation. *Frontiers in Immunology*. 2019;10:3033. **Author role:** Methodology, Validation, Formal analysis, Investigation, Data curation, Writing – original draft preparation, Writing – review & editing, Visualisation, Project administration, Funding acquisition.

A. Dick

Bell OH, Copland DA, Ward A, Chu CJ, Lange CAK, Dick AD. RNA-Seq Reveals Alterations in Homeostatic Microglial Function during Inflammation and Resolution. *Association of Research in Vision and Ophthalmology Annual Meeting*, 28th April–2nd May 2019, Vancouver, British Columbia, Canada. **Author role:** Same as Frontiers in Immunology paper.

Bell OH, Copland DA, Ward A, Nicholson LB, Lange CAK, Chu CJ, Dick AD. mRNA-Seq Identifies Heterogeneity in the Retinal Microglial Function during Acute Inflammation. *BSI Congress 2019*, 2nd–5th December 2019, Liverpool, United Kingdom. **Author role:** Same as Frontiers in Immunology paper.

Tian X, Zheng R, Chu CJ, **Bell OH**, Nicholson LB, Achim A. Multimodal Retinal Image Registration and Fusion Based on Sparse Regularization via a Generalized Minimax-concave Penalty. In 2019 IEEE International Conference on Acoustics, Speech, and Signal Processing, ICASSP 2019 - Proceedings. Institute of Electrical and Electronics Engineers (IEEE). 2019. p. 1010-1014. 8683010. (ICASSP, IEEE International Conference on Acoustics, Speech and Signal Processing - Proceedings); 2019. **Author role:** Investigation.

L.Nicholson

Table of Contents:

Chapter I: Introduction	1
1.1 INTRAOCULAR INFLAMMATION.....	2
1.2 THE EYE	4
1.3 MURINE MODELS OF UVEITIS:	11
1.3.1 Experimental Autoimmune Uveitis	11
1.3.2 Endotoxin-Induced Uveitis	13
1.3.3 In Vivo Clinical Assessment of Intraocular Inflammation	16
1.4 IMMUNITY AND INFLAMMATION	18
1.4.1 Innate Immunity.....	21
1.4.2 Of Monocytes and Macrophages	27
1.4.3. Adaptive Immunity.....	36
1.4.4 Immunological Challenges	39
1.4.5 Tolerance	39
1.4.6 Autoimmunity and Autoinflammation	41
1.4.7 Innate Immune Memory, Adaptation, and Para-Inflammation	44
1.4.8 The Eye and Immune Regulation	50
1.5 MICROGLIA	52
1.5.1 Microglial Phenotypes	56
1.5.2 Retinal Microglia and Homeostasis.....	60
1.5.3 Retinal Microglia and Uveitis.....	63
1.5.4 Monocyte Engraftment and Microglial Depletion	66
1.6 EXPERIMENTAL TECHNIQUES: MRNA-SEQUENCING	70
1.6.1 Experimental Pipelines.....	70
1.6.2 Approaches to Data Analysis.....	72
1.7 THESIS OBJECTIVES	78
Chapter II: Materials and Methods.....	80
2.1 MICE	81
2.2 TAMOXIFEN ADMINISTRATION	85
2.3 <i>IN VIVO</i> MODELS	85
2.3.1 Induction of EAU	85
2.3.2 Induction of EIU.....	86
2.4 <i>IN VIVO</i> IMAGING TECHNIQUES	87
2.5 FLOW CYTOMETRY/FLUORESCENCE-ACTIVATED CELL SORTING	89
2.5.1 Batch Processing	89
2.5.2 Single Sample (or Small Number Batch) Processing	92

2.6 SAMPLE AND LIBRARY PREPARATION FOR SEQUENCING	92
2.7 MRNA-SEQUENCING AND DATA ANALYSIS	93
2.8 QUANTITATIVE PCR	96
2.9 CONFOCAL LASER-SCANNING MICROSCOPY	96
2.10 ANALYSIS.....	97
2.10.1 Image Processing	97
2.10.2 Statistical Analysis	99
Chapter III: Optimisation of Ultra-Low Input mRNA-Seq and Bioinformatic Analysis	100
3.1 INTRODUCTION	101
3.1.1 The Challenge of Ultra-Low Input RNA.....	101
3.1.2 Experimental Design Considerations	103
3.1.3 mRNA-Seq Analysis.....	113
3.1.4 Summary	113
3.2 RESULTS	114
3.2.1 Optimisation of mRNA Isolation and cDNA Generation.....	114
3.2.2 mRNA-Seq of CD4 ⁺ T Cells in EAU	123
3.3 DISCUSSION.....	131
Chapter IV: Validation and Optimisation of the <i>Cx3cr1^{CreER};R26-tdTomato</i> Mouse Line.....	135
4.1 INTRODUCTION	136
4.1.1 The Challenge of Microglial Identification	136
4.1.2 Cre/Lox Systems and CX3CR1	137
4.1.3 The Safety/Toxicity of Tamoxifen, CreER, and tdTomato	142
4.1.4 Tamoxifen Administration Routes	143
4.1.5 Summary	144
4.2 RESULTS	145
4.2.1 Sensitivity of Microglial Tagging.....	145
4.2.2 Specificity of Microglial Tagging.....	151
4.3 DISCUSSION.....	160
Chapter V: Characterising the Temporal Kinetics of the Microglial Transcriptome in EIU.....	163
5.1 INTRODUCTION	164
5.2 RESULTS	165
5.2.1 The Kinetics of EIU in the <i>Cx3cr1^{CreER};R26-tdTomato</i> Mouse Line	165

5.2.2 mRNA-Seq	168
5.2.3 Orthogonal Validation of Selected Markers	174
5.2.4 Stratifying Microglia using C5AR1 Identifies Both Generalised and Restricted Microglial Responses	184
5.3 DISCUSSION.....	187
Chapter VI: Final Discussion and Future Directions.....	194
6.1 SINGLE-CELL MRNA-SEQ	196
6.2 DIGITAL CELL QUANTIFICATION AND DEMULTIPLEXING OF CELLS AND CELL SUBSETS....	201
6.3 FURTHER INVESTIGATION OF MICROGLIA IN EIU	210
6.4 INVESTIGATING MICROGLIA IN EAU	213
6.5 REGIONAL BIOPSIES OF RETINAS FOR ANALYSIS OF INTRA-TISSUE HETEROGENEITY	221
6.6 THREE-DIMENSIONAL OCT DISEASE SCORING.....	225
6.7 SUMMARY	230
Chapter VII: References	231
Chapter VIII: Research Outputs	277
8.1 PUBLICATIONS – THESIS-RELATED	278
8.2 PRESENTATIONS – THESIS-RELATED	278
Oral Presentations	278
Poster Presentations.....	278
8.3 GRANT AWARDS.....	278
8.4 PUBLICATIONS – OTHER	279
Appendix I: mRNA-Sequencing using SMART-Seq and Illumina – Technical Overview	280
Cell Isolation and cDNA Generation	281
cDNA Purification and Quantification.....	283
Tagmentation and Library Preparation	285
Sequencing (Illumina)	287
Measurement Error within Illumina Sequencing	291

List of Tables

<i>Table 1.2.1. Primary components of the retinal layers and their basic function.</i>	7
<i>Table 1.3.1. A summary and comparison of mouse models of uveitis.</i>	15
<i>Table 1.4.1. Specialised region-specific functions of tissue-resident macrophages.</i>	35
<i>Table 1.4.2. Innate immune memory terminology.</i>	45
<i>Table 2.1.1. Details of mice used for experiments.</i>	82
<i>Table 2.1.2. Primer details for genotyping of the Cx3cr1^{CreER}:R26-tdTomato mouse strain.</i>	83
<i>Table 2.1.3. Details of cycling conditions used in genotyping the Cx3cr1^{CreER}:R26-tdTomato mouse strain.</i>	83
<i>Table 2.4.1. Filter information for the exciter/emission positions (on the filter wheel) of the Micron IV: Retinal Imaging Microscope.</i>	88
<i>Table 2.5.1. A list of monoclonal antibodies used for flow cytometry.</i>	91

List of Figures

<i>Figure 1.2.1. A schematic diagram representing the structure of the eye (top) to include cells and layers within the retina (bottom).</i>	5
<i>Figure 1.2.2. A histological section of the retina and choroid highlighting the different segments and their appearances with haematoxylin and eosin staining.</i>	6
<i>Figure 1.2.3. Schematic diagrams of sagittal sections of the human (top) and mouse (bottom) eyes to highlight their similarities and differences.</i>	9
<i>Figure 1.4.1. Developmental summary of blood cells (haematopoiesis) to include their localisation and maturation during key stages.</i>	20
<i>Figure 1.4.2. Pattern recognition receptors (PRRs) and downstream signalling elements.</i>	22
<i>Figure 1.4.3. A schematic of the complement system, highlighting the three initiating pathways and subsequent signalling cascade.</i>	23
<i>Figure 1.4.4. Innate immune responses to pathogen-associated molecular patterns (PAMPs) and the interplay with adaptive immune cells.</i>	25
<i>Figure 1.4.5. An overview of the extravasation process.</i>	26
<i>Figure 1.4.6. Monocyte subsets, defining markers, and functions.</i>	29
<i>Figure 1.4.7. A proposed framework for describing M1/M2 macrophages for better comparability between studies.</i>	32
<i>Figure 1.4.8. The effect of homeostatic tissue signals alone and in conjunction with activation of pattern recognition receptors (PRRs).</i>	33
<i>Figure 1.4.9. Currently known Th cell subsets.</i>	38
<i>Figure 1.4.10. Immune memory and immune adaptation.</i>	47
<i>Figure 1.4.11. Immune adaptation, para-inflammation, and autoinflammation/autoimmunity may represent a spectrum of immune dysregulation and tissue dysfunction.</i>	49
<i>Figure 1.5.1. Microglia possess a variety of important roles relating to both immune surveillance/protection and maintenance of tissue homeostasis.</i>	53
<i>Figure 1.5.2. Phylogenetic relationships and the sequence of evolution predating complex nervous system architectures.</i>	55
<i>Figure 1.5.3. Major types of microglial checkpoint that help to establish and maintain an immunosuppressive environment.</i>	62
<i>Figure 1.5.4. The changes between homeostatic ramified microglia and dysregulated amoeboid microglia during EAU.</i>	64

<i>Figure 2.1.1. An example gel output from the genotyping protocol for the Cx3cr1^{CreER}:R26-tdTomato mouse strain.</i>	84
<i>Figure 2.7.1. The bioinformatics pipeline for processing and analysing the mRNA-Seq data.</i>	95
<i>Figure 2.10.1. tdTomato fluorescence images of a mouse retina both pre- and post-deconvolution using Huygens software.</i>	98
<i>Figure 3.1.1. An overview of the SMART-Seq v4 ultra low input RNA kit pipeline.</i>	102
<i>Figure 3.1.2. Visualisation of batching effects within mRNA-Seq datasets.</i>	105
<i>Figure 3.1.3. Examples of good and poor experimental design with regards to treatment and cage allocations.</i>	107
<i>Figure 3.1.4. Visualisation of batching effects in mRNA-Seq data and processing strategies to normalise for non-biological differences.</i>	110
<i>Figure 3.2.1. Flow cytometric gating strategy for the isolation of microglia by fluorescence-activated cell sorting (FACS) in a naïve retina.</i>	116
<i>Figure 3.2.2. The gel plot, produced from cDNA generated using the SMART-Seq v4 kit as part of the cycle optimisation experiment, on the Agilent 2100 Bioanalyser.</i>	117
<i>Figure 3.2.3. Key quality control parameters (QC) for a representative mRNA-Seq sample calculated by FastQC.</i>	119
<i>Figure 3.2.4. Average base score quality for a representative mRNA-Seq sample (as generated in Partek Flow).</i>	120
<i>Figure 3.2.5. A representative selection of alignment statistics for mRNA-Seq data generated using the ultra-low input RNA pipeline.</i>	121
<i>Figure 3.2.6. Representative fundal and OCT images of a naïve mouse and at peak (D25) EAU from the CD4⁺ T cell mRNA-Seq experiment.</i>	124
<i>Figure 3.2.7. Flow cytometric gating strategy for the isolation of CD4⁺ T cells by FACS in an EAU retina.</i>	125
<i>Figure 3.2.8. A gel plot from the experiment where time-dependent mRNA degradation of samples was observed.</i>	127
<i>Figure 3.2.9. A representative gel plot, produced from cDNA generated from 600 CD4⁺ T cells (equivalent to single-eye mRNA-Seq of microglia) using the SMART-Seq v4 kit, on the Agilent 2100 Bioanalyser.</i>	128
<i>Figure 3.2.10. Principal component analysis (PCA) plot for the CD4⁺ T Cell mRNA-Seq data.</i>	129
<i>Figure 3.2.11. Hierarchical clustering (heatmap) of the DEGs identified from the DGEA on samples of 600 CD4⁺ T cells.</i>	130
<i>Figure 4.1.1. Cre and Lox systems, and their utilisation in conditional gene targeting.</i>	139

<i>Figure 4.1.2. Recombination and the kinetics of fluorescent reporter positivity in the Cx3cr1^{CreER} mouse strain.</i>	141
<i>Figure 4.2.1. Brightfield imaging of wild-type (WT) and Cx3cr1^{CreER}:R26-tdTomato mice highlight no gross perturbations as a consequence of gene editing.</i>	146
<i>Figure 4.2.2. Representative fluorescent fundal images of Cx3cr1^{CreER}:R26-tdTomato mice before and after tamoxifen administration.</i>	147
<i>Figure 4.2.3. Representative fluorescent fundal images of Cx3cr1^{CreER}:R26-tdTomato mice undergoing different tamoxifen administration regimes 4-weeks post-tamoxifen.</i>	148
<i>Figure 4.2.4. Sensitivity of microglial recombination induced in Cx3cr1^{CreER}:R26-tdTomato mice using different tamoxifen administration regimes.</i>	149
<i>Figure 4.2.5. Representative confocal microscopy maximum-intensity projection of a whole naïve retina highlights a physiological morphology.</i>	150
<i>Figure 4.2.6. Flow cytometric histograms highlight tagging of brain microglia and a small number of splenic monocytes following subcutaneous (systemic) tamoxifen administration.</i>	152
<i>Figure 4.2.7. Flow cytometric analysis of peripheral tissues indicates a small, but potentially significant, number of tdTomato^{hi} cells.</i>	153
<i>Figure 4.2.8. Representative images of a naïve and EIU 18h retina in the Cx3cr1^{CreER}:R26-tdTomato mouse line.</i>	155
<i>Figure 4.2.9. Flow cytometric gating strategy used to differentiate immune cell populations present in the retina at peak EIU.</i>	156
<i>Figure 4.2.10. The specificity of different tamoxifen administration regimes for microglial tagging in the Cx3cr1^{CreER}:R26-tdTomato mouse strain during active inflammation.</i>	158
<i>Figure 4.2.11. EIU-mediated inflammation does not alter the number of tdTomato^{hi} cells.</i>	159
<i>Figure 5.2.1. The kinetics of EIU in the Cx3cr1^{CreER}:R26-tdTomato mouse strain.</i>	166
<i>Figure 5.2.2. Confocal laser-scanning microscopy shows changes in microglial morphology over time in EIU.</i>	167
<i>Figure 5.2.3. mRNA-Sequencing of microglia during and after EIU reveals transcriptional alterations that fully resolve.</i>	169
<i>Figure 5.2.4. The transcriptome of microglia during EIU identifies expected changes in previously described microglial genes.</i>	171
<i>Figure 5.2.5. IPA software identifies canonical pathways that are significantly altered in microglia during EIU.</i>	172
<i>Figure 5.2.6. A heatmap shows changes in both z-score and p value over time for significantly-enriched IPA canonical pathways.</i>	173

Figure 5.2.7. A flow-chart demonstrating the selection process of markers for orthogonal validation.	175
Figure 5.2.8. Changes in expression of markers selected for orthogonal validation, as determined by mRNA-Seq of microglia, during EIU.	177
Figure 5.2.9. qPCR validates microglial transcriptomic changes, identified by mRNA-Seq, at the gene-level.	178
Figure 5.2.10. Changes in protein expression of selected markers in microglia, as determined using flow cytometry, over a time-course of EIU.	181
Figure 5.2.11. Confocal-laser scanning microscopy highlights upregulation of CD44 in microglia at peak EIU, compared to naïve controls.	182
Figure 5.2.12. Flow cytometric analysis demonstrates P2RY12 and SIGLECH expression on CD45 ⁺ tdTomato ⁻ non-microglial immune cells (blue) and CD45 ^{lo} tdTomato ⁺ microglia (red) at 18 hours EIU.	183
Figure 5.2.13. Microglia can be stratified based on C5AR1 expression and this correlates with the amount of immune cell infiltrate.	185
Figure 5.2.14. Stratifying microglia using C5AR1 expression identifies both exclusive and generalised responses to LPS in vivo.	186
Figure 6.1.1. Agilent Bioanalyser output of libraries generated through the CEL-Seq2 protocol.	199
Figure 6.2.1. Digital Cell Quantification (DCQ) highlights an abundance of T cell signals in the CD4 ⁺ T cell dataset.	202
Figure 6.2.2. Digital Cell Quantification (DCQ) highlights over-representation of NKT and T effector cell signatures.	205
Figure 6.2.3. Digital Cell Quantification (DCQ) [635] identifies a prominent Th1/Th17 signatures in EAU retinas, in addition to a natural T _{reg} signature.	207
Figure 6.2.4. Differential gene expression analysis (DGEA) of “subtype upregulated” CD4 ⁺ T Cell subset genes highlights general agreement with Digital Cell Quantification (DCQ) results.	208
Figure 6.4.1. Inducing EAU by adoptive transfer of CD4 ⁺ T cells and initial assessment with imaging and flow cytometric platforms.	214
Figure 6.4.2. tdTomato acquisition-normalised fluorescent fundal imaging time-course in a single mouse highlights continuing pathology and microglial association in the EAU model long-term.	216
Figure 6.4.3. Preliminary flow cytometric analysis of microglia during EAU in the Cx3cr1 ^{CreER} :R26-tdTomato mouse strain.	219
Figure 6.5.1. Fluorescent fundal images of tdTomato (microglia) in the Cx3cr1 ^{CreER} :R26-tdTomato mouse line highlights heterogeneity in the microglial response during EAU.	222

<i>Figure 6.5.2. An overview of the regional biopsy technique.</i>	223
<i>Figure 6.6.1. Three-dimensional projections of the retina using OCT.</i>	226
<i>Figure 6.6.2. A series of images showing the key stages of analysis of OCT volume scans using the Imaris software.</i>	229
<i>Figure A1.1. The initial cDNA generation using reverse transcriptase and template-switching, as utilised in the SMART-Seq v4 ultra low RNA input kit.</i>	282
<i>Figure A1.2. The workflow steps required for successful pure isolation of cDNA using the Agencourt AMPure XP beads.</i>	284
<i>Figure A1.3. An overview of the mRNA-Seq library preparation steps utilised in the SMART-Seq v4 pipeline.</i>	286
<i>Figure A1.4. Cluster generation on Illumina flow cells.</i>	289
<i>Figure A1.5. Illumina sequencing overview highlights how it is possible to sequence millions of reads in parallel with accuracy.</i>	290
<i>Figure A1.6. Examples of good and poor experimental design with regards to sequencing flow cells and lane allocation.</i>	292

Abbreviations List

Abbreviation	Expansion
7AAD	7-aminoactinomycin D
AC	Anterior chamber
ACK	Ammonium-chloride-potassium
AD	Alzheimer's disease
AIRE	Autoimmune regulator
ANOVA	Analysis of variance
antig	Allophycocyanin
<i>ApoE</i>	Apolipoprotein E
ARVO	The association for research in vision and ophthalmology
ASPA	Animals (Scientific Procedures) Act 1986
ASU	Animal services unit
AT	Adoptive transfer
ATP	Adenosine triphosphate
Axl	Axl receptor tyrosine kinase
BBB	Blood-brain barrier
BD	Becton Dickinson
BM	Basement membrane (Figure 1.1.3)
BRB	Blood-retinal barrier
<i>Bst2</i>	Bone marrow stromal antigen 2 precursor
BV	Brilliant Violet
BWA	Burrows-Wheeler aligner
<i>C5ar1</i>	Complement component 5a receptor 1
CAG promoter	CMV early enhancer, chicken β -actin TSS, rabbit β -globin intron
CC BY	Creative Commons 'Attribution' licence
CC BY-NC	Creative Commons 'Attribution' licence (non commercial)
CCD	Charge-coupled device
CCL	C-C motif chemokine ligand
CCR	C-C motif chemokine receptor

CD	Cluster of differentiation
cDNA	Complementary DNA
CEL	Cell expression by linear amplification and sequencing
CFA	Complete Freund's adjuvant
CFSE	Carboxyfluorescein succinimidyl ester
CKS	Clinical knowledge summary
CLI	Command line interface
CLR	C-type lectin receptor
CMV	Cytomegalovirus
CNS	Central nervous system
CPU	Central processing unit
<i>Crb1</i>	Crumbs cell polarity complex component 1
Cre	Cre recombinase
CSF1R	Colony stimulating factor 1 receptor
CTLA4	Cytotoxic T-lymphocyte-associated protein 4
CX3CL1	C-X3-C motif chemokine ligand 1
CX3CR1	C-X3-C motif chemokine receptor 1
CXCL	C-X-C motif chemokine
Cy7	Cyanine-7
DAM	Damage-associated microglia
DAMP	Damage-associated molecular pattern
DAVID	Database for annotation, visualization and integrated discovery
DC	Dendritic cell
DCQ	Digital cell quantification
Dd(H ₂ O)	Double-distilled water
DEG	Differentially-expressed gene
DESeq	Differential expression analysis for sequence count data
DGEA	Differential gene expression analysis
DMSO	Dimethyl sulphoxide
DNA	Deoxyribonucleic acid
DT	Diphtheria toxin

EAE	Expeirmental autoimmune encephalomyelitis
EAU	Expeirmental autoimmune uveitis
ECM	Extracellular matrix
EDASeq	Exploratory data analysis and normalization for RNA-Seq
edgeR	Empirical analysis of DGE (digital gene expression) in R
EDTA	Ethylenediaminetetraacetic acid
eGFP	Enhanced GFP (green fluorescent protein)
EIU	Endotoxin-induced uveitis
ELM	External limiting membrane
EMBL-EBI	European bioinformatics institute
ENCODE	Encyclopedia of DNA elements
ER	Oestrogen receptor
ERCC	External RNA controls consortium
ERG	Electroretinogram
ERK	Extracellular signal-regulated kinase
FACS	Fluorescence-activated cell sorting
<i>Fas</i>	Fas cell surface death receptor
FDR	False discovery rate
FISH	Fluorescence <i>in situ</i> hybridisation
FITC	Fluorescein isothiocyanate
FMO	Fluorescence minus one
FPKM	Fragments per kilobase of exon model per million reads mapped
FPR	False positive rate
FPS	Frames per second
G (e.g. 25G)	Gauge (refers to needle diameter)
GCL	Ganglion cell layer
GEO	Gene expression omnibus
GFP	Green fluorescent protein
GO	Gene ontology
GPCR	G protein-coupled receptor
Gpr	G protein-coupled receptor

GSEA	Gene set enrichment analysis
GSNAP	Genomic short-read nucleotide alignment program
GTEX	Genome tissue expression
GUI	Graphical user interface
HISAT	Hierarchical indexing for spliced alignment of transcripts
HLA	Human leukocyte antigen
IFN	Interferon
IL	Interleukin
ILC	Innate lymphoid cell
ImmGen	Immunological genome project
INL	Inner nuclear layer
IPA	Ingenuity pathway analysis
IPL	Inner plexiform layer
IRBP	Interphotoreceptor retinoid-binding protein
IS	Rod and cone inner segment
KEGG	Kyoto encyclopedia of genes and genomes
<i>Lair1</i>	Leukocyte-associated immunoglobulin-like receptor 1
LCM	Laser capture microdissection
LDAM	Lipid-droplet-accumulating microglia
lncRNA	Long non-coding RNA
Loxp	Locus of X-over P1
LPS	Lipopolysaccharide
LRR	Leucine rich repeats
mAb	Monoclonal antibody
MAC	Membrane attack complex
MACS	Magnetic-activated cell sorting
Mafb	v-maf musculoaponeurotic fibrosarcoma oncogene family, protein B (avian)
MAPK	Mitogen-activated protein kinase
M-CSF	Macrophage colony stimulating factor
MDSCs	Myeloid-derived suppressor cells
<i>Mertk</i>	Tyrosine-protein kinase Mer precursor

MFI	Mean fluorescence intensity
<i>Mfrp</i>	Membrane frizzled-related protein
MGI	Mouse genome informatics
MHC	Major histocompatibility complex
<i>Milr1</i>	Allergin-1 precursor
MMLV	Moloney murine leukaemia virus
mRNA	Messenger RNA
mTECs	Medullary thymic epithelial cells
NCBI	National centre for biotechnology information
NFL	Nerve fibre layer
NHS	National health service
NICE	The national institute for health and care excellence
NK cell	Natural killer cell
NLR	NOD-LLR-containing receptor
NO	Nitric oxide
NOD	Nucleotide-binding oligomerisation domain
NP	Neuropeptide
NP-40	Nonyl phenoxyethoxyethanol-40
OCT	Optical coherence tomography
ON	Optic nerve
ONL	Outer nuclear layer
OPL	Outer plexiform layer
OS	Rod and cone outer segment
<i>P2ry12</i>	Purinergic receptor P2Y12
<i>P3h1</i>	Prolyl 3-hydroxylase 1
PAMP	Pathogen-associated molecular patterns
PBS	Phosphate-buffered saline
PC	Principal component
PCA	Principal component analysis
PCR	Polymerase chain reaction
PDE	Phosphodiesterase

PE	Phycoerythrin
PG	Prostaglandin
PGS	Partek genomics suite
PLC	Phospholipase c
PMU	Primed mycobacterial uveitis
PRISMA	Preferred reporting items for systematic reviews and meta-analyses
PRR	Pattern recognition receptor
PTX	Pertussis toxin
QA	Quality-assurance
QC	Quality-control
qPCR	Quantitative PCR
RAM	Recovery-associated microglia
RBP	Retinol binding protein
Rd	Retinal degeneration
RIG-1	Retinoic acid-inducible gene 1
RIN	RNA integrity number
RL	Retinal layers
RNA	Ribonucleic acid
RNA-Seq	RNA-Sequencing
ROS	Reactive oxygen species
RPE	Retinal pigment epithelium
RPKM	Reads per kilobase of transcript per million mapped reads
rRNA	Ribosomal RNA
RSEM	RNA-Seq by expectation maximization
RT	Reverse transcriptase
RUM	RNA-Seq unified mapper
Sc	Single-cell
Sc	Subcutaneous tamoxifen regime
SDS	Sodium dodecyl sulphate
<i>Siglech</i>	Sialic acid binding Ig-like lectin H
<i>Slamf1</i>	Signaling lymphocytic activation molecule

<i>SLR</i>	Single lens reflex
SPF	Specific pathogen free
STAR	Spliced transcripts alignment to a reference
STING	Stimulator of interferon genes
SUN	Standardisation of uveitis nomenclature
SVA	Surrogate variable analysis
TAE	Tris-acetate-EDTA
<i>Tak1</i>	Transforming growth factor beta-activated kinase 1
TBI	Total body irradiation
TCGA	The cancer genome atlas
TCR	T cell receptor
tdTomato	Tandem dimer tomato (fluorescent protein)
TEFI	Topical endoscopic fundus imaging
TGF	Transforming growth factor
T_{hX}	T-helper x
TIFF	Tagged image file format
TLR	Toll-like receptor
TMEM	Transmembrane protein
TMM	Trimmed mean of M values
TNF	Tumour necrosis factor
TNFAIP	Tumour necrosis factor, alpha-induced protein
TPM	Transcripts per million
TPR	True positive rate
T_{reg}	Regulatory T cell
TREM	Triggering receptor expressed on myeloid cells
Tris	Trisaminomethane
tRNA	Transfer RNA
t-SNE	t-distributed stochastic neighbour embedding
TSO	Template-switching oligonucleotide
TSS	Transcription start site
UK	United Kingdom

VB	Vitreous body
VIPER	Visualization pipeline for RNA-Seq, a Snakemake workflow for efficient and complete RNA-Seq analysis
WGCNA	Weighted gene co-expression network analysis
WT	Wild-type
xD	x-day topical tamoxifen regime
YFP	Yellow fluorescent protein

Chapter I: Introduction

1.1 Intraocular Inflammation

Intraocular inflammation, commonly described as uveitis, refers to a spectrum of autoimmune-autoinflammatory diseases of the eye and infection locally to the eye [1]. Non-infectious uveitis is relatively rare, having estimated incidence rates of 17–52 individuals per 100,000 per year and prevalence rates of between 40–400 individuals per 100,000 [2–5] (or 1 in 250–2,500 individuals). It is more common in females than males [6–8]. The large variability in these estimates between studies could be due to the year of sampling, geographical region, or other bias in the sample population. Nonetheless, uveitis is estimated as the commonest cause (1 in 10 cases) of blindness in 20–60 year-olds (the “working-age” population) [9] and the fourth commonest cause of blindness overall in developed countries [1]. Visual impairment is well-characterised to restrict participation in daily activities [10] and lower quality of life [11], as well as increase the risk of mortality by more than two-fold [12]. As a common cause of blindness, uveitis represents a significant health problem.

Describing and classifying uveitis has historically been ambiguous and non-standardised, making interpreting or comparing historical work by different authors difficult. In 2005 the standardisation of uveitis nomenclature (SUN) working group (a group of 45 international uveitis specialists) published a report of classifications, descriptors, and grading scores for uveitis and definitions to address these issues [13]. Uveitis is predominantly classified based on the primary site of inflammation (e.g. anterior, intermediate, posterior, or pan-), but a variety of other descriptors and grading schemes (e.g. acute, recurrent, or chronic) are important so that information from human studies are more readily comparable. Uveitis has a variety of aetiologies; these can be grouped into categories such as infectious or non-infectious, and systemic or local. There are at least 28 major causes of non-infectious uveitis [14, 15] and the majority of cases (~80%) are not associated with other systemic diseases (often referred to as idiopathic autoimmune uveitis) [16]. HLA-B27 is an important allele that associates with both idiopathic forms of anterior uveitis and some systemic-associated forms of uveitis which coincide with diseases such as ankylosing spondylitis, inflammatory bowel disease, and psoriatic arthritis [17]. The other systemic diseases most frequently associated with uveitis include sarcoidosis, Behçet disease, juvenile idiopathic arthritis, Vogt-Koyanagi-Harada syndrome, and multiple sclerosis [18]. Despite the large number of causes, it is well-recognised that commonality exists in disease mechanism i.e. the immune system is dysregulated, that similar or identical cell types participate, and patients typically have some form of persistent inflammation.

The clinical features of uveitis are primarily determined by the anatomical region in which the active inflammation is occurring, and therefore which tissues and structures are most likely altered. It can affect one or both eyes and usually has a rapid and sudden onset. Common symptoms include pain, redness, photophobia, and blurring or other alterations to vision. In severe cases cystoid macular oedema, cataracts (opacification of the lens), synechiae (adherence of the iris to the cornea or lens) and ultimately loss of visual acuity can occur [19, 20].

The National Institute for Health and Care Excellence (NICE) Clinical Knowledge Summary (CKS; it represents the United Kingdom's [UKs] standard national health service [NHS] policy) states that glucocorticoids (steroids) are the first-line treatment for uveitis. Whilst these are efficacious in 60–70% of patients [21], they are well-known to cause a multitude of side effects that coalesce into Cushing's syndrome, making their long-term use inappropriate. If the aetiology is believed to be infectious, then an appropriate antimicrobial agent would also be administered. Other interventions, such as cycloplegic-mydratics, tumour necrosis factor (TNF) inhibitors, laser phototherapy, cryotherapy, or vitrectomy may also be administered [22]. Much work has recently attempted to establish where and when to use the various treatments available at an ophthalmologist's disposal [23]. Nonetheless, current management of uveitis could be enhanced and further developed.

Development of therapeutics that are more efficacious, and potentially have fewer side effects, requires a better understanding of the physiology of the eye and pathophysiology of uveitis; this would allow for the selection of a therapeutic target that is more specific than the generalised immunosuppression that glucocorticoids and other existing treatments exhibit.

1.2 The Eye

The eye is a highly specialised organ dedicated to photoreception – the detection of light energy from the environment by rod and cone cells (types of photoreceptors). Photons of light can interact with these rod and cone cells (the latter being stratified into 3 subtypes in most humans) and become transformed into electrical signals by the process of visual phototransduction. This can ultimately be interpreted by specialised regions of the brain that, along with the eyes (including structures required for accommodation, miosis, mydriasis, and/or those which supporting and nourishing the visual structures) and connecting pathways (e.g. optic nerve [ON]), form the visual system [24]. Sight is relied upon as a principal sensory mechanism in a large number and variety of species, humans included, and has clear evolutionary advantage [25]. In humans, sight is hugely important to participation in daily activities [10].

The eye is a spheroid structure consisting of segments of two spheres. The anterior (and smaller) sphere has a boundary comprised primarily of the cornea and lens, whilst the posterior is contained within the sclera; they contain fluids termed the aqueous humour and vitreous body (formerly humour; VB) respectively [26]. The contents are surrounded by three layers: the corneoscleral (fibrous) coat, uvea (comprising the iris, ciliary body, and choroid), and the retina (neural layer) [27]. A diagram, highlighting key components of the human eye, is shown in Figure 1.2.1.

Light is refracted by both the cornea and lens to focus an image on the retina. The cornea has a fixed refractive power, whilst the lens is variable and can be controlled by tension (or slack) of the suspensory ligaments (also known as the lens zonules or zonules of Zinn) ultimately controlled by the contractile state of the ciliary body – a process termed accommodation [28]. The size of the pupil (aperture) is altered by the iris sphincter muscle or the iris dilator muscle, for miosis and mydriasis respectively, and can be manipulated with pharmacological agents [29]. Aqueous humour is produced by the ciliary body epithelium and drains via the canal of Schlemm [24]. When observing a fundus image (taken from an anterior position), the optic disc (blind spot), fovea (and surrounding macula), and blood vessels (as well as the orange-pink colour of the retina) are apparent [27].

The retina, along with many other structures in the eye, is a complex tissue comprised of multiple cell types and structures. It is stratified into 10 different layers which are visualised in Figure 1.2.1 and 1.2.2 [30]. Each of these layers is briefly summarised in Table 1.2.1.

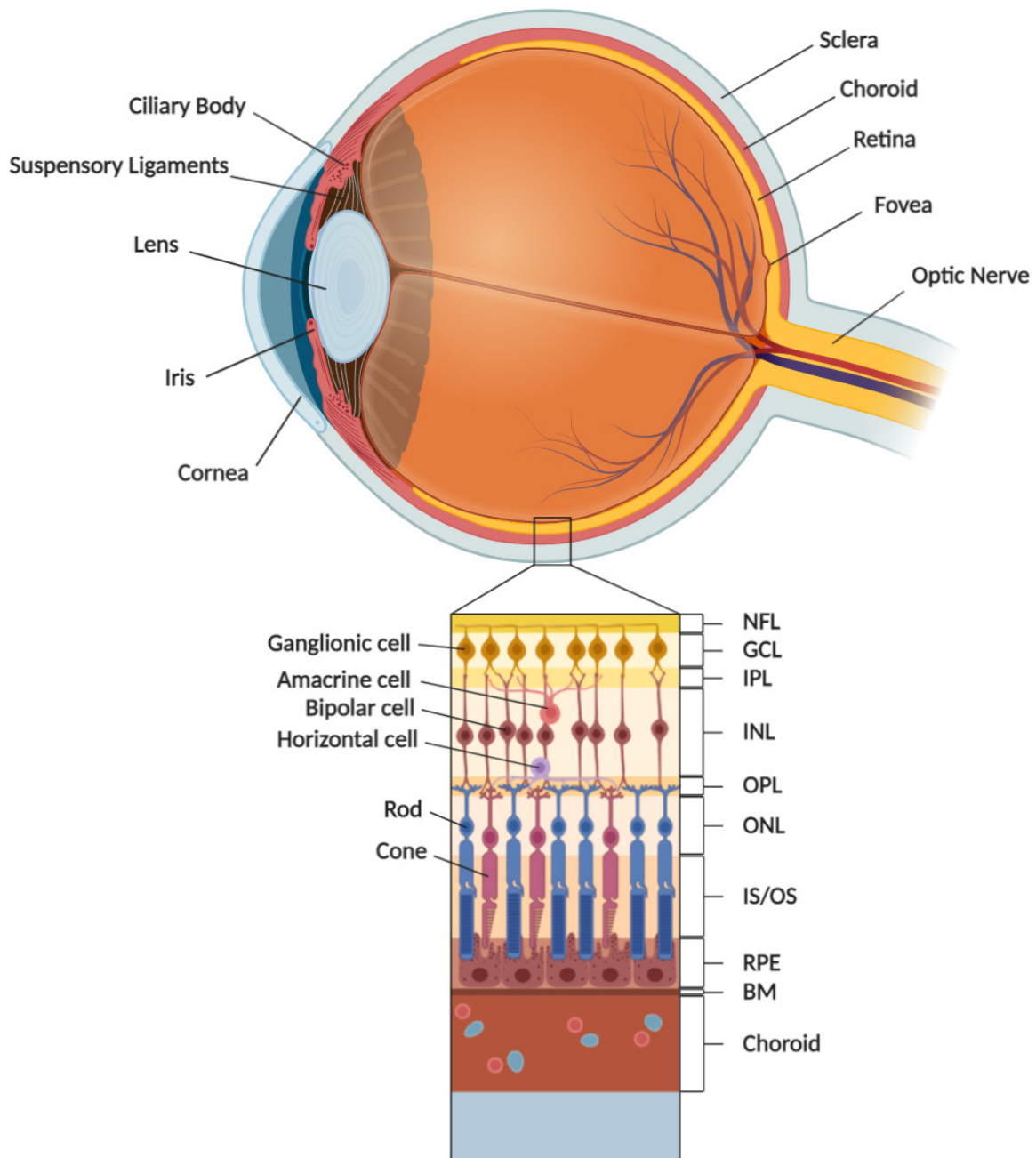


Figure 1.2.1. A schematic diagram representing the structure of the eye (top) to include cells and layers within the retina (bottom). Abbreviations: NFL – nerve fibre layer, GCL – ganglion cell layer, IPL – inner plexiform layer, INL – inner nuclear layer, OPL – outer plexiform layer, ONL – outer nuclear layer, IS – rod and cone inner segment, OS – rod and cone outer segment, RPE – retinal pigment epithelium, BM – basement membrane. Adapted from [31].

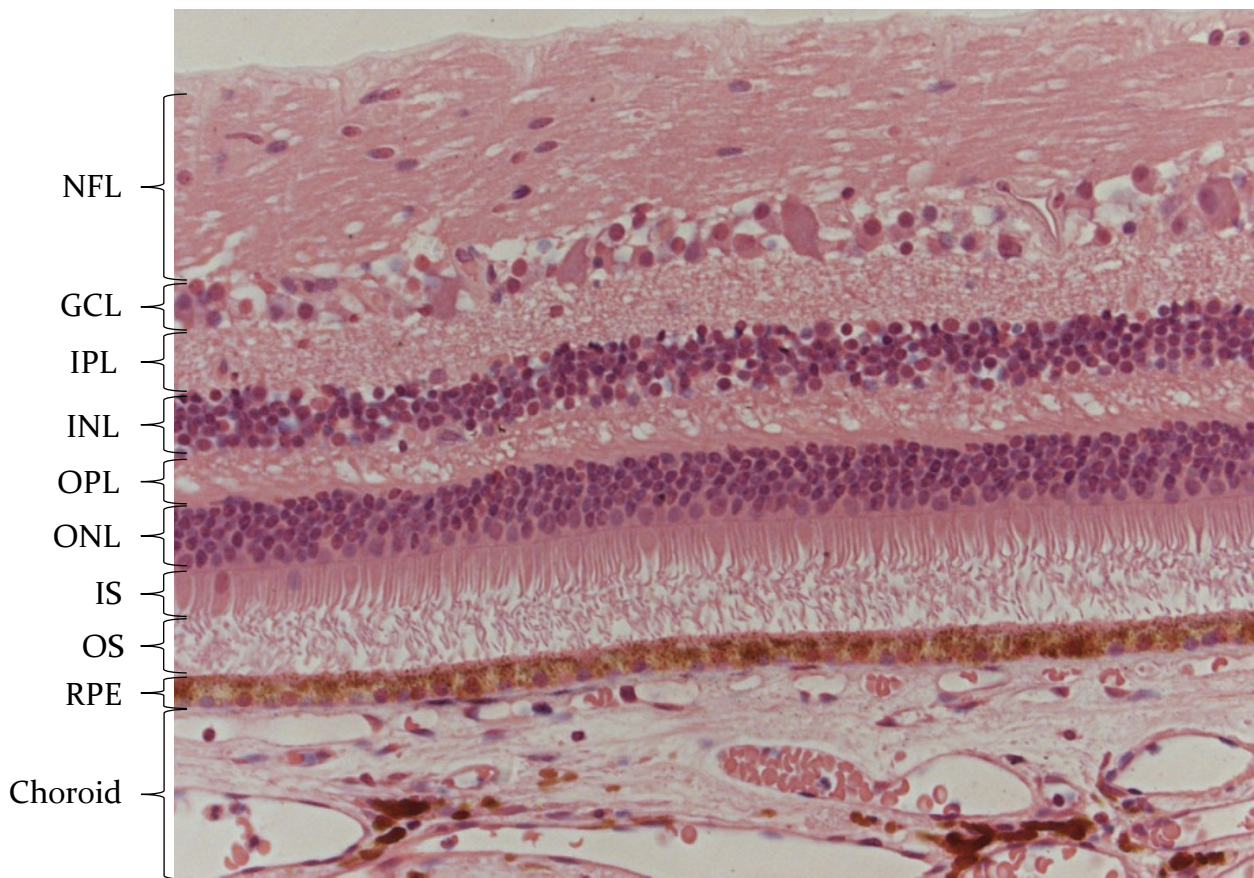


Figure 1.2.2. A histological section of the retina and choroid highlighting the different segments and their appearances with haematoxylin and eosin staining. Haematoxylin stains the nuclei purple whilst eosin stains the cytoplasm and extracellular matrix pink. Abbreviations: NFL – nerve fibre layer, GCL – ganglion cell layer, IPL – inner plexiform layer, INL – inner nuclear layer, OPL – outer plexiform layer, ONL – outer nuclear layer, ELM – external limiting membrane, IS – rod and cone inner segment, OS – rod and cone outer segment, RPE – retinal pigment epithelium, BM – basement membrane. Adapted from [32] and used under licence (CC BY 3.0).

Layer	Primary Components	Function	Reference
NFL	Ganglion cell axons	Transmit action potentials towards the brain (ultimately via the ON)	[33]
GCL	Ganglion cell bodies	Components of the visual system (relating to electrophysiology)	[26]
IPL	Synapses between bipolar cells and ganglion/amacrine cells		
INL	Cell bodies of the amacrine, bipolar, and horizontal cells		
OPL	Synapses between PRs and bipolar/horizontal cells		
ONL	Photoreceptor cell bodies		
ELM	Junctional complexes between PRs and MCs	Mechanical strength and barrier	[34]
IS/OS	PRs	Light detection and conversion into an electrochemical signal	[35]
RPE	Simple cuboidal epithelium	Barrier, and control of substance movement in/out of retina	[34]
BM	Extracellular matrix (collagen)	Structural integrity	[36]

Table 1.2.1. Primary components of the retinal layers and their basic function. Abbreviations: NFL – nerve fibre layer, GCL – ganglion cell layer, IPL – inner plexiform layer, INL – inner nuclear layer, OPL – plexiform layer, ONL – outer nuclear layer, ELM – external limiting membrane, PR – photoreceptor, MC – Müller cells, IS/OS – inner/outer segments, RPE – retinal pigment epithelium, BM – basement membrane.

In addition to the cells which detect light, convert it into an electrochemical signal, and transmit this to the brain there are several other cell types present in the eye important for maintenance of physiological conditions. Microglia and macroglia (astrocytes and Müller cells) are important for supporting neurons in a multitude of ways which have been extensively reviewed recently [37]. Furthermore, there are an abundance of different tissue-resident immune cells, or sentinels, which observe the environment for danger. When required, they can manage threats or escalate by initiating a cascade of events which promote the infiltration of peripheral immune cells to assist. Tissue-resident macrophages and dendritic cells have been observed in the cornea, choroid, iris, and ciliary body, whereas tissue-resident mast cells have been observed in the iris, ciliary body, and choroid of some species [38-40]. Microglia possess an immune function, in addition to their supporting roles, and are discussed in greater detail later in this chapter [41]. The retinal pigment epithelium (RPE) also plays an important role in immune responses and modulation [42].

In addition to this, it is typical to also observe non-tissue resident lymphocytes and other immune cells within non-inflamed retinas; in the absence of inflammation a very small number can still infiltrate and egress without apparent damage or clinical features [40]. Furthermore, it appears possible for tissue-resident T lymphocytes to be present within normal eyes in some species, or for the development of tertiary (or ectopic) lymphoid structures in eyes that have undergone persistent inflammation [43, 44].

The delicate structure of the eye, and its highly important role in daily activities, has meant that investigation using invasive techniques in humans is greatly limited [16]. To overcome these challenges, investigations utilising model organisms have been performed. Mice are commonly employed to model human diseases of the eye and are a prime organism of choice with a variety of models and transgenic lines (relevant models of intraocular inflammation and transgenic lines are discussed later). However, it is noteworthy to highlight key differences between human and mouse exist as they are separated by roughly 87 million years of evolution and around 300 genes are unique to one species or the other [45-47]. With respect to eyes, mice do not possess a macular or fovea, their eye is a single spheroid (still containing both the anterior and posterior chambers), and the lens is considerably larger (Figure 1.2.3) [48]. Nonetheless, human and mouse eyes exhibit a lot of similarities and many advancements in our understanding of eye biology have originated from studies in the mouse.

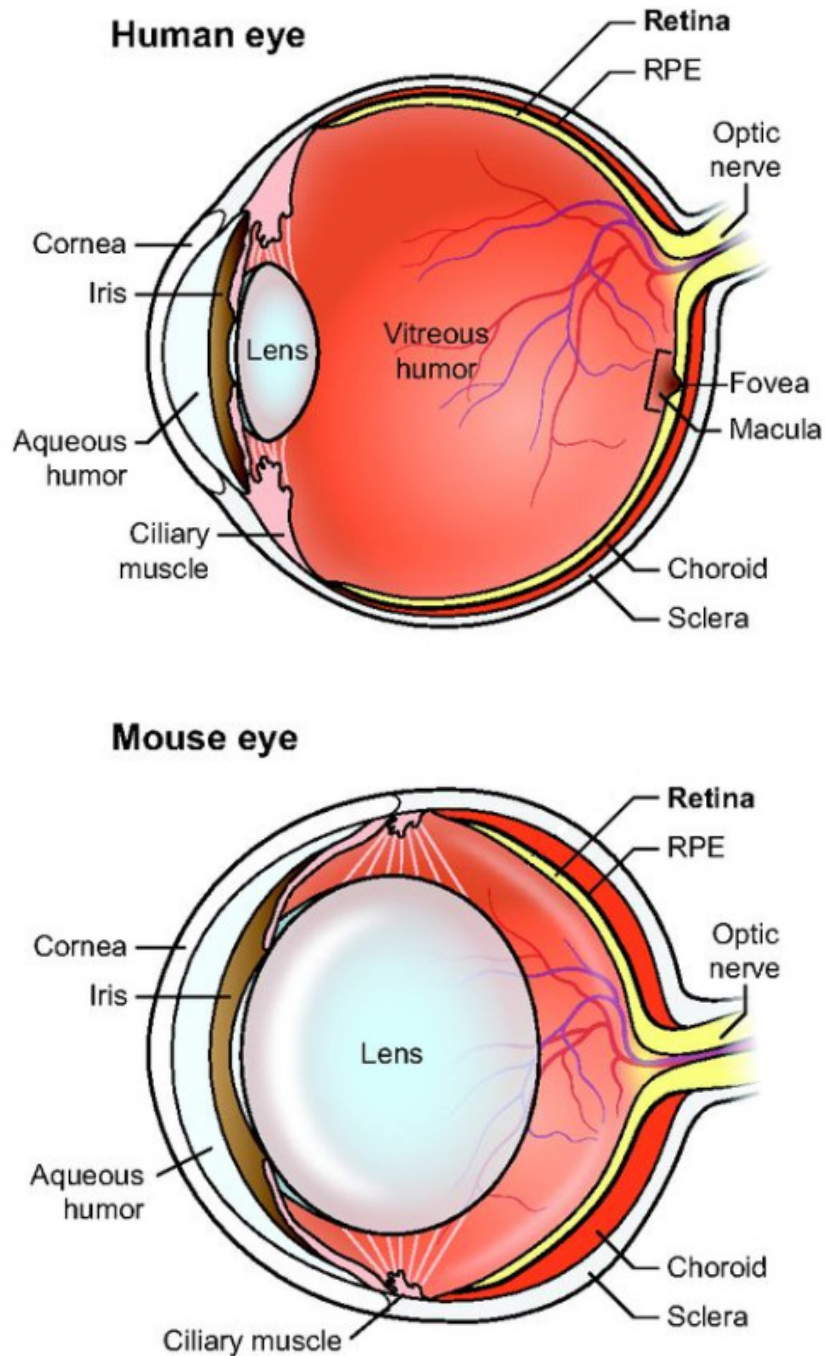


Figure 1.2.3. Schematic diagrams of sagittal sections of the human (top) and mouse (bottom) eyes to highlight their similarities and differences. The primary differences include a relatively larger lens in the mouse in addition to an absence of both fovea and macula. The mouse eye more closely represents a single spheroid as well. Abbreviation: RPE – retinal pigment epithelium. Adapted from [48] and used under licence (CC BY 4..0).

It is also relevant, at this point, to highlight that mouse and human immune systems also exhibit discrepancies despite many similarities. Generally, human blood has a high proportion of neutrophils whilst in the mouse lymphocytes predominate. Mice have considerably more bronchus-associated lymphoid tissue, and haemopoietic stem cells express markers (e.g. c-kit and flt-3) to varying degrees between the species [47]. Whilst many new drugs and targets have translated from mouse to man many others have failed, highlighting underlying differences between the species and/or poor disease modelling [49]. Whilst it would be self-confounding to experiments, there is even data to suggest specific pathogen free (SPF) conditions alter the mouse immune response – with data showing some bystander infections confer resistance to otherwise lethal infections [50]. However, it remains pragmatic to utilise mouse models in situations where no better alternative currently exists, and to try and normalise conditions (and include the proper controls) so experiments are more readily comparable – meaning that control of environmental pathogens and bystander infections is a necessary compromise to reduce confounding within experiments.

1.3 Murine Models of Uveitis:

An early paper describing ocular reactions to exogenously administered substances was published in 1943 [51]. However, it wasn't until the 1980s that the first models of uveitis were developed (in rabbits and rats): experimental autoimmune uveitis (or uveoretinitis; EAU) and endotoxin-induced uveitis (EIU), induced by immunisation and endotoxin respectively [52-54]. Since then, these models have been adapted for the mouse and multiple new variations have emerged: novel vaccination peptides, adoptive transfer (AT) of uveitogenic cells, transgenic mice which develop uveitis spontaneously, infection models with cytomegalovirus or *M.tuberculosis*, and alternative administration routes or substances (for EIU) [55, 56]. Each model generates a different clinical phenotype which can help in modelling different aspects of uveitis and correlation to patient phenotypes. However, none of these models accurately recapitulates human disease [57]. Despite a diverse range of induction approaches, some common effector mechanisms exist to cause disease [57].

1.3.1 Experimental Autoimmune Uveitis

EAU is a model of local non-infectious posterior uveitis, mediated by cluster of differentiation (CD) 4⁺ T cells primarily via the T-helper 1/17 (T_H1/17) axis [1]. It was first described in the mouse in 1988 [58]. EAU is conventionally induced by immunising the mouse against retinal antigens. To achieve this, a mouse is required that has a permissive background (to include possession of a susceptible haplotype) such as a B10.RIII or C57BL/6 strain, but also an encouraging environment so that autoimmune disease can develop [59]. The environment is generated by three major components: complete Freund's adjuvant (CFA), pertussis toxin (PTX – this component is optional, but its use increases the rate of successful induction), and the immunising autoantigen. The peptide is not usually an exact match of a mouse retinal antigen and therefore this system could be considered similar in mechanism to molecular mimicry in terms of how it models autoimmunity. The environment is administered only once and poorly simulates both the burden of infection (or multiple acute events) over the lifetime of an organism and the relapsing nature of uveitis (see Section 1.4).

CFA contains heat-killed and dried *Mycobacterium tuberculosis* of the strain H37Ra dissolved in paraffin oil and mannide monooleate. Adjuvants are used in vaccines and immunisation models as they enhance the immune response to a particular antigen; in the case of CFA, cell-surface antigens of the *M.tuberculosis* strain activates TLR₂, leading to MAPK/ERK activation and expression of TNF- α , leading to acute activation of the innate immune system and up-

regulation of TLR2 and TLR4 [60]. Knockout of the TLR adapter protein, MyD88, results in resistance to EAU induction [61]; however, single or paired TLR2/4/9 knockouts did not induce disease resistance [62] suggesting redundancy within TLR-signalling. Interleukin-1 receptor (IL-1R)-deficient mice are resistant to EAU induction, implying an essential role [61]; IL-1 β is a pro-inflammatory cytokine produced by monocytes, macrophages, dendritic cells, and microglia in response to TLR stimulation, and it causes enhanced endothelium permeability to infiltrating cells such as T lymphocytes [63], highlighting the vital role myeloid cells play in the initiation of EAU. However, TLR agonists have been shown (compared to TLR-knockout mice) to enhance disease severity [62], especially in less-susceptible strains or where low concentrations of antigen are used. This highlights how the local context can influence the sensitivity tuning of the T cell receptor (TCR).

PTX is primarily useful for autoimmune disease induction in the eye because the eye is relatively immune privileged under physiological circumstances. PTX has multiple subunits, organised in a typical A-B structure. PTX raises the permeability of the blood-brain barrier (BBB) [64], which the blood-retinal barrier (BRB) is an extension of, enhancing temporary access of immune cells to the eye. The primary mechanism of action of PTX is to inhibit G_i proteins via ADP-ribosylation via the A-promoter, although it is recognised that PTX has other pharmacological properties too [65]. For example, the B-oligomer acts as an adjuvant, binding to and activating TLR4 to enhance immune responses [66]. PTX has been shown to enhance many CD4⁺ T cell responses [67], in particular T_{h1} and T_{h17} cells indicated by increased interferon- γ (IFN- γ) [68] and IL-17 [69] expression. As *M.tuberculosis* up-regulates TLR4 expression [60], it is likely to have a synergistic interaction with PTX with respect to enhancing immune responses.

The final component, the antigen, is specific to the target the mouse is being immunised against. The antigen chosen, the mass required, and the amino acid residues varies depending on the strain used because their genetic background (primarily major histocompatibility complex [MHC] haplotype) alters susceptibility. For example, the immunisation protocols used by our group for Bio.RIII strains utilise RBP-₃₁₆₁₋₁₈₀ (retinol binding protein-3, also known as human inter-photoreceptor retinoid-binding protein [hIRBP]) whilst in C57BL/6 strains RBP-₃₁₋₂₀ or RBP-₃₆₂₉₋₆₄₃ are used in a much greater final concentration instead.

EAU is a model where, after active immunisation, the first clinical signs of disease (generally swelling and brightening of the optic disc) are observed around days 12–14, followed by perivascular sheathing and the development of spots and/or lesions – which by peak of disease (days 21–27) covers the vast majority of vessels in the C57BL/6 mouse. It is followed by further

structural damage described as a “secondary progression” or resolution phase [70, 71]. In the Bio.RIII strain, disease develops earlier and more aggressively. Whilst EAU was originally considered to model posterior uveitis, features of anterior uveitis have also been observed [72].

Since the report of the original model, several variations have since emerged. These can include immunisation against different peptides or different regions of an already identified uveitogenic peptide [71, 73-77]. However, other variants of EAU include the AT model where lymphocytes with antigen-specificity for retinal peptides are injected into recipient mice [78]. The AT model enables the investigation/delineation of retinal-specific T cells and endogenous T cells which have not (before disease) been selected for retinal antigen activity, especially if allelic markers (such as CD45.1 and CD45.2) are used to differentiate them. The AT model generally has a much faster onset and severity of disease, peaking around day 11 as a more acute form of EAU. Further variants include induction of anterior uveitis using melanin [79, 80], humanised EAU models (these mice have their murine MHC-II replaced with human HLA, with a spontaneous model using HLA-A29 mice – which in humans has a very strong genetic association with birdshot chorioretinopathy [81-83]), other spontaneous models through knockout of the AIRE gene (an important gene for central tolerance as described later) [84]. Lastly, models which mimic infection (linking both the innate and adaptive immune responses), partially diverge in effector mechanism, and therefore are considered separate models to EAU include both primed mycobacterial uveitis (a more anterior disease; PMU) [85] and cytomegalovirus (CMV) infection in immunodeficiency [86]. Generally, the induced models of uveitis tend to have a more acute and greater severity of disease whereas spontaneous models initiate earlier, last longer, and result in a greater loss of retinal function (as measured by electroretinogram [ERG]) [87]. The different peptides used to induce EAU in rodents (and their protocols) have already been comprehensively reviewed [88].

1.3.2 Endotoxin-Induced Uveitis

Endotoxin-induced uveitis (EIU) is another model of uveitis; it was originally induced by subcutaneous or intraperitoneal injection of lipopolysaccharide (LPS – a potent activator of the immune system and component of the outer membrane of gram-negative bacterial that is recognised by TLR4 [89]). It leads to an acute short-lived monophasic reaction that was originally considered synonymous to anterior uveitis [52]; however, it is now recognised to exhibit clinical features that are analogous to posterior uveitis as well [90].

New variations on the EIU model have since emerged, such as administering LPS intravitreally [91]; this approach would simulate local uveitis as opposed to systemic, whilst also greatly reducing the amount of LPS used to induce disease in each mouse eye. Other variations include using different immunostimulatory molecules (such as other TLR agonists) to induce intraocular inflammation [92]. Comparisons between peripheral and local administration of LPS have been made, showing that in the mouse (in which less severe disease is seen with respect to the rat – the originally-described organism for this model) cellular infiltrate is poor when administered systemically, but alterations in cytokine levels that were broadly similar to local administration were observed [93]. It is also recognised that the amount of LPS required systemically for EIU has a multitude of serious adverse effects in the mice that is considered unnecessary suffering – use of local administration in addition to titrating the amount of LPS (or other molecule) administered is a refinement (one of the 3Rs – a framework for more humane animal research [94]) of the model. It is also known that a reduced disease severity could predictively enrich the treatment effect of potential therapies tested downstream [95]. This could be coupled with the recent advancements in analysis of retinal disease models via the development of high resolution *in vivo* imaging platforms and general analytical approaches for images (such as image segmentation [96]) that provide greater ability and sensitivity for detecting and classifying disease in all ocular models. For example, scoring of EIU using optical coherence tomography (OCT)-based methods has been recently reported [97]. Table 1.3.1 summarises multiple different mouse models of uveitis.

Uveitis (Variant) Model	Spontaneous vs. Induced	Overview	Reference
EAU	Induced	Original EAU mouse model, immunisation against RBP-3. Multiple variants against other retinal antigens/regions have since emerged	Original: [58] Variants: [71, 73-77]
EAU (humanised HLA-DR Tg mouse)	Induced	Mice with Tg (human) HLA become susceptible to uveitis induction	[81]
EAU (AT)	Induced	Injection of uveitogenic CD4 ⁺ T cells generated from donor mice	[78]
EAU (Melanin)	Induced	Immunisation against melanin, causing anterior uveitis	[79, 80]
Lens-associated uveitis	Induced	AT of TCR Tg lymphocytes (against HEL) into Tg mice where lens expresses HEL	[98]
PMU	Induced	Systemic priming with <i>M.tub</i> Ag followed by local <i>M.tub</i> Ag. Repeated injections possible for a more chronic disease form	[85]
CMV	Induced	Local administration/infection with CMV	[86]
AIRE KO	Spontaneous	Failure of central tolerance leads to systemic autoimmunity	[84]
HLA-A29	Spontaneous	Insertion of HLA-A29 from birdshot chorioretinopathy patient	[82]
RBP-3 R161H Tg mouse	Spontaneous	Spontaneous EAU in mice with Tg auto-reactive CD4 ⁺ T-cells to RBP-3	[99]
TrP-HEL transgenic mouse	Spontaneous	Spontaneous EAU, utilising HEL system, by crossing melanocyte-specific-HEL mice with HEL-specific TCR CD4 ⁺ T cells	[100]
HEL-transgenic mouse	Spontaneous	Spontaneous EAU, utilising HEL system, by crossing IRBP-HEL mice with HEL-specific-TCR CD4 ⁺ T cells	[101]
EIU (LPS systemic)	Induced	Systemic LPS dosing causes widespread acute inflammation	[52]
EIU (LPS local)	Induced	Local LPS dosing to the eye causing acute inflammation	[91]
EIU (non-LPS)	Induced	Dosing with PRR agonists (such as to TLRs) causing acute inflammation	[92]

Table 1.3.1. A summary and comparison of mouse models of uveitis. Since EAU and EIU were first described in 1988 and 1980 respectively, many variants have since emerged. Abbreviations: AT – adoptive transfer, CMV – cytomegalovirus, EAU – experimental autoimmune uveitis, EIU – endotoxin-induced uveitis, HEL – hen egg lysozyme, HLA – human leukocyte antigen, LPS – lipopolysaccharide, PMU – primed mycobacterial uveitis, PRR – pattern recognition receptor, RBP-3 – retinol-binding protein 3, Tg – transgenic, TLR – toll-like receptor.

1.3.3 *In Vivo Clinical Assessment of Intraocular Inflammation*

The eye permits non-invasive repeatable *in vivo* clinical imaging to monitor disease across a time course and assists in understanding changes in tissue integrity, immune cell recruitment and activation, and assessment of retinal function.

Live imaging techniques have improved dramatically in the last 15 years. Before imaging techniques, it was usual to score retinal disease using semi-quantitative approaches such as histology which was a terminal assay [70]. This greatly increased the number of required mice for an experiment, with exponential increases as more timepoints were used. As individual eyes could not be tracked through disease, this also meant that greater numbers were required to draw conclusions with confidence due to the inherent variability of the disease models. With improvements, approaches such as slit-lamp examination were utilised. The slit lamp is effectively a microscope coupled to a light source which can be focused to shine a thin layer of light into the eye. It permitted scoring in the same mouse across time and cross-correlation of terminal assays to disease within the same mouse [102]. Scoring was based exclusively on anterior features, is both coarse and subjective, and performed only by the researcher(s) completing the examination [103]. It also means that validation of scores by other researchers is not possible, meaning it could be confounded by bias.

Further developments in imaging has enabled retinal diseases to be monitored by acquiring images of the posterior retina (fundal imaging) using topical endoscopic fundus imaging (TEFI – [70, 104, 105]) or by commercial imaging platforms such as the Micron IV [106]. TEFI, put simply, is the attachment of an endo-otoscope to the end of a single lens reflex (SLR) camera but also to a light source (via fibre optic cable) for image capture and retinal illumination, respectively. The Micron IV is a commercial retinal imaging solution (essentially a widefield microscope with condensing lenses) optimised for rat and mouse imaging. These imaging techniques are especially pragmatic as they allow for repeated imaging and monitoring of the same animal, facilitating a reduced requirement in terms of numbers, but also correlation to other *ex vivo* assessments (e.g. flow cytometry and immunohistochemistry) and an ability to remove confounding mice before or during an experiment (i.e. through baseline imaging to identify abnormalities, or confirmation of disease induction before allocation to treatment or control groups in the case of models such as EAU [107]). Additionally, the Micron IV imaging platform enables acquisition of other data in addition to brightfield fundus images: it has the capability to perform OCT (“*in vivo* histology”) and utilise filters for fluorescent imaging. In combination with cell tagging approaches (e.g. carboxyfluorescein succinimidyl ester [CFSE] or

transgenic reporter lines), it would be possible to track specific cell types during disease to better understand their dynamics during disease, and correlation to observed tissue damage or other (terminal) assays.

Additionally, with fundal imaging it is possible to score EAU disease severity using multiple different reviewers who can readily be blinded to treatment groups to prevent potential confounding through bias (without blinding, treatment effect magnitude is estimated to increase by nearly 20% [108]). The convenience of digital images makes it easier to blind images and have multiple reviewers. This makes comparisons and tests of reliability and validity much simpler to perform. Furthermore, other emerging approaches for image analysis have been described. For example, it is possible to use OCT as an unbiased linear approach for scoring retinas during EIU [109]. Briefly, it utilises counts or volume measurements of objects (presumably immune cells) observed inside the vitreous body during inflammation. There is potential for application to EAU and other models where immune cell infiltration occurs as well.

Whilst the imaging techniques allow for *in vivo* analysis, there are limitations in the information they can provide. At the cellular/molecular level, they can provide only minimal information (due to resolution limits – in the Micron IV, this is roughly 2 μm), thus facilitating the need for other *ex vivo* assessment. Nonetheless, the imaging techniques are especially useful in indicating successful induction of EAU, allowing for selection of mice that were successfully induced (incidence of EAU is typically 89-100% [110]) but also selection at a given time-point of the disease (early, peak, late as there can be great variability in the kinetics) so that molecular techniques and/or therapeutic interventions are performed on well-controlled samples. Baseline imaging can also exclude mice with anomalous eyes before use in an experiment. This ultimately means that fewer animals are required in each group to demonstrate significance at a statistical level. Imaging across a time-course also permits determination of good endpoints for an investigation, so that expensive or complicated assays can be performed at the correct time in future/repeat experiments.

1.4 Immunity and Inflammation

The immune system spans the entire organism to maintain health, with well-known functions including protection from infectious diseases and aberrant host cells that have or could form a tumour but additional roles that include tissue morphogenesis, tissue homeostasis, removal of foreign/waste substances (scavenging), wound repair, and many more [111-115]. Underpinning all of these functions is the ability of the immune system to recognise and respond appropriately to self and non-self; where this fails autoimmunity, immune deficiency or other immune disorders such as autoinflammation can arise [116].

The immune system is divided into two arms at the cellular level: innate and adaptive. Key stages of the differentiation of haematopoietic cells (to include leukocytes, erythrocytes, and platelets), in addition to their localisation during these stages, is shown in Figure 1.4.1. The innate immune system is comprised predominantly by cells of the myeloid lineage and is the first arm of the immune system to respond to infection or damage. It does this via pattern recognition receptors (PRRs) which can detect the presence of damage to cells or tissues (damage associated molecular patterns [DAMPs]) or generalised cell-surface molecules which associate with foreign cells i.e. those found on a pathogen (pathogen associated molecular patterns [PAMPs]). Whilst these have a fixed and limited repertoire, each receptor will nonetheless act in a specific fashion. For example, TLR4 recognises lipopolysaccharide (LPS) – a major component of the outer membrane of gram-negative bacteria.

In response to activation, innate immune cells perform functions such as phagocytosis and the secretion of chemokines/cytokines to recruit other immune cells and transiently increase immunological activity in that locale; the response can also enhance immunological surveillance across the body. PAMPs often have critical roles in the survival and function of these foreign cells and therefore cannot be lost or made redundant from them [117]. This partially explains how the innate immune system has retained effectiveness whilst pathogens would be under selection pressures against expression of these molecules (from an immunological perspective). The repertoire of receptors enables the recognition of many different pathogens and damage signatures but nonetheless is limited as there are a finite number of them, pathogens may be capable of altering other surface receptors, and a vast diversity of pathogen species exist. Therefore, innate immune responses are effective, but evolution has also driven the development of adaptive immunity which can combat continually evolving pathogens.

The adaptive immune system, comprised by cells of the lymphocytic lineage (mainly T and B lymphocytes), has the capability to recognise an almost unlimited repertoire of molecules

(termed antigens) and overcomes shortfalls in innate immunity. T lymphocytes act directly on targets whereas B cells typically are associated with differentiating into plasma cells that synthesise antibodies (or immunoglobulins); in short, both major types of lymphocyte assist in target neutralisation. In addition, the adaptive immune system has the capacity for generating immunological memory – where the immune system mounts both a faster and stronger response to subsequent antigenic exposure. However, an effective initial adaptive immune response takes considerably longer to mount than an innate response, and crosstalk can occur between the two arms via mechanisms such as antigen presentation. That said, memory has also been observed in innate immune cells (controlled by epigenetic changes) that can last long-term [118-120].

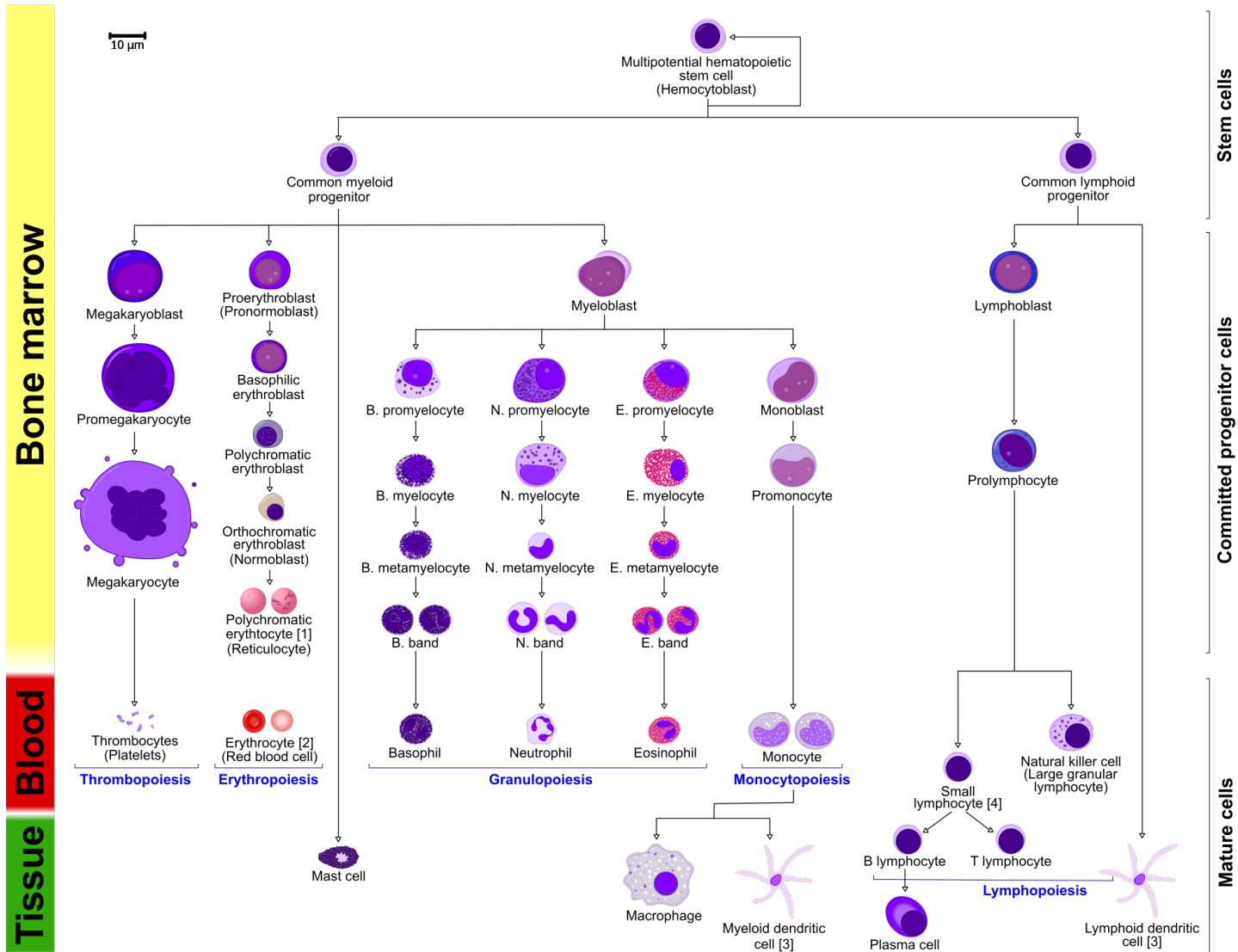


Figure 1.4.1. Developmental summary of blood cells (haematopoiesis) to include their localisation and maturation during key stages. The common lymphoid progenitor gives rise to multiple adaptive immune cells, whilst the common myeloid progenitor gives rise to multiple innate immune cells. Taken from [121] and used under licence (CCo 1.0).

1.4.1 Innate Immunity

Once a foreign cell overcomes anatomical barriers (i.e. the skin and other epithelia), it enters the body. Many mononuclear phagocytes act as sentinels for pathogen entry, residing within the tissue and sensing for danger. They can be found throughout a wide variety of, if not all, tissues of the body and include microglia (brain and eye), Kupffer cells (liver), splenic, lymph node, stromal, cardiac, lung, peritoneal, ileal, and colonic macrophages to name a few [122, 123]. Many types of innate immune cell are also continually circulating within the bloodstream and possess the ability to enter injured or infected tissue as required.

With PRRs, they can recognise generalised patterns of foreign cells or damage and enact initial responses. There are four major sub-families of PRR: TLRs, nucleotide-binding oligomerisation domain (NOD)-leucin rich repeats (LRR)-containing receptors (NLRs), retinoic acid-inducible gene 1 (RIG-1)-like receptors (RLRs), and C-type lectin receptors (CLRs; Figure 1.4.2) [124]. The different types of receptor, ligand they recognise, and their signalling pathways have already been extensively reviewed [125-129]. Furthermore, the context of pattern recognition (e.g. external surface [commensal] or internal [invading pathogen], local damage to tissues, or systemic spread) is utilised to determine the threat level and therefore the required magnitude of the immune response [130].

An alternative initiating mechanism of innate immunity is the complement system (Figure 1.4.3). The main functions of complement include promoting inflammation, phagocytosis, and the formation of membrane attack complexes (MACs). MACs are required for the killing of particular species of pathogen (e.g. *Nisseria meningitidis*) and may enable the passage of degrading enzymes such as lysozyme [131]. Three pathways for complement activation exist: the classical, lectin, and alternative pathway. With differences in initiation, they all have the same downstream effects of chemoattraction, opsonisation, and the formation of MACs via a common signalling pathway from C3 [132]. The classical pathway is activated by antibody-antigen complexes, the lectin pathway activated by lectins (via receptors for unique carbohydrate signatures present on bacteria and fungi), and the alternative pathway initiates by spontaneous hydrolysis of C3 [133].

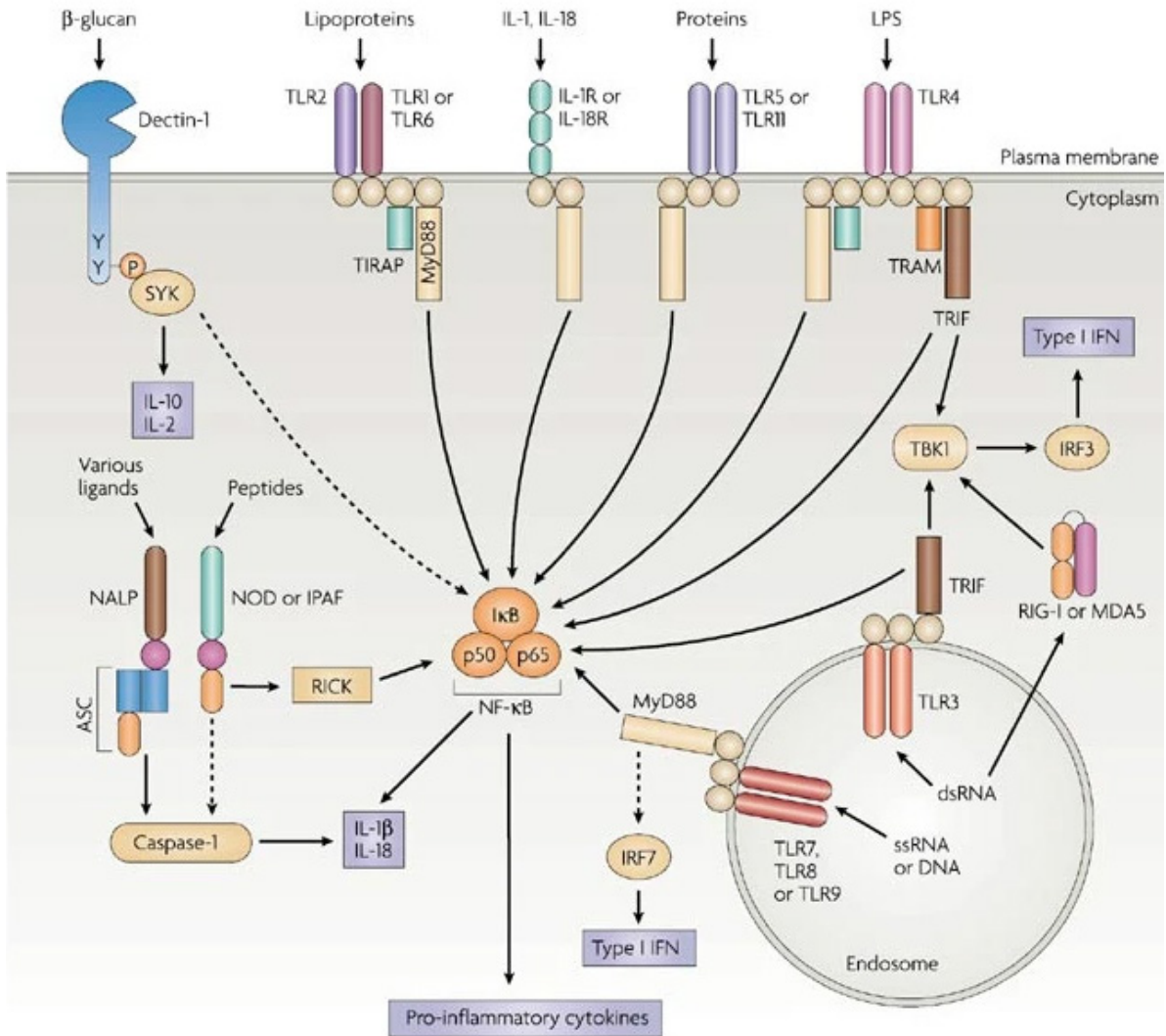


Figure 1.4.2. Pattern recognition receptors (PRRs) and downstream signalling elements. The four major sub-families of PRRs and their signalling adapters are shown: C-type lectin receptors (Dectin-1), Toll-like receptors (TLRs), nucleotide-binding oligomerisation domain (NOD)-leucine rich repeats (LRR)-containing receptors (NLRs), and retinoic acid-inducible gene 1 (RIG-1)-like receptors (RLRs). All PRRs couple to an important pro-inflammatory transcription factor: NF- κ B. Taken from [134] and reproduced with permission from Springer Nature.

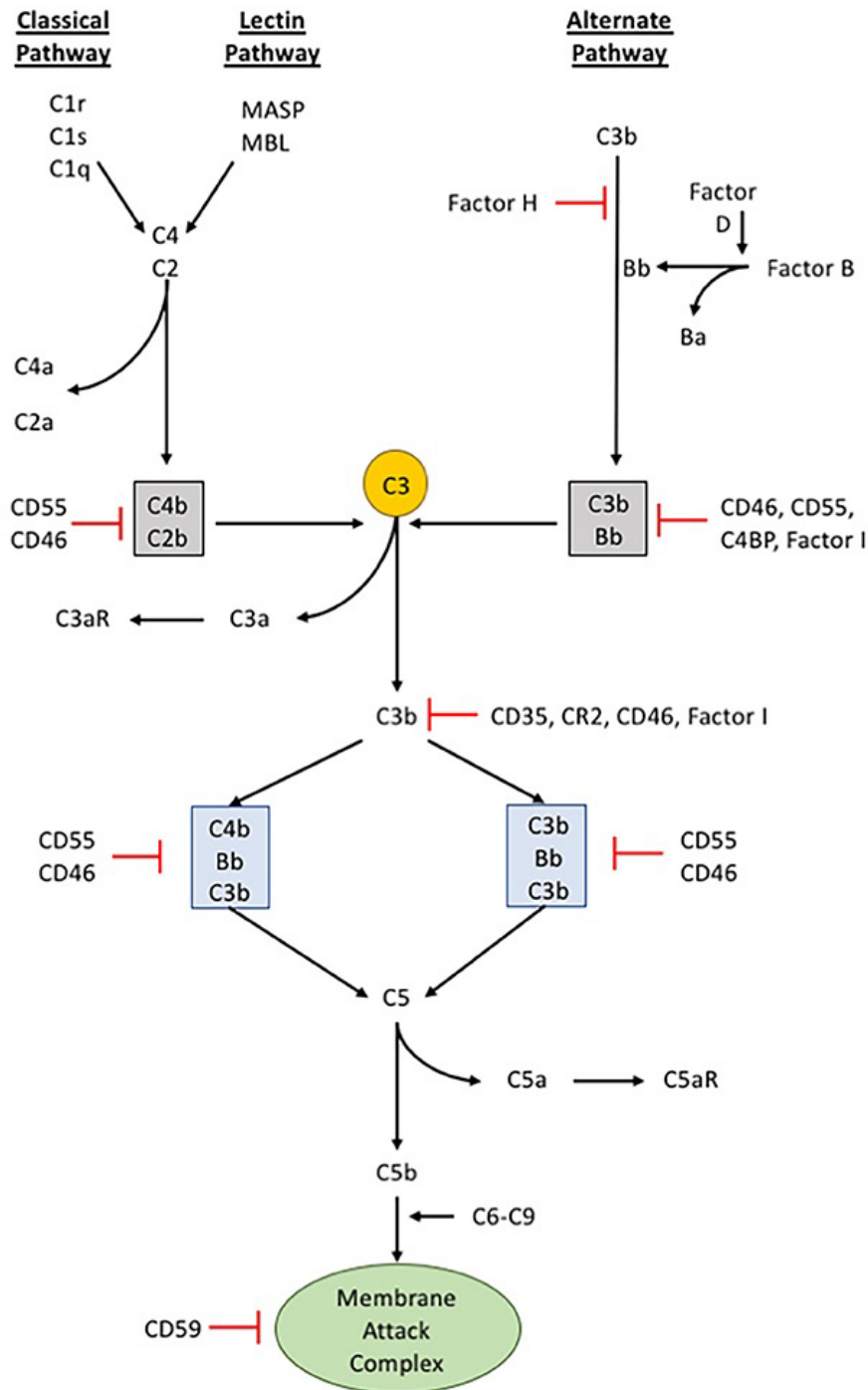


Figure 1.4.3. A schematic of the complement system, highlighting the three initiating pathways and subsequent signalling cascade. The classical pathway is activated by binding to specific carbohydrates associated with pathogens. The alternative pathway is activated by spontaneous activation and binding of C3b to a pathogen, foreign material, or damaged tissues. Both C3a and C5a act as chemoattractants for leukocytes. Endogenous inhibitors of different components of the pathway are indicated in red. Adapted from [135] and used under licence (CC BY 4.0).

After activation, innate immune cells produce effector functions – i.e. phagocytosis of foreign material and pathogens – in addition to secretion of cytokines and chemokines to modulate the immune response and assist with recruitment of other (peripheral) immune cells to that locale respectively (Figure 1.4.4). With regards to effector functions, cytoskeletal changes permit the internalisation and subsequent formation of a phagosome. This fuses with lysosomes, forming a phagolysosome, and ultimately assist in killing the pathogen utilising reactive oxygen species (ROS) and lysosomes [136, 137]. With regards to secreted molecules, these can not only promote inflammation and attract immune cells, but also influence how other immune cells specialise (or polarise) in dealing with the cause of inflammation – both have been extensively reviewed recently [138-140]. Some chemokines are presented on the surface of endothelial cells in addition to other cell-adhesion molecules [141]; these assist in the binding of leukocytes and ultimately their ingress to the inflamed tissue – a process termed extravasation (Figure 1.4.5) [142, 143]. Furthermore, expression of chemokines control the homing of leukocytes between primary lymphoid organs in addition to secondary lymphoid organs and the periphery [144, 145]. It is also appreciated that leukocytes modulate expression of chemokine receptors at different stages of development and activation to facilitate homing.

Phagocytes can process fragments of peptide from the killed pathogen, load it into the MHC and, along with expression of required co-stimulatory receptors/ligands to indicate a danger/damage context, present the fragment to T lymphocytes (Figure 1.4.4) [146]. This process is made feasible through the formation of an immunological synapse and, in addition to activating a T lymphocyte with a complementary TCR to the peptide, assists with T lymphocyte activation and polarisation towards a particular subset [147]. The overall process of loading peptide and exhibiting it to a T lymphocyte is termed antigen presentation, and typically occurs in lymphoid tissues. It is possible for exchange of peptides between different antigen-presenting cells [148], enabling peptide acquired by the initial response of tissue-resident cells to be processed in the lymphoid tissues. Lymphocytes inherently traffic via lymphoid tissue and therefore the probability of a productive interaction (i.e. an interaction/affinity between loaded peptide and TCR that results in activation of the lymphocyte) is greatly increased.

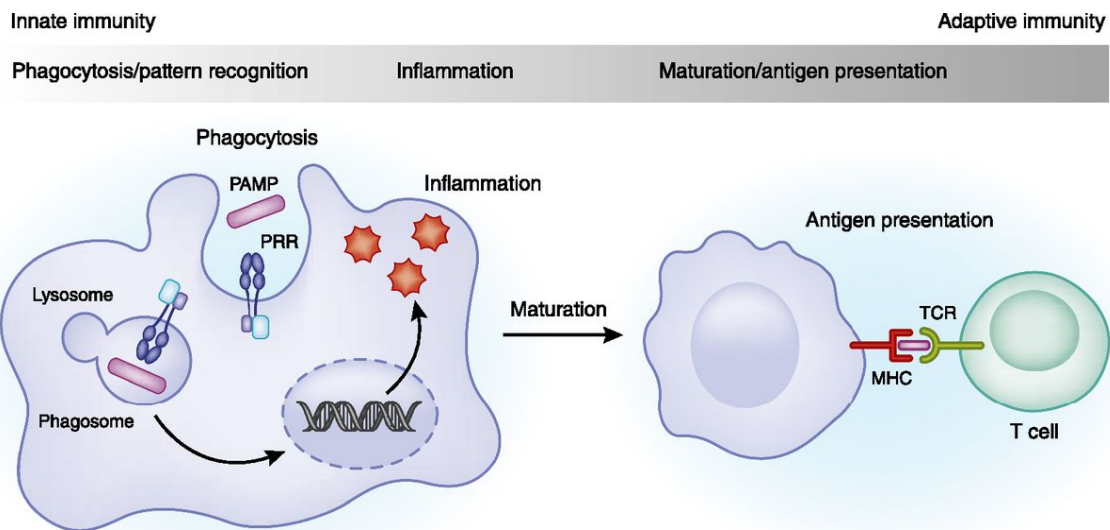


Figure 1.4.4. Innate immune responses to pathogen-associated molecular patterns (PAMPs) and the interplay with adaptive immune cells. Phagocytes can recognise pathogens via PAMPs via their pattern recognition receptors (PRRs), and this causes cytoskeletal re-arrangement and engulfment of the pathogen (phagocytosis). The newly formed phagosome can then fuse with a lysosome to enable degradation of the pathogen. At the same time, signalling cascades (via PRR activation) leads to the expression and secretion of cytokines and chemokines that leads to inflammation. After degradation of the pathogen, fragments of peptides can be loaded into the major histocompatibility complex (MHC) and presented to T cells which, along with secreted cytokines, enables activation and polarisation towards a specific T cell subset upon successful interaction. Taken from [149] and reproduced with permission from the American Society of Nephrology.

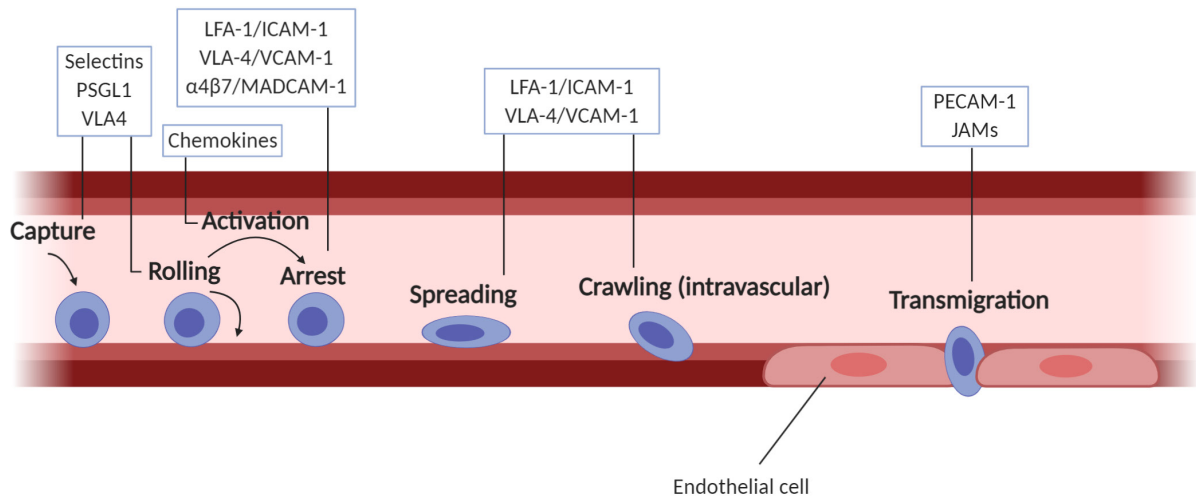


Figure 1.4.5. An overview of the extravasation process. Leukocytes are well-documented to bind and roll alongside the endothelium under physiological circumstances, but when inflammation is occurring locally the presence of chemokines on the endothelium surface activate them and initiate a cascade of events that ultimately leads to their ingress within the tissue. Permission for use of this figure has been sought from the Author. Adapted from [150].

Whilst many phagocytes can present antigen to an experienced T cell (one that has previously been activated), only the mononuclear phagocytes (monocytes, macrophages, and dendritic cells) and B cells have the capability to present antigen to a naïve T cell and induce activation – often leading to their description as professional antigen-presenting cells (APCs) [146, 151]. This means they are critical to initiating adaptive responses. Each of these cell types can be stratified into different subsets with differential responses to stimuli and function. For example, in humans three subsets of monocytes have been identified: classical, intermediate, and non-classical. Classical monocytes are highly phagocytic, intermediate monocytes produce ROS and perform antigen presentation, and non-classical monocytes are considered mobile and often described as “patrolling” monocytes which search for sites of injury [152]. In the mouse, these subsets have also been identified but the markers used for identification are different to those used in humans and do not necessarily align perfectly with the human monocyte subtypes and function [153]. Monocytes also express markers such as C-C motif chemokine receptor 2 (CCR2), C-X₃-C motif chemokine receptor 1 (CX₃CR1), and many other chemokine receptors to varying degrees across the subtypes [154]. They possess the capability to differentiate into both macrophages and dendritic cells (DCs; these are sometimes referred to as myeloid DCs), although DCs and macrophages can be generated via other lineages also [155, 156]. Non-monocyte-derived DCs are stratified into two main subtypes: conventional DCs and plasmacytoid DCs. It is suggested that monocyte-derived DCs are most similar to inflammatory DCs (a rarer and less well-understood subset) [157].

Macrophages comprise the majority of tissue-resident immune cells, in addition to differentiating from monocytes that have ingressed during inflammation; they were originally described as comprising two subsets: M₁ (pro-inflammatory) and M₂ (wound healing). However, it is becoming increasingly recognised that macrophages can possess sub-specialisations depending on the tissue they localise to, and that the M₁/M₂ classification system does not fit all of the inflammatory phenotypes particularly well – with one study highlighting unique profiles of macrophages to many individual stimuli [158-164].

1.4.2 Of Monocytes and Macrophages

As previously mentioned, monocytes are grouped into three main subsets – classical, intermediate, and non-classical – after discovery within humans. Whilst not perfect, broadly similar subsets have also been identified in the mouse. Classical (inflammatory) monocytes predominate in humans, and subsets are typically differentiated based on CD14 and CD16 expression (Figure 1.4.6) [165]. In the mouse, subsets can be differentiated based on markers

including Ly6C, CCR2, and CX₃CR₁, all of which are also differentially-expressed between the human subtypes [166, 167]. Monocytes develop from (common) myeloid precursors located within the bone marrow (Figure 1.4.1), influenced by cytokines such as colony stimulating factor 1 receptor (CSF-1; also known as macrophage colony stimulating factor [M-CSF]). Furthermore, multiple studies have utilised labelling techniques (some in conjunction with transfer of these labelled monocytes) to demonstrate that monocyte subsets retain plasticity, at least in a trajectory from a classical to non-classical phenotype [168-170].

Based on observed expression patterns (both at the gene- and protein-level), the monocyte subsets are believed to possess partial specialisation towards specific innate immune functions [171, 172]; these are summarised in Figure 1.4.6. Furthermore, specific monocyte subsets associate with differentiation preference: classical monocytes associate with macrophage differentiation, non-classical monocytes are argued as capable of macrophage differentiation, and intermediate monocytes are considered biased towards DC trajectories [173-176]. Despite differentiation potential, monocytes also play an important role in responding to both infection and dysregulation within the body and can remain as monocytes during the course of inflammation. For example, monocytes assist in apoptotic cell clearance in addition to degradation/removal of β -amyloid plaques (in the brain) and abnormal connective tissue [177]. Nonetheless, monocyte responses to injury can also exacerbate dysregulation as evidenced through their role in atherosclerosis development (by forming foam cells), tumour progression (acting as myeloid suppressor cells which inhibit T cell responses), and liver fibrosis (by accelerating scar tissue formation) [178].

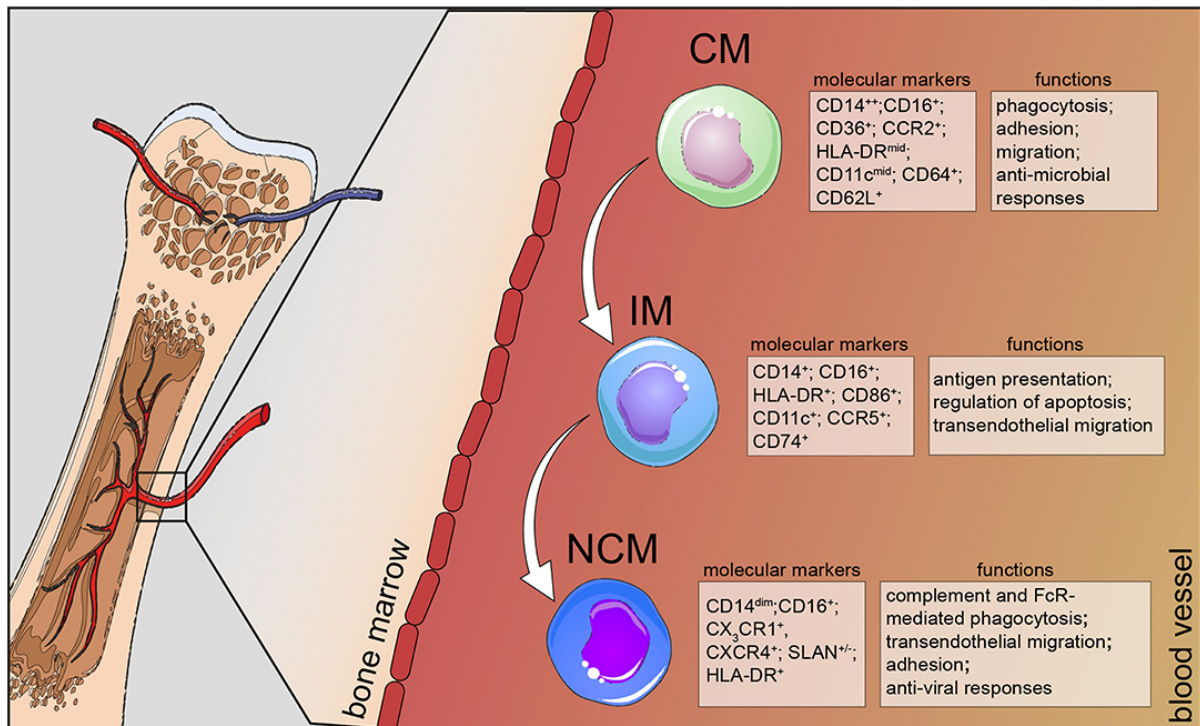


Figure 1.4.6. Monocyte subsets, defining markers, and functions. Three subsets of monocytes emerge from human bone marrow and are typically discriminated based on CD14 and CD16 expression. Classical monocytes (CMs) express proteins associated with phagocytosis and anti-microbial responses, whereas non-classical monocytes (NCMs) associate with directed phagocytosis; intermediate monocytes (IMs) possess functions relating to antigen presentation. Taken from [177] and used under licence (CC BY 4.0).

During inflammation, monocytes can differentiate into macrophages. However, macrophages are also recognised to develop in the bone marrow independently of monocyte-derived origin under the control of the transcription factor PU.1 [179, 180]. Beyond immediate inflammation, many macrophages are found as tissue-resident sentinels and can be found as Kupffer cells (liver), splenic, lymph node, stromal, cardiac, lung, peritoneal, ileal, and colonic macrophages to name a few [122, 123]. Many of these tissue-resident macrophages develop from embryonic progenitors (not monocytes or the bone marrow), are long-lived, and capable of self-replication [181].

Infiltrating macrophages have classically been described as M₁ (pro-inflammatory) or M₂ (wound healing), after these polarisations were discovered *in vitro* [182]. M₁ macrophages canonically express IL-1 β , IL-6, and TNF- α (pro-inflammatory cytokines) whereas M₂ macrophages are associated with expression of IL-10 and arginase [183]. The two phenotypes are summarised in Figure 1.4.7. For these subsets to form, the macrophage requires cytokine signals: priming with IFN- γ and then stimulation with LPS assist in producing an M₁ phenotype whereas M₂ polarisation is considered dependent on IL-4 [184, 185]. Nonetheless, multiple studies have highlighted the problems associated with this simple two-state model (or even considering them polar ends of a spectrum) in that even *in vitro* macrophages receiving different stimuli fit the classification system poorly; some have argued for abandonment of this classification system in favour of a more multidimensional system which is more representative of the highly variable response to stimuli [186, 187]. Others have recommended more standardised nomenclature and reporting of the macrophages and their generation, to better describe them and try to overcome some of these shortfalls [188]. Lastly, 2 new macrophage phenotypes have also been described: regulatory macrophages (also called myeloid-derived suppressor cells [MDSCs]) and “hybrid” macrophages similar to both M₂/wound-healing and regulatory macrophages [187]. MDSCs appear important in immunosuppression within the context of cancer, enabling tumours to develop and progress; they may also play a role in other chronic inflammatory environments [189]. However, these phenotypes have not been widely adopted, nor other classification systems beyond M₁/M₂. Therefore, it is evident that current classification systems leave much to be desired and research is required to develop them into something more reflective of *in vivo* macrophages.

Beyond general phenotypes observed during active inflammation, it is well-recognised that the microenvironment can also influence the macrophage phenotype. For example, tissue-specific factors in addition to the disease-specific microenvironment can play a role in shaping both tissue-resident and infiltrating macrophages (Figure 1.4.8) [190, 191].

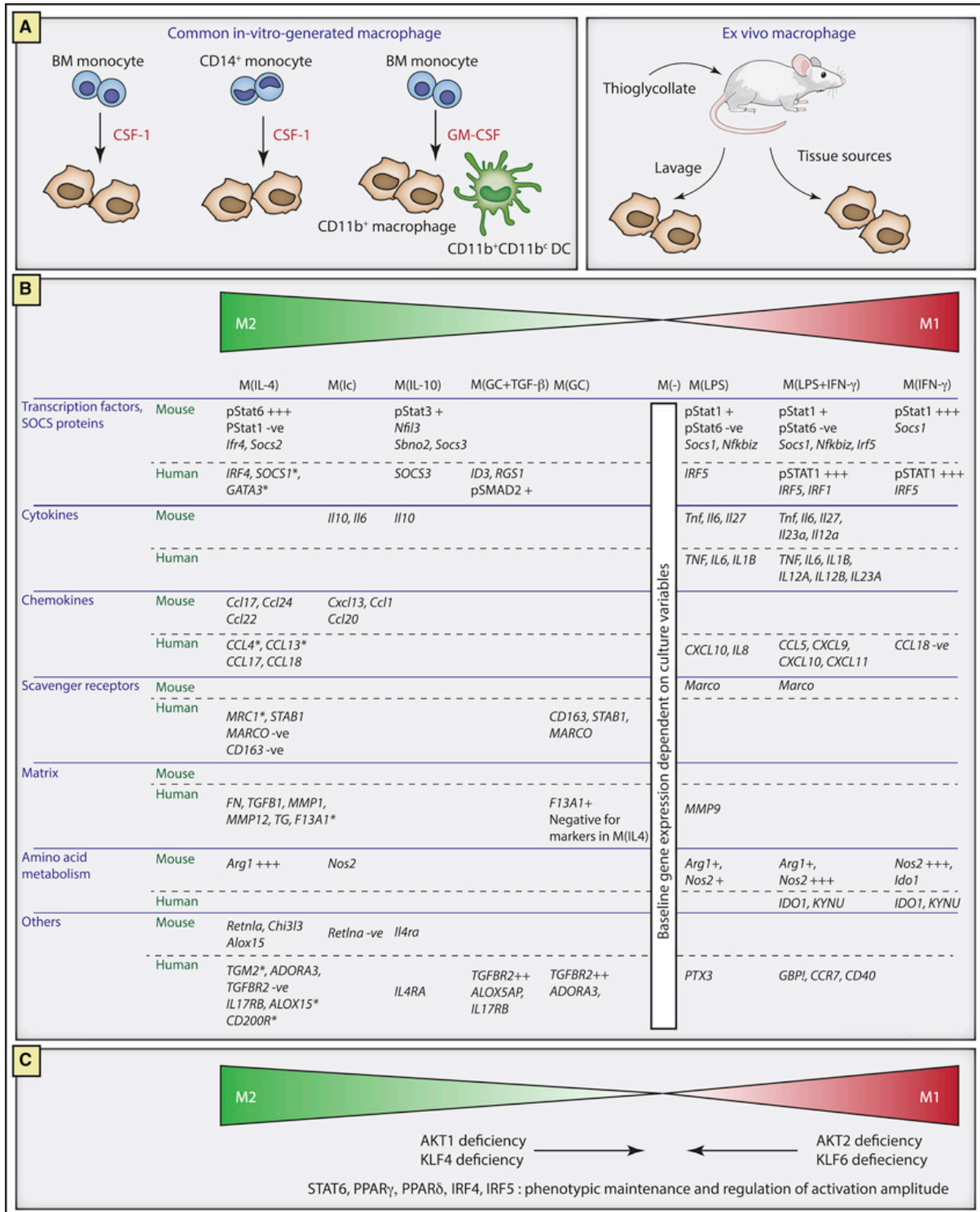


Figure 1.4.7. A proposed framework for describing M₁/M₂ macrophages for better comparability between studies. **A)** There are several methods for generating or isolating macrophages and their subsets, facilitating the need to clearly describe key features such as isolated cells and cytokine/s used in their generation. In the case of ex vivo macrophages, the anatomical location of source in addition to markers/reagents used for their identification would be beneficial. **B)** A variety of different markers (grouped based on general function) are attributed with varying degrees to M₁- or M₂-type macrophages. Taken from [188] and reproduced with permission from Cell Press.

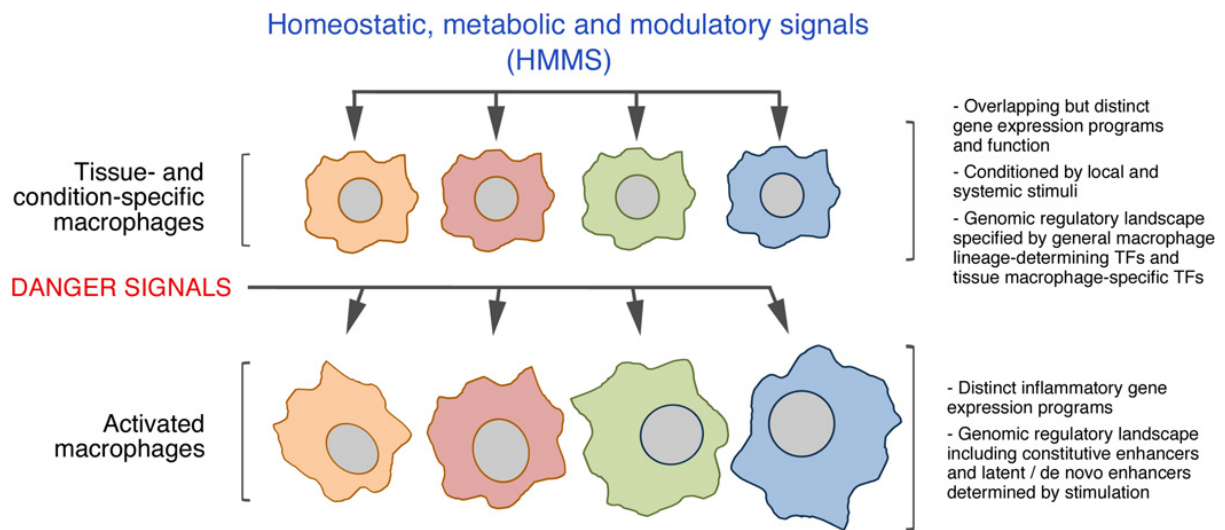


Figure 1.4.8. The effect of homeostatic tissue signals alone and in conjunction with activation of pattern recognition receptors (PRRs). Macrophages located in different tissues will all express typical macrophage genes (including general markers such as *CD45* and *CD11b*) but also genes associated with their local microenvironment (such as *Clec4f*, *Vcam1*, *Itga6*, *Runx3*, and others [192]). When PRRs bind their ligands and transduce pro-inflammatory signals, the combination of this with the homeostatic signals in the microenvironment cause the macrophages to adopt distinctive pro-inflammatory gene expression programmes as opposed to a fixed universal programme. Taken from [190] and reproduced with permission from Springer Nature.

It is well-recognised that tissue-resident macrophages are found in many tissues throughout the body, differentiate from embryonic progenitors (unlike peripheral monocytes and macrophages), and act as sentinels – observing the local environment for danger signals via PRRs and using chemokines and cytokines to recruit and prime peripheral immune cells when required to combat infection and/or tissue dysregulation. Transcriptomic assessment of tissue-resident macrophages can identify genes differentially-expressed based on anatomical location of tissue residency [180]. Nonetheless, core sets of genes expressed by tissue-resident macrophages from different anatomical regions have also been observed [193]. Epigenetic analysis has suggested that the intracellular changes responsible for these observed differences in gene expression are primarily due to alterations in enhancer activity; AT techniques have shown that the vast majority of these epigenetic alterations are shaped by the microenvironment rather than differences during development i.e. it is the context and environment which conditions the macrophage phenotype [192].

The alterations in gene expression allow tissue-resident macrophages to adopt additional functions beyond immune surveillance, enabling contribution towards tissue homeostasis. Additional roles have been observed in many different tissue-resident macrophages and are summarised in Table 1.4.1.

Location	Function	Reference
Bone (via osteoclasts, a myeloid lineage cell)	Regulation of bone remodelling	[194]
Bone marrow	Erythropoiesis and iron recycling	[195, 196]
Brown adipose tissue	Thermogenesis	[197]
Heart	Regulating cardiomyocyte electrical activity	[198]
Lung	Surfactant homeostasis and particle clearance	[199]
Spleen/Liver	Iron recycling	[196, 200]
White adipose tissue	Insulin sensitivity	[201]

Table 1.4.1. Specialised region-specific functions of tissue-resident macrophages. *In addition to immune surveillance throughout the body, many tissue-resident macrophages have adopted additional functions to support homeostasis, controlled by enhancer changes influenced by the microenvironment.*

Beyond providing additional functions in homeostasis, macrophages can be influenced by the microenvironment to generally reduce the propensity for inflammation/activation i.e. immune thresholding. It is believed these immunosuppressive/thresholding functions are important in preserving tissue homeostasis and in minimising inflammation-mediated damage to tissues [202]. For example, tissue resident macrophages have been shown to extend membrane processes around apoptotic cells to inhibit neutrophil activation, and that clearance of apoptotic cells by such resident macrophages does not activate them or promote inflammation [203, 204]. This enables them to manage low-level threats and infrequent occurrences of cell death (in low numbers) within the tissue. It is regulated by the presence of factors within the microenvironment, often derived from other cells in the tissue. For example, in the lung alveolar macrophages are regulated by IL-10, surfactant proteins, CD200R, and transforming growth factor β (TGF- β) [205]. Knock-out of CD200R can lower immune activation thresholds and reduce susceptibility to secondary bacterial infections [206]. However, lack of CD200R during influenza infection leads to greatly increased collateral damage and greatly impaired resolution post-infection [207]. This highlights the importance of localised adaptations and immune thresholding. Within the gastrointestinal tract, macrophages exhibit inflammatory anergy that is orchestrated, at least in part, by TGF- β . Additionally, they possess metabolic adaptations that enable utilisation of locally abundant resources such as glutamine [208, 209]. However, immunosuppression and immune thresholding can extend beyond the tissue-resident macrophages. Kupffer cells (located within the liver) are recognised to express high amounts of membrane-bound TGF- β upon activation, and this can suppress both antigen-specific and antigen-nonspecific CD4⁺ T cell proliferation in the context of inflammation with infiltrating CD4⁺ lymphocytes [210].

1.4.3. Adaptive Immunity

The adaptive immune system is comprised predominantly of two major types of cell: B and T lymphocytes. As with other haematopoietic cells, their progenitors reside within the bone marrow. B cells complete their development here, whereas T cell precursors will migrate to the thymus. Post-development, they enter the bloodstream and circulate through the peripheral lymphoid tissues (lymph nodes, spleen, and other organ-associated lymphoid tissue [e.g. Peyer's patches]) [211]. There are two main types of T lymphocyte: CD4⁺ and CD8⁺ T lymphocytes, which can interact with MHC class II and I respectively. They both recognise targets via their TCR. Canonically, the CD4⁺ T cell is associated with orchestrating clearance of extracellular pathogens whereas CD8⁺ T cells are associated with clearance of intracellular pathogens and

tumour cells. CD4⁺ T cells will typically promote or suppress inflammation by secreting different cytokines required for the infectious context and its resolution. Following productive interaction with an APC, CD4⁺ T cells are polarised into several different T helper (T_h) lineages differing in phenotype and function. They derive from a common precursor but are defined by expression of signature cytokines under the control of a master regulator (transcription factors). Various subsets of CD4⁺ T cell have been identified to include T_{h1}, T_{h2}, T_{h9}, T_{h17}, T_{h22}, T_{fh}, and T_{reg} (Figure 1.4.9) [212, 213]. It should be recognised that T cells exhibit plasticity between these subtypes [214]. CD8⁺ T cells can secrete cytokines but also directly target infected or aberrant cells through the use of perforin and granzymes, as well as induce apoptosis in cells [215]. On the other hand, B cells express a B cell receptor (BCR), can perform phagocytosis, but when activated (via BCR engagement) can differentiate into plasma cells which produce soluble versions of the BCR termed antibodies [216]. Antibodies can have a variety of roles, to include activating complement and enhancing the efficiency/speed of phagocytosis. Both B and T cells possess the capability to generate memory cell subsets, which are long-lived and enable a rapid and more robust immune response upon secondary exposure to the same antigen [217]. Both B cells and T cells possess mechanisms that enable random changes/rearrangement of their receptor during and/or after development to generate novel receptor structures with different affinities; this enables the adaptive immune system to respond to a nearly infinite repertoire of molecules that it may encounter, and ensures that pathogens with novel antigens could still be targeted by the immune system [218].

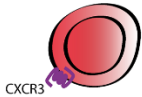
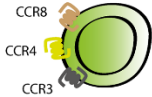

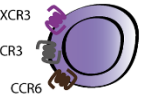
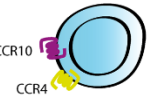


	Th1	Th2	Th17	Th9	Th22	iTreg	Tfh
							
Major cytokines driving differentiation	IL-12	IL-4	TGFβ IL-6	TGFβ IL-4	IL-6 TNFα IL-1β??	TGFβ IL-2	IL-21 IL-6??
Master transcriptional regulator	T-Bet	GATA-3	RORγt	PU.1	AhR?	FoxP3	Bcl-6
Major cytokines produced	IFNγ	IL-4	IL-17	IL-9	IL-22	IL-10 TGFβ	IL-21
Major function	Intracellular infections	Extracellular Infections	Extracellular Infections	Extracellular Infections	Extracellular Infections	Regulation	Extracellular Infections
Major site of effector function	Peripheral tissues	Peripheral tissues	Peripheral tissues	Peripheral tissues	Peripheral tissues	Peripheral tissues & secondary lymphoid organs	Secondary lymphoid organs
Chemokine receptors	CXCR3	CCR3, CCR4 CCR8	CCR2, CCR6, CCR4	CCR3, CCR6, CXCR3	CCR4, CCR10	CCR6	CXCR5
Chemokine ligands	CXCL9 CXCL10 CXCL11	CCL1 CCL11 CCL13 CCL17	CCL2 CCL20 CCL17	CCL11, CCL13, CCL20, CXCL9, CXCL10, CXCL11	CCL17 CCL28	CCL20	CXCL13

Figure 1.4.9. Currently known Th cell subsets. Summary information about their differentiation, function, and expression of key markers highlights differences between them and their differentiation. Taken from [213] and used under licence (CC BY 4.0).

1.4.4 Immunological Challenges

One challenge that makes the immune system different to many other bodily systems is that it is evolving under the influence of multiple directional pressures that can often be at odds with one another. Evolving to become better at killing pathogens risks greater collateral damage to self. Furthermore, hijack of built-in inhibitory mechanisms to protect the host from collateral damage can enable pathogens to survive [219]. This delicate balance of killing and suppression is highlighted by numerous reports identifying the side effects of autoimmunity or other immune-related adverse events caused by immunotherapies aimed at enhancing an anti-tumour response using mechanisms such as checkpoint inhibition, cytokine administration or adoptive immunotherapy – many of which were targeted to a single molecule [220-222]. Therefore, a balanced response is required to both control infection and maintain homeostasis, and inappropriate responses (both mistargeting and excessive reaction) results in damage to self.

Furthermore, the interaction between pathogens, commensals (i.e. the microbiome), and host and their evolution is highlighted in many examples: the complex nature of the immune system, with a wide variety of cell types and subtypes, complex pathogens that utilise a multitude of immune evasion mechanisms and frequent antigenic variation (e.g. CMV and influenza), and the presence of retrovirus DNA, transposons, and other elements in the genomes of many organisms [223-227]. This highlights the requirement for multiple compensatory mechanisms of activation, to cope with the wide diversity of pathogens, and the need for inherent flexibility (i.e. generation of an almost infinite TCR/BCR repertoire via the processes of combinatorial and junctional diversification, and somatic hypermutation [228]) to ensure adequate responses can be generated against novel antigens. However, inherent flexibility in antigenic recognition generates a new problem: how does the immune system cope with randomly generated receptors that recognise self?

1.4.5 Tolerance

As summarised above, it is inevitable that self-reactive lymphocytes will form in an organism during its lifetime. Therefore, the body requires mechanisms to ultimately prevent damage caused by these self-reactive lymphocytes; these are collectively termed tolerance. The first mechanism, which removes these autoreactive cells, is described as central tolerance and occurs during cell development and maturation into a naïve state (in the bone marrow and thymus [for B and T lymphocytes respectively]). In B cells, they can undergo apoptosis, anergy (a state of

permanent unresponsiveness to their antigen) or further receptor editing to see if autoreactivity can be ablated; where central tolerance fails immunologically ignorant B cells (which are autoreactive) can be generated [229, 230]. In the case of T cells, selection is a little more complex because the TCR must be able to interact with MHC molecules (either MHC-I or MHC-II) so that the TCR could activate when a foreign peptide is presented, termed positive selection. However, if the interaction is too strong (i.e. high avidity) then these cells undergo apoptosis or become regulatory T cells (T_{reg}). This is because they will react to either MHC complexes loaded with self-peptide or unloaded MHC complexes [231]. There is debate in the field about whether T cells can undergo receptor editing if they are responsive to self-antigens [232, 233]. It is however evident that a single transcription factor, AIRE (autoimmune regulator), is critical in central tolerance and enabling expression and presentation of a wide variety of tissue-restricted self-peptides in medullary thymic epithelial cells (mTECs) during lymphocyte development; its knock-out results in spontaneous autoimmunity in mice (in humans, mutation of the AIRE gene leads to autoimmune polyendocrinopathy-candidiasis-ectodermal dystrophy). However, the symptoms and autoreactive cells generated are not invariable and highlights the stochastic nature of autoimmune disease [234]. It suggests any peptide not expressed, expressed in low quantities (i.e. cryptic self-epitopes), or spliced (or other amino acid side-chain modifications) so those epitopes are not present, by the mTECs could result in escape of autoreactive T cells from central tolerance mechanisms [235, 236]. Furthermore, low-avidity autoreactive T cells have been shown to routinely escape negative selection [237]. Some of this could be attributed, in part, to the high level of cross-reactivity of the TCR (recognition of up to 10^6 different peptides) [238], although there is evidence of TCR sensitivity tuning to nullify the effect of a peptide with weak binding affinity in the periphery which would (at least partially) overcome this, at least in naïve contexts [239].

Beyond lymphocyte development, multiple other mechanisms of tolerance are also observed, collectively termed peripheral tolerance because it occurs post-development (i.e. in the periphery with respect to their site of development). For example, T and B cells require signalling to be able to activate – from cytokines such as IL-1 β , IL-6, and IL-12 to co-stimulatory molecules such as CD80/86 and CD40/C3b (for T and B cells respectively) – and in the absence of these they can undergo activation-induced death, become anergic, or differentiate into a T_{reg} cell [240-246]. For expression of pro-inflammatory cytokines and co-stimulatory molecules, activation of PRRs that recognise PAMPs or DAMPs (by innate immune cells) is required.

Other tissue-specific immunoregulatory mechanisms are also present. For example, certain regions of the body (e.g. the eye and brain) are relatively inaccessible to lymphocytes under

normal circumstances and it would not be possible for them to therefore engage their respective receptors (TCR/BCR) and induce autoimmunity – these sites are termed immunologically privileged, and in these regions tissue grafts or transplants can survive for extended lengths of time [247]. Likewise, some local environments (i.e. the microenvironment) will include factors that can help to prevent inflammation by functional deviation. In the retina and brain, TGF- β is one such factor that performs this role [248]. Additionally, tissue-resident immune cells (such as the microglia) also play a role in modulating responses and promoting an anti-inflammatory state, at least in naïve circumstances (see the microglial section of this chapter).

T_{reg} cells have the potential to suppress effector cells targeting the same cell or tissue (i.e. spatially-proximal to one another irrespective of antigen specificity) through cytokines such as IL-10, IL-35, and TGF- β , by inducing expression of ligands for co-inhibitory signals on antigen-presenting cells (e.g. cytotoxic T-lymphocyte-associated protein 4 [CTLA-4]), but also through other routes such as killing of effector cells with granzymes, metabolic interruption via hydrolysis of adenosine triphosphate (ATP) to adenosine to signal via adenosine 2A receptor, and a plausible but controversial mechanism of competing with effector T cells for IL-2 [249-251].

1.4.6 Autoimmunity and Autoinflammation

When tolerance mechanisms fail, it creates an environment that is permissive for autoimmunity (such as evasion of central tolerance and survival of autoreactive cells). Likewise, a failure of tolerance at a checkpoint could directly lead to autoimmunity (failure to correctly abrogate an autoreactive lymphocyte peripherally).

Autoimmunity is a state in which discrimination between self and non-self fails (i.e. tolerance mechanisms) and the immune system reacts against healthy cells or tissues. It is well-recognised that autoimmunity is stochastic both in humans and some animal models – it is not a guaranteed event even with a permissive environment or genetic predisposition. For example, people who possess the human leukocyte antigen-B27 (HLA-B27) allele have a 26-fold increased relative risk of uveitis, but nonetheless it is not inevitable [252]. Therefore, other environmental factors are at play for enabling autoimmunity in a permissive environment. For example, it is common for someone diagnosed with autoimmune disease to have a history of recent illness. With inflammation comes an increased density of all peptide-MHC complexes, co-stimulation which alters the functional TCR responses, and changes in the proteasome that could result in generation of novel peptide fragments for presentation [239, 253]. Changes in tissue-resident

immune cells can also occur, even if they are distal to the infection or site of injury [254]. Nonetheless, once established many autoimmune disorders undergo a relapsing-remitting pattern, suggesting phases of activation and subsequent immune regulation [255].

It was originally believed that TLRs were completely specific for PAMPs and were an ideal way of discriminating self from non-self. However, new evidence indicates it is possible for DNA fragments from apoptotic cells to activate TLRs [124] and suggests a possible role for this in autoimmunity – specifically systemic lupus erythematosus [256, 257]. The C-type lectin CLEC2D can also recognise histones released from necrotic cells and stimulate TLR9 [258]. Similarly, when one eye sustains injury it is possible for inflammation to occur in the contralateral eye – a condition termed sympathetic ophthalmia. In very rare circumstances (considering currently available treatments) the injured eye can be enucleated to prevent damage in the contralateral. This highlights how local processes such as cell death and release of DAMPs could enable the activation of autoreactive lymphocytes and differentiation into effector/memory phenotypes to drive disease in the contralateral eye [259]. Sympathetic ophthalmia can occur at least as late as 66 years post-injury, highlighting the stochastic nature of autoimmunity and how multiple environmental factors – in addition to autoreactive cells – are required for its development [260]. Presumably in this case occurring 66 years post-injury, the initial injury generated memory cells which did not re-encounter the antigen (an unknown retinal antigen) until decades later due to anatomical sequestering. For sympathetic ophthalmia to develop, perhaps both co-stimulation and entry of an autoreactive T cell (or several) into the contralateral eye is required to induce inflammation – in addition to a failure of other tolerance mechanisms simultaneously (which itself becomes easier to overcome once memory cells are generated).

It is plausible that the presence of a pathogenic organism can lead to co-stimulation of both pathogen-specific and autoreactive lymphocytes due to its non-specific nature [261]. The presence of systemic infection can activate lymphocytes which have better access through barriers (such as the BRB) enabling temporary lymphocyte access where it was unavailable previously [262]. This could also explain why many people diagnosed with autoimmune illness have a recent history of illness. However, activation of an autoreactive cell in this context depends on a vital assumption: that the antigen encountered peripherally had a sequence/structural similarity to a self-antigen (termed molecular mimicry or cross-reactivity) that would enable the T cell to be autoreactive in the first place, or that an activated antigen-presenting cell presented a retinal-specific self-antigen (presumably in addition to pathogen antigens) and interacted with a lymphocyte in the periphery [263]. In the case of HLA-B27 associated autoimmunity (ankylosing spondylitis), it has been shown that several bacterial

antigens exhibit molecular mimicry to a portion of HLA-B27 and that HLA-B27 itself can be presented – explaining why possessing a HLA-B27 allele does not guarantee development of autoimmunity but with certain environmental factors can lead to it [264].

Additionally, it is plausible that autoimmunity can be triggered by other events. For example, it is possible that infection locally and self-antigens being presented can trigger autoreactive lymphocytes – a phenomenon termed bystander activation [265]. In the case of more persistent inflammation, it is possible that T cells specific for other self-proteins can become activated as the tissue is damaged, releasing more antigen; this is termed epitope spreading [266]. A last mechanism includes persistent infection and activation of B cells, leading to immune complex formation from the various antibodies generated – as observed with hepatitis C virus infection and cryoglobulinemia [267]. The relationship between infection and autoimmunity was summarised in 10 points by Kivity *et al.* [265] listed below:

1. “Infections can cause autoimmune diseases.
2. Different infectious agents (viruses, bacteria, fungus and parasites) can trigger autoimmunity.
3. An infection can trigger an individual with an underlying immune dysregulation to express an overt autoimmune disease.
4. Infectious agents can determine the presence of disease-specific auto-antibodies and clinical manifestations.
5. In many cases, it is not a single infection, but rather the ‘burden of infections’ during life that is responsible for induction of autoimmunity.
6. Infections during childhood can be implicated in the development of autoimmune diseases in adulthood.
7. Infections can protect individuals from some autoimmune diseases.
8. The same infectious agent can induce one specific autoimmune disease and protect from another autoimmune disease.
9. Molecular mimicry, epitope spreading, bystander activation and polyclonal activation can induce autoimmunity after infections via innate and adaptive immune responses.
10. Genetic susceptibility might explain why only a subgroup of individuals will develop autoimmunity after infections.”

In relation to point 10, genetic susceptibility refers to MHC haplotype, but also any other immune regulators (such as the inflammasome) – whether they be costimulatory, inhibitory

receptors, or have other involvement [255]. Current genetic studies implicate small independent effects on susceptibility of several hundred different genetic loci [268].

Autoinflammation refers to a group of disorders where, much like autoimmunity, the immune system is dysregulated. In contrast to autoimmunity (where primarily the adaptive immune system causes damage), autoinflammation refers to diseases (e.g. Behçets or Crohn's disease, or Blau's syndrome) where primarily the innate immune system responds in the absence of an infection and causes injury [269]. However, as both the innate and adaptive immune systems interact, and it is possible for dysregulation of both simultaneously (not necessarily to the same degree) this means that autoimmune-autoinflammatory disorders are generally considered a spectrum with frequent overlap as opposed to two discrete entities [14, 15]. IL-1 β is emerging as a good therapeutic target for some autoinflammatory disorders due to its pivotal role in inflammation caused by myeloid cells [270]. However, new pathways and genes associated with autoinflammatory disorders – such as the stimulator of interferon genes (STING) pathway and deficiency of adenosine deaminase 2 (*Ada2*) – highlight other ways in which autoinflammation can manifest [271].

Whilst autoimmune-autoinflammatory diseases in isolation are generally relatively rare, overall they have a prevalence of around 1 in 20 (5%) and it is becoming increasingly recognised that they have common underlying mechanisms of disease, highlighting the significant burden they represent to society as a whole [272].

1.4.7 Innate Immune Memory, Adaptation, and Para-Inflammation

Innate immune memory describes “a change in the reactivity in innate immune cells previously exposed to various stimuli” [273]. It is generally considered a short-term phenomenon and has also been described “trained immunity”. However, long-lived memory phenotypes of innate immune cells, with a common memory transcriptional/epigenetic programme to lymphocyte memory cells, have also been described [119]. It is proposed, therefore, that immunological memory phenotypes emerged in ancient innate immunity and was inherited when adaptive immunity evolved [274]. Irrespective of origin, various terms have been used to describe innate immune memory and its surrounding phenomena with the potential to cause confusion. Therefore, standardised terminology have been proposed in an effort to minimise this (Table 1.4.2) [273].

Phenomenon	Old Terms	Proposed Terms
Innate immune memory	Innate memory	Innate immune memory Trained innate immunity
Induction of innate memory	Priming Innate immune reprogramming Pre-conditioning	Priming Innate immune reprogramming
Memory-induced decreased responsiveness	Tolerance	Tolerance, trained tolerance (global phenomenon) Contraction, decrease (individual effectors)
Memory-induced enhanced responsiveness	Trained immunity Non-specific acquired resistance	Potentialiation, trained potentialiation (global phenomenon) Enhancement, increase (individual effectors)

Table 1.4.2. Innate immune memory terminology. It describes different phenomena and terms previously used to describe them, as well as suggested new terminology to minimise confusion. Taken from [273].

Innate immune memory has been known about for a long time in the form of priming or tolerisation (primarily with regards to LPS) [275-277], but the mechanisms underpinning it (epigenetic modifications) have only been recently discovered [278-280]. LPS tolerance has been well-studied and reviewed in great detail recently [279].

In the context of peripheral immune cells (with the exception of the possible but rare memory phenotype/subsets), these effects would be short-lived (in the absence of chronic inflammation) as these cells are replaced as part of haematopoietic turnover [281]. Alterations of the progenitor stem cells located within the bone marrow are possible [282]. Furthermore, innate immune memory has the potential for long-lasting or semi-permanent effects on long-lived innate cells such as tissue-resident macrophages or where peripheral immune cells are kept alive by inflammation-associated signals.

Immune adaptation (or differentiation) is considered “a form of adaptation through long-term changes in the functional program of a system (including immune response), determined by a constant change in the environmental conditions or due to a chronic insult (e.g., a chronic infection), leading to a new functional state” [274]. It differs from conventional innate immune memory in that the new functional state is not transient but persists until it is set to a different level. The similarities and differences between the two forms of memory are shown in Figure 1.4.10.

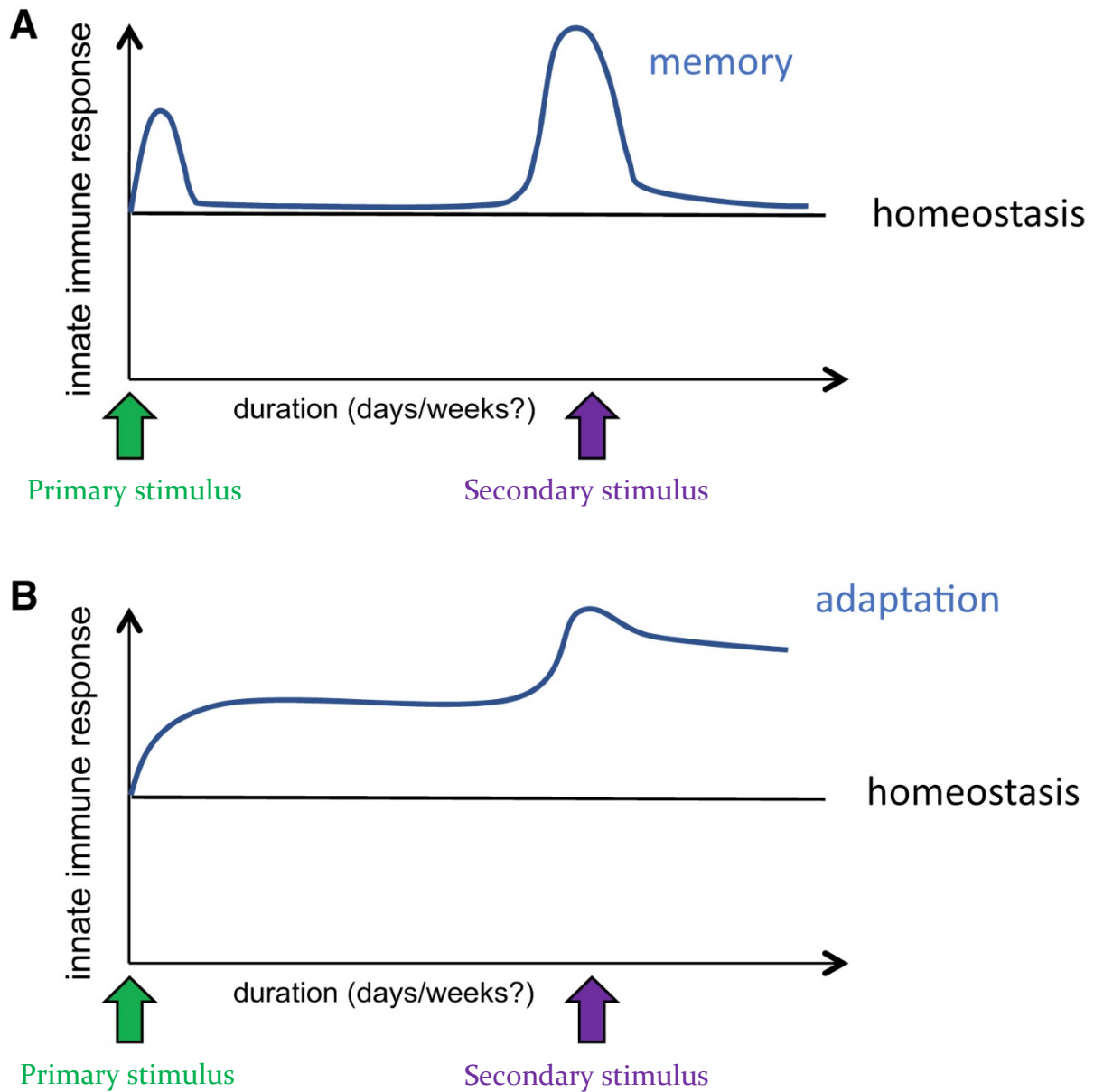


Figure 1.4.10. Immune memory and immune adaptation. **A)** Immune memory describes where the response intensity to a stimulus is altered due to previous stimuli (this can be increased or decreased i.e. priming and tolerance, respectively). The innate immune cells return to a state of homeostasis between stimulation. **B)** Immune adaptation describes a long-term change in the innate immune response which can be altered again in the future. Importantly, the innate immune response does not return to baseline between stimulation. Adapted from [274] with permission from Cell Press.

Currently, most studies investigating innate immune memory have done so *in vitro* or systemically *in vivo*. A small number have identified differential memory responses depending on compartmentalisation [283, 284]. However, it is suggested that innate immune memory could play an important role in chronic diseases (such as atherosclerosis) in addition to autoinflammation/autoimmunity [280, 285].

Para-inflammation is a different phenomenon that is considered a range of inflammation between a full-blown infection response and complete homeostasis; it is believed to be an adaptive response to tissue injury or malfunction [286]. It differs from immune adaptation in that there is continual low-level inflammation occurring in para-inflammation, whereas in immune adaptation only the response to a stimulus is altered. Nonetheless, para-inflammation has been shown as an important process that helps to drive the formation of a wide range of tumours, whilst in the eye can develop into a more chronic inflammation that causes age-related macular degeneration (AMD) [286, 287]. In the eye, this could be triggered by necrotic cell death, ROS (which are generated as part of physiological cell processes), advanced glycation end products, and hyaluronan fragments to name a few [288, 289]. Many age-dependent/para-inflammatory changes have been observed in the eye, such as increases in IL-1 β and TNF- α (pro-inflammatory cytokine) concentrations, breakdown of the BRB, increased complement activation, as well as changes in regulatory cell localisation and morphology [289-291].

It is possible that the “burden of infection” (believed important in autoimmune disease [265]) and/or ongoing changes with age could increase the para-inflammatory state and potential for progression to full-blown autoimmunity or autoinflammation (as barrier integrity is compromised and the microenvironment becomes more pro-inflammatory), increasing the probabilities of leukocyte entry and costimulation of a self-reactive T cell. Furthermore, innate immune memory/adaptation, para-inflammation, and autoimmunity/autoinflammation could represent part of a spectrum of accruing changes/dysfunction to the tissue-resident immune cells and microenvironment (Figure 1.4.11). Whilst this is conceptualised as a spectrum, it should be appreciated that a para-inflammatory state is not necessarily a pre-requisite for autoinflammation or autoimmunity nor is it a guaranteed progression. It is intended to suggest how different severities/degrees of immune dysregulation from homeostasis may link to one another.

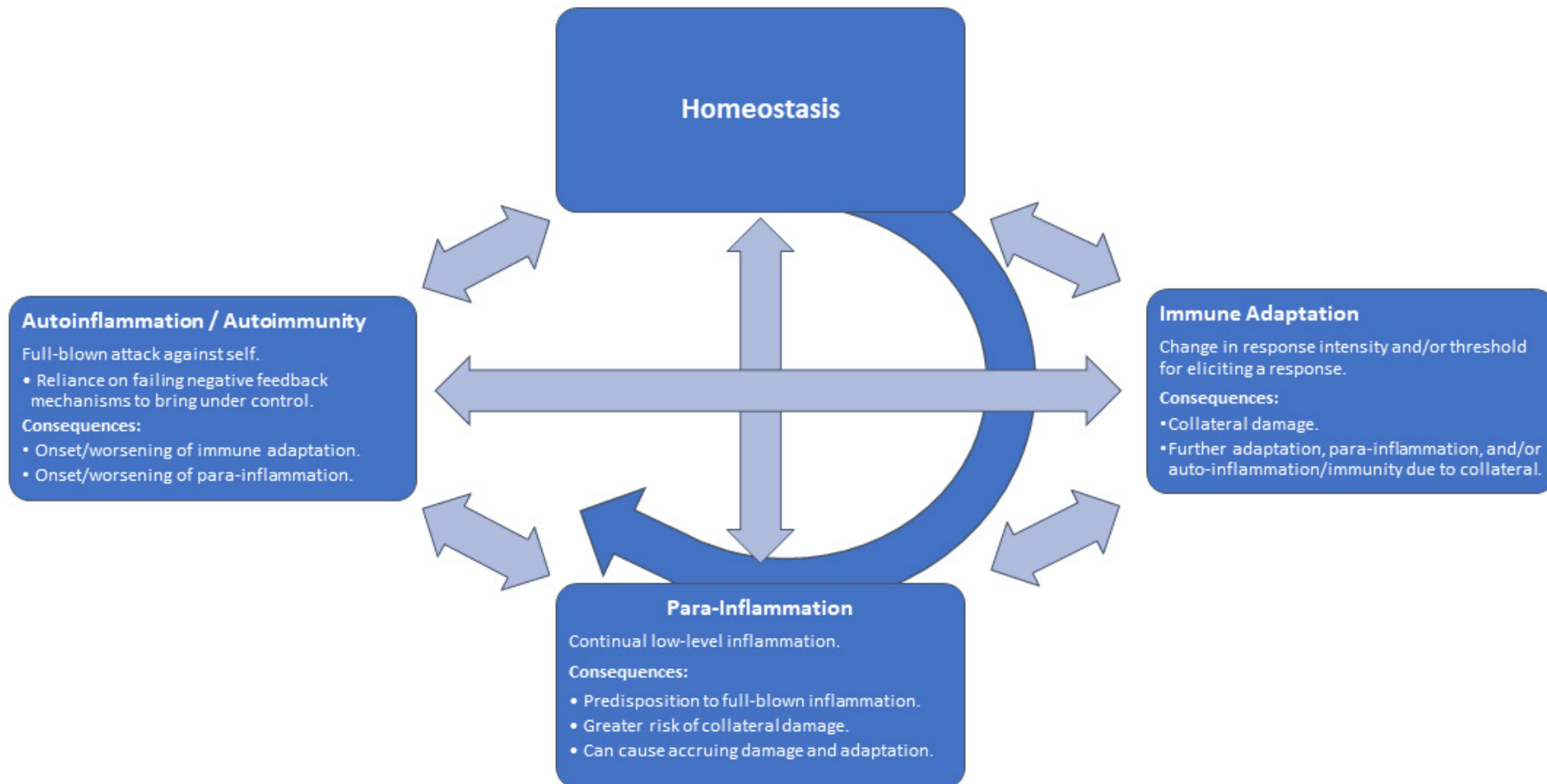


Figure 1.4.11. Immune adaptation, para-inflammation, and autoinflammation/autoimmunity may represent a spectrum of immune dysregulation and tissue dysfunction. Repeated challenges over time can lead to adaptation, predisposing to collateral damage and further adaptation, para-inflammation, and/or autoimmunity. It is possible that steps may be omitted due to other (stochastic) factors such as infection (leading to breakdown of anatomical barriers and expression of co-stimulatory molecules) and genetic risk. Equally, it could be possible for the tissue to regress or return to a homeostatic state.

1.4.8 The Eye and Immune Regulation

Despite multiple tolerance mechanisms to promote safe activation of the immune system (outlined above), the eye contains many unique features which further aid in shaping the immune system and pushing towards regulation – a phenomenon broadly described as immune privilege. For example, it is well-recognised that tissue grafts in the eye can survive for extended periods of time (rejection would occur at other sites) [247]. Furthermore, after a successful graft on the cornea it is possible to administer similar cells/tissues elsewhere in the body without rejection/reaction [292]. Antigens administered to the corneal surface can be tracked to draining lymph nodes and alloreactive T cells specific for these antigens can be detected systemically [293]. Yet, despite the presence of these alloreactive T cells immune responses are not generated. This atypical response (or deviation) has been termed anterior chamber-associated immune deviation (ACAID) [294]. In other studies, xenografts of human uveal melanoma cells form considerably more hepatic micrometastases when administered via the posterior compartment of the eye as opposed to tail vein injection, providing further evidence that eye-specific systemic immune deviation mechanisms exist [295]. It is unclear whether ACAID itself is a physiological phenomenon or purely artificial. However, it highlights that immune-regulating mechanisms are present within the eye.

As described earlier, the eye contains anatomical barriers (i.e. the BRB) which considerably limits the entry of leukocytes and the potential for local immune activation/reactivity. It is likely that considerable local damage and/or microglial activation is required for the breakdown of these barriers to occur to permit large-scale immune infiltration (see 1.5.2 and 1.5.4) and possible collateral damage. However, it is also hypothesised that relative inaccessibility (to leukocytes) limits the effectiveness of peripheral tolerance within the eye (i.e. allows B and T lymphocytes to remain immunologically ignorant) and therefore, ironically, this second defence mechanism could also hypothetically permit autoimmunity within the eye [296] (in conjunction with other circumstances such as local damage/danger context, genetic predisposition, or others as described earlier).

The third main pillar of immune privilege within the eye is the microenvironment, containing a variety of secreted molecules (e.g. TGF- β or TRAIL, the latter promoting apoptosis), expressed receptors (e.g. CX₃CL₁ by neurons), highly-specialised tissue-resident immune cells (i.e. microglia, see later) or other cells capable of immune regulation (e.g. the RPE), constitutive expression of complement inhibitors, and the extracellular matrix – all of which help shape both

tissue-resident and infiltrating immune responses towards regulation or anergy [297-304] (see [305] for a recent review of retinal immune suppression).

In summary, the eye has multiple additional mechanisms that help to promote anergy or a regulatory environment to avoid excessive inflammation and collateral damage – presumably because of both the delicate nature of the eye and the critical role it plays in survival.

1.5 Microglia

Microglia are long-lived tissue-resident macrophage-like cells of the CNS, including the eye. They reside within the retina in addition to many regions of the brain each with varying densities and marker expression, presumably to assist in additional sub-function specialisations [306]. Nonetheless, all microglia express conventional myeloid cell markers. However, despite expression of myeloid markers they have a different origin (they are derived from the embryonic yolk-sac as opposed to haematopoietic progenitors) to other myeloid cells [307]. They exhibit a ramified morphology (unlike the amoeboid morphologies of macrophages) and are well-recognised to express a unique TGF- β -dependent transcriptional profile different to macrophages [308]. Microglia can self-replicate when required but under physiological conditions this is to a low degree. They are incredibly versatile, known to provide immune surveillance of the brain and eye (via movement of the ramified processes [309]), as well as general homeostasis via processes such as synaptic pruning – with dysregulation of the latter linking to schizophrenia [115, 310]. Many microglial functions are summarised in Figure 1.5.1, highlighting a plethora of sub-specialisations beyond immunosurveillance that explains how they differ from macrophages. Furthermore, complement-dependent synapse elimination by microglia is required for the loss of memories, with complement knock-out resulting in reduced cognitive decline in mice [311]. It is well-recognised that microglia, under homeostatic conditions, contribute to an immunosuppressive environment that helps to prevent unnecessary inflammation and/or autoimmune disease [312].

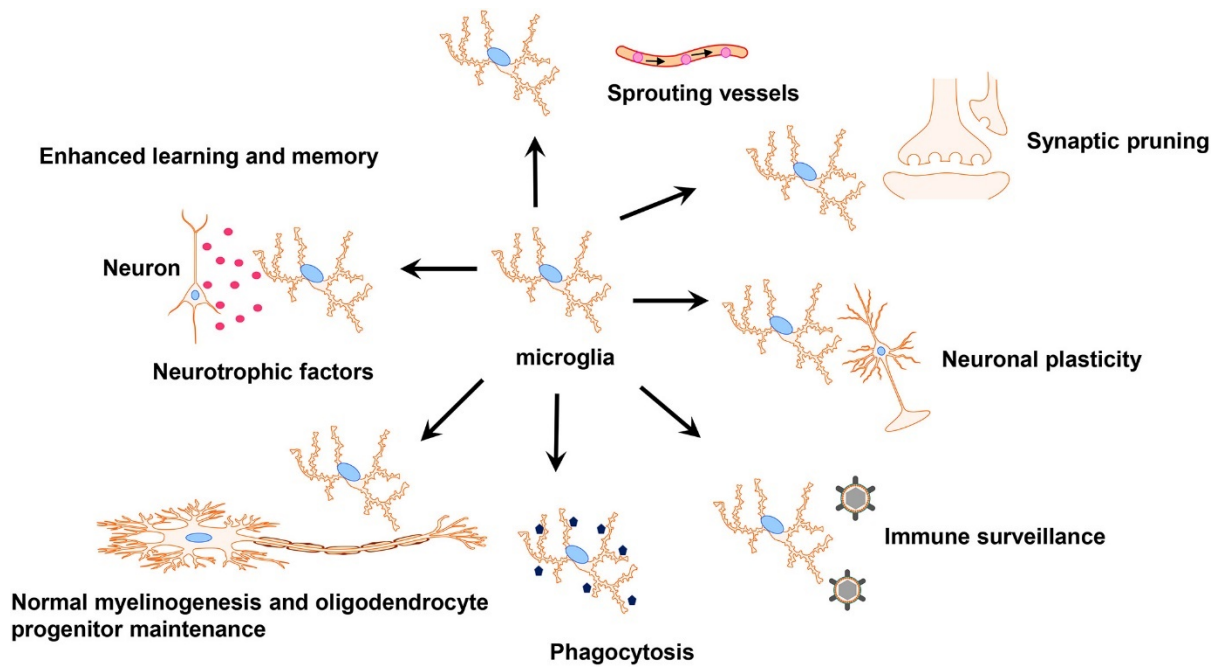


Figure 1.5.1. Microglia possess a variety of important roles relating to both immune surveillance/protection and maintenance of tissue homeostasis. Microglia play an important role in regulating the CNS as highlighted by their repertoire of functions. Overall, they are critical to maintenance of the CNS. Abbreviation: CNS – central nervous system. Taken from [313] and used under licence (CC BY-NC 4.0).

Microglia have been identified in a variety of vertebrates and invertebrates, including mammals, birds, frogs, fish, molluscs, and insects [314-320]. This suggests the existence of microglia predates the Nephrozoan divergence of organisms (into Protostomia and Deuterostomia – that gave rise to molluscs and insects, and chordates respectively) that dates ~600–700 million years ago [321, 322]. Microglia have not been observed in organisms that predate the Nephrozoa (i.e. in Xenacoelomorpha, a clade forming alongside the Nephrozoa from the common ancestral clade of Bilateria), implying their origin in Nephrozoa [323]. Furthermore, neuropeptides (NPs), which are well-characterised to modulate microglial activity [324-327], saw a major expansion in Bilaterians [328]. These events are summarised in Figure 1.5.2. and predate the development of complex nervous system architectures, implying microglia are a critical component or prerequisite for their development and maintenance, and that by extension microglial regulation is critical to homeostasis of the brain but also eye.

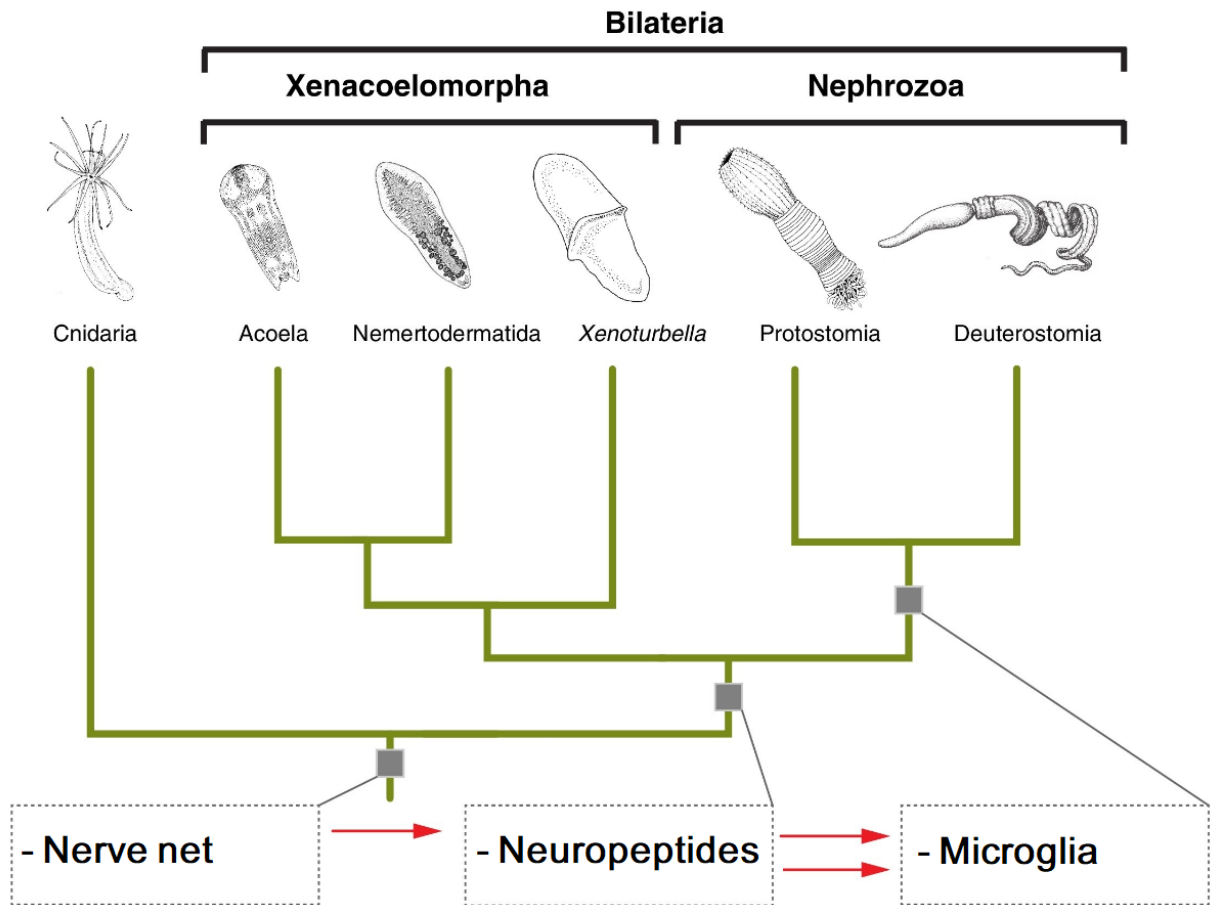


Figure 1.5.2. Phylogenetic relationships and the sequence of evolution predating complex nervous system architectures. Significant developments are highlighted in the boxes below, with an indication of which branch it formed within. Adapted from [329] and used under licence (CC BY 4.0).

Microglia development in mammals occurs in three distinct stages: “early microglia” (until E14), “pre-microglia” (E14 to a few weeks after birth), and “adult microglia” (from weeks after birth henceforth) corresponding broadly to cell cycle, synapse pruning, and immune surveillance functions respectively [330]. During their development, perturbation of microglia can lead to severe consequences. For example, administration of Poly(I:C) (a TLR3 agonist [331]) causes psychopathology when administered during critical gestational time-windows [332]. Furthermore, depletion or alterations in the microbiome can also influence microglia – whether induced by acute changes caused by antibiotics or long-term changes caused through the use of germ-free mice [333, 334]. Additional studies highlight that microglial depletion during development or early post-natal stages can lead to defects in both mouse behaviour and brain physiology [335], cementing some of their critical roles beyond immune surveillance within the central nervous system (CNS).

In adult microglia a core gene expression programme – including *Sall1*, *Mertk*, purinergic receptor P2Y₁₂ (*P2ry12*), and triggering receptor expressed on myeloid cells 2 (*Trem2*) – was observed across species spanning roughly 450 million years of evolution (from leeches to humans, and 16 species between). Additional expression programmes exclusive to large mammals and humans were also identified. It highlighted both similarities but divergences in microglial function in these organisms, and provided implications in the origin of particular neurodegenerative diseases (specific to large mammals and/or humans) and their links to microglia [336].

1.5.1 Microglial Phenotypes

Classically, microglia were considered to possess similar phenotypes and expression patterns to macrophages due to expression of common myeloid markers during a naïve state. However, recent evidence indicates that microglia have distinctive expression patterns and phenotypes that poorly fit “classic” phenotypes of macrophages (i.e. M₁ and M₂ [158]). An investigation to determine differences in adult microglial expression patterns showed that microglia isolated from the eye were distinctive to microglia isolated from other regions of the CNS, but also that microglia isolated from defined anatomical brain regions have subtle differences suggesting localised functional adaptation [308]. Furthermore, sex differences have been observed in brain microglia and their reactivity; sex differences in microglia are believed important in neurological disorders, many of which have a sex bias in incidence [337, 338].

Microglia can be classified generally as primed or acute: an acute microglia is responding to acute injury (such as infection), whereas in contrast a primed microglia is one which exhibits a greater and more prolonged response to challenge (i.e. immune adaptation) – the latter being observed in ageing and neurodegeneration [158, 339]. A core of primed microglial genes was identified, where overlap/consensus between several different models was observed. Nonetheless, model-specific changes were also noted [158]. Furthermore, accumulating evidence suggests the presence of damage- or recovery-associated microglia (DAM or RAM, respectively) in addition to possible transitional phenotypes and quiescent microglia during disease [340-343]. Formal classification and identification of these phenotypes (e.g. specific marker changes) remains to be investigated, although these subpopulations are already being associated to core sets of gene expression changes [344]. Nonetheless, recent efforts have resulted in the development of a 33-module classification system of microglial expression patterns. It was developed using microglial responses to 96 different single stimuli *in vitro* and shows promise in both characterisation and comparability with enough dimensions to resolve multiple hypothetical microglial states [345].

A microglial homeostatic transcript signature has been identified by several groups, with a lot of consensus between them [158, 308, 346-351]. Highly-enriched markers that have been identified in common by multiple groups (such as *Cx3cr1*, transmembrane protein 119 [*Tmem119*], and *P2ry12*) have become the focus of research efforts in generating transgenic mouse lines and antibodies for specific microglial identification. However, it is increasingly recognised that this signature may only be representative of homeostatic microglia as downregulation has been observed in a variety of disease models [158, 341, 342, 352, 353] (for more detail on microglial identification see Chapter IV). More recent work has characterised homeostatic and “reactive” microglia (as separate entities) against macrophage populations, and may assist in the identification of markers specific to microglia in both homeostatic and pathophysiological circumstances [354].

In Alzheimer’s disease (AD), plaque-associated myeloid cells have recently been confirmed as deriving from resident microglia [355]. During disease, they cluster into three main groups: naïve, stage 1 DAM, and stage 2 DAM. The initial key receptors and pathways which trigger stage 1 in this model is unclear, but progression to stage 2 has been shown to be dependent on TREM2 [340]. This dependence on TREM2 for progression was also observed in amyotrophic lateral sclerosis (ALS; also known as motor neurone disease) [353]. In humans, TREM2 variants (which decreased or markedly increased TREM2 binding affinity to its ligands) can predispose to AD [356]. Downstream of TREM2 signalling, expression of apolipoprotein E (*ApoE*) and other genes

associated with lipid metabolism occurs. *Apoe* deletion resulted in considerable normalisation of the transcript signal and suggests this as a specific pathway in neurodegeneration as its upregulation was not observed after stimulation of microglia *in vivo* with *E.coli* or zymosan particles [353]. Expression of *Apoe* was also observed in microglia during other acute and severe neurodegenerative models (the facial nerve axotomy [FNX] and CK-p25 models respectively) [343, 357]. A human allele, *Apoe*², has been shown to reduce pathology in an AD mouse model (synucleinopathy) compared to *Apoe* knock-out and insertion of other human *Apoe* alleles, including those which have genetic associations to cognitive decline (*Apoe*⁴). Furthermore, *Apoe*⁴ had considerably more phosphorylated α -synuclein than knockout or *Apoe*³ mice (not detected in *Apoe*²), although the total α -synuclein burden was similar across alleles and raised in *Apoe* knock-out [358]. This highlights the dual functionality of some genes, where knock-out can simultaneously be better and worse than possessing a functional gene (depending on the allele present) – showing how some alleles confer protective function and others a gain of toxic function. *Apoe* has been implicated in amyloid- β (A β) aggregation and clearance, being at least partially accountable for >99% of late-onset AD cases [359].

Furthermore, lipid-droplet-accumulating microglia (LDAM; they are associated with ageing, but also after LPS stimulation) have been shown (using CRISPR-Cas9 screening) to be regulated by genes associated with neurodegeneration. They produce high levels of reactive oxygen species (ROS), proinflammatory cytokines, and exhibit defective phagocytosis. Furthermore, LDAMs were found to be increased in a dementia model [360]. It is currently unclear if the microglia can reset to a completely homeostatic state after these changes have occurred. As *Apoe* has functions in lipid metabolism and is important in AD pathology [361], it is likely that LDAMs and *Apoe* (known to be important in AD onset) are part of the same mechanism of microglial dysfunction. These LDAMs could represent a critical link between the “burden of infection” and autoimmunity (and perhaps also the microbiota) [265], as the immune response threshold – “the level of immunogenic stimulation required to elicit an immune response” – and the strength of response (i.e. immune adaptation) is altered by accumulating damage [362, 363]. However, it should be appreciated that the TREM2 pathway and lipid-accumulation is neuroprotective (at least in some contexts) as its loss results in increased neurone loss in the cuprizone model (a multiple sclerosis model that bypasses the autoimmune component) [364]. Therefore, it is suggestive that LDAMs themselves are protective short-term by correcting local abnormalities (that would otherwise cause damage) and that they could represent a microglial marker for accumulating damage. However, the altered microglial immune thresholds for activation caused by this process could then predispose towards pathology long-term. These

alterations could represent a key initiator of para-inflammation, although the root mechanisms causing LDAMs remain to be elucidated. Well-designed experiments will be required to demonstrate what is associated with damage (acting as a recovery portion) and what is driving damage in these different contexts/scenarios.

In other AD models (and in humans) nucleic acids associated with β -amyloid plaques have been shown to activate microglia and induce the expression of a type-I interferon (IFN) response, and that exogenous interferon (irrespective of β -amyloid) is able to activate microglia and cause synapse loss via a complement-dependent pathway [365]. Complement component 5a receptor 1 (C5AR1) knock-out results in improved clinical outcomes in AD models, suggesting the IFN response as important in AD pathology and microglial-mediated damage [366]. The complement system also has strong genetic associations to retinal diseases such as age-related macular degeneration (AMD) with most functional implications suggesting loss of inhibitory signals or increased activity [367] – suggesting increased synaptic pruning by microglia as fundamental to establishment and/or progression of these disease processes. As established earlier, loss of synaptic pruning has been linked to schizophrenia [115, 310] which suggests potential therapeutic strategies would need to reduce (but not completely abrogate) this pathway. Ideally biomarkers or risk stratification could inform prophylactic therapies that can be used before the onset of disease and loss of neurones.

Microglia also have been implicated in a wide variety of inherited retinal degenerative diseases observed in mice, including in genes such as phosphodiesterase 6b (*Pde6b*; retinal degeneration 1 [rd1] model), membrane frizzled-related protein (*Mfrp*; rd6), Crumbs cell polarity complex component 1 (*Crb1*), *Cx3cr1* (polymorphisms of which associate with AMD), and prolyl 3-hydroxylase 1 (*P3h1*) [368-373]. In these situations, microglia proliferate and accumulate proximal to areas of retinal damage, enabling phagocytosis. They secrete pro-inflammatory cytokines including TNF- α , IL-1 β , C-C motif chemokine ligand (CCL2), and CCL3 in addition to ROS and nitric oxide (NO) [374, 375]. Some of these genes are expressed exclusively in the retina by microglia (i.e. *Cx3cr1*), implying that microglia can initiate and drive degeneration. However, in other inherited retinal degenerative diseases it appears that the microglial response is secondary to dysfunction.

In autoimmune situations, TGF- β -activated kinase 1 (*Tak1*) has been proposed as pivotal in causing autoimmunity as microglial-specific knock-out demonstrated significantly suppressed disease in the experimental autoimmune encephalomyelitis (EAE) model (EAE models the disease multiple sclerosis) [376]. Further experiments have showed that microglial-specific *Tak1*

knock-out reduces TNF production, and that conditional knock-out of TNF in microglia can also significantly reduce disease severity in graft-versus-host disease [377]. In addition to studies discussed later (within the “Retinal Microglia and Uveitis” section), this implicates a central role for microglia in the development of autoimmune disease.

Beyond surface markers, cytokine production, and gene expression, there is growing evidence of a range of microglial phenotypes at the morphological level that are now being realised. The simple two-state ramified or amoeboid model of microglia (sometimes described in 3 states: compact, longitudinal, and radial [378]) which, whilst useful, is a gross oversimplification. In full, microglia exhibit a multi-dimensional spectrum of morphological phenotypes that facilitates the need for automated analysis strategies [379]. Currently, two dominant approaches for analysing the microglia exist: sholl analysis, and frac-lac [380]. In brief, sholl analysis was developed to characterise neurone morphologies and involves counting intersections between dendrite processes and expanding concentric circles [381]. Frac-lac involves counting of fractal dimensions (which broadly corresponds to complexity) whilst lacunarity helps to describe how the fractal dimensions fill space (a larger lacunarity generally means more or larger gaps) [382-384]. Both approaches can help to describe quantitatively how ramified a microglial cell is, in addition to other parameters such as complexity and shape [385, 386]. These approaches, whilst useful, tend to rely on manual segmentation of each microglia which limits the numbers which can be analysed. However, many more approaches are being developed to increase throughput (to more than 20,000 cells i.e. with phenotypic clustering [387]) or by extracting further information (59 parameters, 17 of which were highly discriminatory in microglial classification on shape [388]) using automated solutions. Despite this, such analyses tend to require technical or coding expertise to execute correctly and obtain results which currently limits their reach and usage. Furthermore, they will rely on and assume the use of a single marker which is both sensitive and specific for microglia along their entire membrane – ergo it tags all microglia, and only microglia – which during severe and chronic inflammation has not necessarily yet been identified or validated.

1.5.2 Retinal Microglia and Homeostasis

Retinal microglia have been shown to reside within both the plexiform layers, forming niches dependent on different cytokines for homeostatic function and survival [341]. Around 50% of microglia within the inner plexiform layer (IPL) depend on IL-34 (an alternative CSF1R ligand [389]) for survival, whilst microglia within the outer plexiform layer (OPL) are IL-34 independent (but are CSF1-dependent as CSF1R blockade can deplete all microglia from the

retina [390]). Furthermore, the IL-34-dependent microglia within the IPL are believed to possess sub-specialisations to their niche and are suggested as key contributors to normal visual function [341].

Retinal microglia constitutively express IL-27 which stimulates photoreceptors to secrete IL-10 [312]. IL-10 is associated with anti-inflammatory activities and has been shown to metabolically reprogram macrophages [391]. This suggests microglia can self-regulate through the IL-27/IL-10 axis. Unsurprisingly, dysregulation of IL-10 increases the risk of autoimmune diseases [392]. Furthermore, microglia can interact with neurones directly, with receptors such as P2RY₁₂, CX₃CR₁, and CD200R assisting with coupling [393]. These localised interactions, like with tissue-resident macrophages in other organs, are believed important in conditioning the phenotype.

There are four major types of microglial checkpoint mechanisms which help to establish an immunosuppressive/homeostatic or “resting” environment: physical barriers (i.e. the BBB/BRB which help to seclude both peripheral immune cells and cytokines or other signalling mechanisms), soluble factors (paracrine signalling via neurons and other local cells e.g. TGF- β , but also through autocrine mechanisms such as TNF- α signalling via TNF alpha-induced protein 3 [TNFAIP3] [394]), cell-cell interactions (e.g. through CD200 and C-X₃-C motif chemokine ligand 1 [CX₃CL1]), and microglial-specific chromatin regulators and transcription factors (e.g. RUNX₁ and SPI₁) which promote the expression of immunosuppressive factors (Figure 1.5.3) [395, 396]. This complex set of checkpoints and interactions highlights the critical need for well-controlled microglial activation.

Soluble Factors

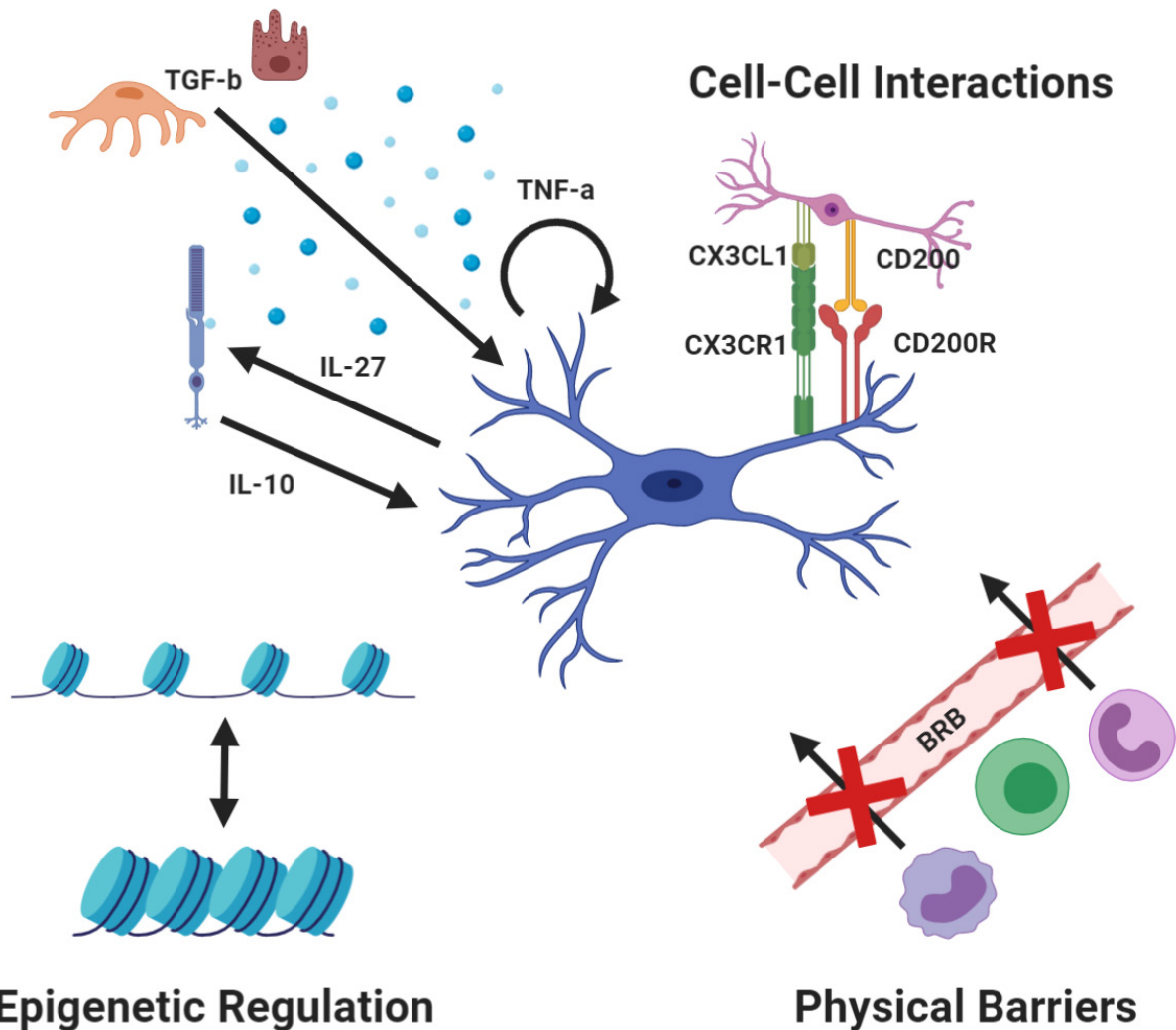


Figure 1.5.3. Major types of microglial checkpoint that help to establish and maintain an immunosuppressive environment. Soluble factors can influence microglial activity, and these can be via autocrine (e.g. TNF- α), paracrine (e.g. TGF- β), or paracrine loop (e.g. IL-27/IL-10) mechanisms. Cell-cell interactions (e.g. CX₃CL₁-CX₃CR₁ and CD₂₀₀-CD₂₀₀R) can aid with microglial localisation. Both soluble factors and cell-cell interactions can influence epigenetic regulation of microglia and activation state of transcription factors via cell signalling, reducing their propensity towards inflammation. Lastly, physical barriers (e.g. the BRB) hinder peripheral immune cells from accessing the retina and their ability to secrete cytokines and interact with microglia to promote inflammation. Abbreviation: BRB – blood-retinal barrier.

1.5.3 Retinal Microglia and Uveitis

The role of microglia in EAU and uveitis are less-well understood and more speculative. Investigation of microglia within inflammatory disease models has been challenging due to their similar phenotype to monocyte-macrophage populations [397]. During early EAU microglia migrate from the inner and outer plexiform layers to other regions of the retina [398], and that during this early stage they secrete peroxynitrite and TNF- α [398, 399] to recruit and activate peripheral immune cells [400]. Microglia also undergo a morphological change from a ramified appearance into a more amoeboid appearance [401], suggesting their activation as important in the early pathogenesis of EAU. The current understanding of microglia during early EAU is summarised in Figure 1.5.4.

Studies have shown that knockout of CD200, an important regulatory glycoprotein expressed by neurones, vascular endothelium, and other activated immune cells, results in accelerated onset and severity of EAU [402]. Recent work suggests that myeloid cells can transfer mitochondria to neurones in a CD200-dependent manner, and this can resolve inflammatory pain in mice [403]. Knock-out of CX₃CR₁, another important microglial checkpoint/regulatory receptor also enhances disease severity [404]. Furthermore, IFN- γ (produced by T_h1 cells, a key mediator of EAU) upregulates IL-27 in microglia which stimulates the production of the anti-inflammatory cytokine IL-10 by photoreceptors [312]. IL-27 also inhibits ROR γ c expression to prevent lineage commitment to T_h17 and expression of IL-17 in CD4⁺ T cells [405, 406]. It is possible IL-27 could induce transformation of T_h17 cells towards a T_h1 phenotype (these are termed non-classical T_h1 or ex-T_h17 cells) [214]; in other contexts T_h17 cells could become T_{reg}-like as well [407]. Moreover, IL-1 β has been shown to induce IFN- γ (a typically T_h1-associated cytokine) in T_h17 cells [408]. As IL-1R knockout mice are resistant to EAU but cellular infiltration can still occur (expression of IL-1 β is an early microglial event) [61, 409], and that IL-27R knockout mice exhibit more severe autoimmune disease in brain contexts [410], this suggests that reprogramming of T cells by microglia (or a critical role for microglia helping to drive uveitis) is plausible. This not only confirms that microglial dysregulation worsens EAU, illustrating direct involvement in disease process, but also suggests that they represent an excellent cellular target for therapeutics in addition to highlighting the critical role several different axes (e.g. IL-27, CD200, CX₃CR₁), or immune checkpoints, can have in regulating the potential inflammatory environment within the eye.

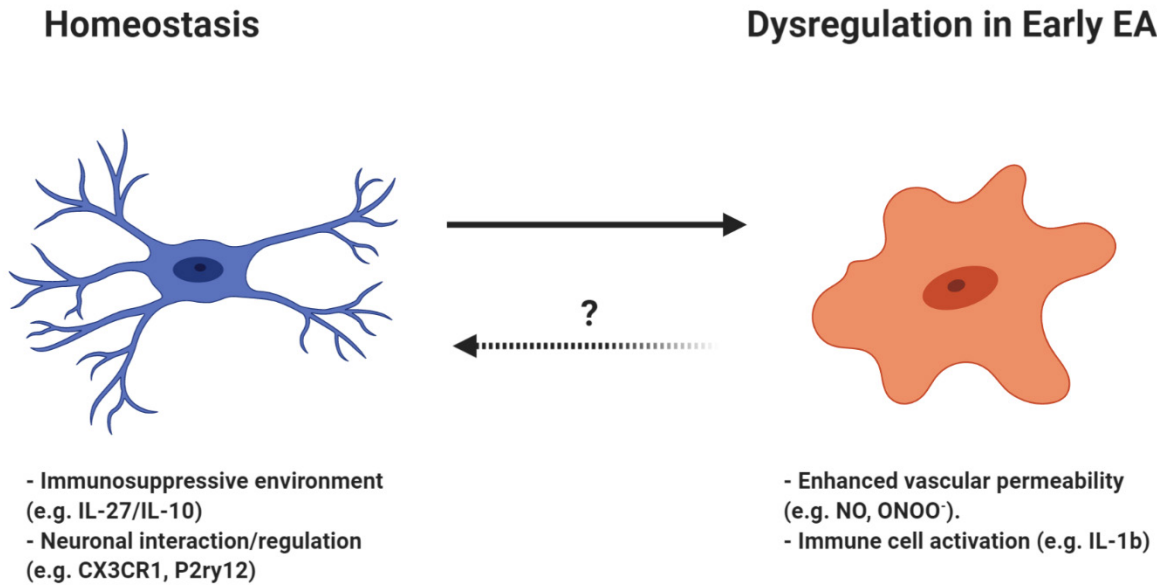


Figure 1.5.4. *The changes between homeostatic ramified microglia and dysregulated amoeboid microglia during EAU. Microglia undergo a morphological transition towards a more amoeboid state, in addition to migration from plexiform layers to other regions of the retina. During this time, the threshold for activation is overcome and a pro-inflammatory environment generated. Microglia are known to release factors enhancing vascular permeability (e.g. NO and ONOO⁻) as well as IL-1 β to activate peripheral immune cells and help to facilitate their entry into the retina. It is currently unknown if microglia can completely reset to their homeostatic state following activation in EAU.*

Microglia are tissue-resident immune cells within the retina, meaning they could be targeted locally by a therapy during remission. Nonetheless, following inflammation it is recognised that the BRB remains permeable, that immune thresholds are altered, and tertiary lymphoid structures may have formed within the eye – these represent other plausible targets during remission also [44, 411]. Targeting microglia (and/or other immune cells that have acquired residency within the tissue) during remission has the potential, in a patient, to enhance the immunosuppressive environment – e.g. in recurrent uveitis, or in drug-induced remission i.e. in chronic uveitis brought under control by steroids that need to be tapered due to its adverse effects – to ultimately prevent relapse. This represents a preferable approach to treatment strategy instead of targeting the peripheral T cells; during relapse, damage and symptoms are already being caused and targeting during remission would likely have an increased side effect profile as it would affect T cells systemically – and they are responsible for adaptive immune responses (in conjunction with B cells) throughout the body.

Determining the role of microglia during the late stages of EAU has been challenging because macrophage infiltration has occurred and reasonable discrimination between these cell types has not been possible (until recently). However, it is plausible that microglia could play a key role in re-establishing an immunosuppressive environment within the eye; for example, through increased secretion of IL-27 (as outlined earlier) but via other mechanisms as well. Overall, this suggests that microglia have both a pro- and anti-inflammatory response in EAU, and that careful manipulation of them with therapies could have a beneficial effect in uveitis.

A recent study cemented the vital role microglia play in uveitis by showing their depletion (using CSF1R antagonism; described later) inhibited the onset of EAU in both conventional immunisation and AT models, yet their depletion during established EAU was relatively inconsequential [390]. Using the EIU model (systemic LPS administration), it was also shown that CSF1R antagonism could prevent BRB breakdown and subsequent immune cell infiltration [412]. This highlights the importance of microglia in enabling immune cell infiltration, through direct interaction with leukocytes through the vascular wall and/or indirect effects via the vascular endothelium, but how other immune cells (such as monocytes and macrophages) could functionally mimic them and compensate for their loss once autoimmunity was established, or that they were obsolete by this point. They did not observe the effects of complete microglial depletion (e.g. using CSF1R antagonism) long-term, and it would be interesting to see if disease continued with a different severity due to their loss, because their potential pro-resolution response would no longer be present. However (as discussed in the next section) there is potential for myeloid cells to adopt programmed microglial niches of residency, acquire a

microglia or microglial-like role, and help to also resolve disease. As this adopted residency and functional adaptation takes time to complete, then resolution of disease could still be delayed compared to an absence of microglial depletion.

1.5.4 Monocyte Engraftment and Microglial Depletion

The understanding of monocyte and microglial dynamics within the brain has been difficult to establish due to similarities between the cell types. Nonetheless, it is well-characterised that microglia can be replaced by monocytes in the retina and brain by a process termed engraftment. The monocytes/monocyte-progenitors differentiate into microglia or microglia-like cells, adopting their function and niche of residency. Post-engraftment, tissue-resident CD11b⁺ populations have their enhancers shaped by the local microenvironment (tissue- and lineage-specific transcription factors in addition to the microbiome) and this enables them to acquire the required phenotype for the niche they occupy [192, 413]. This may also explain why loss of a homeostatic microglial signal is observed in many microglial cell lines and cultures – i.e. because they are removed from this regulatory microenvironment [414].

It has been shown that infiltration and engraftment of monocytes (for at least 6 months post-radiation) into the brain only occurs after total body irradiation (TBI) and not after head-protected irradiation (HPI) [415]; engraftment by monocytes occurs in a dose- and time-dependent manner [416].

More recent work, using $Cx3cr1^{CreER/+};Csfr^{Flox/Flox}$ (CSF1R signalling is a vital microglial survival signal, and therefore its removal results in their death) mice fed tamoxifen-containing chow, shows that microglia are capable of self-replication (in the presence of partial loss) to maintain their physiological count (as compared to $Cx3cr1^{+/+};Csfr^{Flox/Flox}$ controls) [417]. They also showed that both sorted and circulating blood monocytes were able to occupy the brain only in the *CreER* heterozygotes after tamoxifen administration (in a chimera with donor cells labelled). Engraftment occurred with or without the presence of a CSF1R inhibitor (it was exacerbated in its presence) and was confirmed it as genuine through use of the $Cx3cr1^{+/-};Csfr^{Flox/Flox};R26^{yfp}$ mouse (where microglia would express yellow fluorescent protein [YFP⁺] and lose *Csfr* expression, whilst peripheral cells would be negative). It was also shown that the peripherally-engrafted cells had a transcriptional signature that was different from microglia; the unique signature was similar to intestinal serosal macrophages, lung CD11b⁺ macrophages, and small intestine lamina propria macrophages determined from microarray data acquired as part of the Immunological Genome Project (ImmGen) [418]. However, it should be noted that the atlas has

a bias towards certain cell types and others are under-represented or not present at-all. For example, currently no microglial data is included. Overall, the data suggests that tissue-residency of microglia or microglia-like immune cells can only occur in predetermined regions commonly referred to as niches, and that in the absence of free/available niches this process cannot occur. It is suggestive that the spatial distribution of the niches, in conjunction with extension/retraction of microglial ramified processes, enables adequate microglial coverage of the tissue to both provide total immunosurveillance and enable completion of sub-specialised tasks unique to each microenvironment within the CNS.

Other studies show that wide-scale microglial depletion (using Cre recombinase [Cre]/diphtheria toxin [DT] receptor systems) results in self-renewal of those which survive. With irradiation, engraftment of peripheral cells could occur [419]. Therefore, it was suggested that unless the BBB is disrupted (i.e. by irradiation), the “niches” (programmed regions in which a microglia or microglial-like cell can reside – as described by [417]) are filled by self-renewing microglia. Through blockade of IL-1R, it was showed that microglial renewal is significantly delayed and that engraftment does not occur despite the niches being empty long-term, confirming that disruption to the BBB to permit cellular entry is required in addition to empty niches [419]. As CSF1R is vital for microglia, and they die without it [420], it is suggestive that the cell death resulting from experiments targeting CSF1R to deplete microglia could lead to the disruption of the BBB through the release of DAMPs or other signals to indicate tissue damage (CSF1 would be produced in a typical retina, and absence of its signalling could suggest tissue abnormalities) – which could disrupt the BBB and permit engraftment. The mechanism of cell death via DT systems is apoptosis as a result of inhibition of protein synthesis [421], meaning that release of DAMPs or danger signalling molecules may not occur as they cannot be synthesised, and this may explain why engraftment does not occur in this context. Irrespective of the conflicts, both studies independently identified microglial unique gene signatures, that were already widely-believed to be microglial-specific, when compared to the engrafted cells [417, 419] (e.g. *P2ry12*, *Tmem119*). In agreement, other reports suggest that TMEM119 marks only microglia within the human brain and not monocytes [422]. However, in these experiments (performed on human tissues post-mortem) it remains unclear whether the monocytes have persisted long-term and are engrafted cells or are infiltrating due to inflammation. Furthermore, during disease states it is becoming increasingly recognised that downregulation of the microglial transcriptional programme occurs, including *Tmem119* [353]. Nonetheless, it is understood that engrafted monocytes can be morphologically indistinguishable from yolk-sac derived microglia, but that it is possible to fate-map them using *Ccr2* transgenic mouse lines (i.e. using *Ccr2^{Cre}* instead of

chimeric techniques) as microglia do not express *Ccr2* but most monocytes/monocyte progenitors do [423]. It is likely that their differential transcriptomes could be due to different differentiation pathways and lineages (i.e. origins) leading to epigenetic differences in these cells that cannot be fully overcome by the microenvironment and other local regulators.

Whether these engrafted cells are beneficial or detrimental to tissue homeostasis is likely to be context-dependent with research supporting both outcomes [423, 424]; further research is required before their role and potential can be realised. Assuming monocyte-engrafted cells retain some epigenetic footprint of a monocyte progenitor, it would follow that these cells are inherently more predisposed towards a pro-inflammatory state. This could be helpful or harmful depending on the context. For example, monocyte-engrafted cells could become better at clearing and scavenging as well as dealing with infection (beneficial) whilst at the same time predisposing to inflammation in unnecessary contexts that could lead to collateral damage (detrimental). In the context of lipid-droplet accumulation, replacement of these microglia (LDAMs) by the monocytes could result in a more anti-inflammatory environment; whilst this would certainly be context-dependent on the proportion of LDAMs present, there is potential for engrafted cells to be beneficial and/or detrimental to the immune state of the retina. Furthermore, recent research shows that partial depletion of microglia and subsequent self-renewal results in reduced neuronal damage in models of traumatic brain injury compared to controls which did not perturb the microglia, and that this is an IL-6-dependent process [425]. Whilst these experiments were performed on microglia located within the brain, these results could explain observations in the retina on partial depletion as they are likely to be similar in mechanism. This data suggests it could be repopulation of the retina, and not necessarily a specific cell type or progenitor (i.e. microglia or engrafted cell), that associates with protective effects. Further work comparing the IL-6 repair process between self-replicating microglia and engrafting monocytes, in addition to the context(s) in which this is beneficial would be useful in delineating the finer aspects of this phenomenon.

It should, however, be noted that the experiments involving irradiation and large-scale depletion of microglia may not be representative of disease processes in humans. However, during inflammation (either locally or systemically) the ability for engraftment to occur, as the BBB/BRB is disrupted, is plausible. In humans, engrafted microglia-like cells have been observed in AD whilst in the mouse they have been shown to express genes associated with AD DAMs in naïve mice (engraftment procedure aside) [426, 427].

Further work to establish whether engraftment is a genuine feature of inflammatory disease models of the brain and retina, and the effect this has on a disease course or future inflammatory processes, is required. It is, however, well-recognised in ageing that cells exhibiting a microglial morphology are more pro-inflammatory (generally primed) compared to their younger counterparts – it is unclear if these are general replacement of microglia with engrafted cells with time, or genuine changes in the embryonically-derived microglia over the lifetime of an organism (such as lipid accumulation and para-inflammation). It is possible that a threshold for these changes (i.e. a more pro-inflammatory state) is required before autoimmunity or neurodegenerative disease becomes feasible and could explain why the burden of infection, LDAM accumulation, immune adaptation, and para-inflammation could be important to its onset.

1.6 Experimental Techniques: mRNA-Sequencing

Messenger ribonucleic acid sequencing (mRNA-Seq) is a technique that enables the quantification of mRNA inside a cell or group of cells, and has the potential to identify differences in expression of any gene, splice variants, and/or mutations (or SNPs) in different experimental groups – whether that be physiological and disease groups, treatment groups, others, or a combination [428]. The aim is to characterise changes between experimental groups in an unbiased manner to determine the changes occurring to cellular behaviour at the molecular level. For the study of microglia, this approach has improved our fundamental understanding through the identification of specific candidate markers which has enabled the generation of transgenic microglial reporter mouse lines, compendiums of key/homeostatic microglial transcripts, and meta-analyses of multiple microglial datasets to identify genes associated with varying microglial states (e.g. acute vs. primed) in attempts to begin classifying different microglial subtypes [158, 308, 346-351, 376, 429] (see the microglial phenotypes section of this Chapter and the challenge of microglial identification section within Chapter IV). mRNA-Seq is a powerful tool for interrogating the whole transcriptome and understanding changes to cellular behaviour at a broad level, and has the potential to elucidate mechanisms of action, signalling, and side effects induced by therapeutics. The general aspects of experimental and analytical pipelines for mRNA-seq are summarised and discussed herein; specifics of the mRNA-Seq pipeline selected for the experiments conducted as part of this thesis are described within Chapter III and Appendix I.

1.6.1 Experimental Pipelines

Cell Isolation Methods

When performing mRNA-Seq on whole tissues derived from organisms, there will inevitably be a mixture of cell populations. This poses several challenges, chiefly that the mRNA isolated for sequencing would be a mixture of all the cell-types present in that tissue or organ. This causes significant problems in that the signal from your population of interest will be diluted by the others, and any treatments or other experimental procedures you wish to investigate would yield a summary picture of the largest/average changes from the cells types blurred into one – as opposed to specific changes at given times within a defined cell population. This can become further complicated if there is differential transcriptional amplification between cell types – transcriptional amplification being when a cell expresses more mRNA (or in the case of repression, less), leading to potential bias in identifying differentially-expressed genes (DEGs)

[430]. This may also result if there are changes in the proportions of cells of the different types or cellular infiltration (as would be seen in inflammatory models). Despite this, and approaches for cell isolation being well established, studies based on whole tissue approaches are being published currently [102].

To overcome some of these limitations, two main methodologies for bulk mRNA-Seq have been widely-adopted: fluorescence-activated cell sorting (FACS) and laser capture microdissection (LCM) [431]; the former involves dissociation of cells into a single-cell suspension, staining with antibodies conjugated to fluorophores (or use of fluorescent tagging beforehand), and then sorting of populations based on a gating strategy (determined by size and fluorescence intensity in the channels). LCM involves fixation and sectioning of tissues, optional staining, and use of a microscope-guided laser to isolate the region of interest (in this case a cell or group of cells). It is argued by many that LCM will be more representative of the mRNA being expressed by the cell as fixation “flash freezes” mRNA early-on in the preparation process, whilst there is a greater window of opportunity for transcriptional changes to occur with FACS-isolated mRNA due to the length of time required for preparatory steps such as staining protocols. However, it is also recognised that contaminant mRNA from surrounding areas/cells can also be captured using LCM. Nonetheless, both are valid ways of obtaining cells for mRNA-Seq as controls within each experiment are likely to be confounded by the same limitations and thus change in a similar way – when analysing, these artefacts would then be excluded as noise which would not achieve the required statistical threshold, and/or not be observed as different between experimental groups. Furthermore, a study investigated the two methodologies head-to-head by profiling single cells from chicken embryos; good correlation between samples acquired using the two cell isolation methodologies (FACS and LCM) was observed, suggesting the two techniques are comparable [432]. Beyond the two initial approaches, it is possible to utilise other technologies such as magnetic-activated cell sorting (MACS) for mRNA-Seq [433]. However, this approach is less widely adopted due to limitations of lower specificity and reduced sample viability of MACS compared to either LCM or FACS [434, 435].

Sample and Library Preparation

Following isolation, cells require careful processing and preparation for sequencing. If not performed initially during the isolation step, the cells need to be lysed; this can be performed using snap freezing but is commonly performed with a lysis buffer (usually containing an RNase inhibitor). The mRNA is then isolated, stabilised, and sometimes amplified from the mixture of cellular contents (the latter step is required in the case of low input amounts from few or single cells). This can be performed through polyA selection or ribosomal/transfer RNA (rRNA/tRNA)

depletion. The former is considered superior for mRNA-Seq, but rRNA/tRNA depletion helps to retain more long non-coding RNAs (lncRNAs) and other small RNAs [436]. Other approaches, such as using TRIzol reagent, also exist [437]. The aforementioned approaches are not compatible with formalin-fixed and paraffin-embedded samples – which is the way many tissue banks preserve and store patient samples – and therefore specialised extraction pipelines for these types of samples have also been developed [438].

The mRNA is then converted into complementary DNA (cDNA) using reverse transcriptase (RT) because cDNA is considerably more stable [439]. Before proceeding to cDNA synthesis, protocols often test the quality of the mRNA if it was purified as part of processing; the RNA Integrity Number (RIN) is the gold-standard for this [440]. In the original mRNA-Seq pipelines developed, random hexamer primers (in addition to d[T] primers specific for the beginning of the poly[A] tail) are used to amplify the cDNA first-strands generated by PCR. However, this process leads to a strong GC bias. Enhancements to this process now include the use of template switching to facilitate introduction of equivalent sequences at the 5' end of the transcript to overcome this limitation [441]. Other pipelines bypass the use of PCR entirely, instead utilising a different process called *in vitro transcription*, which is considered to introduce less bias and is used in microarray platforms (the predecessor transcriptomics platform which mRNA-Seq has now effectively superseded) [442]. At this point, the cDNA is usually quantified and then processed for library preparation (where each sample is barcoded and prepared for sequencing; see Appendix I for the intricacies of this process), in addition to quantification post-library generation. A variety of techniques are available, such as the conventional nanodrop approach, but Qubit and Agilent TapeStation approaches are more sensitive, accurate, and reliable, and remain two commonly-used approaches to this end [443].

From this point, the samples are then loaded onto the flow cell (sometimes called chip) and sequenced. A variety of sequencing machines are available, depending on the throughput or technology required; the vast majority of mRNA-Seq is performed using the Illumina technology. A small proportion of mRNA-Seq is also performed using the Ion Torrent platform. Both perform similarly well, but the choice of sequencing platform affects how the data should be processed (for example, some aligners perform better or worse for each technology) [444].

1.6.2 Approaches to Data Analysis

Whilst there is no gold-standard for data analysis approaches, good practice does exist and a survey on best practices was recently performed to help compile these in one place [445]. Before

detailing the available packages, software, and/or code to carry out analysis functions it is important to recognise the infrastructure and technical challenges relating to these tools and their use.

Bioinformatics Tools

The majority of tools available for use have been released as packages (or plugins) within Bioconductor. This is an add-on platform for the open-source R statistical package and is specifically aimed at the analysis and visualisation of data generated from high-throughput biological assays (e.g. mRNA-Seq, proteomics, flow cytometry) [446, 447]. This platform enables anyone to author a package (a plugin/addon for Bioconductor) and holds several advantages such as faster and better collaboration opportunities, being open-source so that the code can be critiqued and edited/refined by users, and an ability to write custom code if a desired function does not yet exist. However, it also holds several disadvantages such as a need for experience with command line interfaces (CLI). Packages can also become obsolete and dysfunctional within the Bioconductor environment if they are not maintained because Bioconductor itself is continually being updated. University computer systems often restrict user permissions and this can make troubleshooting or running of certain packages more challenging because the R environment defaults to using the C: drive (restricted) and it isn't usually possible to edit the java runtime environment (default installation is also to the C: drive) which R depends on. Additionally, writing code for novel tasks/functions is non-trivial and requires expertise with coding languages.

Other tools have also been developed and released in different ways. A large compilation of tools have been written by the Bioinformatics group at the Babraham Institute and the Broad Institute, whilst many other tools and/or data repositories are integrated on websites including the European Bioinformatics Institute (EMBL-EBI; to include the Expression Atlas and many more), the Database for Annotation, Visualization and Integrated Discovery (DAVID), the ImmGen project, the National Centre for Biotechnology Information (NCBI, to include the Gene Expression Omnibus [GEO]), Mouse Genome Informatics (MGI), and Ensembl [418, 448-457]. Beyond this, numerous commercial packages for analysis have also been released such as the Partek suite of software, Ingenuity Pathway Analysis (IPA) and CLC Genomics Workbench (the latter two from Qiagen) – these utilise graphical user interfaces (GUIs) instead of CLIs which makes them considerably more user friendly. Open-source all-in-one packages with a GUI, such as the Visualization Pipeline for RNA-Seq, a Snakemake workflow for efficient and complete RNA-seq analysis (VIPER) have also been released [458]. However, these GUI-based applications will have functionality limited to what has been implemented within them already,

usually with inaccessible/protected source code meaning that users rely on new versions solely from the developers. This can limit the rate of adoption of the latest innovations in the field and available options for analysis within these environments.

It is evident that there are a variety of bioinformatics tools at a scientist's disposal each with benefits and drawbacks. A more exhaustive list of over 100 mRNA-Seq bioinformatics tools, and their original papers for further reading, can be found on Wikipedia [459]. A different review paper also summarises and discusses many 'omics tools and their utility in systems immunology [460].

Analysis of mRNA-Seq Data – Principles and a “Good Practice” Pipeline

Once data has been acquired, it is first quality-checked and pre-alignment processing performed. Tools such as FASTQC are used to check the Phred scores (defined as $-10 \log_{10}P$ where P is the probability of an error in base-calling [461]), GC content (highlighting PCR bias), base distribution across read position (highlighting abnormalities in a sample), and many other parameters which can be informative about the quality of the output (e.g. adapter contamination) [462]. From here, bases are trimmed – typically to remove adapter sequences, but also to remove poor quality reads at the 3' end – so that alignment to a reference genome or *de novo* assembly would be more accurate and valid; low-quality reads can also be discarded [463]. Alignment, especially of small or microRNA molecules, would be highly inaccurate if contaminating adapters were still present or base calling was not accurate. Adapter sequences are dependent on the library preparation kit used (and hence vary considerably, although a list of many Illumina adapters can be found at [464]), but trimming from the 3' end of a read on a Phred score of ≥ 20 is considered good and ≥ 30 ideal.

At this point, dimension-reduction algorithms (such as principal component analysis [PCA]) are often performed on the data to enable visualisation of broad patterns. For example, segregation of samples would be anticipated based on factors such as experimental group, tissue the sample was derived from, time, etc [465]. Samples can also be correlated to one another to help identify outliers for exclusion (e.g. $R^2 \geq 0.9$ for cell lines of the same experimental group). However, in heterogeneous *in vivo* disease models this is not well understood and no defined set of criteria for exclusion exists, possibly because each disease model is unique and could vary in correlation due to genuine biological variation [466, 467].

The reads are then mapped to an organism's genome or transcriptome, or sometimes (usually in the case of a poorly annotated organism) are used to create a *de novo* assembly, using an aligner. This process associates each read with a specific region (or regions) that it matches

within the genome, which itself associates with a specific gene. When mapping to the genome, it is also possible to identify new transcripts and splice variants [468]. For the creation of an assembly or to identify novel splice variants, considerably more and longer paired-end reads are generally required¹. A huge variety of different aligners exist including bowtie 2, Burrows-Wheeler aligner (BWA), genomic short-read nucleotide alignment program (GSNAP), hierarchical indexing for spliced alignment of transcripts (HISAT2; a successor to the popular TopHat2), Isaac 2, MapSplice, RNA-Seq unified mapper (RUM), and spliced transcripts alignment to a reference (STAR) [469-477]. When selecting an aligner for use, the main considerations include available random access memory (cRAM) of the processing machine (some aligners require large amounts of cRAM, and would not run on smaller systems such as desktop personal computers), read length of your data (some aligners are optimal for only certain length reads [i.e. ~25, ~75, ~200, or even larger]), mapping accuracy (higher being more desirable), splice awareness (if using mRNA-Seq data, this is critical or reads spanning an exon-exon boundary will align to multiple places within the genome unnecessarily and this can affect results), and to some extent the speed at which the algorithm can align. To this end, STAR is a prominent and popular aligner because it is splice aware, can be used on reads of any length, is comparably accurate in mapping to many other aligners, and has a fast mapping speed – it is up to ~55 times faster than TopHat2 [475]. Furthermore, it can utilise only 16 Gb of cRAM in sparse mode, which would enable its use on high-end desktop machines and all servers.

Once alignment has been performed, quality control (QC) steps are carried-out to check various basic metrics including alignment rate and unique alignment rate, but also more advanced metrics such as coverage uniformity, mapped reads distribution, and splice junction annotation [478, 479]. Generally, a total alignment rate of 80–90% is considered ideal, with a unique alignment rate of 70–80% also desired – assuming you are mapping to a well-annotated genome (e.g. human or mouse). Unique alignments describe where that read mapped to only one position within the organism's genome; because of some repeat sequences and similarity in sequence between paralogous genes, some non-unique alignments are anticipated. In some organisms, such as the zebrafish, whole-genome duplication events occurred in evolutionary history (for the zebrafish, this is termed the teleost-specific genome duplication and represents a third-round compared to the two observed in tetrapods) and means that a greater proportion

¹ Five to twenty-five million reads are required for gene expression analysis, 50–70 million reads for transcript-level analysis, and ≥90 million reads for identifying novel transcripts or *de novo* assembly. This rule applies well to genomes comparable to the mouse or human, but otherwise the required number of reads can vary depending on the size of the organism's genome (fewer for smaller genomes and vice versa).

of non-unique alignments would be anticipated compared to other organisms [480, 481]. Relatively uniform coverage is expected across the genome, so over-representation of sequences from one region of the genome can be an indicator of QC issues in the sample or problems with processing steps.

The next step requires quantification of the reads and this can occur at the gene-, transcript-, or exon-level. A variety of packages can perform this function, including those such as Cufflinks, NOISeq, exploratory data analysis and normalization for RNA-Seq (EDASeq), Sailfish, and HTSeq [482-486]. Unfortunately, many (if not all) appear to struggle with reliable and valid quantification of reads that map in a non-unique fashion – which typically correspond to paralogous genes – as there is no simple (if any) way of differentiating them [487]. After quantification, the raw reads require normalisation because normalisation, or lack of, can have a profound effect on expression values and the subsequent detection of DEGs [488]. There are many normalisation strategies, but some of the commonly-used approaches include: RPKM, fragments per kilobase of exon model per million reads mapped (FPKM), transcripts per million (TPM), trimmed mean of M values (TMM), PoissonSeq, RNA-Seq by expectation maximization (RSEM), eXpress, or through the use of synthetic spike-in controls (e.g. ERCC spike-ins) of known concentration before sample processing begins [467, 489-496]. It is also possible to normalise using housekeeping genes: this could include the use of one or a set of predefined genes. Normalisation models which assume that roughly half of the transcriptome does not change across experimental groups have also been developed [497].

Quantified reads can then be analysed by differential gene expression analysis (DGEA) to identify DEGs. As before, many tools can be used for this (and some provide their own normalisation too); two of the best currently available packages include empirical analysis of digital gene expression in R (edgeR) and differential expression analysis for sequence count data 2 (DESeq2) [498-500]. Once DEGs have been identified, it is important to nonetheless validate them. Performing quantitative PCR (qPCR) on the samples (if there is leftover material) can validate both the mRNA-Seq itself and the analysis as it uses the same original material. This is important, because if validation at the protein level was discrepant it would be unclear if the mRNA-Seq and/or analysis was valid or not, and discrepancies between proteome and transcriptome have already been observed [501]. The best approach to confirm change at the protein-level (i.e. with techniques such as Western blotting, fluorescence microscopy, and flow cytometry to name a few) will depend on a variety of factors [502].

From here, the list of DEGs can be used for secondary analysis such as gene set enrichment (or pathway) analysis (GSEA) [503]. Two databases predominate in this type of analysis: gene ontology (GO) terms, and the Kyoto encyclopedia of genes and genomes (KEGG) pathways [504-506]. This type of analysis can help to group DEGs which are related in a specific pathway, and put them through a second statistical test: the proportion of DEGs in that pathway (to those not) are compared to the proportion of all DEGs to the list of genes in the database (in essence, a repeated version of the Chi-Squared test for each pathway in the list) [507]. It arguably corrects for DEGs which may otherwise be noise (i.e. false positives) as multiple DEGs from a single pathway will be required before significance is achieved, and the probability of this occurring by random chance becomes considerably smaller. Despite this, these approaches are limited because they rely on coupling data to annotated databases and pathways primarily determined by genes with known functions. It can lead to the loss of information relating to genes which have been poorly characterised or are novel. The second main limitation is that it does not show directionality of the pathway change and uncertainty as to whether the changes in gene expression correspond to activation or inhibition of the pathway, or if there is functional antagonism and therefore no overall change to the pathway. However, the IPA tool can perform a modified GSEA which predicts activation/inhibition of the pathway to help understand which pathways are both significant and have a directionality bias. Despite these shortfalls, GSEA remains a very useful tool for filtering results into meaningful changes, mechanistic/signalling changes, or for further lines of investigation. It can also confirm at a broad level if the results are in general agreement with the known pathways and processes (e.g. you would anticipate immune-related processes to be identified as significantly enriched if you were investigating transcriptional differences during an autoimmune disease). Further to this, some tools (including weighted gene co-expression network analysis [WGCNA]) permit the generation of novel clusters/gene sets and statistical comparisons between samples and clusters [508]; the use of such tools generally require large datasets, often compiled from multiple sources.

Lastly, a variety of other tools can also be utilised in conjunction with mRNA-Seq data such as genome browsers, generation of Sashimi plots (to visualise splice junctions), gene fusion discovery, volcano plots, and many other types of visualisation or investigation. However, these are generally limited to specific or a small set of genes [445].

1.7 Thesis Objectives

Uveitis is a group of autoimmune/autoinflammatory conditions of the eye and is the commonest cause of blindness in the working-age, representing a significant health burden. EAU and EIU are mouse models of non-infectious uveitis that enables us to manipulate and investigate the mechanics and kinetics of ocular autoimmune disease. The interplay of innate and adaptive responses, driven by macrophages and T cells, underpins immune-mediated pathology associated with non-infectious intraocular inflammation. Additionally, the retina is endowed with regulatory networks to maintain tissue homeostasis and neuronal function and to respond appropriately to danger. However, when homeostasis is lost immune-mediated inflammation and damage can ensue.

At the current time, it is evident that microglia are more than mere bystanders during uveitis. They are suggested to be critical in initiating ocular autoimmunity, with some understanding of basic mechanisms by which they can achieve this. Alterations in critical sensing and regulatory microglial proteins have been shown to have profound effects on the permissibility of autoimmunity and severity of inflammation. Microglia are also known to influence leukocytes within the eye and have the potential to restore tissue homeostasis and resolve inflammation. However, little is known about their role in the later stages of uveitis, whether it is beneficial or detrimental overall, if tissue homeostasis ever returns or how it could be modulated.

Furthermore, no markers for microglial-specific identification have been validated despite many promising candidates. Conventional transgenic models such as the *Cx3cr1^{GFP}* mouse strain are known to tag microglia in addition to subsets of monocytes and other immune cells and this limits its utility in microglial investigation. In contrast, the *Cx3cr1^{CreER}:R26-tdTomato* mouse strain holds promise but is currently unclear if it will overcome shortcomings in microglial identification during inflammation so that the microglial role could be better investigated. Provided it is sensitive and specific, the *Cx3cr1^{CreER}:R26-tdTomato* mouse strain would permit valid usage of established techniques that utilise fluorescence-based detection, and the coupling of these to high-throughput techniques such as mRNA-Seq for unbiased characterisation. The synthesis of these tools with repeatable *in vivo* imaging techniques should ultimately enable discovery of changes to microglia and more understanding about their role in uveitis.

In summary, the hypotheses on which this thesis is based were specifically formulated to focus on determining the transcriptional changes that occur in retinal microglia in response to inflammation, comprising both a technical and biological question:

- An enhanced ability to transcriptionally characterise samples acquired from ultra-low cell numbers.
- Use of this platform to ask whether the homeostatic threshold of retinal microglia remains perturbed in response to acute and chronic inflammation.

To test these hypotheses, this thesis aimed to:

- Optimise and validate a FACS-Seq pipeline that would permit isolation and characterisation of defined/small numbers of immune cells from a single retina.
- Characterise whether the *Cx3cr1^{CreER}:R26-tdTomato* reporter strain was a sensitive and specific tool that would permit the isolation of microglia from retinas with intraocular inflammation.
- Determine what changes occur in the microglial transcriptome in response to acute challenge using the EIU model.
- Determine what changes occur in the microglial transcriptome in response to persistent inflammation using the EAU model.

Chapter II: Materials and Methods

2.1 Mice

C57BL/6J drug and test naïve 7-week-old SPF female mice were obtained from Charles River Laboratories International, Inc. (Oxford, UK). C57BL/6 *Cx3cr1^{CreER}:R26-tdTomato* mice were obtained from Clemens Lange (University of Freiburg, Germany) and re-derived by embryo transfer; breeding colonies of homozygotes were established from the offspring, and homozygotes were crossed with wild-type (WT) mice to generate heterozygotes for experiments. C57BL/6 *Cx3cr1^{GFP/+}* mice were obtained from Heping Xu (Queen's University Belfast; the mice were originally obtained from The Jackson Laboratory, Bar Harbor, ME), re-derived and bred as described for the *Cx3cr1^{CreER}:R26-tdTomato* mice. Genotyping (via PCR) of breeding pairs was performed to validate homozygosity of breeders. Mice were confirmed as negative for the *Rd8* mutation [509]]. The details of mice used for experiments are listed in table 2.1.1.

For genotyping, DNA was extracted from mouse ear notches by overnight digestion in a solution containing 100 mM Trisaminomethane (Tris)-Cl, 5 mM ethylenediaminetetraacetic acid (EDTA), 0.2% sodium dodecyl sulphate (SDS), 200 mM NaCl, and 100 µg/mL proteinase k (P2308-100MG; Sigma-Aldrich, Poole, UK) at 56°C. Samples were then centrifuged and 250 µL of supernatant was transferred to a new Eppendorf containing 250 µL ice-cold pure isopropanol. This was then washed with 75% v/v ethanol (diluent was distilled water [dH₂O]), air-dried, and resuspended in 20 µL double-distilled water (ddH₂O). A PCR mastermix was made, using Phusion Green Hot Start II High-Fidelity PCR Master Mix (F566L; Thermo Fisher Scientific) at 1:2 and primers at 0.2 µM to a total volume of 11.5 µL per sample (adding ddH₂O as necessary). Half a microlitre of the DNA solution was added to each sample and mixed. The samples were then ran through the thermocycler programme for amplification. All run batches included both positive and negative (water) controls for validation. The primer sequences and cycling conditions are detailed in Tables 2.1.2 and 2.1.3, respectively.

After amplification, the product was separated using gel electrophoresis and visualised under UV light. Briefly, 1.5% w/v agarose gels (in Tris-acetate-EDTA [TAE] buffer containing 100 ng/mL ethidium bromide [E7637; Sigma-Aldrich]) were ran for ~22 minutes at 120 V (400 mA). A band (using the *Cx3cr1^{CreER}* primer set) 750 bp in length is observed in a WT mouse (i.e. without insert), and a band 304 bp in length if present. In the case of the tandem dimer tomato (fluorescent protein [tdTomato]) insert in ROSA, a 297 bp band is observed in a WT mouse, and a band of 169 bp is observed if present (Figure 2.1.1).

Experiment (Chapter X)	Disease Model	Strain	Gender	Age (at disease induction)
III	EAU	C57BL/6 (WT)	Female	7 weeks
IV	EIU	C57BL/6	Male	8–10 weeks
V		<i>Cx3cr1^{CreER}:R26-tdTomato</i>		

Table 2.1.1. Details of mice used for experiments. The *Cx3cr1^{CreER}:R26-tdtomato* mice received a course of tamoxifen 4 weeks prior to disease induction. Abbreviations: EAU – experimental autoimmune uveitis, EIU – endotoxin-induced uveitis, WT – wild-type.

Primer Name	Primer Set	Forward/Reverse	Sequence (5'->3')
Cx3cr1CreERF	For genotyping the CreER insert (in the <i>Cx3cr1</i> gene)	Forward	CCTCTAAGACTCACGTGGACCTG
Cx3cr1CreERR		Reverse	GACTTCCGAGTTGCGGAGCAC
Cx3cr1CreERSpec		Reverse	GCCGCCACGACCGGCAAAC
RsTom-F	For genotyping the tdTomato (and stop/ locus of X-over p1 [loxP] sites) insert (in the <i>Rosa26</i> gene)	Forward	CTGTTCTGTACGGCATGG
RsTom-R		Reverse	GGCATTAAAGCAGCGTATCC
RsTomWT-F		Forward	AAGGGAGCTGCAGTGGAGTA
RsTomWT-R		Reverse	CCGAAAATCTGTGGGAAGTC

Table 2.1.2. Primer details for genotyping of the *Cx3cr1^{CreER}:R26-tdTomato* mouse strain. Two primer sets were used to determine the presence of the two genetic inserts in this transgenic mouse strain.

Stage	Temperature (°C)	Length (minutes)
Pre-heat	105	0
Initial (Heat Activation)	94	5
Cycles (repeats 33 times)	Denaturation	94
	Annealing	58
	Extension	72
Final Extension	72	5

Table 2.1.3. Details of cycling conditions used in genotyping the *Cx3cr1^{CreER}:R26-tdTomato* mouse strain. The same conditions were used for both genotyping sets of primers.

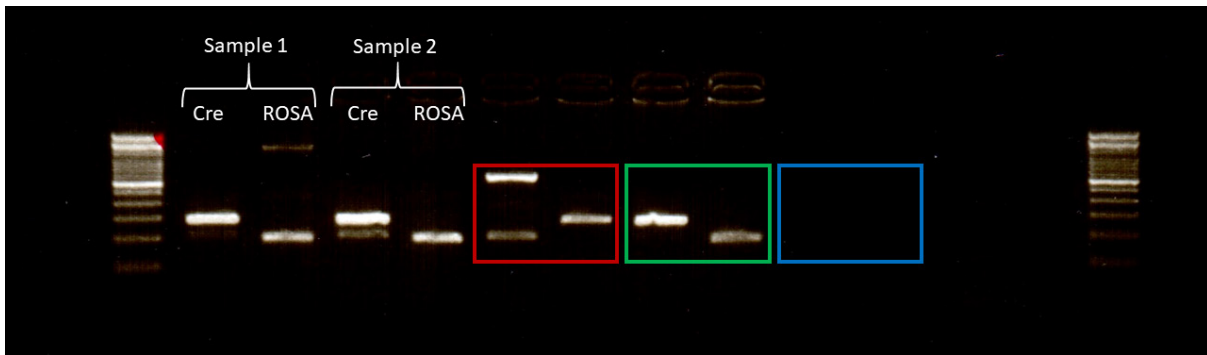


Figure 2.1.1. An example gel output from the genotyping protocol for the $Cx3cr1^{CreER}:R26$ - $tdTomato$ mouse strain. Ladders flanking the samples enable confirmation of expected band size. Output from each of the primer mixes is indicated, and these alternate within the gel meaning that every 2 lanes represents results from a single biological sample. A wild-type control, positive control, and negative (water) control are shown in red, green, and blue, respectively. The ladder used has steps 100 bp in size, starting from 100 (the brightest band nearest to the bottom represents 500 bp).

The *Cx3cr1^{CreER}:R26-tdTomato* mice were weaned at ~4 weeks of age. All mice were housed in groups of 2-5 in Tecniplast 1284L conventional cages (Tecniplast, Buguggiate [VA], Italy) on a 12-hour light/day cycle at room temperature. They also had access to EURodent Diet 22% food (LabDiet, St. Louis, MO) and water *ad libitum*, and environmental enrichment in the form of cardboard play tunnels/huts, wood gnawing blocks and sizzle nests. Welfare-related assessments were performed at least daily. The number of mice in each experiment was chosen so that, despite variability in disease incidence and severity/development of EAU [110] (EIU has a disease incidence of 100%, although there is a rare risk of protocol failure), suitable mice could be selected for sequencing to provide adequate power.

All work was performed within the Animal Services Unit (ASU) at the University of Bristol, where the mice are housed, in concordance with the Animals (Scientific Procedures) Act 1986 (ASPAs) and The Association for Research in Vision and Ophthalmology (ARVO) Statement for the Use of Animals in Ophthalmic and Visual Research.

2.2 Tamoxifen Administration

Tamoxifen (T5648; Sigma-Aldrich) was dissolved in corn oil (C8267; Sigma-Aldrich) to a concentration of 21 mg/mL or 5 mg/mL, for subcutaneous injection and topical administration respectively. The solutions were freshly prepared by overnight incubation in an orbital shaker at 42°C and 300 rpm. Mice were injected with 200 µL subcutaneously (100 µL into both the lower [inguinal] left and right quadrants using a 25-gauge [25G] needle) on days 1 and 3; alternatively, mice were administered 10 µL (using a Gilson pipette) topically to the eye 3 times daily (minimum gap of 2 hours between dosing) for up to 4 days (post-optimisation, a 3-day protocol was used). The subcutaneous regime was provided by Clemens Lange (with the *Cx3cr1^{CreER}:R26-tdTomato* mice) whilst the topical regime was obtained from a paper using CreER mice and induction of recombination within the eye [510]. The local method of administration was compared to subcutaneous in case extraocular recombination occurred within long-lived cells that entered the eye during inflammation.

2.3 In Vivo Models

2.3.1 Induction of EAU

Female mice were immunised for disease at 8 weeks of age (typical mean weight of 19.3 ±1.0 g), with constrained randomisation within blocks (cages, which represent mice from the same litter) being performed in Excel (Microsoft, Redmond, WA) to select unimmunised mice as

naïve controls. An experimental unit is considered a collection of mice that were all immunised (or kept unimmunised) at the same time.

Mice were immunised by injecting 500 µg/mouse hRBP-3₁₋₂₀ or 400 µg/mouse RBP-3₆₂₉₋₆₄₃ in phosphate-buffered saline (PBS) with 2% v/v dimethyl sulfoxide (DMSO). This was added 1:1 v/v to CFA; 1 mg/mL supplemented with 1.5 mg/mL *Mycobacterium tuberculosis* H37 RA (Becton Dickinson [BD] Biosciences, Oxford, UK), to a total volume of 100 µL/mouse, subcutaneously. Mice were also injected with 1.5 µg *Bordetella pertussis* toxin (Sigma-Aldrich), diluted to a volume of 100 µL in PBS, intraperitoneally.

2.3.2 Induction of EIU

Prior to anaesthesia, mouse pupils were dilated using topical tropicamide 1% w/v and phenylephrine 2.5% w/v (Minims; Chauvin Pharmaceuticals, Romford, UK).

The mice were then anaesthetised by intraperitoneal injection of 90 µL/10 g body weight of a solution containing 6 mg/mL ketamine (Ketavet; Zoetis Ireland Ltd., Dublin, Ireland) and 2 mg/mL Xylazine (Rompun; Bayer plc, Newbury, UK; diluent was dH₂O). This anaesthetic combination and route of administration was used as it is a well-established and safe method of anaesthesia, used both within and beyond our group, to provide sufficient sedation for imaging/intravitreal injections whilst allowing for relatively quick recovery.

Mice were selected for injection using randomisation as described before. The eye (left or right) was also randomised.

Intravitreal injections were performed under an operating microscope by Dave Copland [97]. In summary, 2 µL volume of PBS containing 10 ng LPS from *E.coli* 055:B5 (Sigma-Aldrich) was delivered into the intravitreal space via the pars planar. The eye was proptosed and held in position with a pair of forceps, then carbomer eye gel 0.2 % w/w (Viscotears; Novartis Pharmaceuticals, Camberley, UK) was applied and a circular coverslip (7 mm diameter) placed over the eye. A 33G hypodermic needle, mounted on a 5 µL Hamilton syringe (CAL7633-01; Hamilton, Reno, NV), was inserted approximately 2 mm circumferential to the corneal limbus with a ~45° injection angle. The needle bevel was guided into the VB, stopping between the lens and the optic disc (from the relative viewpoint of the surgeon, this is above/covering the optic disc – approximately 1.5 mm from the site of insertion), and 2 µL of LPS (at 5 ng/µL in PBS) was slowly injected. The needle was held in-place briefly (to reduce the amount of reflux of injectate) and removed. Post-injection, the site was treated with 1% w/w chloramphenicol ointment

(Martindale Pharma, Romford, UK) and the globe repositioned by release of the forceps. Post-injection, mice were monitored for vital signs (breathing, movement, heart rate, reflexes) and kept on a heated pad until recovered.

2.4 *In Vivo* Imaging Techniques

Disease progress was monitored using the Micron IV: Retinal Imaging Microscope (Phoenix Research Labs, Pleasanton, CA). Imaging was performed in the morning, working in ascending mouse number within each cage and by alphabetical cage lettering.

The Micron IV had the following attachment: OCT1. Prior to imaging, the Micron IV charge-coupled device (CCD) was calibrated using the auto-white balance, and the OCT attachment was calibrated in accordance with the manufacturer's protocol. For brightfield fundus images, the gain was set to +3 dB, frames per second (FPS) to 15, and a 544/211 exciter filter with 700 nm shortpass emission filter was used. For fluorescence imaging, the brightness, gain, and FPS were adjusted so that (using the log histogram function of the Streampix software) the brightest non-dead pixels (representing the brightest spots of the fluorescently-labelled cells) were at an intensity just above 200: for tdTomato imaging, this typically required maximum brightness on the analogue dial, a gain of +11 dB, and FPS of 2 (or a gain of +18 dB and FPS of 4); for green fluorescent protein (GFP) or fluorescein imaging this typically required maximum brightness, a gain of +15 dB, and FPS of 4. Gain-normalised settings (to the typical parameters – for comparison across a time-course) were acquired for each retina, in addition to tuned settings for each eye so that images were not under- or over-exposed and would be suitable for deconvolution or other image analysis. The exciter/emission filter combinations used for fluorescent imaging is detailed in Table 2.4.1. For OCT, the parameters were defined according to the manufacturer's protocol, and all scans were taken 30 times in rapid succession and averaged. Full-length line B-scans were taken horizontally and vertically with the optic disc centred; other features of interest, identified through fundal imaging, were also scanned. Full-length circle B-scans were taken centred around the optic disc. Additionally, 512 half-length line B-scans running superiorly (with respect to the target box area; scans obtained without averaging) can be acquired in quick succession for acquisition of a 3D, or volume, scan. Images were stored in the tagged image file format (TIFF).

Filter Position	Exciter/Emission (Barrier)	Specification	Λ Range (nm)	Source
1	Exciter	544/211 bp	438.5-649.5	Stock (Phoenix Research Labs)
	Emission	700 sp	-700	
2	Exciter	468/35 bp	451.5-486.5	
	Emission	488 lp	488-	
3	Exciter	550/25 bp	537.5-562.5	Edmund Optics (Barrington, NJ)
	Emission	590 lp	590-	
4	Exciter	715 lp	715-	Phoenix Research Labs
	Emission	512/30 bp	497-527	Edmund Optics

Table 2.4.1. Filter information for the exciter/emission positions (on the filter wheel) of the Micron IV: Retinal Imaging Microscope. Exciter and emission filters can be used independently of each other. Common combinations of filters used (x - y , where x is the exciter and y is emission) include: 1-1 (brightfield), 3-3 (tdTomato), 2-4 (GFP/Fluorescein). Excitation filters were 25 mm in diameter and mounted, with a max thickness of 5 mm; emission filters were 12.5 mm in diameter and unmounted, with a max thickness of 3.5 mm. Filters were installed according to the Micron IV manual.

Prior to imaging (both techniques), mouse pupils were dilated as described previously.

When using the Micron IV, mice were anaesthetised (as described previously; in some cases, a lower dose of the anaesthetic solution was administered in conjunction with isoflurane by inhalation), transferred to the animal stage, and carbomer eye gel was administered for coupling to the objective lens. The mouse was positioned so the eye was perpendicular and near to the lens with the iris roughly equidistant from pupil to sclera on the viewing plane on the computer monitor (the ideal position is to have the optic disc centrally-positioned with an unobscured view of the retina surrounding – with the space between optic disc and iris equidistant – this roughly corresponds to the iris-sclera positioning described above, but can vary slightly based on anatomical variation found between mice; some optic discs are found centrally to this position, but are usually slightly offset). An image was captured (for QC purposes), and then the lens was moved closer to the eye so that the retina occupied the full image space. The focus and illumination were adjusted (for brightfield – for fluorescent imaging, the settings are described above) to obtain a good colour balance and images were captured. Videos, whilst slowly rotating the focus dial (starting from above the focal-plane of the retina until below) were also captured to assist in the acquisition of the sharpest/most in-focus images. Post-imaging, mice were monitored for vital signs (breathing, movement, heart rate, reflexes) and kept on a heated pad until recovered.

2.5 Flow Cytometry/Fluorescence-Activated Cell Sorting

2.5.1 Batch Processing

Mice were euthanised by cervical dislocation, eyes enucleated and spleens dissected, and both were placed in PBS on ice. The eyes were dissected under a microscope to isolate the retinas; a 27G needle was poked through the corneal limbus, 100 μ L of ice-cold PBS was added, and then micro surgical scissors were used to cut along the remainder of the boundary. The anterior fragment, along with the lens, was removed and discarded. The retina was then gently teased apart from the RPE and, with the PBS, transferred to an Eppendorf where it was mechanically disrupted by scratching along the surface of an Eppendorf rack. The retinas were transferred to a 60 μ m nylon mesh filter plate and centrifuged at 300 xg and 4°C for 5 minutes. The filtrate was then transferred to a V-bottom 96 well plate for staining. Spleens were prepared by mashing, transfer through a 70 μ m cell strainer and centrifuged at 400 xg and 4°C for 3 minutes (subsequent centrifugation steps use these settings, unless otherwise stated). The supernatant was discarded, and the pellet was resuspended in 10 mL Ammonium-Chloride-Potassium (ACK)

lysing buffer (8.29 g/L NH_4Cl , 1 g/L KHCO_3 , 372 mg/L Na_2 -Ethylenediaminetetraacetic acid [EDTA] in dH_2O) for 3 minutes on ice (to lyse erythrocytes), centrifuged and the supernatant discarded, re-suspended in 5 mL PBS and 200 μL transferred to the plate. A 200 μL aliquot of the spleen cell suspension was killed by heating to 95°C for 15 minutes.

For staining, the V-bottom plate was centrifuged, the supernatant discarded, and each well re-suspended in 100 μL 2.4G2 cell supernatant (or 50 μL Fc block [#553142 (BD Biosciences)] at 1:50) and incubated at 4°C for 10–15 minutes. 100 μL of an antibody cocktail (or 50 μL if using the Fc block) containing fluorochrome-conjugated mAbs (see Table 2.5.1) was added and incubated at 4°C for 20–30 minutes. One μL of mAbs were also added to one drop of compensation beads (OneComp eBeads [Thermo Fisher Scientific], Anti-Rat Ig, κ /Negative Control Compensation Particles Set [BD Biosciences], or AbC total antibody compensation bead kit [Thermo Fisher Scientific]) to prepare single-stain controls for compensation; for live-dead compensation, a mix of live and heat-killed spleen cells were used re-suspended in 7-aminoactinomycin D (7AAD) at 1:500 (Thermo Fisher Scientific) diluted with staining buffer. Fluorescence minus one (FMO) controls were also prepared. Post-staining, the plate was centrifuged and the supernatant discarded, re-suspended in 200 μL staining buffer, and centrifuged with supernatant discard as a wash step. Cells were re-suspended in 250 μL 7AAD as before and kept on ice until sorting on a BD Influx Cell Sorter (in some sorting experiments DRAQ7 [DR77524; Biostatus, Shepshed, UK] was added instead – for flow cytometry, the 7AAD was added in conjunction with the antibodies); beads were re-suspended in staining buffer. Data was acquired using a BD LSRFortessa X-20 flow cytometer.

Target (synonym)	Fluorophore	Clone	Supplier
B220	FITC	RA3-6B2	BD Biosciences
CD3	APC	145-2c11	
CD45	PE-Cy7	30-F11	
Gr-1 (Ly6C/Ly6G)	Alexa-700	RB6-8C5	
CD11b	APC-Cy7	M1/70	
Milr1 (Allergin-1)	BV421	TX83	
C5ar1	BV510	20/70	
CD44	Super Bright 600	IM7	Thermo Fisher Scientific
Siglech	BV650	440c	BD Biosciences
Fas (CD95)	BV711	Jo2	
Mertk (Mer)	BV786	108928	
Slamf1 (CD150)	FITC	9D1	Thermo Fisher Scientific
Bst2 (CD317)	PE-eFluor610	eBio927	
Lair1	PE-Cy5.5	113	Novus Biologicals*
P2ry12	APC	S16007D	Biolegend
CD4	FITC	RM4-4	BD Biosciences
CD8	PE	H35-17.2	Thermo Fisher Scientific

Table 2.5.1. A list of monoclonal antibodies used for flow cytometry. *Novus Biologicals (Centennial, CO). Abbreviations: Milr1 – allergin-1 precursor, Siglech – sialic acid binding Ig-like lectin H, Fas – fas cell surface death receptor, Mertk – tyrosine-protein kinase mer precursor, Slamf1 – signaling lymphocytic activation molecule, Bst2 – bone marrow stromal antigen 2 precursor, Lair1 – leukocyte-associated immunoglobulin-like receptor 1, FITC – fluorescein isothiocyanate, APC – allophycocyanin, Cyx – cyanine-x, BV – brilliant violet, PE – phycoerythrin.

Cells were sorted (using a BD Influx Cell Sorter) into 0.2 mL tubes containing 0.05 μL RNase inhibitor, 0.95 μL lysis buffer, and a variable amount of nuclease-free water depending on the number of cells collected – $9.5 - \left(\frac{x}{850} * 3\right) \mu\text{L}$, where x is the number of cells you are sorting (e.g. 600 cells occupy 2.1 μL , so 7.4 μL ddH₂O is added; components of the SMART-Seq v4 Ultra Low Input RNA Kit for Sequencing; Takara Bio USA, Inc., Mountain View, CA) as per the user manual (to calculate the volume of nuclease-free water, preliminary experiments determined the volume of 850 microglia to be 3.0 μL). Sorting was performed by the University of Bristol Flow Cytometry Facility. Samples were sorted in a constrained randomised order in blocks; blocks were made as small as possible and consisted of a balance of every tissue type and disease status (naïve or immunised) so that observable effects between groups were not due to a time-/order-dependent effect of when they were sorted.

Gating strategies for cells are shown and described in the relevant results sections.

2.5.2 Single Sample (or Small Number Batch) Processing

In a variation of the above protocol, it is possible to prepare samples as required/in batches to minimise mRNA sample degradation when performing FACS. Some sample degradation was observed in early experiments, and therefore batches of samples (for cell-surface staining prior to sorting) were restricted to a maximum of 8 at a time (with later batches of samples being staggered and prepared later [i.e. whilst the first batch was sorting]).

For samples where sorting was performed purely using fluorescent markers (e.g. tdTomato or GFP), it was possible to prepare the samples by dissecting, scratching, spinning through the filter plate, adding the DRAQ7 and sorting with minimal preparation time. In these experiments, samples could be prepared individually (or a pair if taking both retinas from the same mouse) but it was determined that batches of 2-4 retinas worked best as single retina preparations were not very practicable, and that these small batches were fast enough to obtain high quality cDNA output for all samples.

2.6 Sample and Library Preparation for Sequencing

Samples were prepared for sequencing through use of the SMART-Seq v4 Ultra Low Input RNA Kit for Sequencing, according to the user manual, to generate cDNA from the mRNA and amplify by Long Distance PCR; for the latter step, 16 cycles were used (for 600 cells) as determined by an optimisation experiment (see Chapter III; 15 cycles was optimal for 1,000 cells). Subsequently, the cDNA was isolated using the Agencourt AMPure XP Kit (Beckman

Coulter, Brea, CA) and quantified using the Agilent High Sensitivity DNA Kit on an Agilent 2100 Bioanalyser (Agilent Technologies, Santa Clara, CA), by the University of Bristol's Genomics Facility, as per the protocols in the SMART-Seq v4 Ultra Low Input RNA Kit for Sequencing user guide. The library was then prepared by the Genomics Facility using the Nextera XT DNA Library Preparation Kit (Illumina Inc., San Diego, CA), following the Nextera kit reference guide, using 150 pg cDNA as the starting input.

2.7 mRNA-Sequencing and Data Analysis

Samples were sequenced to depths of up to 33.3 million single-end 75 nt length reads per sample using the Illumina NextSeq 500/550 High Output v2 kit (75 cycles) on an Illumina NextSeq 500 Sequencing System. Based on new data, and depth vs. replicates data published elsewhere (as described in Chapter III), a sequencing depth of ≥ 11.1 million reads per sample was determined as optimal (the SMART-Seq kits allow for preparation of samples in multiples of 12 [where kits can be used singly to mitigate the risk of contamination from "double-dipping"], and the sequencing flow cell provides up to 400 million reads [$400/36 = 11.1$], making this choice a compromise between depth and kit usage). Image analysis, base calling, and generation of sequence reads were produced using the NextSeq Control Software v2.0 (NCS) and Real-Time Analysis Software v2 (RTA). Data was converted to FASTQ files using the bcl2fastq v2.20 software (Illumina Inc.).

Sequencing data was uploaded to a cluster of computers for alignment and initial analysis; the cluster consisted of a master (consisting of a 12-core central processing unit [CPU] and 32 Gb cRAM) and 2 worker nodes (consisting of a 16-core CPU and 64 Gb cRAM each) running on a 64-bit linux operating system (v3.13.0-40-generic). The data was then processed through an analysis pipeline using the Partek Flow (Build version 6.0.17.0614; Partek Inc., St. Louis, MO) software with the following task nodes (non-default parameters are specified in brackets): Trim adapters (inputting Nextera XT Index Kit v2 adapter sequences as provided by Illumina [464]), Trim bases (From 3' end, 1 base), Trim bases (from 3' end with minimum quality score [Phred] of 30), Align reads using STAR (2.5.3a using mm10 as the reference index), Quantify to transcriptome (Partek E/M using mm10 – Ensembl Transcripts release 89 as the reference index).

The data output from Partek Flow was then downloaded to a local computer, and further analysed using Partek Genomics Suite (PGS; version 6.6, Build 6.16.0812). PGS normalises data using the RPKM approach and performs differential gene expression analysis using an analysis of variance (ANOVA) model; a gene is considered differentially-expressed if it had an FDR step-

up p value ≤ 0.05 and fold-change $\geq \pm 2$. The fold-change and p-values were then imported into IPA version 01-13 and analysed according to the manual. PGS and IPA were both used to generate figures. A summary of the analytical pipelines is shown in Figure 2.7.1.

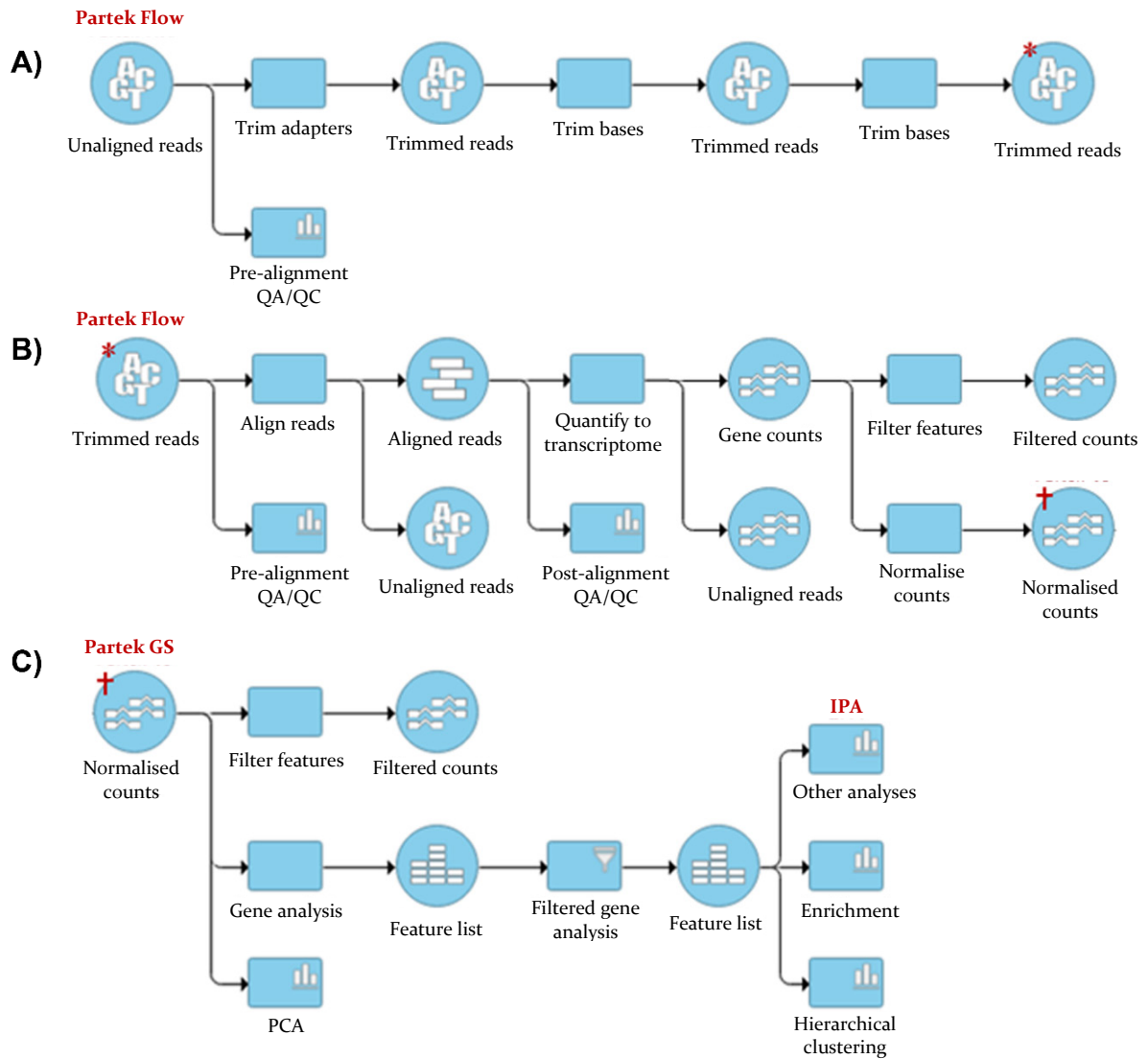


Figure 2.7.1. The bioinformatics pipeline for processing and analysing the mRNA-Seq data. A) The bioinformatics analysis shown starting with the unaligned reads and pre-alignment processing, B) alignment, alignment QC and quantification of reads, and C) differential gene expression analysis (DGEA) and filtering/visualisation; Partek Flow was used for pre-processing, alignment, and quantification of the data whilst Partek Genomics Suite (PGS) was used to normalise the data and perform DGEA. Both PGS and Ingenuity Pathway Analysis (IPA) were used for visualisations and further analysis of the data and pathway enrichment.

2.8 Quantitative PCR

The remaining cDNA generated from the sorted cells was used for transcript-level validation. qPCR was performed using the TaqMan Universal Master Mix II, with UNG (4440038) and TaqMan gene expression probes (4331182) on a Quantstudio 3 Real-Time PCR system (A28137; all products from Thermo Fisher Scientific). Samples were run in technical duplicate, using 1 ng as the input amount, and analysed using the equation: $2^{Cq(\text{mean (control)}) - Cq(\text{sample})}$.

The probes used were: *Bst2* (mm1609165_g1), *C5ar1* (mm00500292_s1), *Cd44* (mm01277161_m1), *Fas* (mm01204974_m1), *Lair1* (mm00618113_m1), *Mertk* (mm00434920_m1), *Milr1* (mm01242703_m1), *P2ry12* (mm01950543_s1), *Siglech* (mm00618627_m1), *Slamfi* (mm00443317_m1).

2.9 Confocal Laser-Scanning Microscopy

Mice were euthanised by cervical dislocation, their eyes nucleated and placed in 4% v/v PFA (in PBS) for 1 hour. The anterior components were removed (to isolate the “eyecup”) by dissection under a microscope as described previously, with the following modification: the 27G needle was poked through the sclera, circumferential to the corneal limbus (as opposed to at the corneal limbus), with micro surgical scissors used to cut the remainder.

After isolation, the eyecup is carefully placed into an Eppendorf containing 100 μ L of a solution containing 1% v/v BSA and 3% v/v Triton x-100 (both Sigma Aldrich) in PBS and rocked on a 3D rocker at room temperature and 70 rpm for 20 minutes. The retinas were washed two more times, before blocking for 2 hours in the same solution containing 5% v/v normal goat serum (Vector Laboratories Ltd., Peterborough, UK). Eyecups were then incubated at 4°C overnight with a rabbit anti-mouse anti-RFP mAb (600-401-379; Rockland Immunochemicals Inc., Limerick, PA) and for target validation experiments a Super Bright 600-conjugated anti-mouse CD44 mAb was used in combination. They were washed three times, and then incubated overnight (as per primary antibodies) with the secondary antibody goat anti-rabbit Alexa-633 (A21070; Thermo Fisher Scientific). Eyecups were then washed three more times.

The retina was then isolated from the eyecup by gently teasing as described before. However, micro surgical scissors were used to cut the ON (as opposed to tearing it – careful handling and preservation of the structure is necessary for confocal preparations). The retina was then cut in four places by incising from the peripheral retina one-third to halfway to the ON (the incisions are on imaginary horizontal and vertical lines running perpendicular through the ON). They

were then flat-mounted in Vectashield hard-set antifade mounting media (H-1400; Vector Laboratories Ltd.) by placing the sample in the centre of a “sticky ring” on a microscope slide or coverslip and then attaching a coverslip on top. A secondary seal, using nail varnish, can be added to the edge of the interface between slide and coverslip. Slides were kept at 4°C until imaged on a Leica SP5-AOBS confocal laser scanning microscope attached to a Leica DM I6000 inverted epifluorescence microscope (Leica Microsystems Ltd., Wetzlar, Germany). Images were acquired with an xy pixel size ≤ 200 nm, and a z-step size of ≤ 400 nm.

2.10 Analysis

2.10.1 Image Processing

Huygens professional software (Scientific Volume Imaging B.V., Hilversum, The Netherlands) was used to deconvolve the Micron IV fluorescent images and fluorescence microscopy (Figure 2.10.1). For the Micron images, the following parameters were used: lens immersion = 1.343 (refractive index of the 0.2% w/w carbomer eye gel [511]), embedding = 1.377 [512], peak emission = 581 nm, numerical aperture = 1.25, and xy pixel size of 130 nm; the background was estimated at 2 and a signal-to-noise ratio of 15 was used. Hot pixel correction (with a sensitivity of 4) was used prior to deconvolution. For fluorescence microscopy, the parameters were imported from the microscope and the default settings were used.

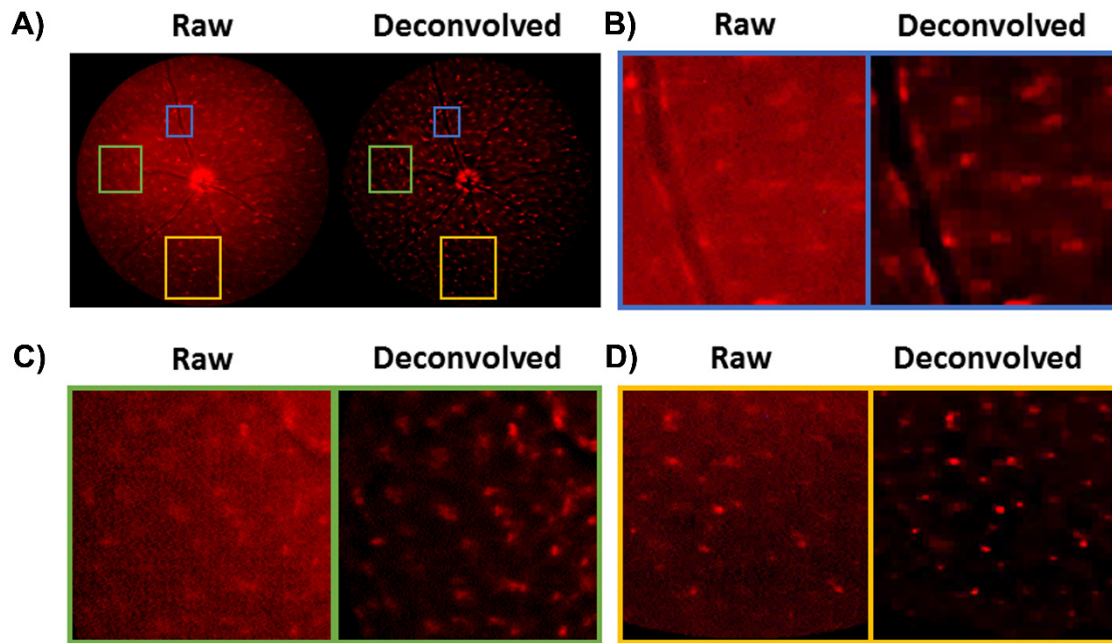


Figure 2.10.1. *tdTomato fluorescence images of a mouse retina both pre- and post-deconvolution using Huygens software. A) Fluorescent fundal images were acquired from naïve $Cx3cr1^{CreER};R26$ -tdTomato mice 4 weeks following tamoxifen administration. Paired raw and deconvolved images show how the software algorithm improves the image detail quality. Full fundal distribution of microglia and close-up images of cells located in **B)** peri-vascular, **C)** central and **D)** peripheral retinal regions. Due to the resolution limits of the Micron IV ($2\ \mu\text{m}$) it is not possible to readily visualise all but the largest of the ramified processes; ramified processes are well-known to be typically 0.5 – $1.0\ \mu\text{m}$ in diameter.*

Microscopy images were processed using the Leica LAS X software (Leica Microsystems Ltd.) and FIJI (a distribution of ImageJ [513]). Other images, and figures, were processed using Photoshop (Adobe Inc., San Jose, CA) and Powerpoint (Microsoft).

2.10.2 Statistical Analysis

Data were analysed using GraphPad Prism 7 software (GraphPad Software Inc., San Diego, CA). The One-way ANOVA with Tukey's multiple comparisons test was used to compare multiple groups of data to a control group. FDR step-up correction was also applied. A p value ≤ 0.05 was considered significant. For a comparison between two groups, the t-test was used. For correlative measures, the Pearson's test was used.

Chapter III: Optimisation of Ultra-Low Input mRNA-Seq and Bioinformatic Analysis

3.1 Introduction

3.1.1 *The Challenge of Ultra-Low Input RNA*

It has been previously shown that the mouse retina contains approximately 1,500 microglia using histological-based approaches [514]. Flow cytometric analysis has indicated it is possible to reliably recover 1,000 microglia per retina [413]. However, it is well-recognised that cell sorting may recover as low as 30% of the cells present in the original sample, meaning that recovery numbers could be as low as 450 microglia per retina [515]. This low number limits the use of many mRNA-Seq sample and library preparation kits which typically require much higher input amounts of mRNA (corresponding to $\geq 10,000$ cells). Furthermore, pooling of multiple retinas (≥ 10) is not feasible/practicable for several of reasons: 1) the time required isolate these high numbers means that the mRNA may be degraded or of poor quality for input, potentially resulting in very low numbers of samples obtained and poor statistical power or failure of experiments entirely; 2) the use of large numbers of mice to obtain limited data could be considered unethical/excessive and not in accordance with the principles of the 3Rs [94]; 3) the breeding, handling, and effective monitoring of mice with disease may not be feasible in the numbers required; 4) information about disease grading and the ability to associate this with the transcriptome will be greatly limited, reducing the utility of the hypothetical dataset.

After careful consideration and support from the University of Bristol Genomics Facility, the SMART-Seq Ultra Low Input RNA kit by Clontech (with Nextera XT DNA Library Preparation kit by Illumina) was adopted for our requirements of low cell input mRNA-Seq [516-518]. The pipeline (which is recommended by Illumina for single-cell and ultra-low input) is summarised in Figure 3.1.1 but is discussed in greater technical detail within Appendix I.

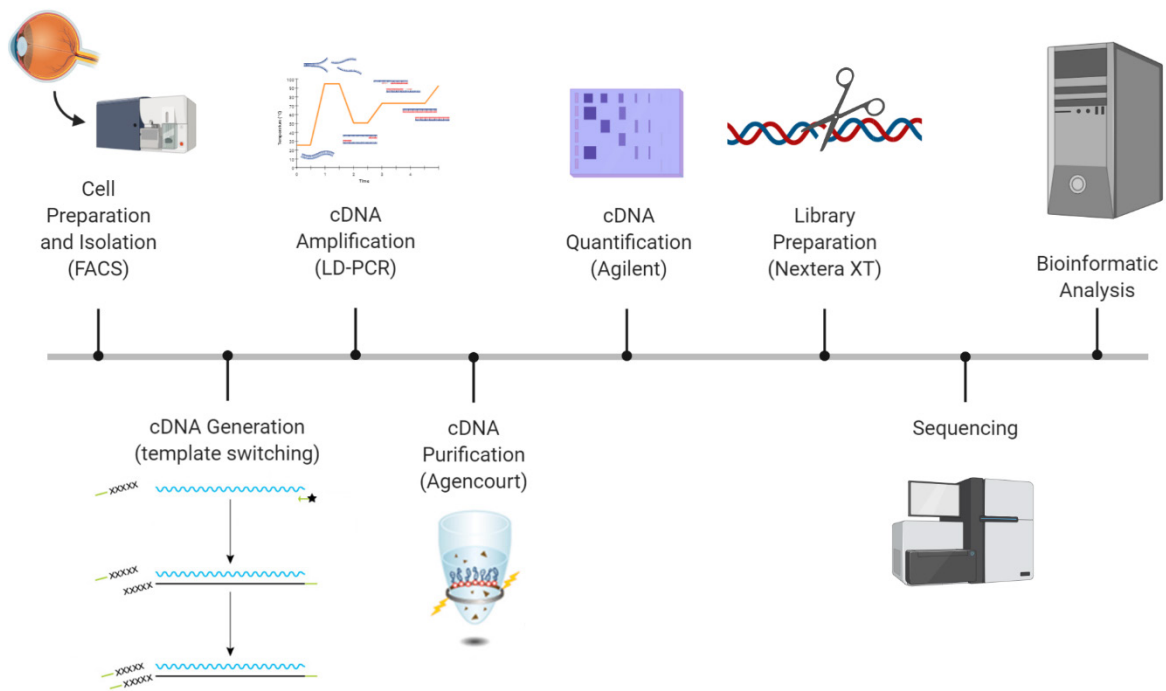


Figure 3.1.1. An overview of the SMART-Seq v4 ultra low input RNA kit pipeline. Firstly, cells are prepared for isolation by fluorescence-activated cell sorting (FACS). From the poly(A) tail, copying of mRNA is performed in addition to template-switching to incorporate primer sequences flanking the mRNA transcript. This is then amplified – to increase yield – utilising long-distance polymerase chain reaction (LD-PCR), purified utilising magnetic beads (Agencourt), and quantified utilising a high-sensitivity gel electrophoresis approach (Agilent). Lastly, the cDNA is processed for library preparation using the Nextera XT kit and sequenced on an Illumina machine ready for data analysis. This figure was prepared utilising modified images from both the SMART Seq v4 kit and Agencourt manuals.

3.1.2 Experimental Design Considerations

Design of mRNA-Seq experiments, but also any experiments involving high-throughput techniques, are a subject of intense debate. It is possible (and has indeed happened) for an mRNA-Seq experiment to be confounded, and yet nonetheless be accepted for publication after vigorous peer review. Later, after replication experiments, these claims have been retracted and the experiment identified as confounded in some fashion [519]. More generally, problems with reproducibility are common within the biomedical sciences [520]. Fisher's book on the design of experiments notes that the two grounds upon which evidence is disputed are "that the interpretation of the experiment is faulty" (i.e. that the Author is "incompetent in statistical technique") or that "the experiment itself was ill designed or... badly executed" [521]. The book also discusses three key principles of design: randomisation, replication, and blocking. Approaches to data analysis are discussed later, but it holds the advantage of capability to repeat/permutate an unlimited number of times. Therefore, if the analysis is believed found wanting by reviewers it is relatively easy for an Author to correct this.

In contrast, a possible confounder in experimental design may be difficult to identify (particularly in the absence of information about the experimental design within the manuscript), but also impossible to correct without replicating the entire experiment at huge cost to the Author. This high cost may have contributed to whether an Author has performed repeat experiments of their initial sequencing or high-throughput experiment in the initial instance. It is also not practicable (or expected) for an Author to validate all of the findings of their experiment (e.g. performing orthogonal validation on 1,000 differentially-expressed genes [DEGs] would be far too costly in terms of time and resources for a lab), meaning only a small subset of DEGs would be validated (likely the most promising DEGs identified by the high-throughput technique). A reviewer must therefore have very strong grounds to make an objection based on experimental design, and criteria such as the number of replicates is relaxed in lieu of the fact that sequencing is both difficult and expensive to perform (for example, the encyclopedia of DNA elements [ENCODE] guidelines suggest two replicates for mRNA-Seq experiments, but that it is possible to justify only one replicate [522]). This explains how it is possible (or perhaps easier) for confounded studies using high-throughput techniques to be published. In typical studies, a minimum of three biological replicates is usually expected, and for randomisation to be performed. With one or two replicates, and difficult-to-obtain samples (e.g. human tissue from a biobank) it may not be possible to randomise or effectively block or

even obtain a reasonable estimate of the variation, meaning there can arguably no basis for inference [523].

Sequencing is a rapidly-developing field, and whilst attempts have been made to suggest standardised reporting and design/execution of experiments (e.g. depth) – i.e. the ENCODE guidelines [522] – these are far from complete and have become obsolete quickly (for example, the field of single-cell [sc-]mRNA-Seq has now emerged and only some of the ENCODE guidelines would be applicable/relevant to those experiments). Nonetheless, the best practices by other researchers – that will be incorporated into this work where possible – will be described herein.

Batching Effects

With regards to mRNA-Seq, the multiple sources of variation can be separated into biological/experimental variation (i.e. due to the intrinsic variability of organisms and the interventions being investigated) and “batch effects” – the sources of variation unrelated to the biological/experimental variables of the study (e.g. usage of different batches of reagents, flow cells, lanes on a flow cell, litters of organisms [resulting in a different microbiome], a different researcher or lab performing the experiment, etc) [524]. Batch effects are the variability that well-designed experiments attempt to minimise and/or mitigate. With highly dimensional data such as mRNA-Seq, batch effects can be readily identified using dimension-reduction visualisations (e.g. PCA, where different “batches” will separate into different regions of the plot as it represents a major source of variation). Batch effects can cause significant problems for the analysis of data, lead to artefacts, and may render the data relatively meaningless/invalid (in a worst-case scenario) with regards to the original biological questions being asked.

Batch effects can be separated into three main groups: biological variation, technical variation, and measurement error [525]. With adequate blocking, randomisation, and replication through a well-designed experiment, these effects can be mitigated. Furthermore, it is possible to use computational methods to (at least partially) correct for batching effects, but to be successful it requires that a form of blocking and replication be incorporated into the experimental design prior to data acquisition. These approaches are further discussed later but the basic concept of batch effects and correction are shown in Figure 3.1.2.

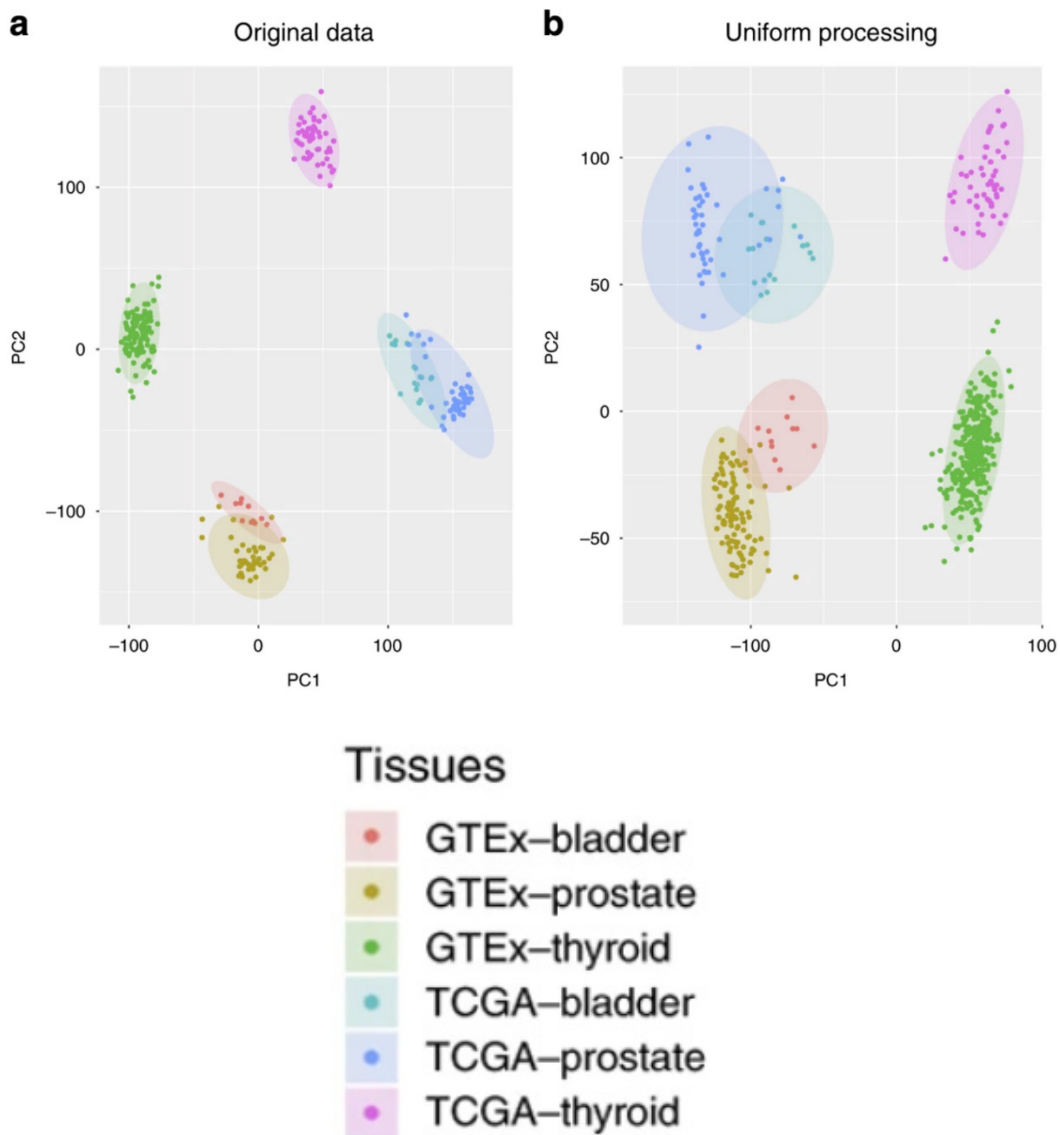


Figure 3.1.2. Visualisation of batching effects within mRNA-Seq datasets. A) PCA plot of original processed mRNA-Seq data (each atlas utilised different processing strategies) highlights a batch effect between the two compendiums and represents most of the variability observed within the dataset (PC#1; GTEX and TCGA). B) PCA plot of data when processed uniformly helps to reduce the batch effect partially but not fully because samples isolated from the same tissue map with greater distance than samples isolated in the same lab (reduced variation results in batching effects observed on PC#2 as opposed to PC#1). Abbreviations: GTEX – genome tissue expression, TCGA – the cancer genome atlas, PCA – principal component analysis. Adapted from [526] and used under licence (CC BY 4.0).

Biological variation can be caused or introduced when experiments use organisms that may have differences prior to the experiment. For example, differences in the microbiome of organisms could be caused by organisms originating from different litters, or being kept in different cages (in the case of animal research) and this could have different effects on organismal response to treatments, induction of disease models (i.e. incidence and/or severity), and many other measurements [527]. A simple, but confounded experiment design may involve treatment of one cage of mice and use of a different cage of mice as a control. In this situation, differences in the data obtained could be due to the treatment, or due to the cage effect, or a combination of both; due to the experimental design it would be impossible to delineate. A more balanced (but complex) design would involve treatment of 50% of mice from each cage so that the potential cage effect is blocked (or mitigated) across the samples. This concept is visualised in an experimental design schematic (Figure 3.1.3). In large-scale studies with multiple experimental groups, experimental design could become exponentially more complicated and impractical (if not impossible – e.g. with organisms in cages of 4, based on litter, any experiment with 5 or more experimental groups would be impossible to block in a perfect manner) to perform adequately, and highlights a potential major issue when scaling-up.

Technical variation refers to artefacts that are not due to biological variation but occurs prior to acquiring the data (i.e. introduced during mRNA isolation/amplification and other pre-processing required). This can include a large variety of factors such as the batch of reagent used, when and how many times the mice were anaesthetised, and many more. It may also include the variability (precision) of inducing a disease model, performing a technique on the model organism, or differences in the ability of the researcher to isolate a tissue in a pure manner. The simplest way of blocking for these is to allocate samples from each experimental group across the various runs/experiments (if running more than one experiment – if running one experiment these factors will require less consideration) so that any technical variation is equally-spread and successfully mitigated. Where possible, organisms should be treated as equally as possible with all handling and interventions. Samples from an experiment could also be acquired in a random (or random but balanced) order as well for example. The same researcher/team could also be used (where possible) to help minimise the technical variation.

Measurement error has well-established practices for its mitigation, and delve into the intricacies of the sequencing technology and are therefore summarised within Appendix I.

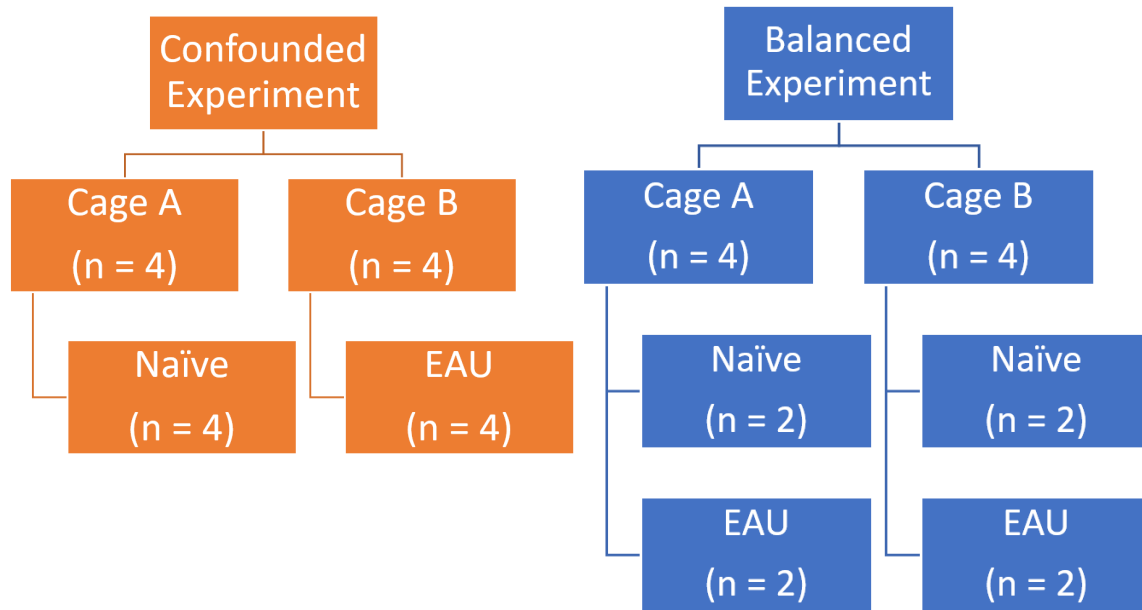


Figure 3.1.3. Examples of good and poor experimental design with regards to treatment and cage allocations. In the confounded design, experimental groups are allocated according to the cage in which mice reside (this typically represents the litter they were derived from). When performing analysis, differences between cage conditions and/or litter microbiomes could confound the results. In the balanced experiment, all experimental groups are allocated across each cage in a constrained randomised fashion and ensures results obtained are not due to litter or cage confounding effects.

The overall implications are that experimental design and good practices for mRNA-Seq is continually evolving, and that there are no formal up-to-date standardised design procedures. Nonetheless, there are good principles of experimental design (some adopted from the wider field that have been well-known for decades) that can be implemented with careful planning. In larger-scale experiments, it becomes increasingly difficult to satisfy all of these requirements in a fully balanced manner. Therefore, a compromise between the perfect experimental design and practicability may be pragmatic (for example, if a design became too complex the probability of mistakes by a researcher may increase – such as which mice receive what treatments/dose – which would be more confounding to an experiment than a minor design imperfection), and in the case of large-scale studies replication (provided the experiment is reasonably designed, i.e. has no major flaws) will help to mitigate these. Overall, experimental design should not be overlooked, and should be carefully included in any experiment using high-throughput technologies in particular.

Batching Effects: Can we do Anything about them?

It is possible to compare results obtained from different laboratories or even different experiments, although it should be appreciated there are challenges and limitations to using the data in this way. Batch (confounding) effects are effects or results observed in the data due to non-biological factors. This could include different reagents, laboratories, experiments, researcher/s, lot number of reagents, experimental pipeline used, and many other factors which could cause a difference in the data which isn't due to the independent variable (i.e. experimental groups). In some cases, observed differences between laboratories can be larger than tissue differences (e.g. when comparing expression data from the same tissues generated by the cancer genome atlas and gene tissue expression databases; Figure 3.1.2) [526].

The ability to summate different datasets and perform meta-analyses of them is pertinent for several reasons: 1) it enables interrogation of large numbers of samples which would be impractical and too costly for a single experiment or series; 2) it adds additional utility to existing datasets and enables investigation of novel questions, reducing the need to generate new data which is both costly and time-consuming; 3) it could enable direct comparison of datasets in the same area or field and help to establish where consensus exists (for example, in mechanisms and pathways that are altered). This could highlight critical pathways or molecules altered in all variants of a disease model, or all dysregulated states of a specific cell type. In fact, use of datasets from different labs might be more beneficial in identifying critical pathways as biases that may be specific to a strain of model organism, reagents used, or processing pipelines

– all of which may be specific to a single research group – will be mitigated by such an analysis. Much like meta-analysis of clinical trials or other data, summing mRNA-Seq data could provide novel insight and prove to be very powerful if done in an appropriate fashion.

For analyses wishing to compare samples obtained from multiple experiments (e.g. different papers published), it may be possible to compensate for/correct batching effects via different strategies. This can be done provided the different datasets contain equivalent samples (e.g. a reference sample, such as a naïve sample) and can be performed in several different ways: 1) the two datasets could be analysed independently, using their own internal reference/controls, and DEGs compared between datasets (this might be useful so that a standardised analysis approach – for both alignment and DEG identification – was adopted, as the two datasets may have undergone different analytical strategies in the original papers. This type of strategy has been used to create, compare, and refine consensus gene lists [158]); 2) the datasets could be analysed together, but by using a paired design allowing for comparison of each dataset to their own reference sample as part of a conglomerate (particularly useful if the experiments replicated conditions between them, as this type of analysis would enhance the power through increased numbers of biological replicates); 3) the reference sample can be used in conjunction with a batch effect remover (such as ComBat or surrogate variable analysis [SVA] [528-530]) – batch effect removers may be particularly helpful on both internal and external large-scale datasets that inherently need to be performed in multiple batches (i.e. availability of researchers, model organisms, patients, cell isolation machines, etc, may not be possible simultaneously all within relevant timescales for mRNA-Seq processing). The use of approaches 2 and 3 would improve the power of the analysis (ability to detect DEGs), and arguably increase the validity of results obtained. A comparison between uniform processing (1) and batch effect removal (3) can be seen in Figure 3.1.4.

Batch effect removal can also include the use of QC samples (such as sequencing a specific cell line to sequence what should in theory produce identical results), although these have been shown to provide little benefit [531]. It has been shown that batch effect removers tend to generally perform better than analyses which do not use them [532]. Whilst useful, it should be noted that batch effect removal can itself lead to false discoveries. The results obtained from analyses utilising batch effect removal should be considered as obtained from an imperfect study design, and therefore identified DEGs or changes to critical pathways should also be validated rather than blind trust placed in the data [533].

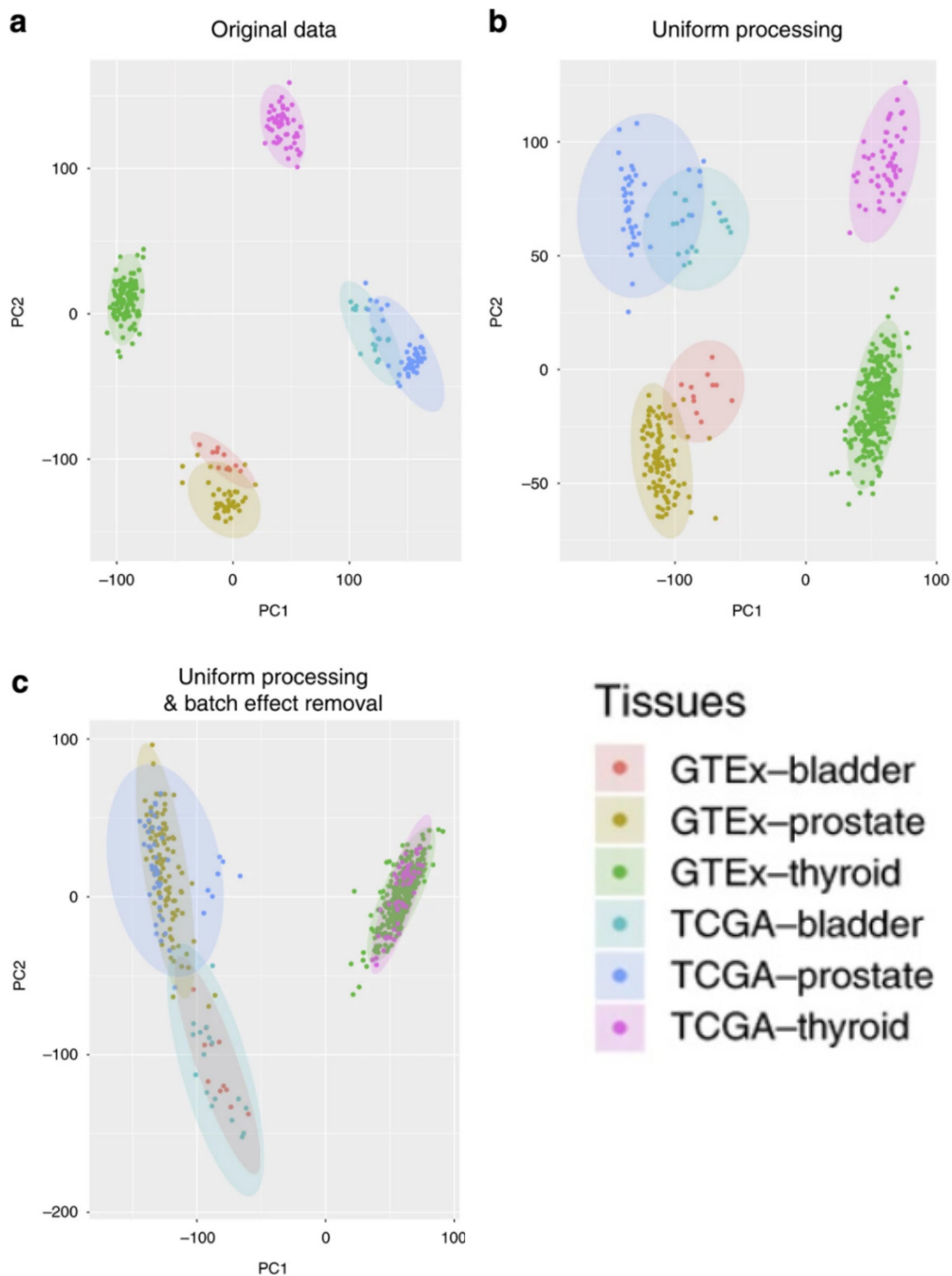


Figure 3.1.4. Visualisation of batching effects in mRNA-Seq data and processing strategies to normalise for non-biological differences. A) PCA plot of original processed data without uniform processing highlights a batch effect between the two compendiums (GTEX and TCGA). B) PCA plot of data when processed uniformly helps to reduce the batch effect partially. C) PCA plot of data when processed uniformly and normalised using a batch remover algorithm helps to greatly reduce the batch effect, allowing for analyses to be performed with increased numbers of replicates and therefore power. Abbreviations: GTEX – genome tissue expression, TCGA – the cancer genome atlas, PCA – principal component analysis. Adapted from [526] and used under licence (CC BY 4.0).

Power of mRNA-Seq Experiments

For mRNA-Seq, the depth (i.e. number of reads per sample) obtained and number of replicates is also a topic of hot debate. The ENCODE guidelines suggest a minimum of two biological replicates, with a minimum of 30 million reads [522]. However, other research has suggested this is not necessary for experiments aiming to identify DEGs. For example, correlation coefficients between samples (and their various quartiles of genes based on expression level) plateau at 10 million reads per sample in chicken lung RNA preparations [534]. Another team showed that all genes fall within a 2-fold change of final expression at 10 million mapped reads, and that nearly all of the moderately-expressed genes ($\sim 95\%$ – 10-99 reads per kilobase of transcript per million mapped reads [RPKM]) and all of the highly-expressed genes (>99 RPKM) were quantified within 20% of their final expression value within samples (based on the values obtained for the maximum depth of 45 million mapped reads utilised in this experiment), suggesting that a higher depth may providing diminishing returns with respect to the ability to identify DEGs at a considerably increased cost [535]. Whilst higher depths of sequencing allow for improved quantification of splice variants and isoform expression, the relatively short reads that Illumina sequencing provides has been superseded by different technologies which can sequence whole mRNA molecules without the need for polymerase chain reaction (PCR) steps (to introduce potential bias) or fragmentation (e.g. the nanopore technology) [536].

In these experiments, the number of replicates is also an important factor to consider. It is generally accepted that as many replicates should be used as can be afforded. Investigations have performed comprehensive comparisons into various algorithms used to identify DEGs but also into the number of replicates and how that alters both the true positive rate (TPR) and false positive rate (FPR), or the number of DEGs identified as a proxy. For example, one group used both simulated and real mRNA-Seq data to investigate 11 different algorithms and concluded that all the algorithms perform poorly on less than 3 biological replicates [537]. Another team suggested that at least 6 biological replicates were necessary [538]. However, the real data (in both these papers) was concatenated from various sources and may have been confounded by batching. Therefore, another group sought to create a high number of biological replicates ($n = 42$ or 44 “clean replicates”) in a single experimental system to conclusively address the question of biological replicates; they also compared various algorithms for detecting DEGs [498]. They performed DEG analysis with each algorithm by bootstrapping the number of replicates per condition and making a total of 100 iterations. In agreement with others, they also suggested a minimum of 6 biological replicates per condition. However, the TPR for 3 replicates (for a fold-change of $\geq \pm 2$; a commonly-used criteria in the absence of calibration using spike-in controls

such as those made by the external RNA controls consortium [ERCC]) was close to 0.95 for many tools (i.e. $\alpha \sim 0.05$, a commonly-used statistical threshold) [498]. They also show (within their system) that the likelihood of obtaining anomalous samples (when performing 48 replicates) was relatively low although not impossible [466].

However, both depth and replicates need to be considered together when designing an mRNA-Seq experiment. Consider a hypothetical flow cell which contains a total of 400 million reads, and you wish to conduct an experiment involving 2 experimental groups. You have the ability to sequence 4 samples ($n = 2$) to a depth of up to 100 million reads per sample, 6 samples ($n = 3$) to a depth of up to 66.6 million, 12 samples ($n = 6$) to a depth of up to 33.3 million, and so forth. An experiment ideally achieves the “golden” 80% power (β) with significance below 0.05 (α) but irrespective of this the depth and number of replicates could be optimised to achieve the highest cost-efficiency – either to reduce the overall cost of the experiment to achieve power, or to maximise attainable power for a given cost. One research group considered the two values in tandem and showed that both depth and number of replicates are important; however, they indicated that 10 million reads per sample (allowing for more replicates – in this example 6) allowed detection of far more DEGs than the other permutations, and attainment of a power of 0.8 (with a significance threshold of 0.05 after false discovery rate [FDR] step-up correction) [539]. Their data shows that 6 replicates at 10 million reads detected ~4,500 DEGs, 4 replicates at 20 million reads detected ~3,000, and 2 replicates at 30 million reads detected ~2,500 (equivalent total numbers of reads sequenced). They also showed, with their experimental pipeline for performing mRNA-Seq, that having 10 million reads per sample was the most cost-efficient for the power it provided between 2-6 replicates (at 7 replicates it was marginally outperformed by 5 million reads) [539].

A major flaw of the aforementioned studies is that much of the analysis is based on cell lines where there is likely to be a reduced biological variability than what may be observed within a whole organism. Therefore, it may be possible that a higher number of biological replicates is required to achieve optimal power *in vivo*. Nonetheless, the above studies indicate that the 2 replicates and 30 million reads suggested by the ENCODE guidelines are not optimal with respect to detecting DEGs in the most cost-efficient or powerful manner (for a fixed cost). Ideally, a pilot study should be performed using the pipeline an experimenter wishes to utilise, and a power analysis (as well as a cost analysis) be performed for their individual experiment as there are many pipelines with different costs and advantages/drawbacks, and that sequencing costs can greatly vary between institutions primarily depending on which sequencer machines are available (higher throughput sequencers provide greater cost efficiency but assumes enough

samples require sequencing – either within an experiment or compounded between several researchers).

Published data utilising the Smartseq2 pipeline (on which the SMART-Seq v4, the selected kit for our pipeline, is based) indicates correlation between samples peaks at around 5 million uniquely mapped reads [517]. Cost estimates were compared for mRNA-Seq using the SMART-Seq 4 kit and internal University Genomics Facility Sequencing versus the power data generated by *Liu et al.* [539]: it indicated that, in the context of the SMART-Seq pipeline (where preparatory costs are generally higher than most mRNA-Seq pipelines due to its specialist capabilities), the most cost-effective mRNA-Seq experiment overall (£ per power) contained 4 biological replicates per group at a depth of 10 million reads per sample. However, as advised by Schurch *et al.*, at least 6 biological replicates were also considered to achieve adequate power ($\beta = 0.8$) [498], noting that this recommendation was based on *in vitro* cell lines. Ultimately, a pilot study and power analysis would best inform experimental design, but nonetheless existing data suggested sequencing 5–10 million reads per sample was optimal.

3.1.3 mRNA-Seq Analysis

There are no special considerations for mRNA-Seq analysis beyond what was described in the first chapter, and the pipeline can be analysed using the gold-standard approaches (i.e. adapter trimming, trimming based on quality, use of the appropriate splice-aware aligners, typical quantification and normalisation algorithms, etc; see Figure 2.7.1).

For analysis, the University of Bristol's Genomics Facility provide access to Partek Flow and PGS, software that can perform all aspects of the analytical pipeline (from raw data processing and identifying DEGs to pathway analysis and more).

3.1.4 Summary

The aims of this chapter were to optimise both the experimental and analytical aspects of the mRNA-Seq pipeline, performing QC checks and confirming expression/non-expression of expected genes in samples, and to determine whether it would be possible to sequence microglia isolated from single retinas. Having identified a pipeline that would be appropriate for the research objectives to investigate the transcriptome of the microglia, the results of optimisations for ultra-low input mRNA-Seq are presented herein.

3.2 Results

3.2.1 Optimisation of mRNA Isolation and cDNA Generation

The first experiments required involved optimising the pipeline for sorting the cells, to confirm the ability to generate suitable material for mRNA-Seq. For initial experiments, microglia were sorted based on their CD45 and CD11b expression (Figure 3.2.1). Informed by the SMART-Seq kit guidance, 1,000 microglia were sorted from pooled retinas (comprising the left and right eyes from a single mouse) to generate cDNA using a 10-cycle amplification programme with subsequent Agencourt AMPure isolation (magnetic beads) and quantification with the Agilent Bioanalyser tapestation. The rationale for pooled retinas was to ensure 1,000 microglia were accurately sorted into each sample tube (the recovery rate of the cell sorter was not known at the time, but based on existing knowledge it seemed unlikely that a single retina would yield 1,000 sorted microglia) so that large quantities of starting mRNA could be utilised for the cDNA generation and amplification steps. Taking this approach allowed experimental risks to be mitigated until the sorting and cDNA generation was optimised.

Unfortunately, cDNA was not detected on the Agilent bioanalyzer in the first experiment meaning it was unclear if kit components were functioning correctly or whether there was an error in a different part of the pipeline until that point. Therefore, a similar follow-up experiment was conducted using sorted microglia from both WT and *Cx3cr1-GFP^{+/-}* mice (using CD45 and CD11b gating; see Figure 3.2.1); conceptually, it would allow comparison of hypothetical differences in the transcriptomes caused by the transgenic alteration as it was unknown if haploinsufficiency occurred below the detection threshold/sensitivity of conventional phenotyping approaches (such as fundal imaging) that had not detected gross abnormalities. In this experiment, the positive control RNA (from the SMART-Seq kit) and a negative (water) control were both included so that kit components could be validated as functional and the absence of contamination also confirmed. Cycle optimisation was also performed by running a sample from each strain for 12-, 15-, or 18 cycles, numbers higher than recommended in the kit manual (this was done in case low cycle number was the reason for no detectable yield in the first experiment). This resulted in cDNA generation from both the 15- and 18 cycle conditions and a barely detectable amount with 12 cycles (Figure 3.2.2), confirming low cycle number was the primary reason for failure in the first experiment. The cycling conditions for the positive control were as expected/indicated as per the manual, suggesting them as accurate to the amount of input RNA. In-line with the kit's guidance, 15 cycles for 1,000

sorted cells was selected for subsequent experiments (as opposed to 18) as over-cycling can lead to amplification bias and skewing of the cDNA generated (the output from 15 cycles most closely resembled the exemplary bioanalyser output figures from the manual). Additionally, sorting of residual volumes of the samples into empty tubes indicated it was possible to isolate ~1,200–1,500 microglia per pool, suggesting that it would be possible to reliably isolate 600 microglia per retina for single-eye sorting in the future.

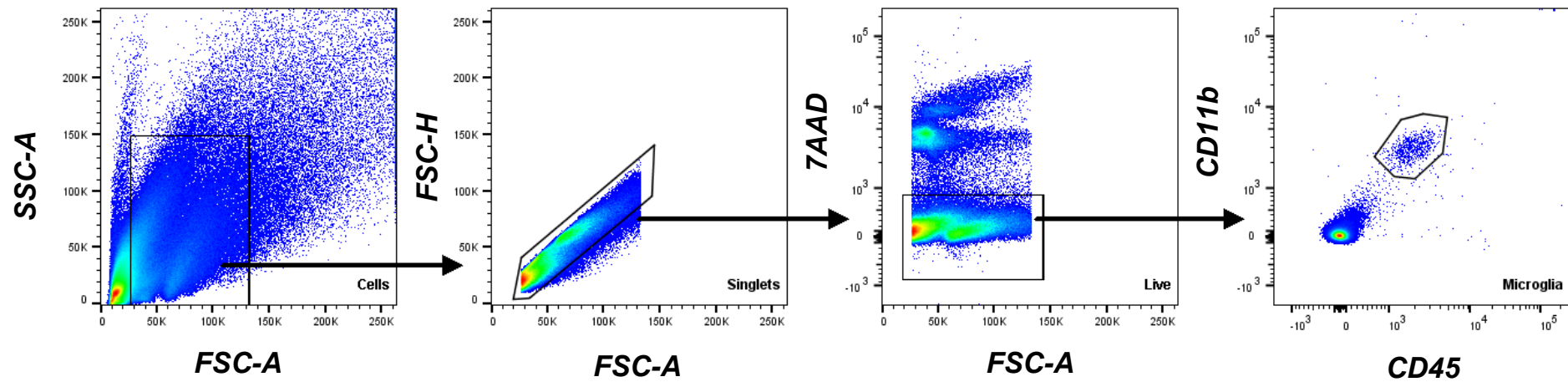


Figure 3.2.1. Flow cytometric gating strategy for the isolation of microglia by fluorescence-activated cell sorting (FACS) in a naïve retina. 1) Cells are gated-for on size and granularity; 2) singlets are gated using cell area (size) and height; 3) live cells are gated using 7AAD; 4) microglia are gated using CD45 and CD11b.

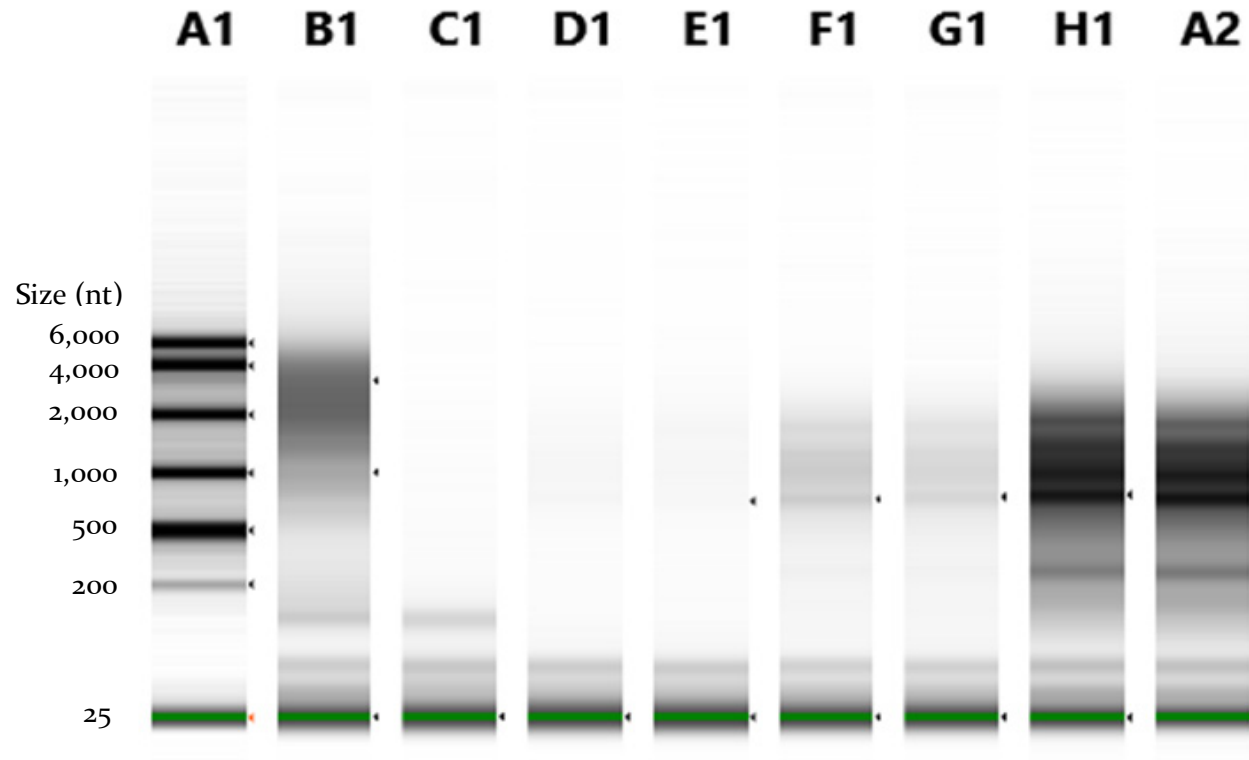


Figure 3.2.2. *The gel plot, produced from cDNA generated using the SMART-Seq v4 kit as part of the cycle optimisation experiment, on the Agilent 2100 Bioanalyser. The following lanes represent different samples and controls: A1 (ladder), B1 (positive control RNA sample [as provided in the kit]), C1 (negative control sample), D1–E1 (12-cycle wild-type and *Cx3cr1-GFP*^{+/-} microglia respectively), F1–G1 (15-cycle wild-type and *Cx3cr1-GFP*^{+/-} microglia respectively), H1–A2 (18-cycle wild-type and *Cx3cr1-GFP*^{+/-} microglia respectively). The positive control had a peak around 2,000 nt as expected, whilst the samples had consistently sized peaks corresponding to just under 1,000 nt – which falls within the normal anticipated range for a sample generated using this kit. The green line indicates the 25 bp spike-in in each sample used for calibration purposes.*

The cDNA from the second experiment was then sequenced and QC was assessed using FastQC; the results demonstrated very low N content, sporadic sequence content for the first 15 bases with stabilisation afterwards (normal), a near-normal GC distribution, and sequence duplication (expected) as a consequence of the LD-PCR amplification (Figure 3.2.3).

As there are multiple measures of sequence quality and there is no single parameter which can define good-quality mRNA-Seq data, quality assurance (QA)/QC measures were also performed using Partek Flow. The average base quality score per position (using Phred scoring) was ~35, with the vast majority of reads having an overall quality of 34 or 35 (Figure 3.2.4).

The above information indicates that the sequencer was very accurate in its base calling (a Phred score above 30 indicates an error rate below 0.01%, low N content, expected sequence content), but indicates little about the quality of the input material beyond having a near-normal GC distribution and that it was able to generate quality reads of at least 75 bp in length. To further assess the quality of the input material, the alignment stats were also assessed. The total alignment for samples was ~90%, with a total unique alignment rate of ~80% – which are generally considered the ideal metrics for mRNA-Seq data (Figure 3.2.5). Comparison of the alignment rates between paired-end reads (what was generated in initial experiments) and single-end reads demonstrated negligible differences between the two; therefore, future experiments utilised single-end reads as an improvement in cost-efficiency.

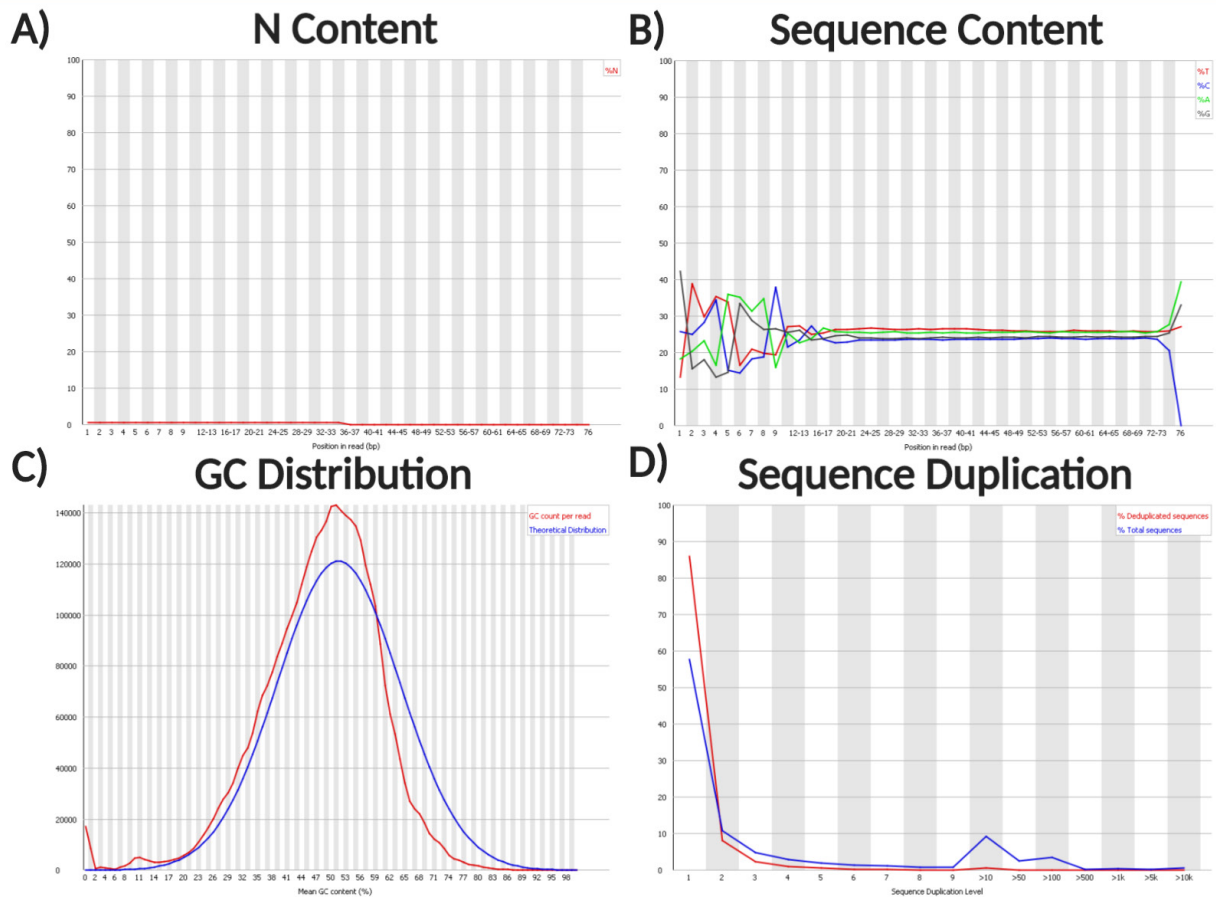


Figure 3.2.3. Key quality control parameters (QC) for a representative mRNA-Seq sample calculated by FastQC. A) Percentage N content (y) per base position (x) for all reads (1–76). **B)** Percentage sequence content (y; TCAG) per base position for all reads (x). An unusual sequence content is anticipated for the first 12–18 bases, after which stabilisation (as observed) is expected. **C)** GC distribution (x; percentage content) of each read plotted as a line (red; y, number) with a theoretical perfect distribution line shown (blue), indicating a near-normal GC content distribution. **D)** Percentage (y) sequence duplication levels (x; duplication level) indicated with a blue line compared to a theoretical perfect duplication level line (by random chance; red) which indicates sequence duplication occurred in the sample; this was anticipated as cDNA samples were amplified by LD-PCR as part of the preparation process before library generation, meaning duplication was an inevitable part of the preparation process.

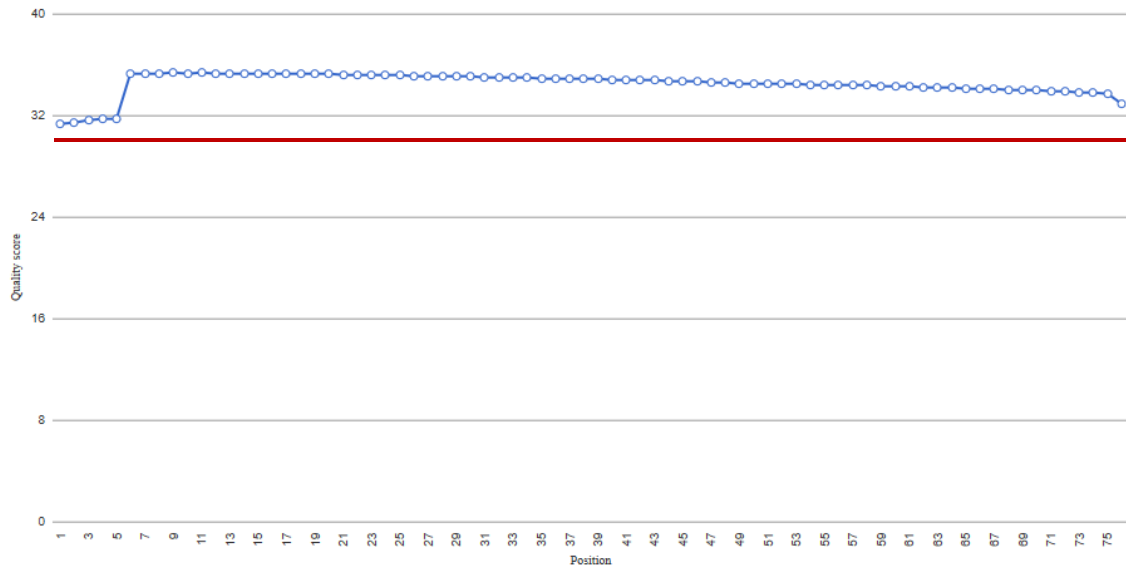
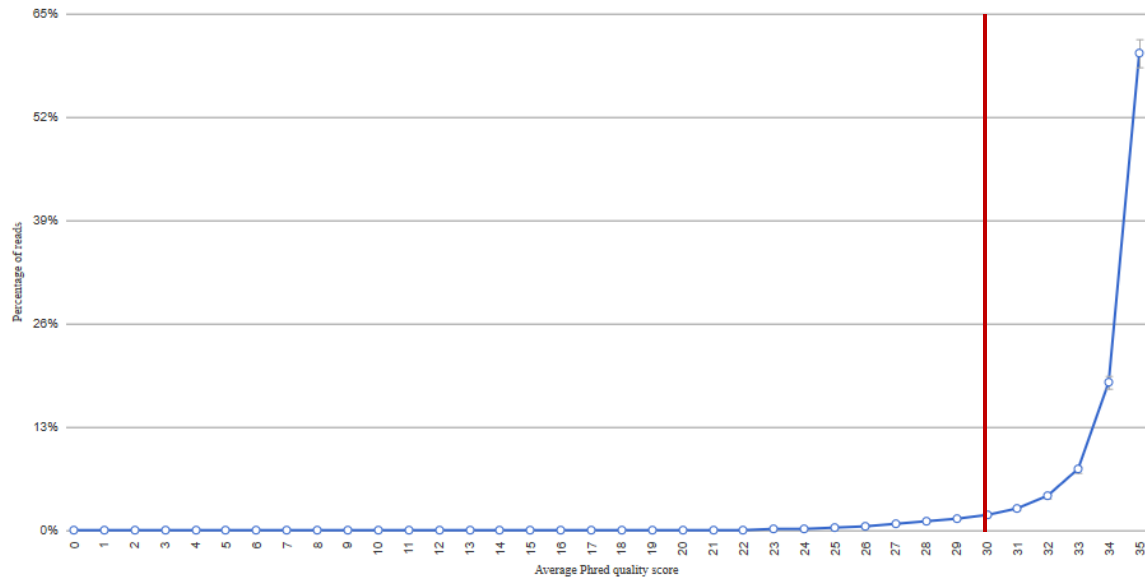
A)**Average base quality score per position****B)****Average base quality score per read**

Figure 3.2.4. Average base score quality for a representative mRNA-Seq sample (as generated in Partek Flow). **A)** The average base quality score per position is shown, with a red line to indicate a Phred quality score of 30 (0.1% error rate in base-calling), with the average (and SD) falling above this (indicating ideal base-calling). **B)** The average base quality score per read is plotted as a histogram of frequencies; a red line indicates a Phred quality score of 30, which the vast majority of reads fall to the right of (indicating ideal base-calling for the vast majority of reads).

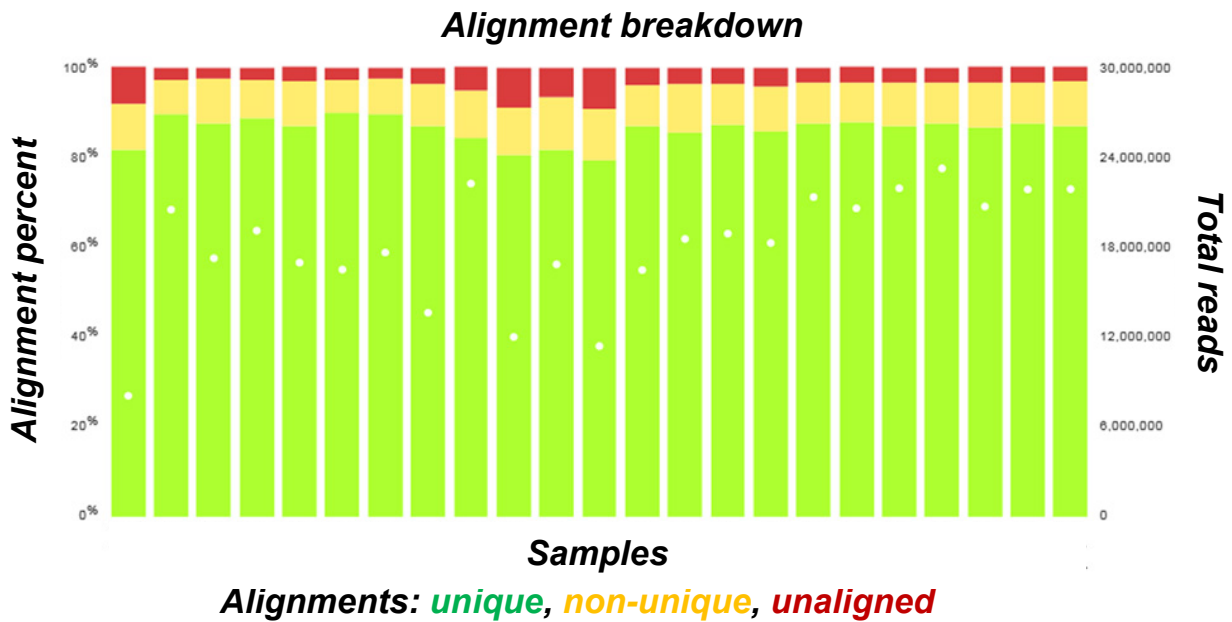


Figure 3.2.5. A representative selection of alignment statistics for mRNA-Seq data generated using the ultra-low input RNA pipeline. Each bar represents a different sample, which are colour-coded according to how the reads mapped to the mouse genome. Green represents unique alignment (where the read aligned to only one location of the genome), yellow represents non-unique alignments (where the read aligned to more than one location of the genome), and red represents unaligned reads (where it did not align to the genome). Non-unique alignments are possible because many genes may have arisen from a common predecessor via gene duplication events (i.e. paralogous genes), meaning that identical (or near-identical) regions of two paralogues will inevitably exist. Generally, a unique alignment of ~80% (with total alignment of ~90%) is considered the ideal/gold-standard results for mRNA-Seq. The white dots represent exact numbers of reads aligned, which remain relatively consistent across an experiment.

Using PGS, analysis indicated expression of “top microglial genes” (e.g. *Slfn2*, *Gpr84*, *Bcl2*, *Olfml3*), expression of many “microglial-enriched genes” (e.g. *Olfml3*, *Siglech*, *Tmem119*, *Cx3cr1*, *Slc24a3*, *Sparc*) and an absence of expression for markers canonical to T cells, endothelium, and photoreceptors which otherwise could be suggestive of sample contamination (*Cd3*, *Cd4*, *Cd31*, *Map2*, *Tubb3*) in the four samples sequenced [158, 308, 346-348].

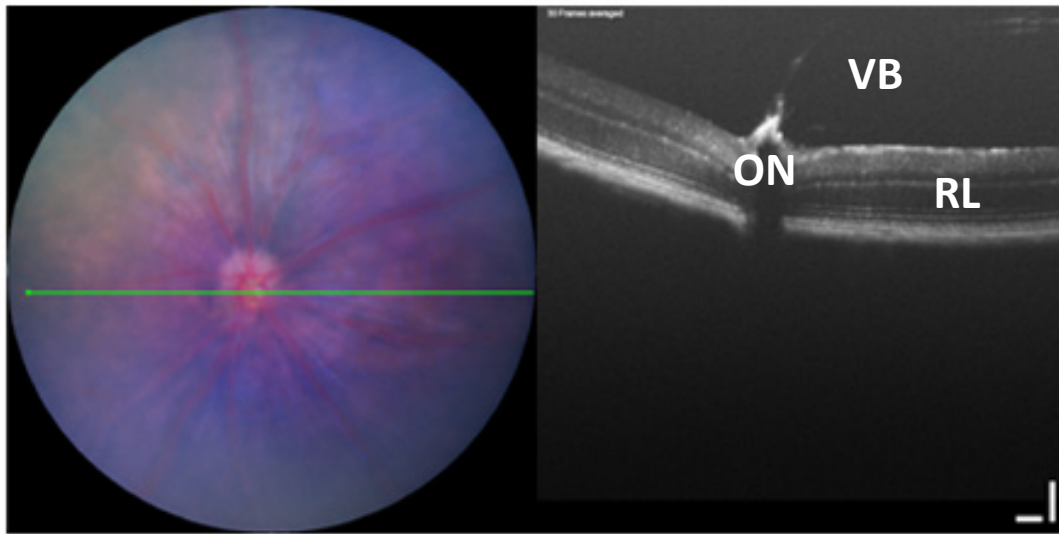
However, it became apparent during analysis that the two experimental groups were very similar, as few DEGs were identified and PCA was unable to delineate the groups. Robust final checks for QA would require samples obtained from two different experimental groups to enable identification of larger numbers of DEGs and run unsupervised analyses (such as PCA) to see if delineation between the groups occurs, both of which would indicate the ability to detect broad differences between experimental groups using this pipeline. However, until the experiment comparing microglia from different transgenic lines was performed, it was unknown whether microglia isolated from WT and *Cx3cr1^{GFP/+}* mice would be similar or have differences.

For a follow-up experiment, use of the *Cx3Cr1^{GFP}* mouse strain would result in samples containing mixed-cell populations as the strain does not retain microglial specificity during inflammatory contexts [540] and this would limit the utility of a dataset generated with such mice. Informed by publications, acquisition of a new reporter line from collaborators was initiated to circumvent these issues of microglial specificity (see Chapter IV) [376]. However, there were anticipated delays in the acquisition and rederivation process required to establish a colony locally. Therefore, investigation of a different cell type during retinal inflammatory contexts would provide data most useful in understanding the disease process of uveitis whilst allowing for robust final QA checks to further validate the mRNA-Seq pipeline. As EAU is a CD4⁺ T cell-mediated disease [1], investigation into these cells was performed.

3.2.2 mRNA-Seq of CD4⁺ T Cells in EAU

Based on the preliminary work on microglia, it was evident that isolation of 600 cells per retina would be both feasible and reliable; therefore, this was the target for the number of sorted CD4⁺ T cells. This would enable validation of single-retina sequencing for microglia, as a proof-of-concept, whilst simultaneously providing a representative sample of the CD4⁺ T cells isolated from an inflamed retina for insights to that aspect of disease. WT C57BL/6 mice were immunised for disease with the aim of taking retinas and spleens from mice exhibiting peak disease at day 25 (Figure 3.2.6); in C57BL/6 mice, peak disease is typically observed around days 23–25 (following approximately 8–12 days of no clinical features) with a secondary progression that can last at least 100 days post-immunisation [541, 542]. Additionally, spleens from naïve mice were utilised as controls because CD4⁺ T cells are not present in large numbers in a normal retina. The sorting strategy is highlighted in Figure 3.2.7. The results are generated from two independent experiments with experimental groups balanced between them to combat hypothetical batching effects.

Naïve



D25 EAU

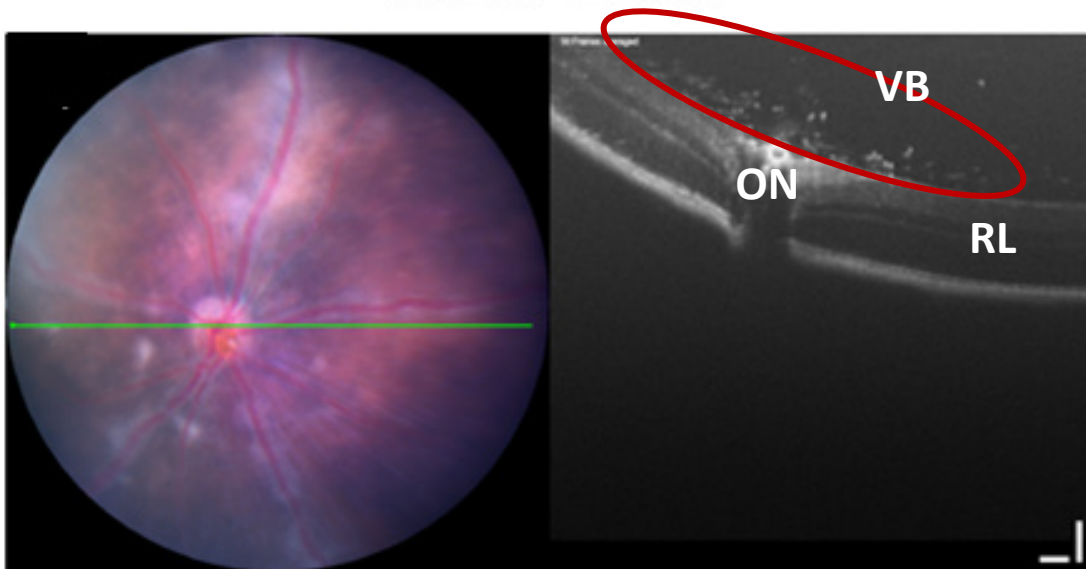


Figure 3.2.6. Representative fundal and OCT images of a naïve mouse and at peak (D25) EAU from the CD4⁺ T cell mRNA-Seq experiment. Perivascular sheathing, lesions, and retinal damage are evident at D25 EAU (fundal image) with signs of cellular infiltrate on the OCT scan (circled red; scan line indicated in green). The naïve retina appears as expected. Abbreviations: EAU – experimental autoimmune uveitis, OCT – optical coherence tomography, ON – optic nerve, RL – retinal layers, VB – vitreous body.

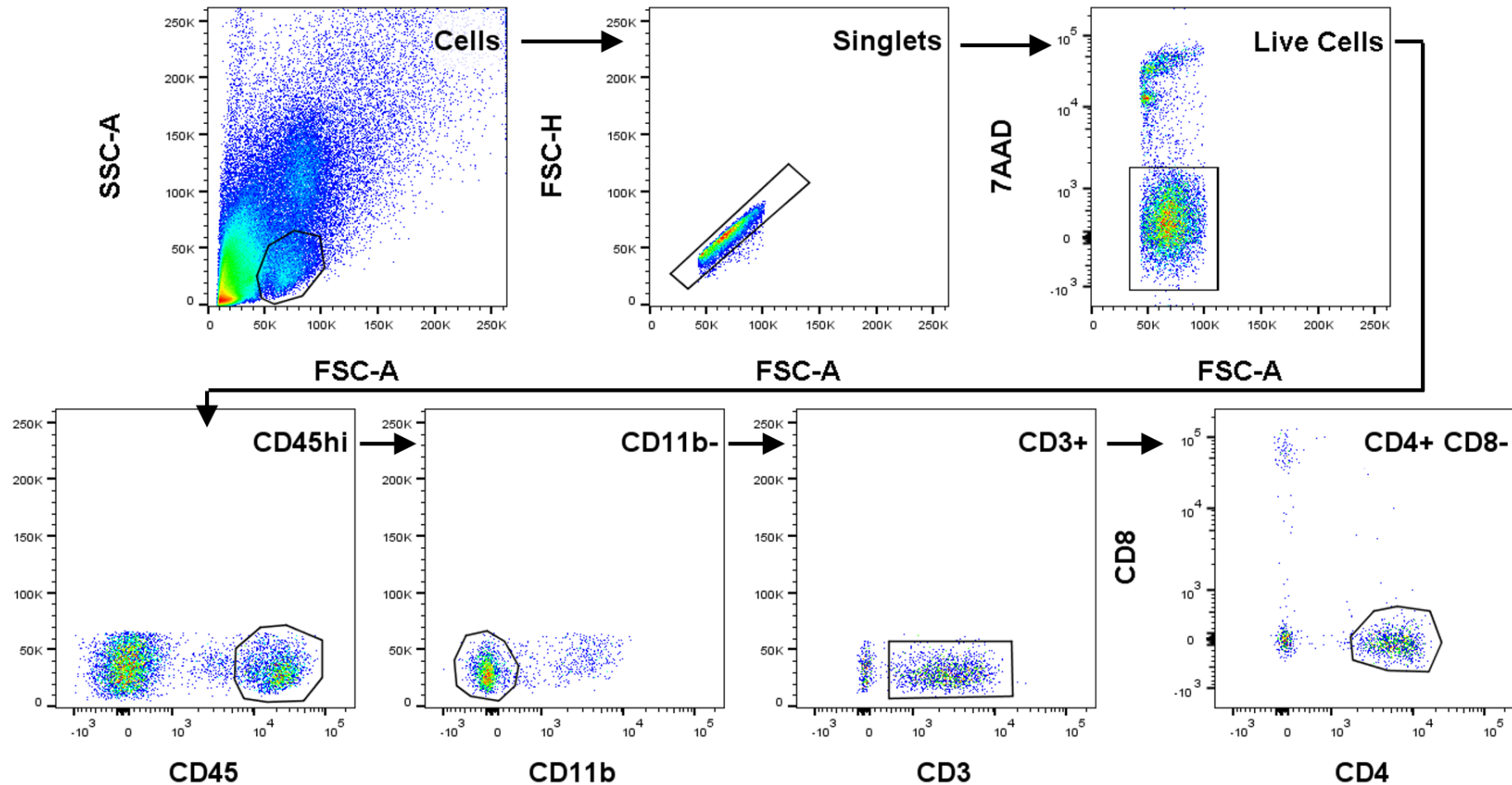


Figure 3.2.7. Flow cytometric gating strategy for the isolation of CD4⁺ T cells by FACS in an EAU retina. Cells are gated initially as per figure 3.2.1 (live cells). They are then gated for CD45^{hi} (immune cells), CD11b⁻ (non-myeloid cells), CD3⁺ (T cells), and CD4⁺ CD8⁻. Abbreviations: EAU – experimental autoimmune uveitis, FACS – fluorescence-activated cell sorting.

However, in the first CD4⁺ T cell experiment a phenomenon we describe as “time-dependent RNA degradation” occurred; it describes where cDNA yield is reduced in a time-dependent manner across samples (i.e. the order in which they were sorted) and is likely due to RNA degradation due to necrotic/apoptotic processes that occur prior to the formation of holes within the membrane (which viability dyes could then identify cells as dead). It occurred due to a few factors causing time delays such as technical difficulties with the cell sorter that arose after mouse termination and a complicated experimental design involving preparation of multiple tissues simultaneously; these factors ultimately increased the time taken between mouse termination and sorting of cells into lysis buffer (this phenomenon was observed at around 3-3.5 hours post-termination) and highlights the fragility of the first protocol step to partial failure (Figure 3.2.8, red box). It is noteworthy to mention that the cells (according to the viability stain) appeared live and it was not possible to predict this outcome until after performing processing steps. Therefore, future experiments used a protocol amendment where small batches (containing samples from every experimental group where possible) of 1–5 were prepared and sorted in a staggered fashion to mitigate risks from this occurring in future. Nonetheless, the data indicates it is possible to generate high quality cDNA from 600 cells isolated from an individual retina as a proof-of-concept for single-eye microglial sorting in the future.

The subsequent experiment adopted this refined protocol, and all samples acquired in this experiment were of the expected yield and quality (Figure 3.2.9). In total, 2 naïve spleens, 2 EAU peak disease spleens, and 8 EAU peak disease retinal samples were sequenced. PCA was able to readily delineate the three groups, indicating genuine and broad differences between the samples (Figure 3.2.10). Interestingly, retinas obtained from the same mouse clustered more closely together on the PCA plot than retinas obtained from different mice. The spleens, irrespective of disease status, clustered more closely together. A total of 991 unique DEGs were identified by the three comparisons in the ANOVA model (953 from naïve spleen to diseased retina, 147 from diseased spleen to diseased retina, and 59 from naïve spleen to diseased spleen). These are visualised by hierarchical clustering in Figure 3.2.11, highlighting a dynamic transcriptional landscape. In summary, a group of genes upregulated in CD4⁺ T cells in EAU retinas are highlighted in black; genes downregulated in EAU (spleen and retina) compared to naïve controls are highlighted in blue; those downregulated in EAU retinas (but not spleen) in green; and those upregulated in EAU spleens only in brown.

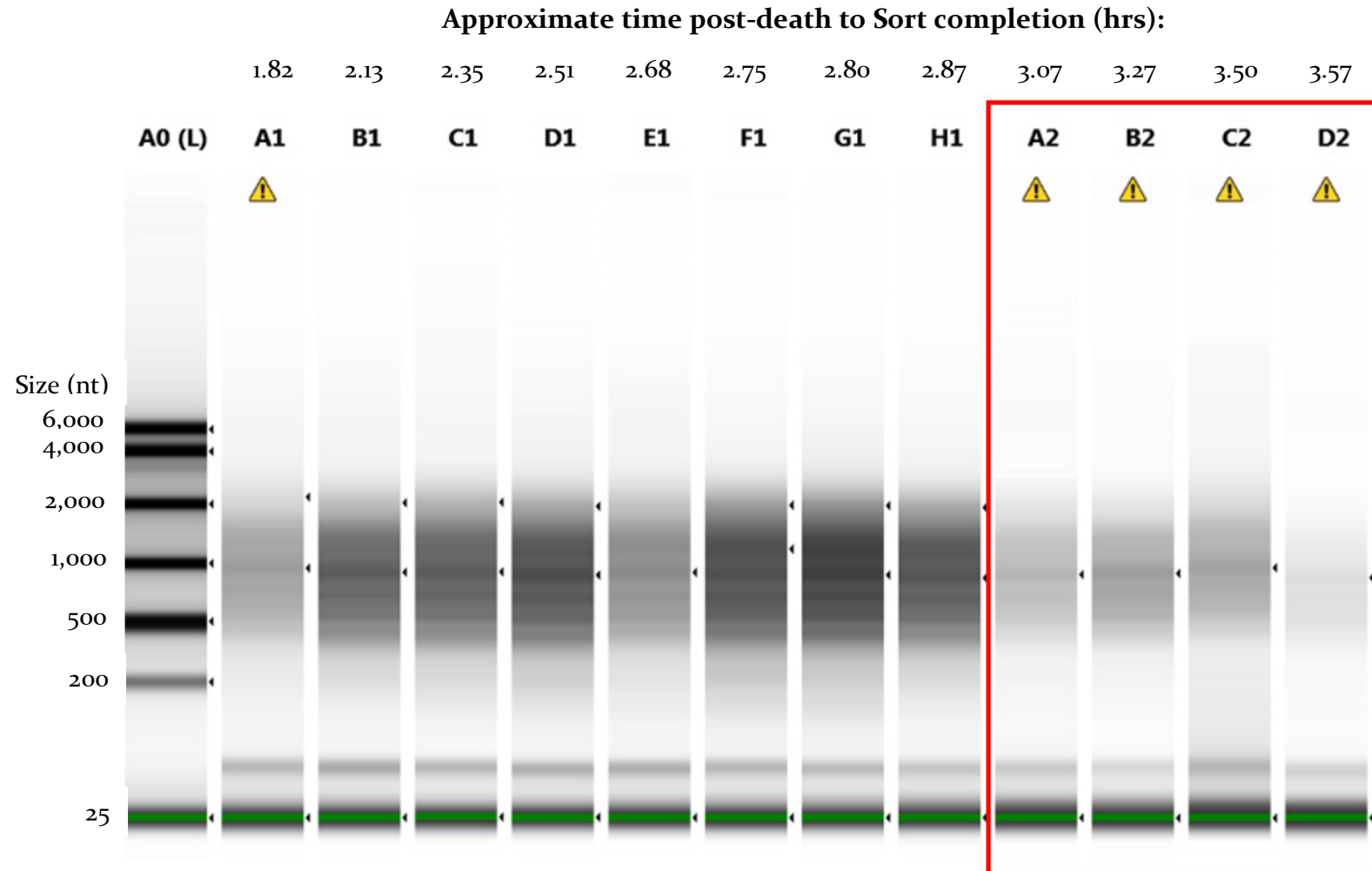


Figure 3.2.8. A gel plot from the experiment where time-dependent mRNA degradation of samples was observed. The gel indicates cDNA was generated for samples B₁–H₁ (a mixture of retinal and spleen samples), but a reduction in yield (resulting in almost none detected) was observed for samples A₂–D₂ (red box). The samples on this gel are arranged in the order they were sorted in (with A₁ being sorted first, and hence the shortest time post-termination, and D₂ being sorted last). The green line indicates the 25 bp spike-in in each sample used for calibration purposes.

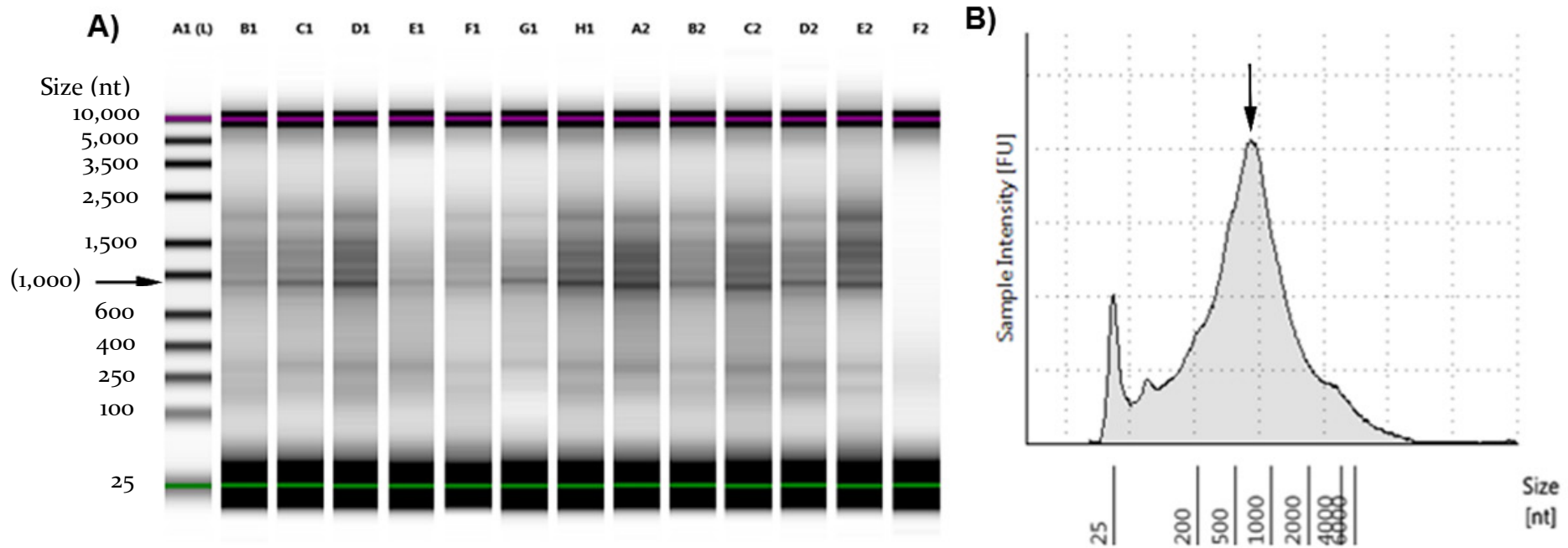


Figure 3.2.9. A representative gel plot, produced from cDNA generated from 600 CD₄⁺ T cells (equivalent to single-eye mRNA-Seq of microglia) using the SMART-Seq v₄ kit, on the Agilent 2100 Bioanalyser. **A)** The following lanes represent different samples and controls: A₁ (ladder), B₁–E₂ (16-cycle CD₄⁺ T cells), F₂ (water control loaded onto the gel to estimate background signal). **B)** Single gel trace for a sample, showing a clean peak observed at just under 1,000 nt. Green line – 25 nt spike-in; purple line – 10,000 nt spike-in. Both spike-ins assist in calibration.

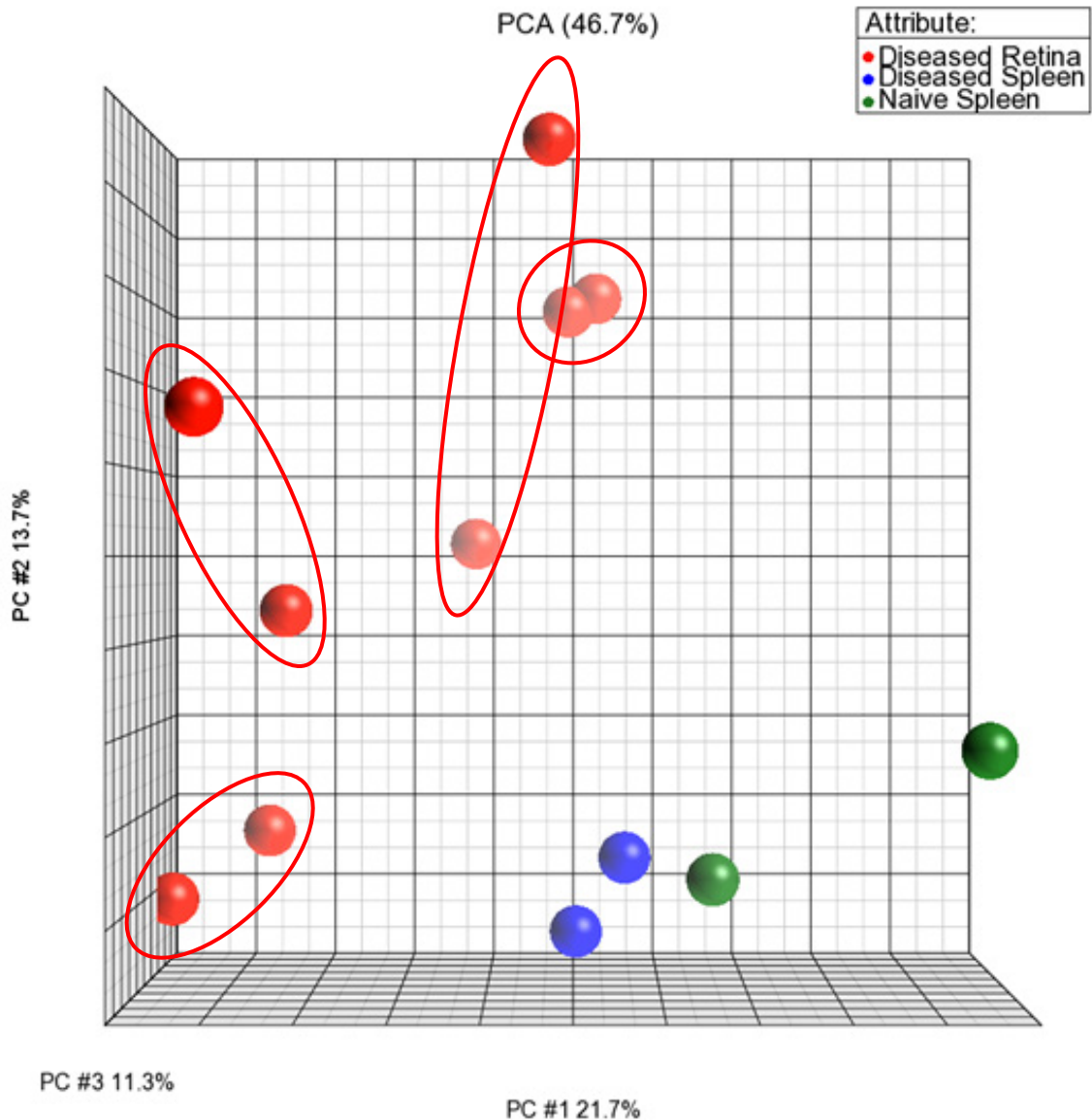


Figure 3.2.10. Principal component analysis (PCA) plot for the $CD4^+$ T Cell mRNA-Seq data. The first three PCs are plotted which represent 46.7% of the variation between the samples. Samples are labelled according to their anatomical origin and disease status: naïve spleen (green; $n = 2$), diseased (EAU) spleen (blue; $n = 2$), and diseased retina (red; $n = 8$). Increasing loss of colour intensity on a sample indicates a more posterior position on PC#3. Retina pairs (obtained from the same mouse) are indicated with red circles. Abbreviations: EAU – experimental autoimmune uveitis, PCA – principal component analysis.

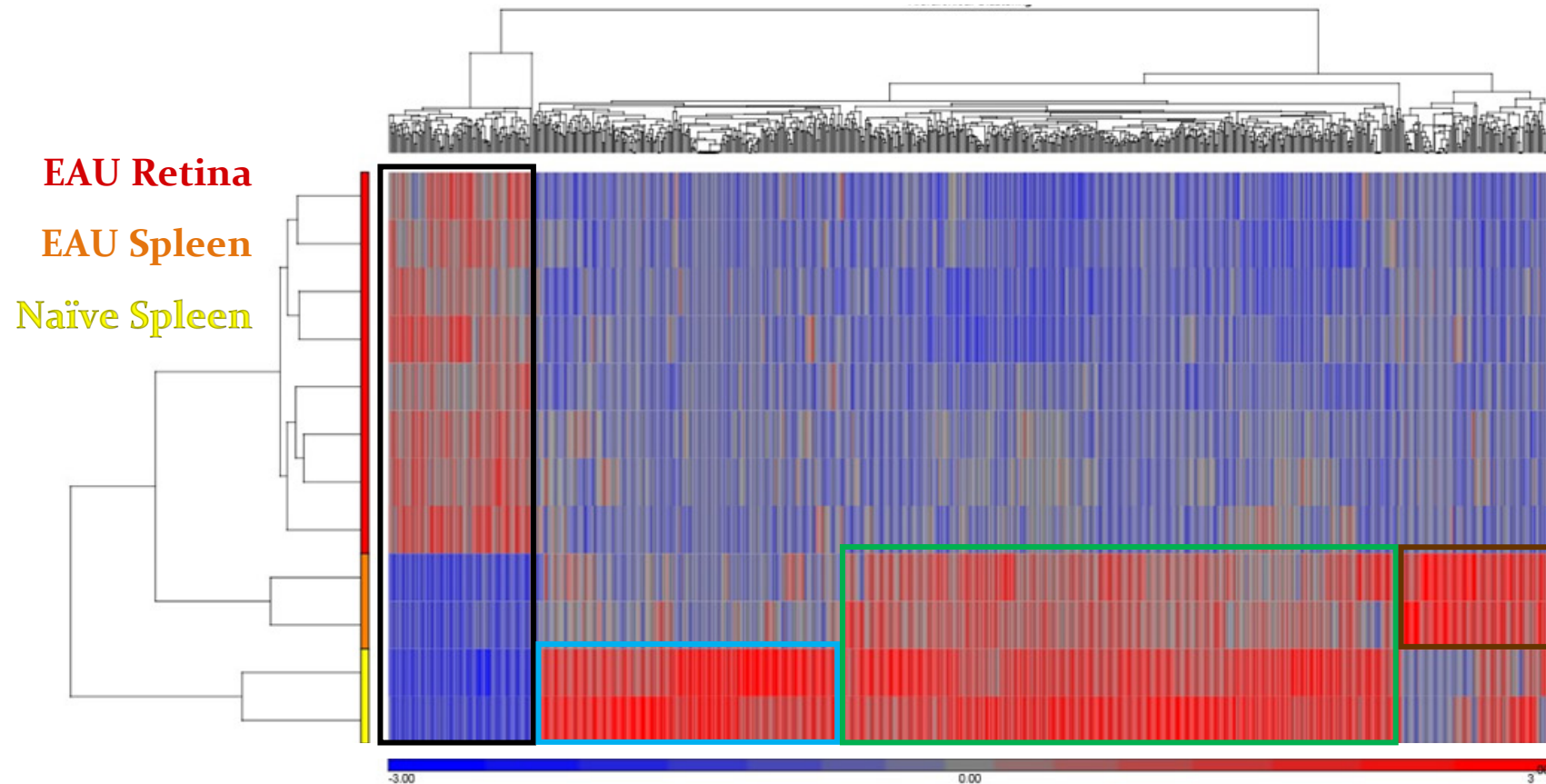


Figure 3.2.11. Hierarchical clustering (heatmap) of the DEGs identified from the DGEA on samples of 600 CD₄⁺ T cells. Comparisons were made between naïve spleen (yellow; $n = 2$), diseased (EAU) spleen (orange; $n = 2$), and diseased retina (red; $n = 8$) are highlighted with coloured boxes. Raw expression values (on a per gene basis) were shifted to a mean of 0 and scaled to an SD of 1 for easier comparability as part of the visualisation process. Genes were clustered based on their similarity in expression profile, as were samples – both to create dendrograms illustrating the relationships. Abbreviations: DEGs – differentially-expressed genes, DGEA – differential gene expression analysis, EAU – experimental autoimmune uveitis.

3.3 Discussion

The main aims of this chapter were to optimise both the experimental and analytical aspects of the mRNA-Seq pipeline, and to determine whether it would be possible to sequence microglia isolated from single retinas as a proof-of-concept for utilising this pipeline to assess mRNA differences in microglia before, during, and after models of uveitis.

Initial experiments, performed with naïve microglia, highlighted several factors that can alter the quality of the output material. Firstly, careful optimisation of cycling conditions for the cDNA amplification step is required; secondly, that high-quality output depends on streamlining of the experimental pipeline so that optimal timing for the isolation of cells is maintained. Preliminary experiments using sorted microglia did not generate detectable amounts of cDNA. The hypothesis was that material had been generated, but it was too low a yield for detection. To test this, a cycle optimisation experiment was performed where the cycle conditions was changed from 10 to 12, 15, and 18. Upping the cycling conditions to 12 generated barely detectable amounts of cDNA, with greatly increased yield with 15 and 18 cycles. This confirmed the experimental pipeline as functional and indicates that the initial experiment likely generated cDNA but at a level below detection thresholds.

The cycling conditions used were discrepant to the guidance provided in the SMART-Seq kit user manual. It is well-known different cell types can express different amounts of mRNA, and that transcriptional amplification occurs in immortalised cell lines [430, 543-545]. The SMART-Seq kit manual indicates that the cDNA synthesis protocol was tested and validated using cultured cells, supporting this notion. Whilst cDNA was generated from microglia with 18 cycles, the output from 15 cycles was sufficient to produce libraries, and the kit's guidance indicates the fewest number of cycles required to construct a library should be used. This is because higher cycle numbers can lead to a phenomenon described as “overcycling”, which results in a coarse distribution of sizes and can affect downstream results. The output from 12 cycles was barely detectable and therefore was too low to select for future experiments. Therefore, 15 cycles was selected for 1,000 cells henceforth.

Whilst all care was taken to ensure high-quality mRNA products were obtained, and haste (with accuracy) in the protocol, on one experiment a time-dependent degradation of mRNA was observed. A variety of factors caused this, such as a complex experiment for preparation (lengthy antibody staining protocols, in addition to preparation of retina, spleen, and blood simultaneously) and unanticipated technical difficulties with the cell sorter which arose after the mice had already been terminated. As an amendment, future work will utilise small-batch

preparations of samples to mitigate the risk of this in the future. Experiments utilising the *Cx3cr1^{CreER}:R26-tdTomato* line may permit sorting of microglia using tdTomato alone (provided the tdTomato tag is both sensitive and specific for microglia), which would considerably shorten the preparation time and streamline the process as no Fc block or antibody staining would be required. This might make future experiments at a reduced risk of failure or problems, therefore.

There is no clear consensus in the literature about the length of time mRNA remains viable post-termination, other than that it is a short time and processing should be as rapid as possible. A recent publication suggested a maximum processing time of 5 hours for a sc-mRNA-Seq method [546]. However, our own findings suggest a time of 3–3.5 hours post-termination (following the protocol described in Chapter II with samples on-ice) as a cut-off for an experimental sample unlikely to yield high-quality or large amounts of cDNA suitable for sequencing. Other approaches that could help bypass this issue include fixation, but for this ultra-low input pipeline the kit manual explicitly stated it was incompatible with fixed mRNA and therefore fresh preparations are required for this pipeline.

Addressing both the cycle optimisation and timing issue, the data generated possessed the ideal (Gold-standard) QA/QC parameters (low N content, normal base composition per position, near-normal GC content to a theoretical, some sequence duplication as a consequence of the LD-PCR, high Phred scores, and excellent alignment metrics); data generated from isolated microglia also had expression of both highly-expressed microglial genes and enriched microglial markers, and an absence of non-microglial gene expression which is suggestive of a valid and successful transcriptomics experimental pipeline. The near-normal GC content, in contrast to the heavy GC bias observed with historical mRNA-Seq protocols, is enabled due to template switching (which incorporates the same, or GC-equal, primer regions for amplification; Appendix I), allowing for unbiased selection and coverage of the transcriptome. However, the SMART-Seq technology does have certain limitations that should be recognised. For example, strand-specificity is not preserved, and the current kit format prevents multiplexing of the samples until library preparation – the latter driving up costs associated with an experiment. Additionally, in contrast to mRNA-Seq experiments using alternative preparatory approaches, there was no loss in Phred score at the 3' end of the transcript.

However, one major limitation of these initial experiments on microglia were that the experimental groups were too similar, meaning that unsupervised algorithms were unable to delineate them. To fully test the platform and validate the pipeline, isolation of cell types under different states (or different cell types) were required. Due to known limitations with the

Cx3cri^{GFP} model in specific labelling of microglia, and the time required to establish the *Cx3cri^{CreER}:R26-tdTomato* strain locally, characterisation of CD4⁺ T cells at EAU peak disease enabled validation of the pipeline whilst simultaneously generating novel and useful data in understanding uveitis (as a CD4⁺ T cell-mediated disease). Performing mRNA-Seq on 600 CD4⁺ T cells also acted as a proof-of-principle for single retina sorting of microglia (the number that could be reliably isolated from single-eyes).

Hierarchical clustering also indicates that many genes are down-regulated when CD4⁺ T cells are present in the retina. Some of these could be explained by tissue factors (i.e. spleen vs. retina), although it is difficult to delineate this as CD4⁺ T cells are not tissue-resident immune cells and hence there is no ideal control. However, as ingress to the eye is a part of the disease and something inherent to uveitis, whether the changes are caused by activation or the microenvironment could be inconsequential provided they can be characterised and assist in understanding how the CD4⁺ T cells are altered in uveitis. Other studies investigating T cells also utilise spleen preparations as controls, but sometimes include an absence of activation markers (e.g. CD62L⁺, CD25/69⁻, etc) to ensure the T cells are in a naïve state. This indicates a line of investigation equivalent to good and currently established practice was undertaken with regards to controls for this type of experiment. It is entirely possible there is no perfect control for investigating T cells in uveitis.

Genes that up-regulate in the EAU retina have great variability, and this could be due to two factors: there is inherent variability in the EAU disease model itself (in terms of severity), and/or that the mice were at different stages of disease severity. A linear, unbiased method of scoring retinas for disease would permit the use of parametric correlative statistics and this could ultimately identify markers which associate with disease. In the spleen, there were fewer DEGs between a diseased and naïve state, although roughly a third of downregulated genes in the retina are also downregulated in the spleen simultaneously during EAU. There is also a small group of genes that are upregulated only in diseased spleens, indicating active changes occurring there in addition to the retina. As the T_{H1}/T_{H17} axis is pivotal in uveitis [1], a way of delineating T cell phenotypes from the mRNA-Seq data (and how they change across EAU) would be pertinent. As the spleen samples were prepared from eyes at peak EAU disease, it isn't possible to extrapolate whether these changes preclude infiltration of T cells into the retina or represent changes occurring from T cells that recirculated from the retina, or both. However, it adds to compounding knowledge that the peripheral lymphoid tissues are altered during inflammation, even at distal sites to the inflammation.

The further analysis of the experimental groups with PCA and hierarchical clustering also support our pipeline for transcriptomic analysis as valid, building a platform which can then be used for analysis of the microglial transcriptome. Unsurprisingly, the spleen samples were found closer together on the PCA plot than the retinal samples which indicates more similarity to each other than to the retinal samples. Paired retinal samples from the same mouse were also closer together than samples from a different mouse. This questions whether contralateral eyes are true biological replicates, as the peripheral immune cells which infiltrated the retinas are derived from the same pool. Furthermore, there is evidence to suggest untreated contralateral eyes can experience changes (with regards to the microglia) in the presence of pathology in the ipsilateral [547]. However, in both mouse and man it is well-recognised that the two eyes can experience different disease kinetics, with complete disease asynchrony in some rare cases [548]. This therefore demonstrates that they cannot be technical replicates. Overall, paired retinas could be considered neither biological replicates or technical replicates, and there may not be an existing term or statistical model that can analyse them in a completely valid manner in light of this (statistical models tend to assume different samples are biological replicates as technical replicates are commonly employed for evaluation of variability within a model, system, or assay).

In summary, successful optimisation of mRNA-Seq for ultra-low input samples (equivalent to single-eye microglial mRNA-Seq) and an analytical pipeline were achieved, both of which will be utilised as a robust platform for investigation of the microglial transcriptome in the retina before, during, and after uveitis.

Chapter IV: Validation and Optimisation of the *Cx3cr1^{CreER}:R26-tdTomato* Mouse Line

4.1 Introduction

4.1.1 The Challenge of Microglial Identification

Investigating microglia within inflammatory diseases has been historically very challenging. Microglia are historically differentiated as CD45^{lo}/CD11b⁺ [397]. However, there is overlap between CD45^{lo} and CD45^{hi} populations, meaning that during inflammation where infiltration of monocytes and macrophages (CD45^{hi}/CD11b⁺) occurs discrimination is poor.

When activated, microglial expression of CD45 has been argued to increase to CD45^{hi} [549, 550]. However, there is evidence suggesting that microglia retain the ability to differentiate into other immune cells and this could explain the observed increase [551]. Many other groups have been able to modestly discriminate a CD45^{lo} population during inflammation [348, 552, 553]. In other studies it has been shown that infiltrating monocytes can differentiate into microglia [554], or even that down-regulation of CD45 occurs in monocytes that are CD62L⁻ as compared to CD62L⁺ [555]; CD62L loss is associated with activation of immune cells [556]. A final group used chimeric techniques to conclusively show that microglia can up-regulate CD45, and that monocytes can down-regulate CD45 [415]. This raises questions about what the population of CD45^{lo} cells during inflammation might be, if there is a way to discriminate them with greater resolution, and ultimately discriminate microglia from that pool.

Until recently, there have been no markers that reasonably discriminate microglia from monocyte/macrophage populations. One marker, *Cx3cr1*, is a gene that is enriched in microglia within naïve organisms [557]. A transgenic mouse line was generated that replaced the first 390 bp of exon 2 of the *Cx3cr1* gene with GFP (and a single LoxP site) [429] and was believed would allow for the isolation of microglia; however many peripheral immune cells are GFP⁺ in naïve organisms, and other immune cell populations up-regulate *Cx3cr1* during EAU (and other inflammatory processes) making the mouse line an improvement but still unsuitable/inadequate for specific microglial identification [540]. CD44 is a newly-discovered marker [558, 559] which appears to resolve the CD11b⁺ CD45^{lo/hi} populations with greater resolution [558]. TMEM119 is a second such marker and has been reported by several teams using orthogonal methods to indicate it as a promising microglial-specific marker [352, 422, 560] that can differentiate them from other immune cells. However, it should be noted that infiltrating monocytes have been shown to adopt a microglia phenotype [415, 554] and hence TMEM119 may not permit discrimination of microglia derived from different origins (i.e.

embryologically-derived [yolk-sac] vs. resident-proliferating vs. monocyte/bone-marrow progenitor-derived microglia). TMEM119 has been argued to specifically label embryonically-derived microglia within the brain [422]. However, some very recent sc-mRNA-Seq data on a spontaneous EAU model (*Aire*^{-/-}) identifies expression of TMEM119 on a subset of monocyte/monocyte-lineage cells identified because they mapped separately to microglia using dimension-reduction algorithms [561]. Additionally, loss of *Tmem119* expression has been observed in activated microglia [340].

Nonetheless, the ability to label a pure population of tissue-resident microglia prior to the induction of inflammation (e.g. EAU/EIU) would be pragmatic and allow one to deconvolve and investigate the microglial kinetics. It would also allow for validation of novel microglia markers and activation markers, so that WT or other transgenic mouse lines could be used for further investigation of microglia in the future. This would bypass potential confounders of transgenic models (as you could utilise WT mice) or enable the use of alternative transgenic lines (e.g. some disease models are themselves transgenic lines, or other lines could be used to investigate how alterations to a molecular target changes both microglia and the model) without the need for complex breeding regimes to a line that tags microglia. A novel strain of mouse, called the “*Cx3cr1*^{CreER}:R26-tdTomato” mouse, is considered to allow for binary discrimination of tissue-resident microglia from other cells [376].

4.1.2 Cre/Lox Systems and CX3CR1

Cre recombinase (Cre) is an enzyme from the P1 bacteriophage. It uses a tyrosine residue within the active site to recombine specific DNA sites termed LoxP sites and is used for genetic manipulation [562]. It can be placed downstream of DEGs to create conditional gene targeting; for example, if placed downstream of *Cx3cr1*, only cells expressing *Cx3cr1* will express Cre and undergo recombination events at inserted LoxP sites within the genome. The *Cx3cr1*^{Cre} mouse line has been shown as able to tag microglia, but also many other types of macrophage found throughout the body, similarly to the *Cx3cr1*^{GFP} strain [540]. Cre and Lox systems are summarised in Figure 4.1.1.

CreER is a hybrid of the Cre gene and the oestrogen receptor (ER) gene, which is only activated when 4-hydroxytamoxifen (and some other ER partial agonists or antagonists) are bound but not oestrogen at physiological concentrations [563]; this allows for control of when recombination events occur, rather than occurring constitutively upon Cre expression. In other words, recombination only occurs when the ER partial agonists/antagonists are administered,

and therefore only cells expressing CreER at that specific point in time will undergo a recombination event [563]. However, it has been noted that some tamoxifen-independent recombination can occur in CreER (both CreER and CreER^{T2} [second-generation]) systems [564], particularly when CreER is inserted downstream of a highly-expressed promoter by a specific cell type [565].

Another commonly-used gene in transgenic mouse models is *Rosa26* because it is ubiquitously expressed in both embryonic and adult cells of the mouse [566]; a stop codon, flanked by LoxP sites, followed by the gene for a fluorescent protein are inserted downstream of the *Rosa26* promoter to create a reporter for Cre lines. *Rosa26* is commonly used as any target cell will express the fluorescent protein (or other insert) after a recombination event because it is ubiquitously expressed [566, 567]. It is noteworthy to mention that daughter cells (of those which have recombined) formed via mitotic division will also inherit this recombined variant, as it is permanent.

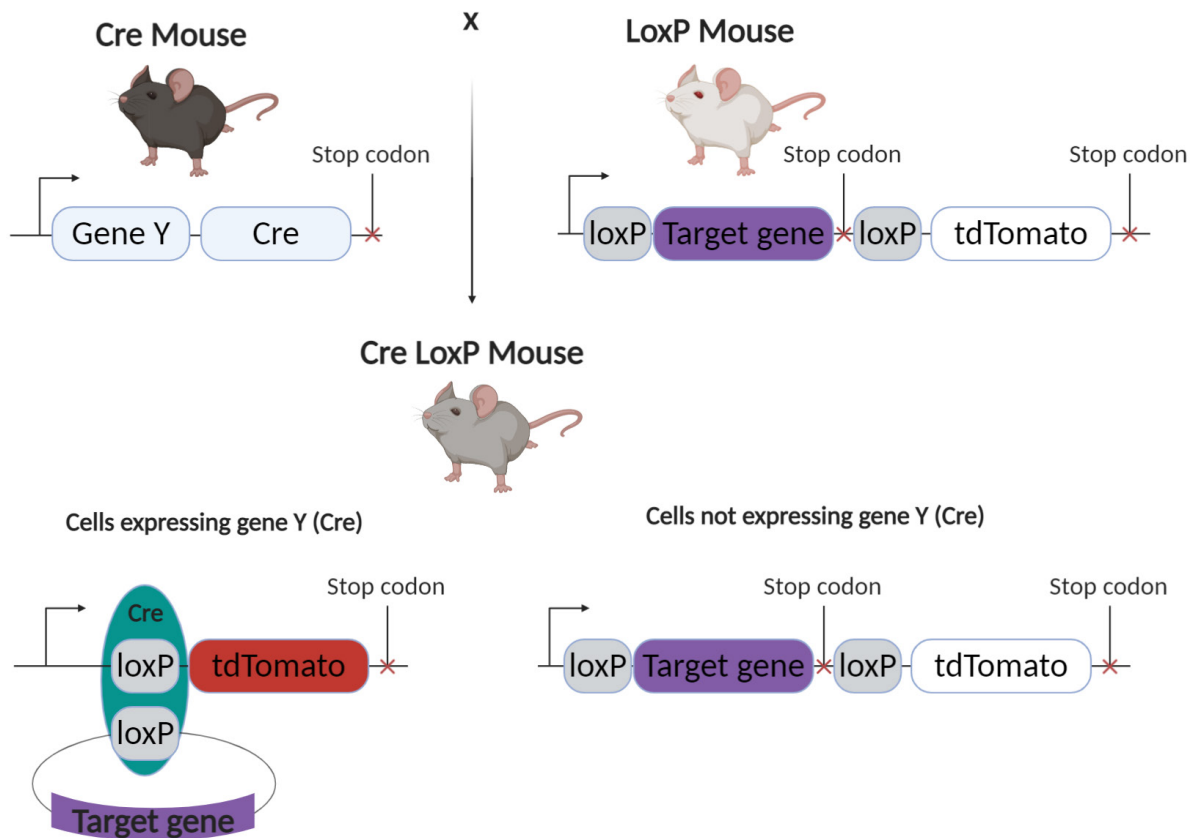


Figure 4.1.1. Cre and Lox systems, and their utilisation in conditional gene targeting. Homozygous mice for a Cre insert (downstream of a specific promoter) can be bred to LoxP homozygous mice (which contain Loxp [recombination sites], typically flanking a stop codon and with a fluorescent reporter downstream) to create Cre LoxP mice which enable conditional gene targeting. Only cells which express the promoter that Cre was inserted into have the capability to excise the region between the LoxP sites, resulting in removal of the stop codon and expression of fluorescent reporter (in this example, tdTomato). This system can be very useful in the conditional targeting of gene disruption, and/or fluorescent tagging of cells that have expressed a promoter for lineage-tracing studies.

In the *Cx3cr1^{CreER}:R26-tdTomato* mouse, *CreER^{T2}* replaced the 390 bp of exon 2 of *Cx3cr1* [540]. *Cx3cr1* is a microglial-enriched gene that is also expressed in lower amounts by other myeloid cells in naïve organisms [557], and therefore CreER is only expressed by myeloid cells. This means that only myeloid cells can undergo a recombination event and only when an ER partial agonist/antagonist is present. The CAG “promoter” (CMV early enhancer, chicken β -actin transcription start site [TSS], and rabbit β -globin intron), stop codons flanked by LoxP sites, and tandem dimer (td) Tomato fluorescent protein was also inserted downstream of the *Rosa26* promoter [568]. Therefore, until a recombination event occurs and the stop codon is excised, tdTomato cannot be expressed (in theory, although very low-levels of expression of tdTomato in the reporter mice – even in the absence of Cre – have been noted [569]).

As *CreER* is located downstream of *Cx3cr1*, only myeloid cells can potentially undergo a recombination event. Upon tamoxifen administration, myeloid cells undergo recombination and express tdTomato. Because *Cx3cr1* is a microglia-enriched gene [348], this genetic model tags microglia most effectively, although other myeloid cells are tagged too initially [376]. As myeloid cells are short-lived, with the exception of microglia which are long-lived with self-replicative potential [570, 571], after 4 weeks the other cells will have perished (as part of haematopoietic turnover) leaving microglia as the only cells tagged. In the original describing study, they indicate that a large proportion (~85%) of the microglial population are tagged using this transgenic model (Figure 2.1.2) [376]. This means that techniques such as FACS or flow cytometry, confocal microscopy, or others that use fluorescence-based detection will be able to identify tissue-based microglia. With a combination of other markers (e.g. CD44, CD45, TMEM119, CD11b, etc) it could allow for discrimination between monocyte/macrophage populations, for validation of these cell markers, and to investigate other avenues such as whether monocytes can differentiate into microglia (or microglia-like cells) and whether this occurs during chronic inflammation (e.g. EAU).

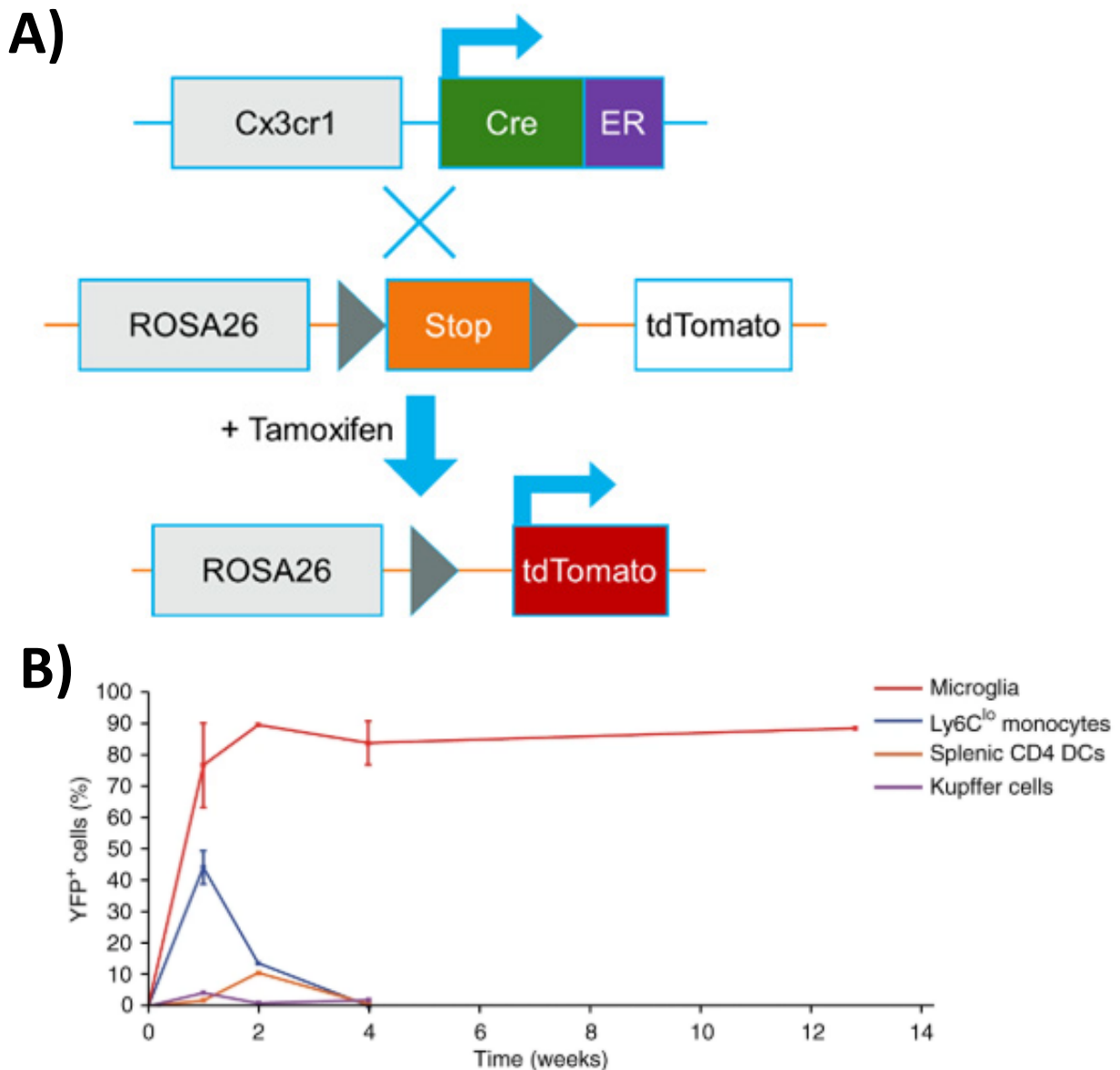


Figure 4.1.2. Recombination and the kinetics of fluorescent reporter positivity in the $Cx3cr1^{CreER}$ mouse strain. **A)** Schematic for inducing recombination in the $Cx3cr1^{CreER};R26-tdTomato$ mouse – loxP sites are indicated with grey triangles. **B)** A time-course highlights induction of recombination in a variety of cell types, with progressive loss of all but microglial cells by 4 weeks post-tamoxifen in the $Cx3cr1^{CreER};R26-eYFP$ mouse strain. Recombination persists in microglia long-term. Adapted from [376] and reproduced with permission from Springer Nature.

4.1.3 The Safety/Toxicity of Tamoxifen, CreER, and tdTomato

Tamoxifen is a known chloride channel blocker and has been shown to inhibit microglial process formation/extension, compromising their neuroprotective function after lesions were formed by lasers [572]. Whilst tamoxifen administration is acute, and occurs 4 weeks prior to the usage of mice, it is unclear if this would have long-term effects on the microglia and their function. Therefore, experiments to confirm a normal disease course/process will be required in the *Cx3cr1^{CreER}:R26-tdTomato* mouse line as altered *in vivo* kinetics would impact experimental time-points at which microglia are isolated for downstream sequencing. It is well-recognised that CreER mouse lines can also have off-target effects and use of heterozygotes in experiments helps to mitigate these as it ensures that there are functional variants of all proteins in the organism. Nonetheless, the effect of a haplosufficient heterozygote compared to a WT homozygote is unknown as it is specific for each mouse strain. However, as discussed earlier, use of this transgenic line represents one of the only currently available approaches of specifically isolating microglia (until specific markers are identified, potentially through use of this transgenic line) which justifies its use.

In the literature there are many reports of CreER being toxic and causing severe side-effects on mice via the cells they are expressed in, irrespective of whether they had received tamoxifen or not [573]. A different study in the eye was conducted to establish the potential toxic or other effects that CreER and tamoxifen administration might have. For this study, three different Cre mouse lines (CAGGCre-ERTM [which should tag all retinal cells, including microglia], α -Cre, and LMOP-Cre) were used to investigate whether Cre expression and/or tamoxifen treatment would alter retinal structure/function, neuronal vulnerability or glial reactivity in the mouse eye [510]. *Ex vivo* assessments included confocal laser scanning microscopy of histological tissue sections (to visualise potential morphological changes in individual cell types, but to also perform measurements of the INL thickness) and qPCR of microglial activation markers, a macroglial development factor, and neuroprotective factors. Additionally, clinical *in vivo* assessments in the form of fundal images and ERGs of the retina, and neuronal vulnerability to light damage (measured by a TUNEL assay) were performed. In summary, they showed that Cre or CreER and tamoxifen did not influence retinal function, expression of neuroprotective factors, macro-/microglial reactivity, and neuronal vulnerability. This suggests that the eye is not compromised by Cre toxicity and/or tamoxifen treatment. There are no known abnormalities in the *Cx3cr1^{CreER}:R26-tdTomato* mouse line, but these studies highlight the need for good controls (i.e. at least from the same transgenic line, but ideally littermates) but also confirmation of typical

disease kinetics (despite no detectable retinal abnormalities in other Cre lines) as it has been shown that perturbation of microglia can inhibit establishment of ocular disease in the EAU model [390].

Lastly, it is well-recognised that fluorescent proteins have the potential to be both immunogenic and toxic to cells [574]. tdTomato is a tandem-dimer, making it in effect a monomer with double the molecular weight, that was engineered not to oligomerise which has helped reduce its toxicity potential. It is recognised that (detectable) toxicity is rare in currently-used fluorescent reporters [575]. tdTomato has a relatively low potential for phototoxicity due to longer-wavelength excitation (with respect to many other fluorophores) [576]. It is also noteworthy to mention that tdTomato is extremely bright and has very high photostability as well, making repeated *in vivo* imaging unlikely to cause issues with respect to our detection of the microglia [577]. It would be important to characterise the mice post-tamoxifen to confirm the microglia as physiological, and to use equivalent controls so that tdTomato presence/absence does not potentially confound experiments.

The overall emerging picture from the use of transgenic mice (e.g. Cre lines), fluorescent reporters, and tamoxifen is that equivalent controls (if not littermates) should be used where possible to mitigate any possible (even if not detected) confounding caused by the transgenic line, tamoxifen treatment, CreER, and/or fluorescent protein.

4.1.4 Tamoxifen Administration Routes

Various routes of tamoxifen administration (for activating CreER systems) have been described previously. Research groups commonly employ subcutaneous injection [376] or oral gavage [540] (also in food), but topical administration (as a 4-day regime) has also been described recently as both safe and effective [510]. Therefore, we sought to compare the subcutaneous and topical administration routes of tamoxifen (200 μ L of a 21 mg/mL solution on days 1 and 3, and 10 μ L of a 5 mg/mL solution to each eye 3 times daily for 4 days, respectively) – one systemic approach compared to the local approach – to identify whether one was superior with respect to both the sensitivity of inducing recombination in, and specificity for microglia (i.e. the proportion of microglia that are tagged using the approaches, and the frequency of recombination events in non-microglial cells and their presence in the retina under inflammatory conditions). This would enable us to determine which is the most suitable regime for use in our experiments in the *Cx3cr1^{CreER};R26-tdTomato* strain.

4.1.5 Summary

The *Cx3cr1^{CreER}:R26-tdTomato* transgenic mouse offers great potential as a tool for investigating microglia, but many questions needed to be asked such as whether the Cre/Lox system alters microglial behaviour and disease model kinetics, whether it is indeed sensitive and specific for microglia, and if this is universal or biased towards a particular tamoxifen administration route.

The major aims of this chapter were to characterise the sensitivity and specificity of different tamoxifen administration regimes for retinal microglial tagging in the *Cx3cr1^{CreER}:R26-tdTomato* to confirm whether it would be suitable (alone or in combination with antibody staining) for retinal microglial isolation and downstream transcriptomic assessment during inflammatory states.

4.2 Results

4.2.1 Sensitivity of Microglial Tagging

Firstly, confirmation was sought that the retina in the *Cx3cr1^{CreER}:R26-tdTomato* mouse line was physiological and no perturbations were observed. Secondly, confirmation that it was possible to tag retinal microglia using tamoxifen and the *Cx3cr1^{CreER}:R26-tdTomato* mouse line was required. Thirdly, a comparison between the different tamoxifen regimes (topical 3x daily lasting for 1–4 days, a subcutaneous approach with injections on days 1 and 3, and no-tamoxifen controls) was required to observe if they tagged microglia differentially and if one was superior compared to the others for use in continuing work. Brightfield fundal imaging of WT and *Cx3cr1^{CreER}:R26-tdTomato* mice revealed no gross differences between the retinas, suggesting a physiological state, in a naïve context at least (Figure 4.2.1). A fluorescent fundal imaging time-course (with gain-normalised settings) indicates that, following systemic administration, retinal tdTomato fluorescence has not stabilised by 2 weeks post-tamoxifen; it reaches a maximum by 4 weeks however (Figure 4.2.2). Fluorescent imaging of retinal tdTomato undergoing the different tamoxifen regimes, 4 weeks post-tamoxifen, suggested (as a qualitative readout) that a minimum of 2 days of the topical regime was required for full tagging (Figure 4.2.3). It also indicated that a modest proportion of microglia can recombine in the retina independently of tamoxifen administration (tamoxifen-independent, or constitutive, recombination).

However, a quantitative assay that was more absolute and sensitive would confirm whether all retinal microglia were tagged (sensitivity) and if other retinal cells were also labelled following tamoxifen administration (specificity). To assess this, flow cytometric analysis was performed on the retinas using a panel to include the microglial markers CD45 and CD11b (good markers of determining microglia in a naïve retina). This demonstrated that a 3- or 4-day topical, or subcutaneous (days 1 and 3) regime was required for full microglial tagging and that the other regimes (including 2-day topical) were insufficient (Figure 4.2.4).

As a final confirmation confocal laser-scanning microscopy, performed on retinal flatmounts, permitted assessment of the spatial distribution and morphology of the tdTomato^{hi} cells; they exhibited the ramified morphology typical of microglia which also suggested that there were no gross perturbations in the retina or microglia as a consequence of the transgenic line or treatments (Figure 4.2.5).

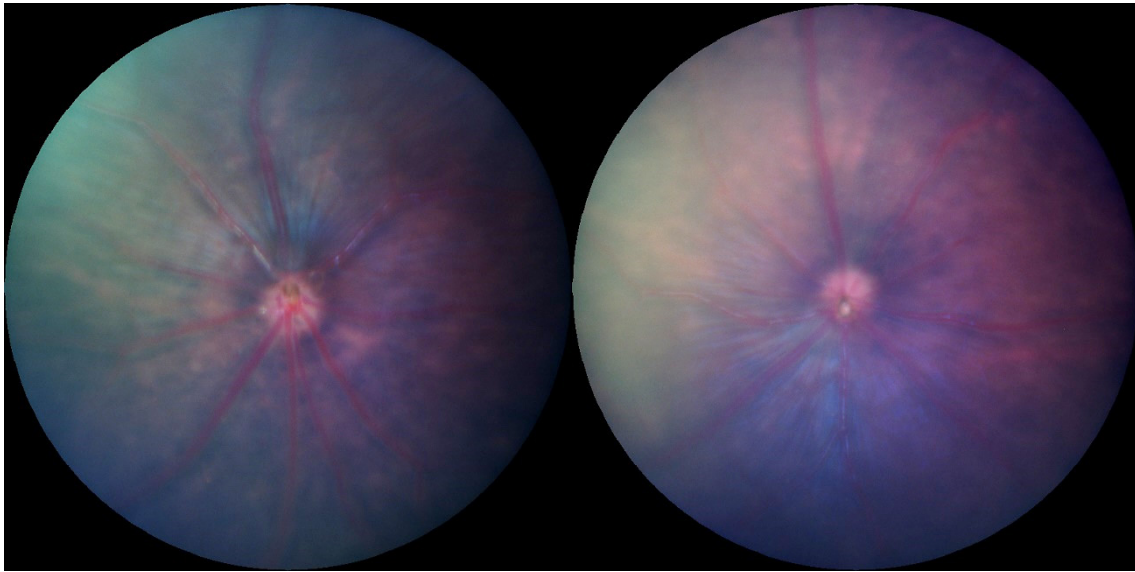
Wild-Type**CX3Cr1^{CreER}:R26-tdTomato**

Figure 4.2.1. Brightfield imaging of wild-type (WT) and $Cx3cr1^{CreER}:R26-tdTomato$ mice highlight no gross perturbations as a consequence of gene editing. Representative fundal images are shown, where mice exhibit a typical appearance that lacks retinal scarring, inflammation, or degenerative phenotypes.

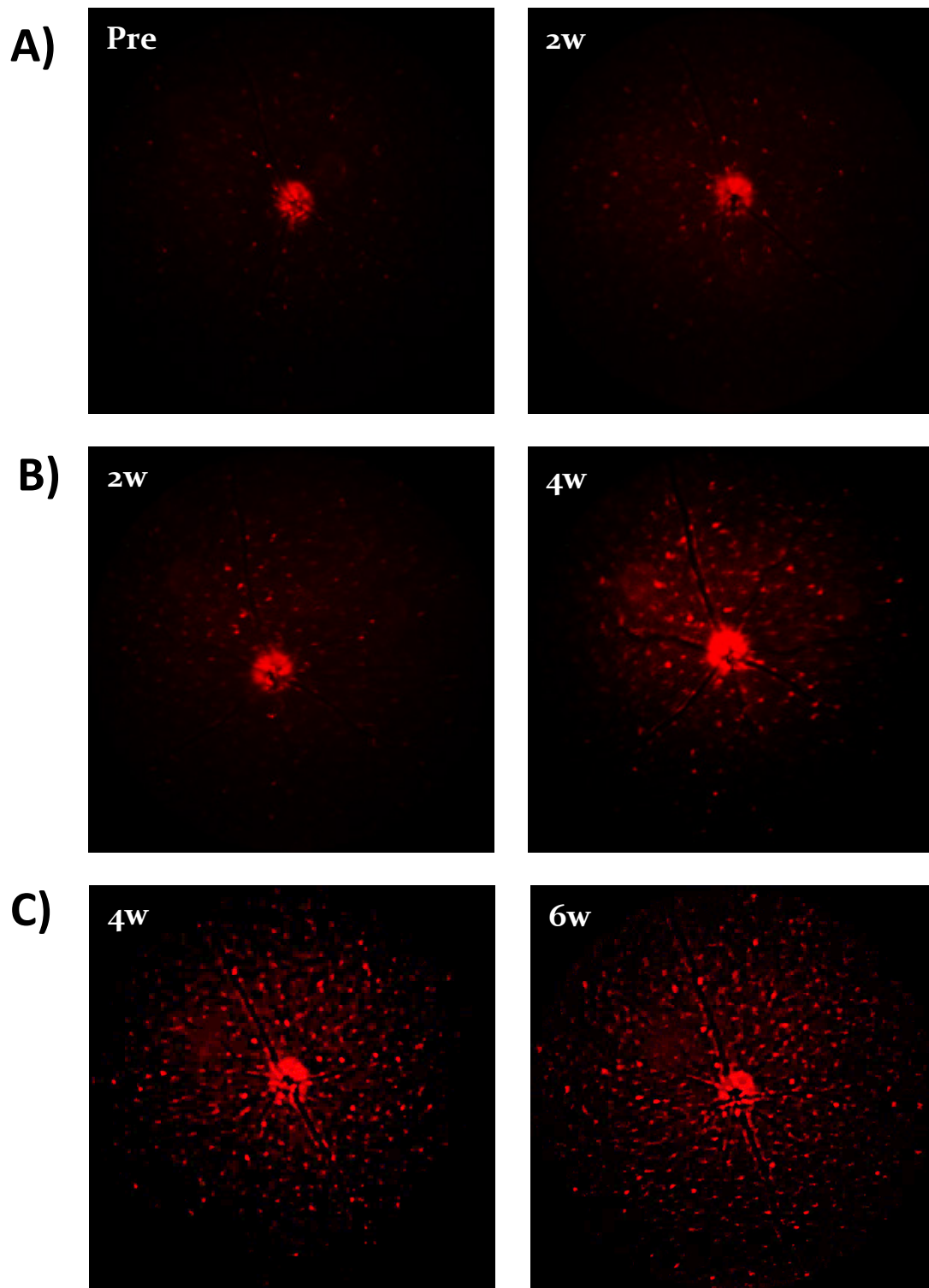


Figure 4.2.2. Representative fluorescent fundal images of $Cx3cr1^{CreER};R26-tdTomato$ mice before and after tamoxifen administration. **A)** Images pre- and 2 weeks post tamoxifen indicate a slight increase in fluorescence. **B)** Fluorescence greatly increases between 2- and 4-weeks post-tamoxifen. **C)** Fluorescence intensity does not change after 4 weeks post-tamoxifen, indicating stabilisation. All mice (different in each panel) received a subcutaneous tamoxifen administration regime and were 5 weeks old when tamoxifen was administered.

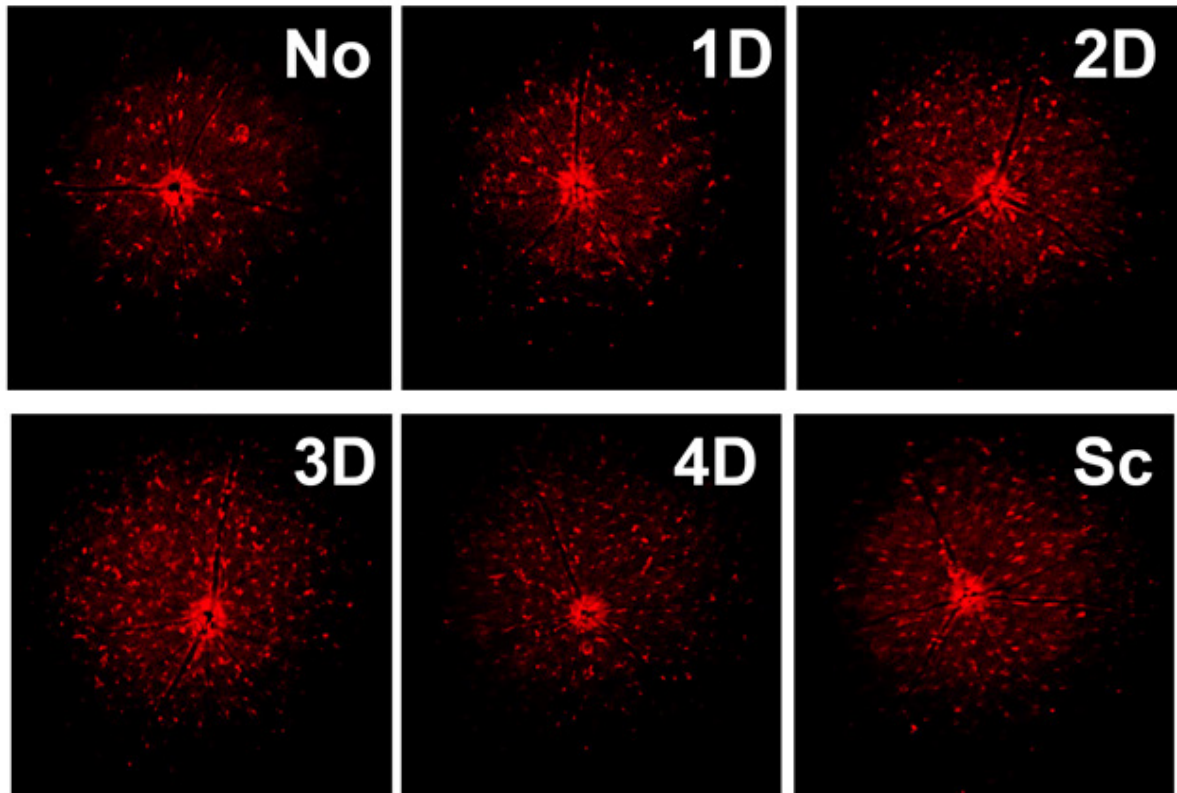


Figure 4.2.3. Representative fluorescent fundal images of $Cx3cr1^{CreER};R26-tdTomato$ mice undergoing different tamoxifen administration regimes 4-weeks post-tamoxifen. There is clear evidence of recombination and tdTomato expression in a no-tamoxifen mouse, but more microglia are tagged when tamoxifen is administered; it is difficult to discern differences between 2D–4D and Sc retinas. The results are representative of two independent experiments, with at least 4 biological replicates per group. Abbreviations: No – no tamoxifen administered, xD – x-day topical tamoxifen regime, Sc – subcutaneous tamoxifen regime.

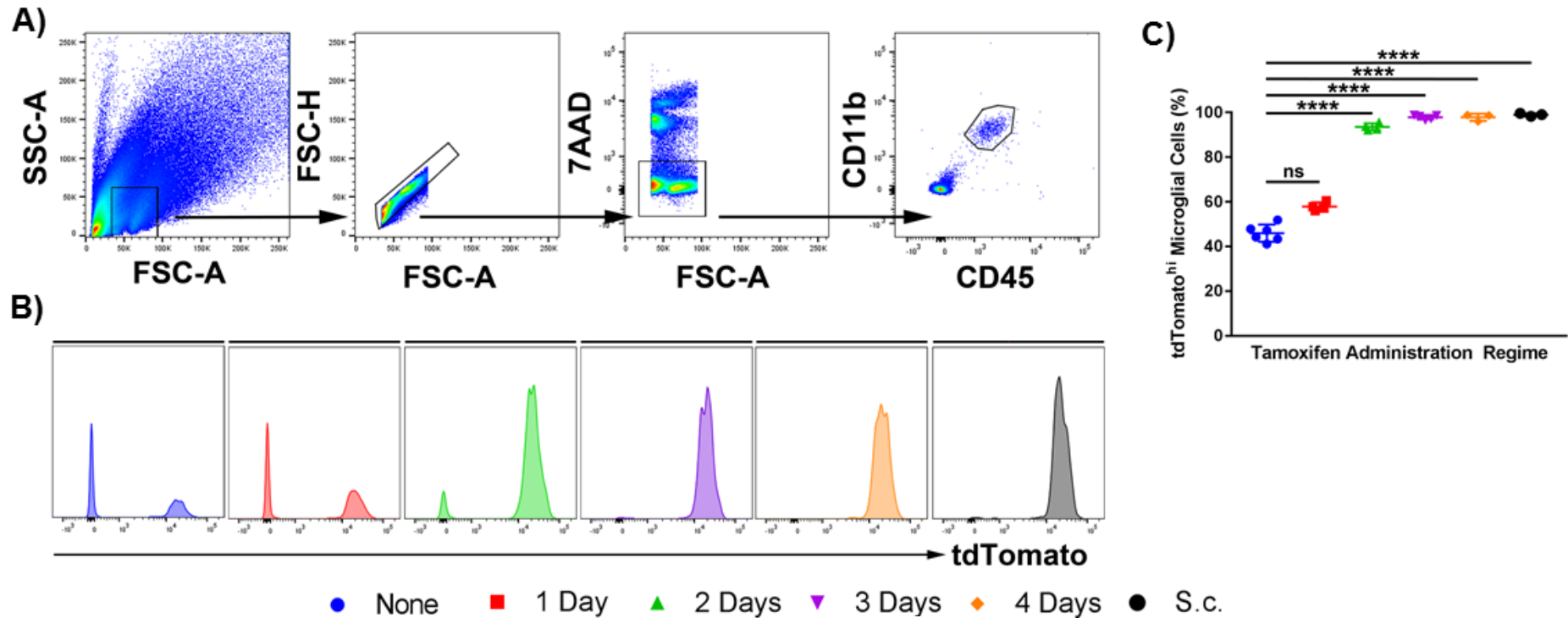


Figure 4.2.4. Sensitivity of microglial recombination induced in $Cx3cr1^{CreER};R26-tdTomato$ mice using different tamoxifen administration regimes. **A)** A representative flow cytometric gating strategy used to identify microglia in a naïve retina based on CD45 and CD11b expression. **B)** Representative tdTomato histograms (unit area scaling) on gated microglia from various tamoxifen administration regimes. **C)** Aggregate data demonstrating the percentage of microglia that were tdTomato^{hi} (as quantified by flow cytometry) shows that a 3-day and 4-day topical, in addition to subcutaneous, regimes result in full microglial tagging (n = 3-6). Abbreviations: None – no tamoxifen administered, 1D – one-day topical tamoxifen regime, 2D – two-days topical tamoxifen regime, 3D – three-days topical tamoxifen regime, 4D – four-days topical tamoxifen regime, Sc – subcutaneous tamoxifen regime. For statistical analysis, One-way ANOVA with Tukey's post hoc test was used. **** = p ≤ 0.0001, ns = not significant.

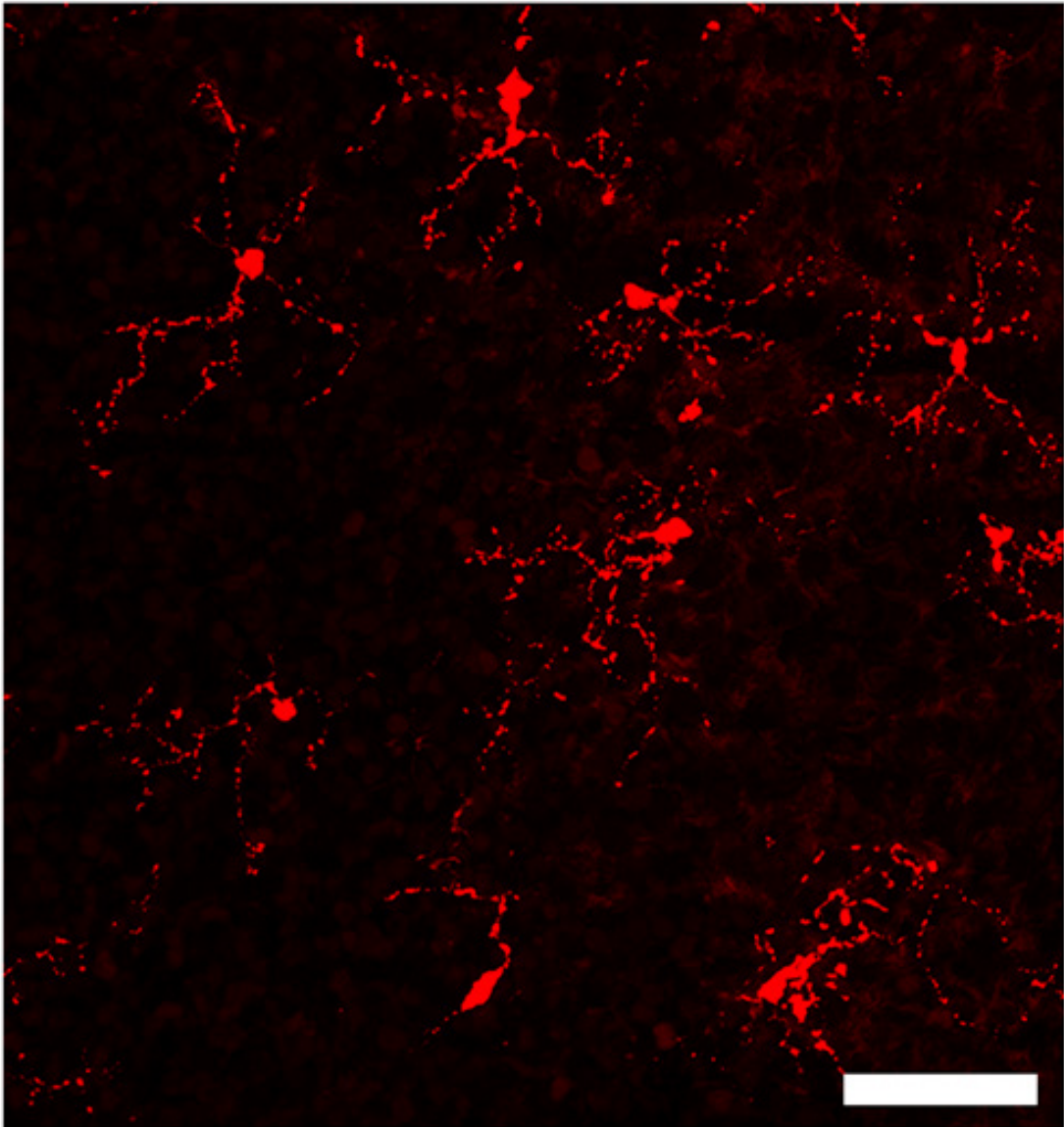


Figure 4.2.5. *Representative confocal microscopy maximum-intensity projection of a whole naïve retina highlights a physiological morphology. Retinal flatmount prepared from a mouse that received the 3-day topical tamoxifen regime. The microglia exhibit a physiological ramified morphology, suggesting no gross perturbations in the microglia as a consequence of the transgenic model and tamoxifen administration. Scale bar = 30 μ m.*

4.2.2 Specificity of Microglial Tagging

Having confirmed that a 3- or 4-day topical tamoxifen regime or sub-cutaneous approach was required for full retinal microglia tagging, subsequent experiments sought to compare differences in the specificity for microglial tagging using these routes (i.e. if extraocular cells underwent recombination). This was important for the planned transcriptomic assessments of microglia before, during, and after intraocular inflammation as these would require “pure” populations of retinal microglia and it is well-known that other cells ingress to the retina during inflammation.

Initial experiments sought to characterise the full extent of tdTomato expression following topical and subcutaneous administration. Tissue samples were prepared for flow cytometric assessment using an immunophenotyping panel (containing B220 [a B cell marker], CD3 [a T cell marker], CD11b [a myeloid cell marker], CD45 [an immune cell marker], and Gr-1 [an antibody that binds Ly6C and Ly6G with different affinities to differentiate “resting/patrolling” and “inflammatory” monocytes in addition to granulocytes]) to identify whether there were tdTomato^{hi} cells present in non-retinal tissues (blood, bone marrow, brain, kidney, liver, lung, and spleen), but also whether there was a predisposition to a given cell type – as use of the tag in conjunction with other markers may nonetheless permit specific microglial identification. The sub-cutaneous approach resulted in full tagging of brain microglia due to the systemic administration; in comparison, the topical approach and no-tamoxifen controls resulted in 40–50% of microglia being tagged (Figure 4.2.6).

With the sub-cutaneous approach, there were also ~2.2 times more tdTomato^{hi} splenic monocytes as compared to a topical approach (Figure 4.2.6). Furthermore, the presence of a small number of tdTomato^{hi} cells were observed in other peripheral tissues (Figure 4.2.7). Whilst the absolute numerical differences in cells (or percentages) are low, this could be pertinent in the context of the eye where only a small number of microglia are found; numbers of tdTomato^{hi} cells ranging in the hundreds (if they infiltrate the eye) as observed could greatly reduce the specificity of the mouse line.

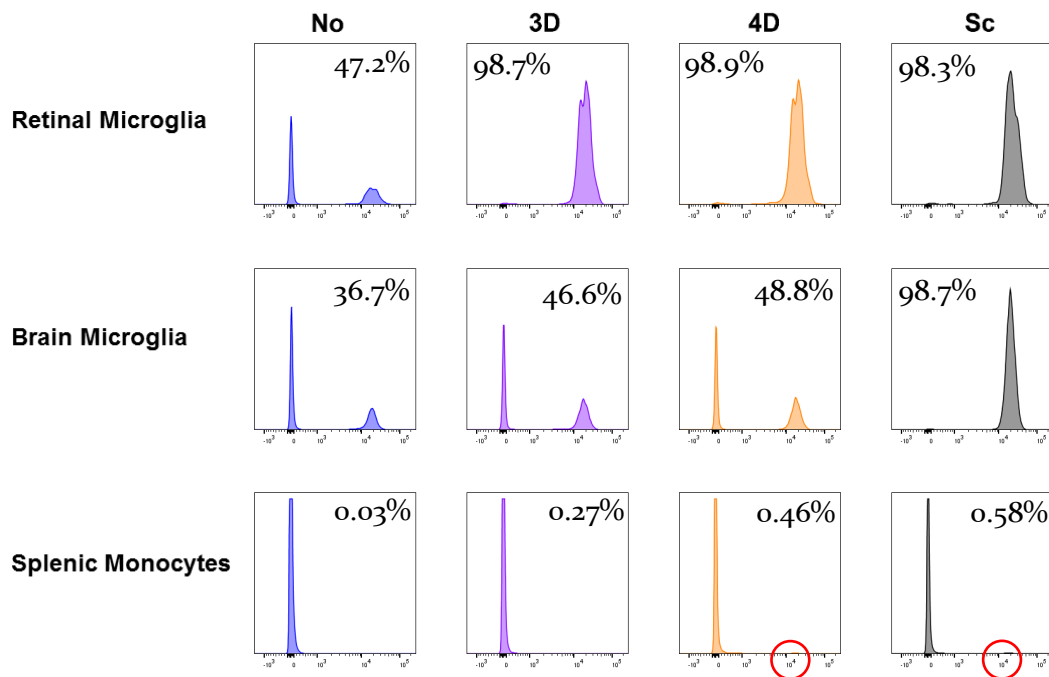


Figure 4.2.6. Flow cytometric histograms highlight tagging of brain microglia and a small number of splenic monocytes following subcutaneous (systemic) tamoxifen administration. Histograms for different tamoxifen administration regimens are displayed for retinal microglia, brain microglia, and splenic monocytes alongside the percentage positive of each cell type for tdTomato. Histograms containing a small number of positive cells are highlighted with circles. Abbreviations: No – no tamoxifen administered, 3D – 3-day topical tamoxifen regime, 4D – 4-day topical tamoxifen regime, Sc – subcutaneous tamoxifen regime ($n = 1$).

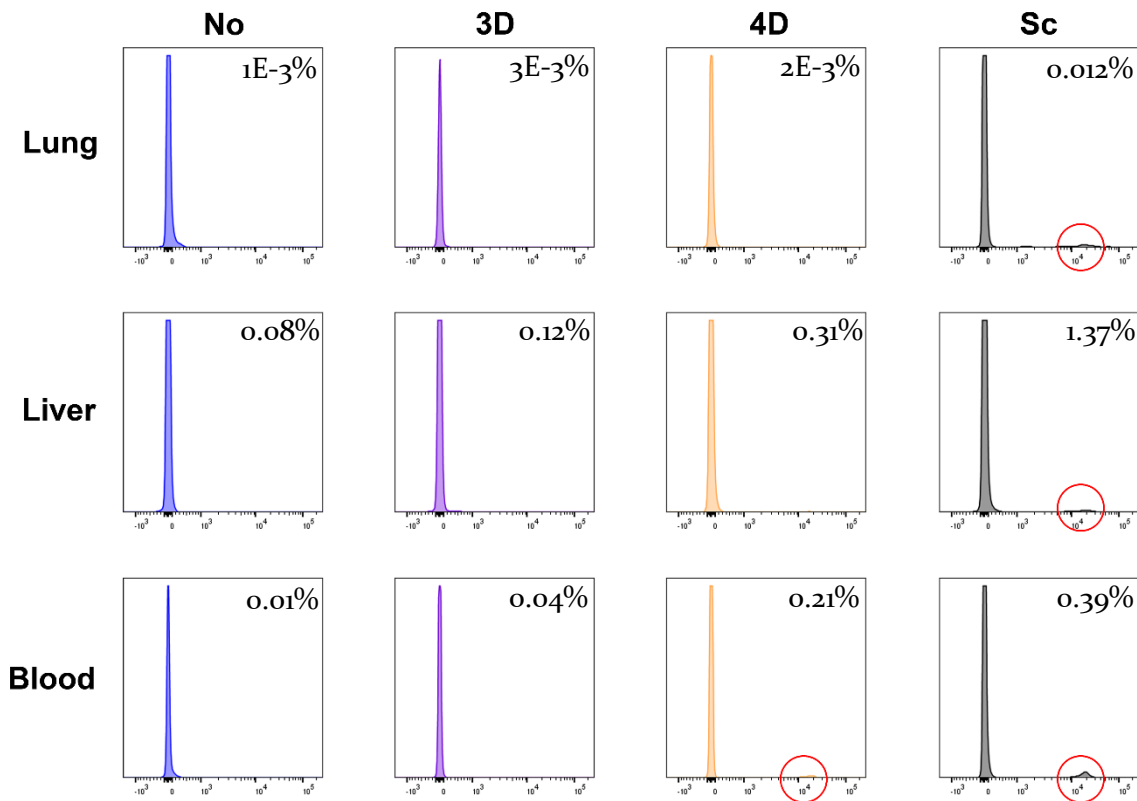


Figure 4.2.7. Flow cytometric analysis of peripheral tissues indicates a small, but potentially significant, number of tdTomato^{hi} cells. Tissues were gated for cells, singlets, live cells, and then for myeloid cells (CD45⁺, CD11b⁺). Histograms of tdTomato fluorescence intensity from the different tissues are shown alongside the percentage positive for tdTomato. Histograms containing a small number of positive cells are highlighted with circles (these samples contained a minimum 3-figure number of tdTomato^{hi} cells). Abbreviations: No – no tamoxifen administered, 3D – 3-day topical tamoxifen regime, 4D – 4-day topical tamoxifen regime, Sc – subcutaneous tamoxifen regime (n = 1).

Nonetheless, the presence of peripherally recombinant cells (including brain microglia) is not necessarily of concern (with respect to retinal microglial specificity) if they do not infiltrate the eye during inflammation. Therefore, to test this comprehensively a model where immune cell infiltration to the eye occurs was required. EIU, as a model of acute endotoxin-induced inflammation, was selected for this purpose because it has a robust and reliable onset of disease with peak immune cell infiltrate observed within the retina and VB at 18 hours post-induction (typically by intravitreal injection of LPS).

Before testing, it was important to first confirm the EIU model kinetics in the *Cx3cr1^{CreER}:R26-tdTomato* mouse line were equivalent to the WT C57BL/6J mouse (see Chapter V, Figure 5.2.1). This would allow the isolation of retinas for flow cytometry during the peak cellular infiltrate stage of EIU (18 hours post-injection) to test the specificity.

Flow cytometry was performed on the retinas during peak cellular infiltrate (as confirmed by OCT of the retinas; Figure 4.2.8) and the immunophenotyping panel was used so that various immune cell populations could be gated and checked for their expression of tdTomato (Figure 4.2.9).

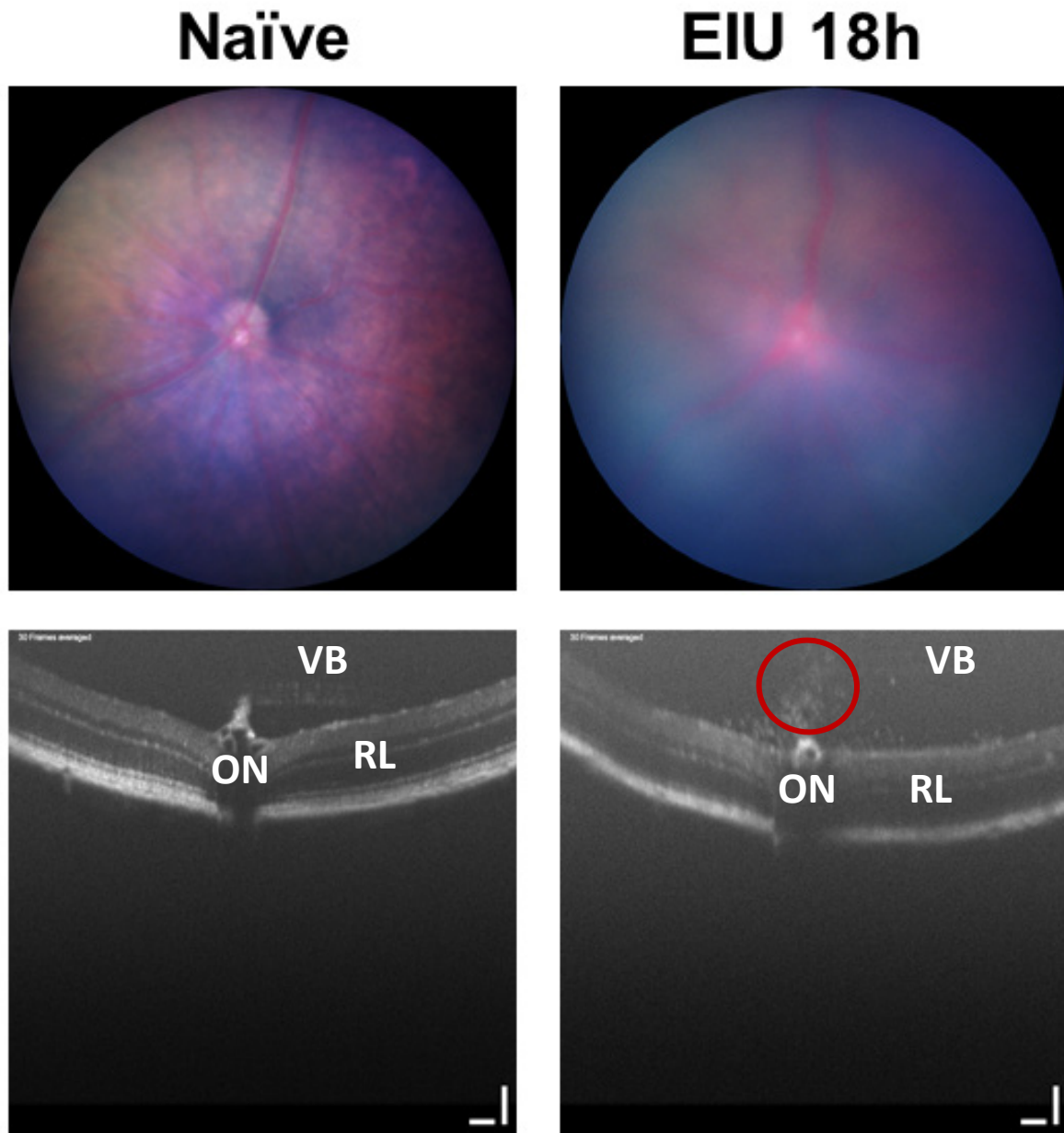


Figure 4.2.8. Representative images of a naïve and EIU 18h retina in the $Cx3cr1^{CreER};R26-tdTomato$ mouse line. Fundal images (top) show a generalised haze, including over the optic disc (nerve), which OCT (bottom) confirms as cellular infiltrate in the vitreous (circled). Abbreviations: EIU – endotoxin-induced uveitis, OCT – optical coherence tomography, ON – optic nerve, RL – retinal layers, VB – vitreous body.

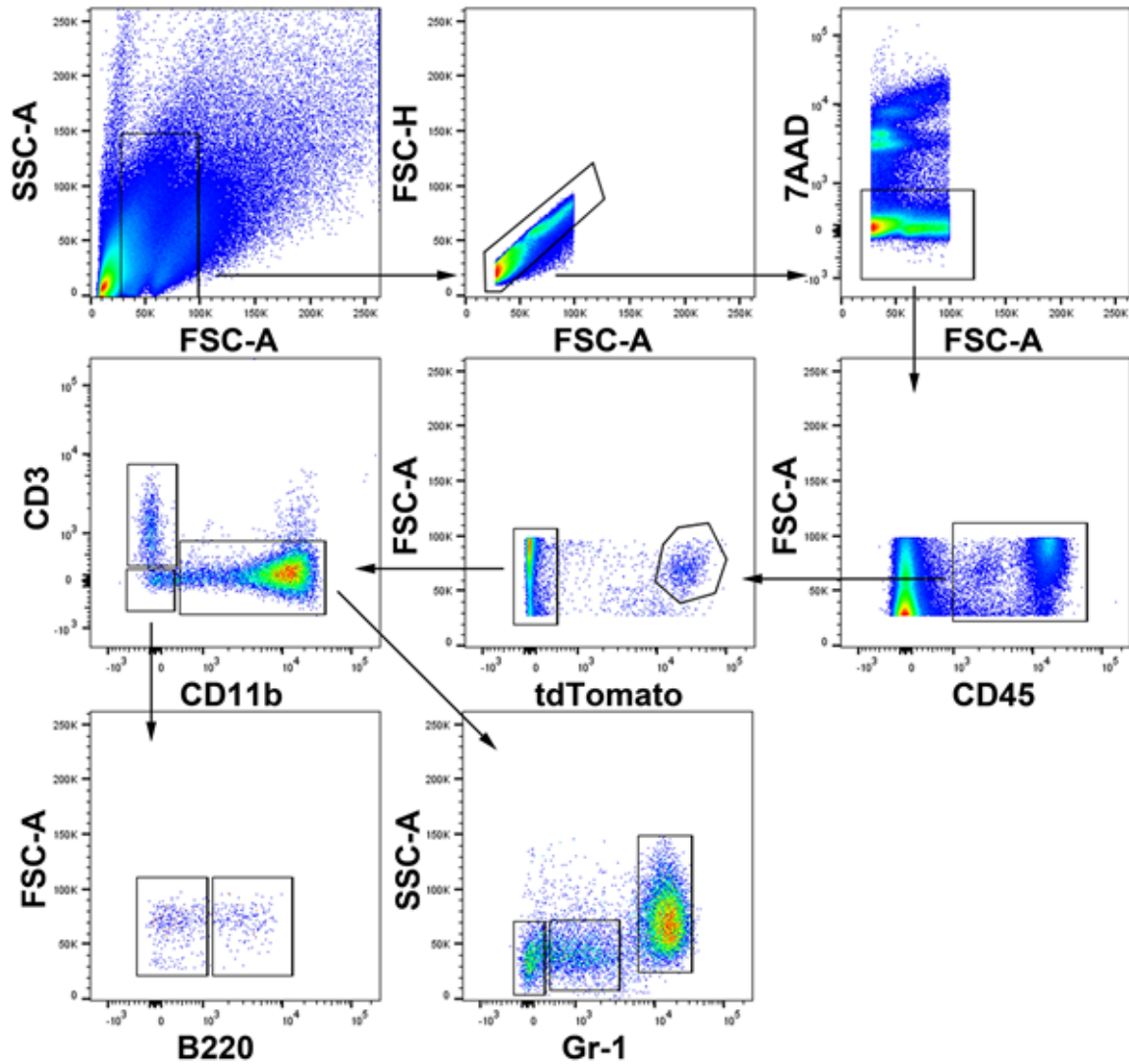


Figure 4.2.9. Flow cytometric gating strategy used to differentiate immune cell populations present in the retina at peak EIU. Retinas were gated for cells, singlets, live cells, and CD45⁺ immune cells. They were then separated into tdTomato^{hi} (which we hypothesised were microglia) and tdTomato^{lo}. The tdTomato^{lo} cells were then gated for myeloid cells (CD11b⁺), T cells (CD3⁺), and other (CD3⁻, CD11b⁻), with the myeloid cells further discriminated into Gr-1^{lo} (Ly6G⁻), and Gr-1^{hi} (Ly6G⁺) cells. The “other” cells were gated on B220 to identify B cells.

To test for specificity, tdTomato^{hi} cells were gated from live cells (as per Figure 4.2.9; Figure 4.2.10a) and then subsequently back-gated for microglia based on CD45 and CD11b expression. In the 4-day topical and subcutaneous approaches, the presence of non-microglial cells in the tdTomato gate was observed (Figure 4.2.10b, circled), indicating a slight reduction in specificity. Gating for microglia without first gating for tdTomato^{hi} cells results in the inclusion of many tdTomato⁻ cells which are not microglia, and greatly compromises the specificity (Figure 4.2.10c, blue). The results indicate that a 3-day topical approach had the highest specificity (equivalent to a no-tamoxifen control, where incomplete microglial tagging but no peripheral tagging has occurred), followed by the 4-day topical approach and lastly sub-cutaneous (Figure 4.2.10d). Nonetheless, use of any tamoxifen administration regime considerably trumped the use of conventional CD45/CD11b gating.

However, a possible limitation to this approach for distinguishing the retinal microglia (CD45^{int} CD11b⁺ tdTomato^{hi}) from the tdTomato^{hi} group is that non-retinal microglial or non-microglial cells which possess a similar transcriptional profile (e.g. infiltrating monocytes or brain microglia) could be falsely identified as retinal microglia. Therefore, the total counts of the tdTomato^{hi} group, from naïve and peak EIU retinas (3-day topical tamoxifen regime), were compared and no significant difference was observed confirming a pure retinal microglial population (Figure 4.2.11). All subsequent experiments used the 3-day topical tamoxifen regime.

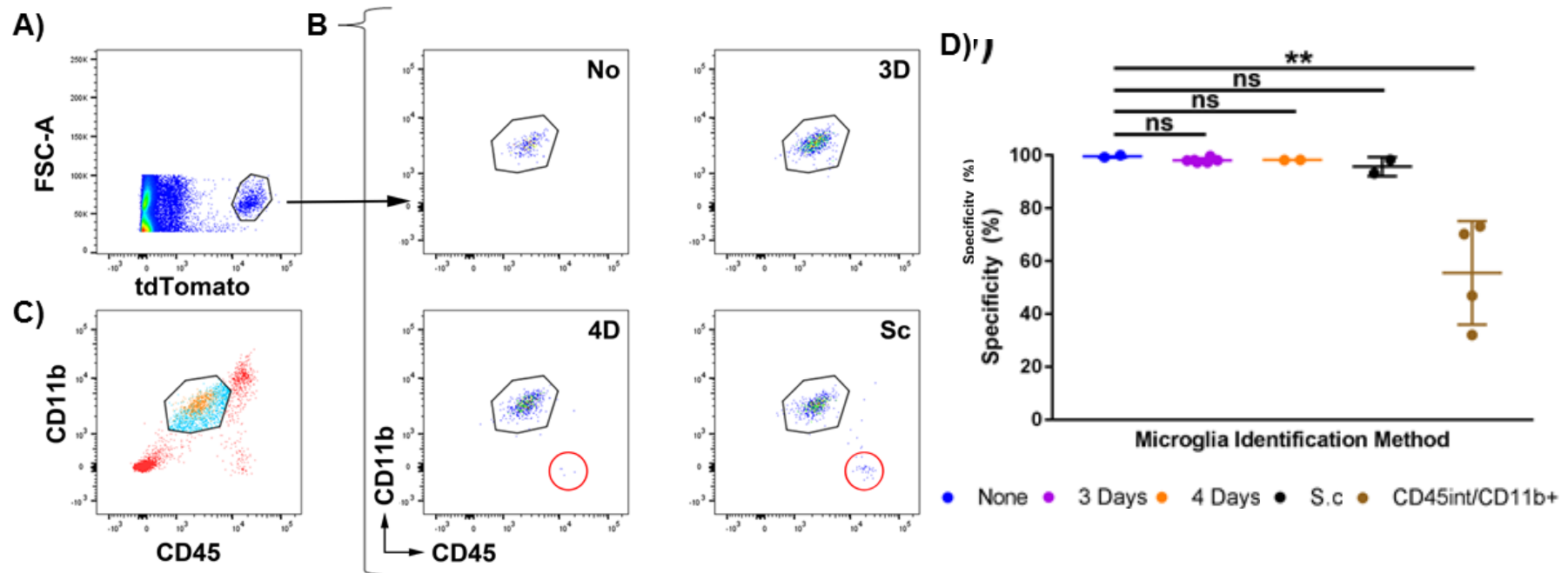


Figure 4.2.10. The specificity of different tamoxifen administration regimes for microglial tagging in the *Cx3cr1^{CreER}:R26-tdTomato* mouse strain during active inflammation. **A)** Peak EIU retinas following different tamoxifen administration regimes were prepared for flow cytometry. Live, cell singlets were gated based on tdTomato^{hi} expression. **B)** tdTomato^{hi} cells were gated based on CD45^{int} and CD11b⁺ expression, and in the 4-day and subcutaneous tamoxifen treated groups, non-microglial cells (CD45^{hi}, CD11b⁻) were present (circled). **C)** Gating microglia based on CD45 and CD11b expression alone results in the inclusion of infiltrating immune cells (tdtomato⁻, blue) in addition to retinal microglia (tdTomato^{hi}, orange) but exclusion of cells not fitting the microglial expression profile (CD45^{hi/-}, red). **D)** Aggregate data on the percentage specificity for microglia demonstrates that the 3-day topical route results in high specificity for microglia using tdTomato. The CD45^{int}/CD11b⁺ group uses the microglial gating strategy (from live cell singlets without using tdTomato) shown in panel B for a comparison of the mouse strain to conventional microglial identification strategies (n = 2–5). Abbreviations: None – no tamoxifen administered, 3D – three-days topical tamoxifen regime, 4D – four-days topical tamoxifen regime, Sc – subcutaneous tamoxifen regime. For statistical analysis, One-way ANOVA with Tukey’s post hoc test was used. ** = p ≤ 0.01, ns = not significant.

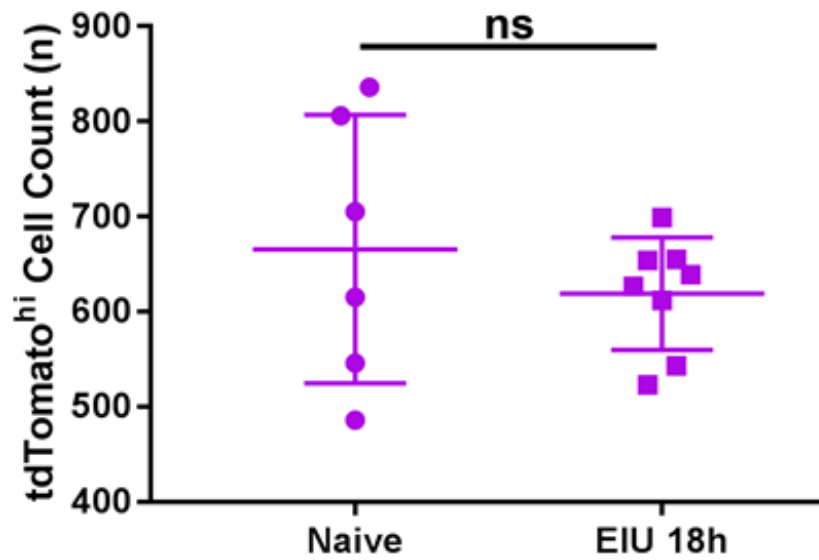


Figure 4.2.11. EIU-mediated inflammation does not alter the number of tdTomato^{hi} cells. The retinas from naïve and EIU 18h mice were processed for flow cytometry and gated for live tdTomato^{hi} singlets. All mice underwent a 3-day topical tamoxifen regime. For statistical analysis, the t-test was used. Ns = not significant (n = 6–8).

4.3 Discussion

The *Cx3cr1^{CreER}R26-tdTomato* mouse line is both highly sensitive and specific for microglia, and irrespective of tamoxifen administration routes is a considerable improvement on the previously available methods of microglial isolation (whether that be by cell-surface markers such as CD45 and CD11b, through use of the *CX3CR1^{GFP/+}* mouse line, or other approaches). This is especially important as a clear marker to distinguish long-lived, yolk-sac derived microglia from infiltrating myeloid cells is critical to our future investigation into the transcriptome of the microglia.

In concordance with previously published work, our results suggest that the *Cx3cr1^{CreER}:R26-tdTomato* mouse strain do not possess any gross abnormalities and that the microglial morphology (as identified using confocal laser-scanning microscopy) is physiological (ramified). The use of appropriate controls (transgenic mice under the same tamoxifen regimen) is necessary to mitigate any potential confounding effect of the transgenic line and/or tamoxifen treatment; this will be implemented for future experiments as there could be perturbations in the mice which are beyond the detection limits of these assays. Further investigation of this might be possible through comparison of microglial morphologies (between *Cx3cr1^{CreER}:R26-tdTomato* and WT C57BL/6 strains) using Frac-Lac or Sholl analysis on microscopy images. Nonetheless, despite this potential caveat other studies that used more sensitive approaches to assess functionality within the retina (e.g. ERG, qPCR, and cell death due to a light-induced damage model) were unable to detect perturbations due to the presence of CreER and/or tamoxifen administration [510].

The results showed a high level of tamoxifen-independent (constitutive) recombination in the microglia. Whilst this was unexpected, it has been reported in CreER models previously and so is certainly not exclusive to this CreER line or investigations – it is suggested that high expression of the CreER, dependent on which promoter it is inserted downstream of, can lead to tamoxifen-independent (or constitutive) recombination [564, 565]. Constitutive recombination is a well-recognised phenomenon within the field of receptor biology [578], and in a simple two-state (active or inactive; on or off) model of receptors an equilibrium between these two states (with the position, in the absence of an agonist, being far to the inactivated side) is present. This means that it is entirely possible for a receptor to be in an active conformation even in the absence of a ligand. Therefore, the higher the expression of CreER (but also the longer the time the expression persists, or the receptor lasts before recycling, for) the greater probability of a tamoxifen-independent recombination event occurring. As

microglia highly express *Cx3cr1*, this explains why we observe this phenomenon. Nonetheless, this phenomenon is of no major concern with regards to microglial tagging as full tagging occurs after a tamoxifen regime. A more pertinent question is whether chronic inflammation (and possible engraftment of monocytes/bone marrow progenitors) leads to sustained expression of *Cx3cr1* in and survival of other cells (whether this be non-yolk sac-derived microglia – or microglia-like cells – or in other immune cell populations) and if this may lower the specificity of the *Cx3cr1^{CreER}:R26-tdTomato* mouse line for microglia. Based on the current observations, this does not appear to be the case for the EIU model but remains to be seen for the EAU and other disease models and necessitates testing on a per-model basis. It also raises the question of what exactly a microglia is, and whether stratification based upon their origin, or clarification of their origin (when isolated for downstream assays) may be necessary for future work so that studies can be better compared to one another, particularly if conflicting results are obtained due to different isolation strategies.

As indicated by the imaging, the tdTomato fluorescence intensity does not stabilise until 4 weeks post-tamoxifen in naïve microglia. This suggests that even if non-microglial cells were to undergo a constitutive recombination event, they would not necessarily have the tdTomato fluorescence intensity equivalent to a microglial cell unless they survived/persisted for lengthy periods of time. This assumes expression of the CAG promoter is not greatly altered by inflammation (which we have not tested). The only way to conclusively confirm this hypothesis would be using a high-throughput method (such as mRNA-Seq, proteomics, etc) with single-cell resolution, and even this carries the underlying assumption that the yolk-sac derived microglia remain different to the infiltrating cells to enable unsupervised delineation of them using a dimension-reducing algorithm.

The 3-day topical regime is fully sensitive and highly specific for microglia during EIU. Whilst other approaches also fully tagged the microglia (e.g. 4-day topical and subcutaneous regimes), they are associated with a reduced specificity in the context of immune cell infiltration. The non-microglial CD45⁺ tdTomato^{hi} cells identified in the eye were negative for the full panel of markers (which covered all the major types of immune cell). They may represent a population of innate lymphoid cells (ILCs). ILCs do not express the typical cell-surface markers of other lymphocytes (such as B220 or CD3), but some ILC subtypes are known to express high amounts of *Cx3cr1* and can also be long-lived [579-582]. This may explain how they could be tagged, survive more than 4 weeks, and subsequently be observed within the retina during EIU after a course of subcutaneous tamoxifen. It is unclear whether the tagging in a 4-day topical regime is due to systemic reabsorption of tamoxifen to a concentration above a threshold to activate

recombination in a smaller fraction of these cells, or if activation is happening locally to the site of administration.

Whilst the specificity data is calculated based upon back-gating of microglia using CD45 and CD11b expression (and it is possible that non-retinal microglial or non-microglial cells could have similar levels of expression of these markers and be incorrectly classified), we are confident that the 3-day topical regime in this Cre line is specific because the total numbers of tdTomato^{hi} cells did not vary from a naïve organism through to the peak cellular infiltrate phase of EIU; it is well-known that microglia do not egress from the retina, but can migrate to different retinal layers or the subretinal space (which would still allow for isolation using our approach), upon inflammation [341]. This data also supports recent studies of microglia that highlight the need to confirm the specificity for microglia in their disease model and employ techniques with single-cell resolution to resolve the non-microglial cell populations [341, 583].

Lastly, this series of experiments have also enabled us to explore the possibility of implementing the 3Rs in our work (principles of animal welfare [94]), specifically refinement. We showed that the optimal tamoxifen administration regime is both beneficial to the sensitivity/specificity for microglia but also for the animal's welfare via reduced confounders of handling and procedures; a topical regime is a sub-threshold technique resulting in only the inherent stress that handling brings as opposed to the mild severity that a sub-cutaneous injection would bring. Furthermore, we showed it was possible to shorten the originally published regime to 3 days.

In summary, we show that a 3-day topical tamoxifen regime results in complete and specific tagging of microglia in the *Cx3cr1^{CreER}:R26-tdTomato* mouse line before, during, and after EIU that permits valid investigation of them using fluorescence-based detection and isolation approaches such as the mRNA-Seq pipeline (using FACS) that was optimised and described in Chapter III.

Chapter V: Characterising the Temporal Kinetics of the Microglial Transcriptome in EIU

5.1 Introduction

EIU is a self-resolving model of acute TLR4-mediated ocular inflammation, that following a single inflammatory insult generates acute immune cell infiltration [52, 584]. It typically has the kinetics of an acute short-lived monophasic reaction.

Microglial activation by LPS has been characterised before, with co-expressional meta-analysis identifying a core set of microglial “LPS” genes in addition to generic activation markers of microglia in various pathological states [158]. A common microglial transcriptional signature has been described by several groups [158, 308, 346-348]. Furthermore, the microglial transcriptional signature is well-documented to be disrupted during an activated state – with many homeostatic genes downregulated including *P2ry12*, *Siglech*, *Cx3cr1*, and *Tmem119* – whether that be due to ageing, neurodegeneration, acute responses (such as to LPS), and many others [158, 341, 342, 352, 353]. Depending on the context and kinetics, microglia can promote or regulate inflammation [390, 585].

Developing our understanding further, both inherent and acquired heterogeneity (i.e. during a response) are being observed within microglial populations. Microglia are known to exist in two distinct niches within the retina and exhibit differential regulation because of inherent microglial heterogeneity [341]. Microglial heterogeneity has been observed in LPS responses (brain microglia following a systemic dose), AD, and ocular light-damage models *in vivo* [340-342, 344, 586]. *C5ar1* was identified as a DEG between microglial subtypes during an LPS response [342], making it a candidate marker for differentiating microglial subtypes; other reports showed that C5AR1 is required for microglial polarisation to a pro-inflammatory state with deficiency of C5AR1 signalling resulting in reduced activation/induction of inflammatory genes and improvements in outcomes from an AD model [366].

Furthermore, it is now recognised that other similar cell types (i.e. macrophages) exhibit a highly-plastic transcriptome during an LPS response [587]. The transcriptional kinetics have not been investigated in microglia nor the microglial behaviour/activity post-“resolution”, and the degree to which homeostatic restoration is achieved or if they remain permanently altered (whether this be more pro- or anti-inflammatory) after an insult.

Therefore, the aims of this chapter were to utilise the knowledge from the previous chapters to characterise the plasticity of the microglial transcriptome over time during an LPS response but also to see if the homeostatic state was restored after resolution.

5.2 Results

5.2.1 The Kinetics of EIU in the $Cx3cr1^{CreER};R26-tdTomato$ Mouse Line

For investigation of EIU, the kinetics needed to be characterised to observe if they were consistent with reports in WT mice so that appropriate timepoints could be selected for microglial isolation and sequencing [97]. To this end, imaging was performed on mice to obtain a time-course which confirmed the kinetics as typical, with peak cellular infiltrate at 18 hours post-injection and resolution by 2 weeks (Figure 5.2.1). Clinical assessment demonstrated few changes in the microglia at 4 hours post-injection, although a slight widening of vessels was apparent. By 18 hours, the uniform distribution of microglia was altered, cell bodies possibly appeared larger suggesting retraction of ramified processes to form a more amoeboid morphology, and vessels were larger still. Cognisant that the Micron IV imaging platform does not possess the high resolution required to reliably detect changes to the microglial ramified processes, retinal flatmounts were prepared for acquisition by confocal laser-scanning microscopy to visualise these in high-resolution (Figure 5.2.2). Microglia were observed to have a ramified-to-amoeboid transition by 4 hours which persisted through to 18 hours but resolved to a ramified state by 2 weeks. With evidence of microglial perturbation at 4 hours post-injection, we sought to then characterise the microglial transcriptome during the early stages of EIU, peak cellular infiltrate, and after resolution.

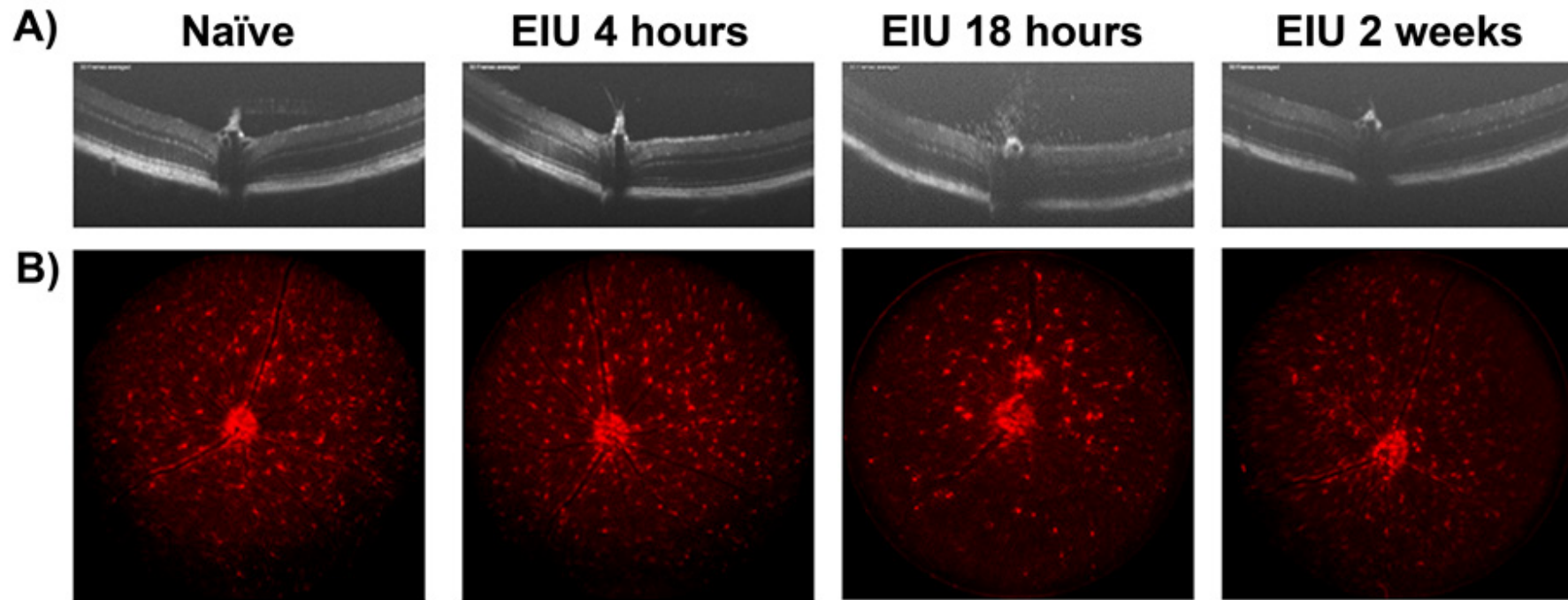


Figure 5.2.1. The kinetics of EIU in the $Cx3cr1^{CreER};R26-tdTomato$ mouse strain. A) OCT images showing disease-course in a single mouse demonstrates the presence of infiltrating cells in the vitreous body at 18 hours post-injection with resolution by 2 weeks. B) Deconvolved fluorescent fundal images acquired simultaneously show few changes in the distribution of microglial cells at 4 hours post-injection, but clear changes in their distribution and brightness (in addition to vessel dilation) at 18 hours which have resolved by 2 weeks.

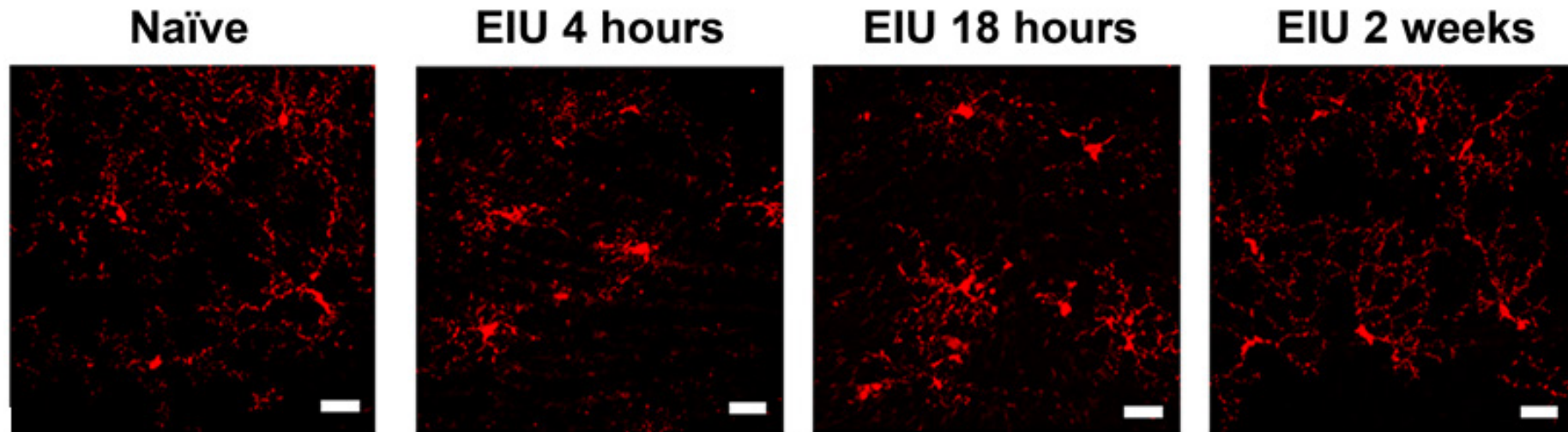


Figure 5.2.2. Confocal laser-scanning microscopy shows changes in microglial morphology over time in EIU. High-resolution images reveal retraction of ramified processes (indicator of activation) between a naïve organism and EIU 4 hours, with resolution after 18 hours but by 2 weeks. Scale bars = 30 μ m.

5.2.2 mRNA-Seq

Initially, a pilot study to include the naïve (no injection), 18 hours EIU, and 2 weeks EIU groups in addition to the contralateral (uninjected) eyes was performed so that a power analysis (with an α of 0.1 and β of 0.8; standard parameters) could be completed to further inform the subsequent experiments and the required numbers per groups. The power analysis indicated that to detect changes in 50% of genes with a fold-change of 2, 6.92 samples were required (50th percentile of a given fold-change is the most-commonly used metric according to the PGS software documentation). This agreed with published reports on power analysis that suggested 6 biological replicates were required for adequate power when detecting DEGs with a fold-change criterion of $\geq \pm 2$ (at a depth of 10 million reads per sample) [498]. Furthermore, unanticipated changes in gene expression between the contralateral eyes and naïve controls indicated that true naïve controls were more appropriate than using the contralateral eyes. In agreement with our findings, a single report in the literature also identified changes to microglia in eyes contralateral to a procedure inducing glaucoma, suggesting a mechanism of microglial or general communication between eyes [547].

Following the pilot study, a new study was initiated that included the 4-hour EIU group and utilised naïve eyes as controls. It was split into two independent blocked experiments with the aim of at least 6 biological replicates per group; cDNA was generated from samples with a 93% success rate, resulting in 5–10 biological replicates per group from these experiments. The analysis identified 1,069 unique DEGs (613 at 4 hours, 537 at 18 hours, and 0 at two weeks; all compared to naïve controls) visualised by hierarchical clustering that highlights a highly-plastic transcriptome with most up-regulated genes being mutually exclusive at different timepoints but a common/core set of downregulated genes (Figure 5.2.3). Boxes highlight clusters of genes that were normal at 4 hours but up-regulated at 18 hours (yellow), those which were up-regulated at 4 hours but not 18 hours (brown), those which were up-regulated at both timepoints (green), those which were down-regulated at 4 hours but recovered to pre-EIU levels by 18 hours (light blue), and those which were down-regulated at both 4- and 18 hours (black). Restoration back to a homeostatic signal was observed by 2 weeks because unsupervised clustering failed to discern between samples in the naïve and 2-week post-injection experimental groups.

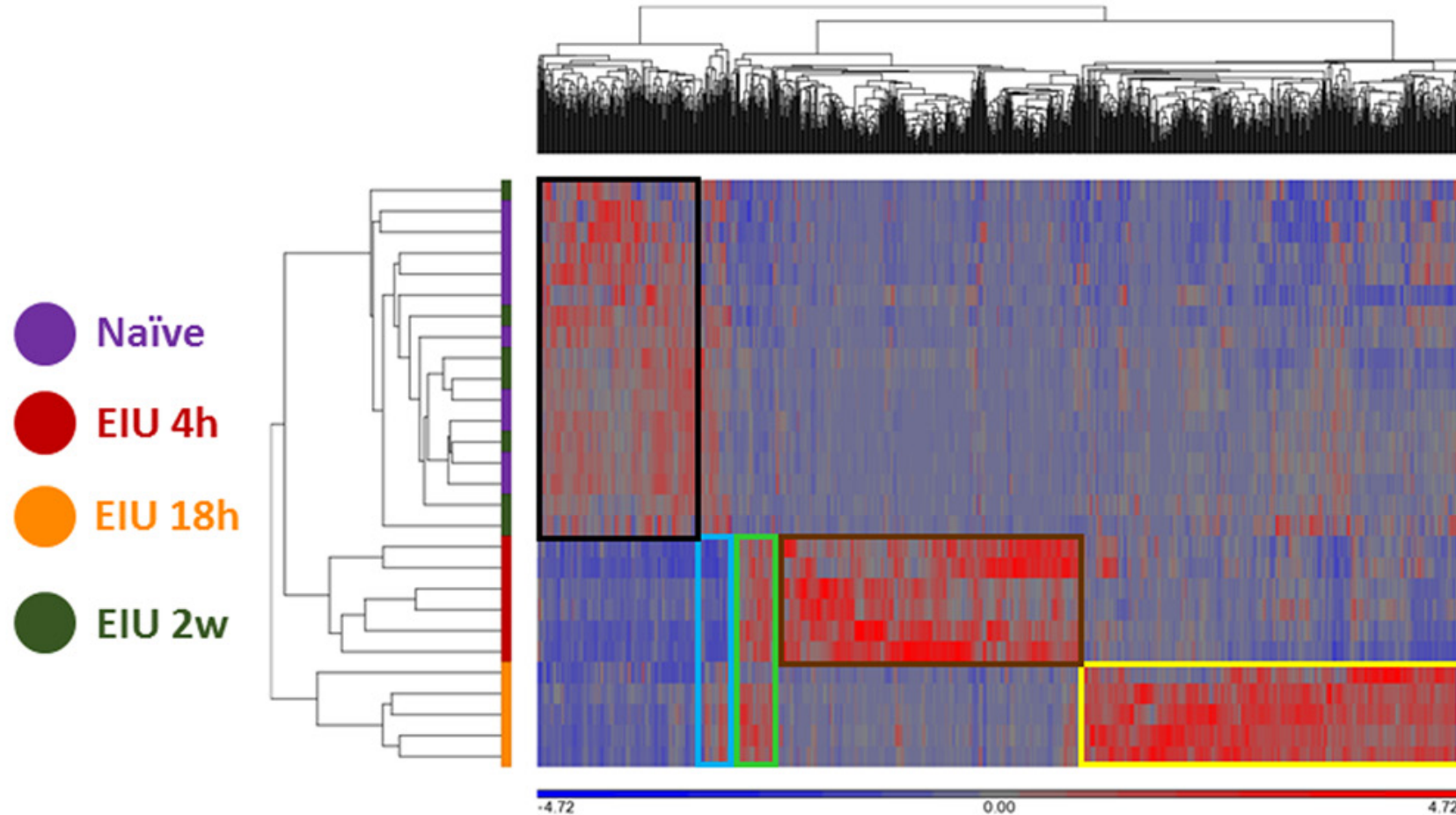


Figure 5.2.3. mRNA-Sequencing of microglia during and after EIU reveals transcriptional alterations that fully resolve. Hierarchical clustering of DEGs shows differences in the kinetics of the microglial transcriptome during EIU. Boxes highlight clusters of genes with different kinetics, and a restoration back to a homeostatic signal by 2 weeks ($n = 5-10$).

Despite all of the previous QC checks, it was nonetheless important to compare this dataset to the published literature to observe whether this data was concordant or not. Therefore, gene lists generated from a co-expression meta-analysis and other consensus lists of microglial homeostatic genes were checked against gene expression values from this dataset. Gene lists included those representing microglial homeostatic genes (e.g. G protein-coupled receptor 34 [*Gpr34*], v-maf musculoaponeurotic fibrosarcoma oncogene family protein B [avian] [*Mafb*]), microglial activation (generic) genes (e.g. C-X-C motif chemokine 10 [*Cxcl10*]), microglial LPS activation genes (e.g. *Map3k8*), and “primed microglia” response genes (e.g. axyl receptor tyrosine kinase [*Axl*]) [158, 342, 588]. On this basis, downregulation of homeostatic genes, upregulation of activation genes, and no expression of primed genes were expected. For clarification, the “primed microglia” response genes were observed and characterised in neurodegenerative conditions but not in acute activation. The expected changes were observed within the dataset; a representative selection of RPKM scatterplots, highlighting this agreement, is displayed in Figure 5.2.4.

Consensus on these select genes was encouraging but it was also important to compare the data at a broader level using pathway analysis. This was performed using the GO terms, KEGG pathways, and IPA canonical pathways. Enriched canonical pathways when naïve and 4 hours EIU groups were compared included: TREM1 Signaling, iNOS Signaling, Th17 Activation Pathway, TNFR2 Signaling; for the naïve and 18 hours comparison, enriched pathways included: EIF2 Signaling, Interferon Signaling, Gαq Signaling (Figure 5.2.5). No enriched pathways were identified between the naïve and 2 weeks EIU groups because it is not possible to perform pathway analysis without DEGs. To better represent the time dimension of the dataset a heatmap of the significantly-enriched canonical pathways over time was created, highlighting how both the p value and z-score (directionality score) change across the timepoints with resolution/homeostatic restoration to baseline by 2 weeks (Figure 5.2.6). LPS was found to be a “master regulator” by IPA as expected.

Enriched GO terms (enrichment score) when naïve and 4 hours EIU groups were compared included: immune system process (60.9), regulation of cytokine production (56.0), and response to stress (52.7). Similarly, the enriched KEGG pathways included: NF-Kappa B signaling pathway (34.1), toll-like receptor signaling pathway (31.7), and TNF signaling pathway (25.3). For the naïve and 18 hours EIU comparison GO terms included: cytosolic part (89.7), extracellular organelle (70.7), translation (65.8), and immune system process (29.8); enriched KEGG pathways included: ribosome (58.8) and proteasome (42.9).

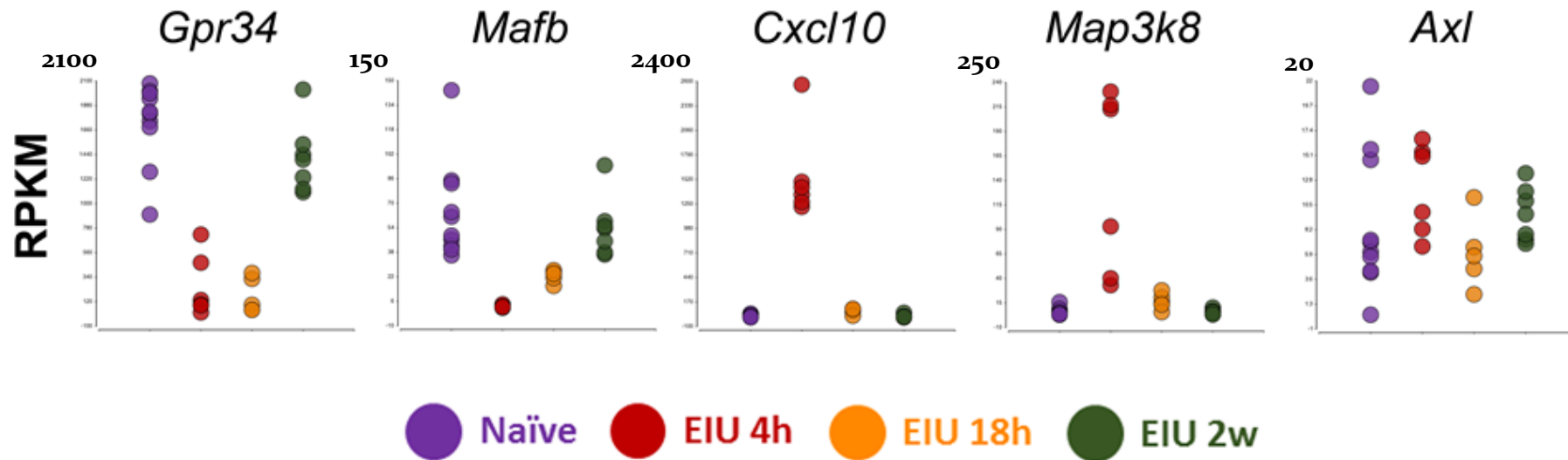
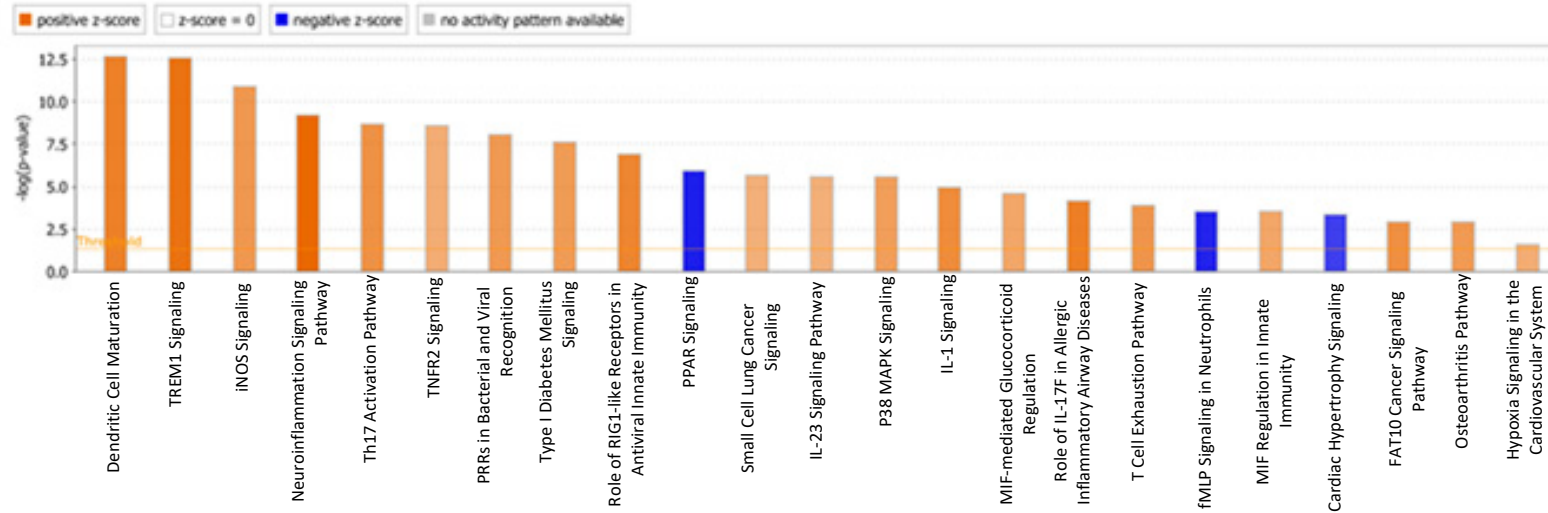


Figure 5.2.4. The transcriptome of microglia during EIU identifies expected changes in previously described microglial genes. Scatterplots show expression levels of a homeostatic gene (*Gpr34*), a homeostatic transcription factor (*Mafb*), a generic microglial activation gene (*Cxcl10*), an acute LPS-response gene (*Map3k8*), and “primed microglia” gene (*Axl*). The observed changes in expression (or absence of) are consistent with previously published reports ($n = 5-10$).

A) EIU 4h vs. Naïve



B) EIU 18h vs. Naïve

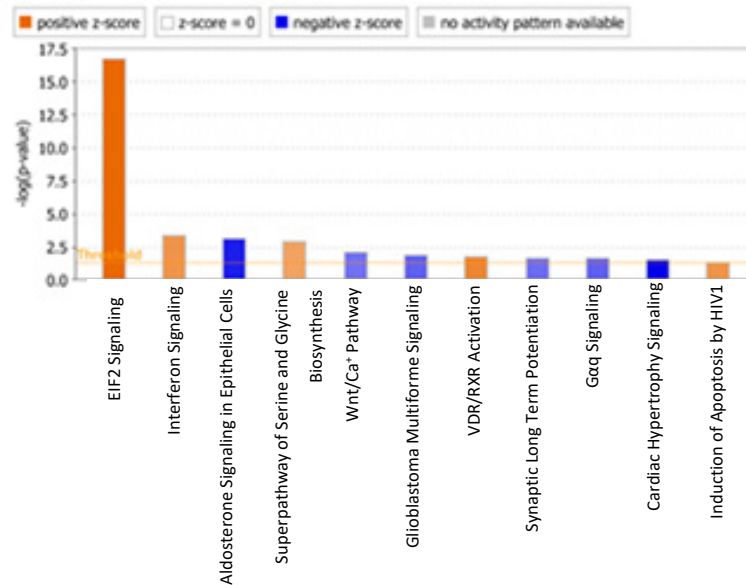


Figure 5.2.5. IPA software identifies canonical pathways that are significantly altered in microglia during EIU. A) Significantly altered pathways at 4 hours post-injection and B) 18 hours post-injection are shown. A p value threshold of ≤ 0.05 is indicated by the horizontal line. The shading intensity of the bars indicates how strongly positive (orange) or negative (blue) the z-score (directionality score) was for each pathway. There were no significantly-enriched pathways at 2 weeks post-injection.

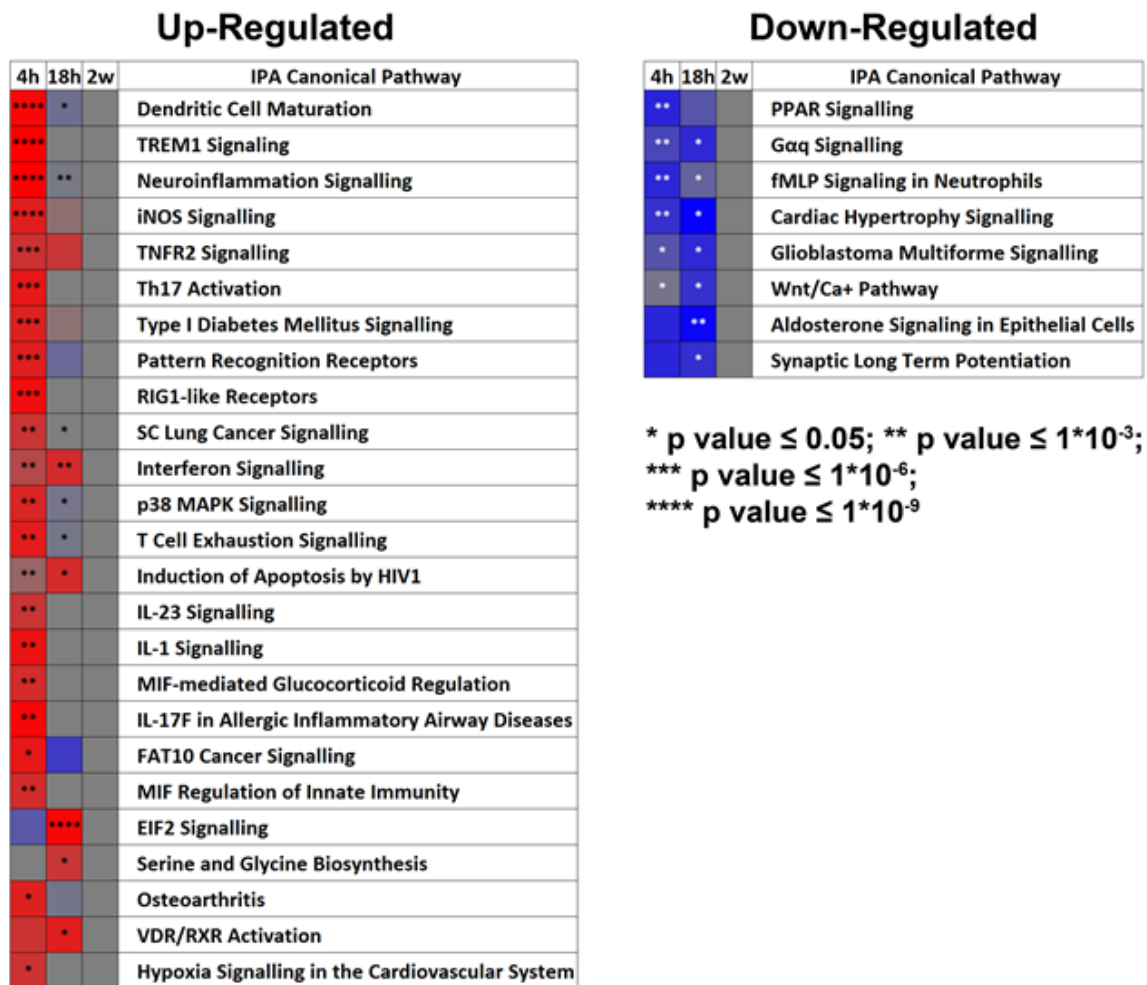


Figure 5.2.6. A heatmap shows changes in both z-score and p value over time for significantly-enriched IPA canonical pathways. The pathways are arranged in ascending order based on their overall (summary) p value with colour-coding to indicate the magnitude of change in z-score (red representing an increase in pathway activity, and blue representing a decrease in pathway activity). All pathways resolved to the equivalent of a naïve state by 2 weeks post-injection.

5.2.3 Orthogonal Validation of Selected Markers

Identification of recognised DEGs and canonical pathways reported in the literature was encouraging, but orthogonal validation of the dataset (to include at the protein-level) was required as the transcriptome and proteome do not necessarily correlate. A full proteomics assessment was not feasible in the current study as very limited numbers of specialised pipelines can handle low cell input (<10,000) and require custom-made reagents and/or equipment (e.g. microfabrication of glass chips using photolithography) [589, 590]; utilising one of these pipelines would have considerably increased the cost of experiments beyond the current budget in addition to requiring further extensive optimisation. Whole retinal protein-level analysis could identify differentially-regulated proteins but would be unable to distinguish the individual contribution of distinct cell types and validate them as altered in microglia [591]. Therefore, a limited number of key markers would need to be selected for validation testing.

Flow cytometry was chosen as the technique of protein-level validation as it has single-cell resolution and would enable the assessment of potential microglial heterogeneity that is becoming increasingly recognised. Nonetheless, a hypothetical discrepancy between the mRNA-Seq data and flow cytometric data could question the accuracy and validity of the sequencing, and therefore direct validation of the mRNA-Seq on the same material used to generate the libraries was required to confirm if sequencing results were inaccurate or a genuine discrepancy between gene-level and protein-level was present. For this qPCR, using highly sensitive and specific TaqMan probes, was utilised. As flow cytometry can be performed on samples with limited numbers of markers in parallel and low amounts of cDNA remained from the original samples for qPCR (limiting the number of runs that could be performed), a selection process for determining a small number of key markers for validation was required. Furthermore, not all DEGs identified had commercially available antibodies suitable for flow cytometric analysis or fluorophore conjugations that were compatible in the same panel.

Markers were initially screened by systematic assessment based on magnitude of the relative change in expression, membrane localisation, and the availability of testing reagents. The final markers were selected based on novelty, lack of prior validation at the protein level, whether they were a previously suggested microglial marker, and/or were in contrast to or appeared crucial in light of other reports. A total of 10 markers were selected (from a total of 44 suitable candidates), to include one identified from the pilot study (Figure 5.2.7).

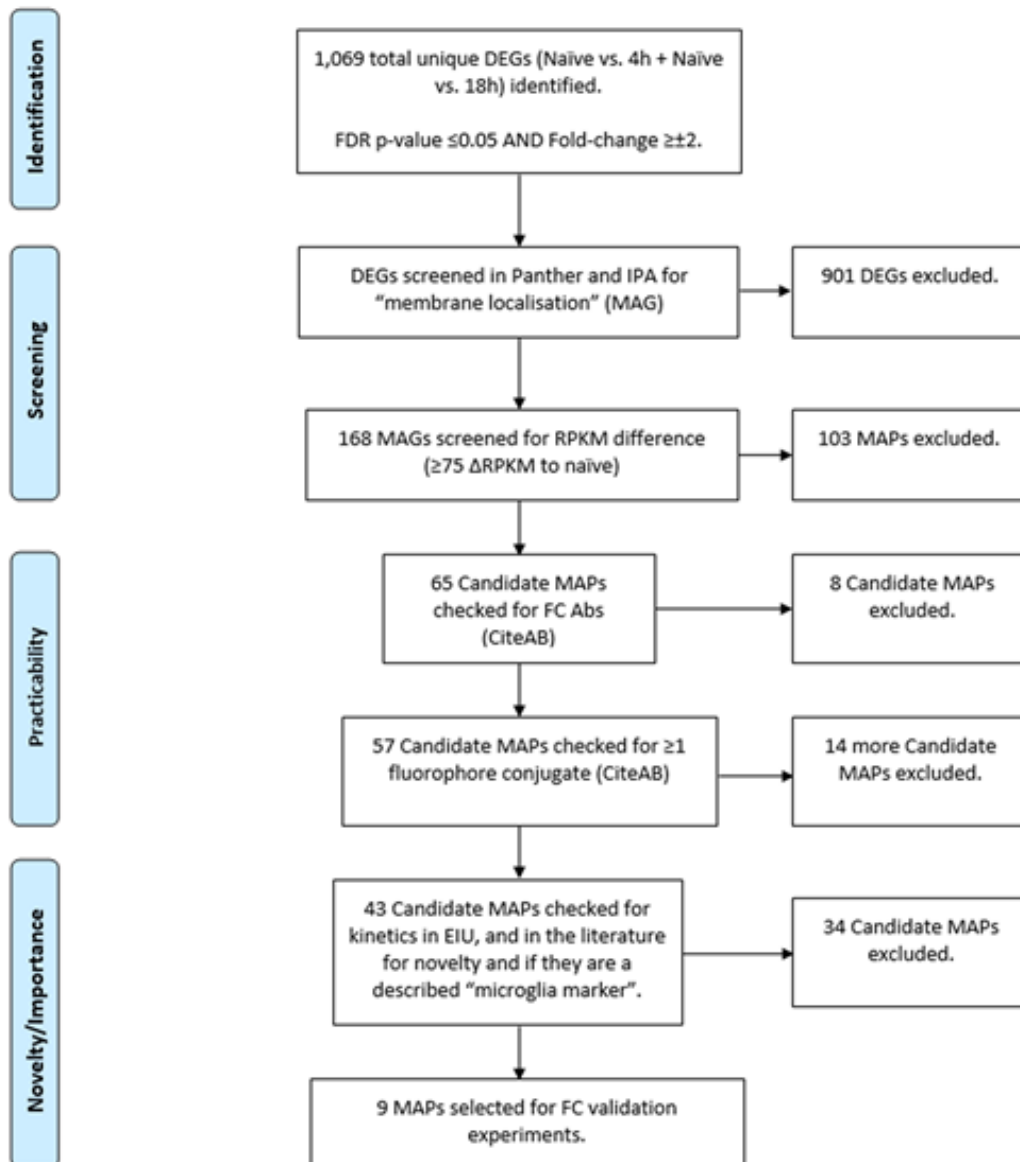


Figure 5.2.7. A flow-chart demonstrating the selection process of markers for orthogonal validation. One thousand and sixty-nine DEGs identified (possible targets) were screened for membrane localisation (for simple flow cytometric validation), large RPKM difference, and availability of conjugated antibodies. Targets were selected based on whether they were novel with respect to describing microglial activation (*Milr1*) or without validation beyond the transcript level (*Bst2*, *Fas*, *Lair1*, *Slamf1*) [592-596], whether they were a previously specific or enriched microglial marker (*P2ry12*, *Siglech*) [308, 348], whether our data was in contrast to previous reports (*Mertk*) [597], or appeared crucial in light of other reports (*C5ar1*) [342]. The other marker (*Cd44*) was selected for testing based on results of a pilot study and its previous description as a possible microglial marker [558]. This diagram was generated using the PRISMA word document template [598]. Abbreviations: DEG – differentially-expressed gene, MAG – membrane-associated gene, MAP – membrane-associated protein, FC – flow cytometry.

In line with published reports and an activated state, pro-inflammatory markers (*Slamfi*, *C5ar1*, *Fas*, and *Cd44*) were all upregulated at 4 hours following LPS challenge. In addition, a novel microglial associated transcript, *Milr1* (a negative regulator of mast cell activation) and *Bst2* (a previously validated marker of late activation) were elevated by 18 hours. In contrast, constitutively expressed microglial genes, including homeostatic genes, (e.g. *P2ry12*, *Siglech*, *Mertk*, and *Lair1*) were downregulated at the early timepoint. RPKM values for the markers are shown in scatterplots within Figure 5.2.8.

In general, qPCR analysis validated the transcript-level changes observed at each timepoint, confirming resolution and return to baseline levels by 2 weeks (Figure 5.2.9). However, markers such as *C5ar1* and *Siglech* did not reach statistical significance despite following the same trend (with regards to up- or downregulation).

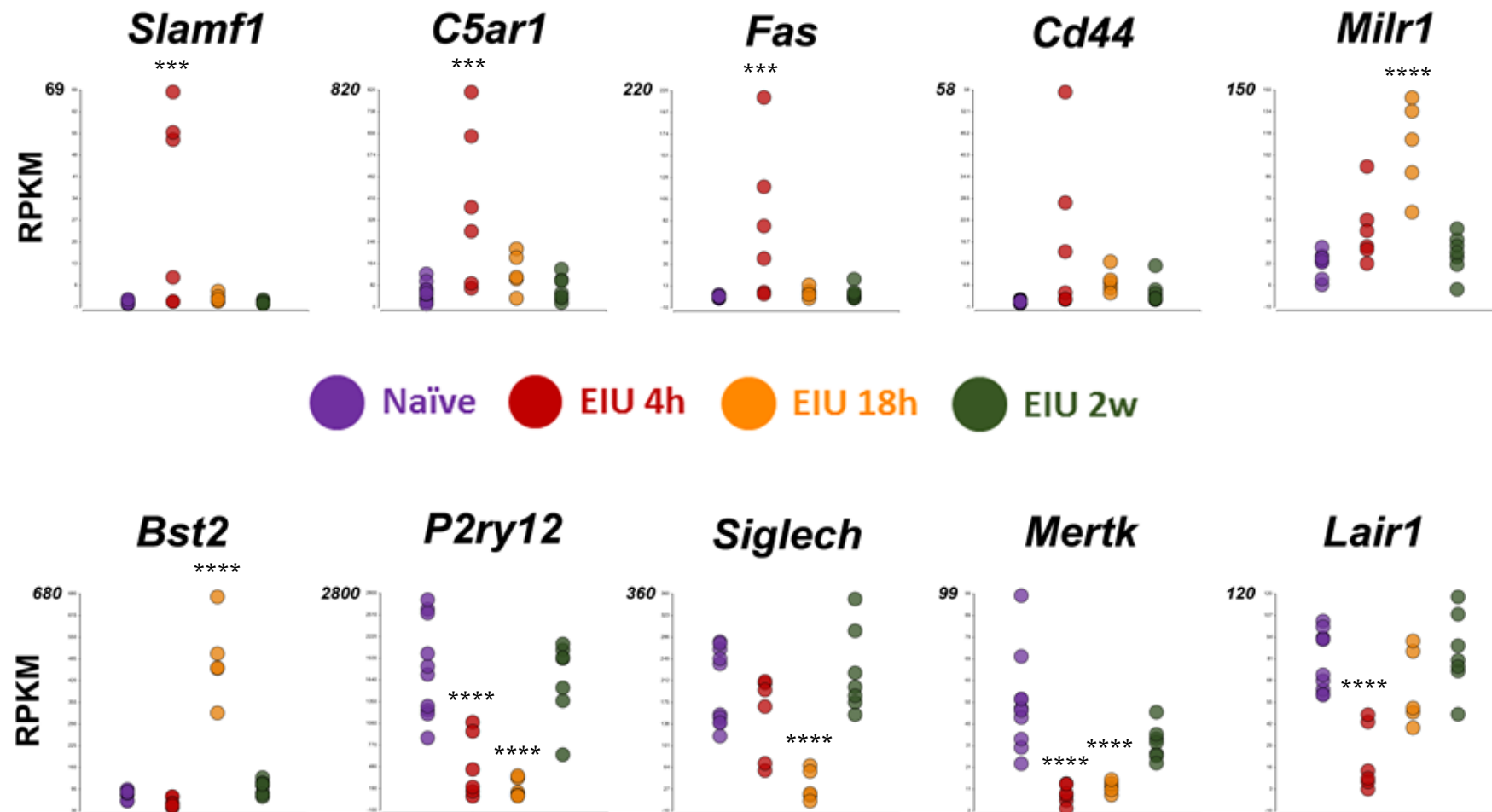


Figure 5.2.8. Changes in expression of markers selected for orthogonal validation, as determined by mRNA-Seq of microglia, during EIU. RPKM values show how expression of selected markers change during the course of EIU ($n = 5-10$). *** = $p \leq 0.001$, **** = $p \leq 0.0001$ (comparisons to naïve). For statistical analysis, ANOVA (with FDR step-up correction) was performed on the full mRNA-Seq dataset.

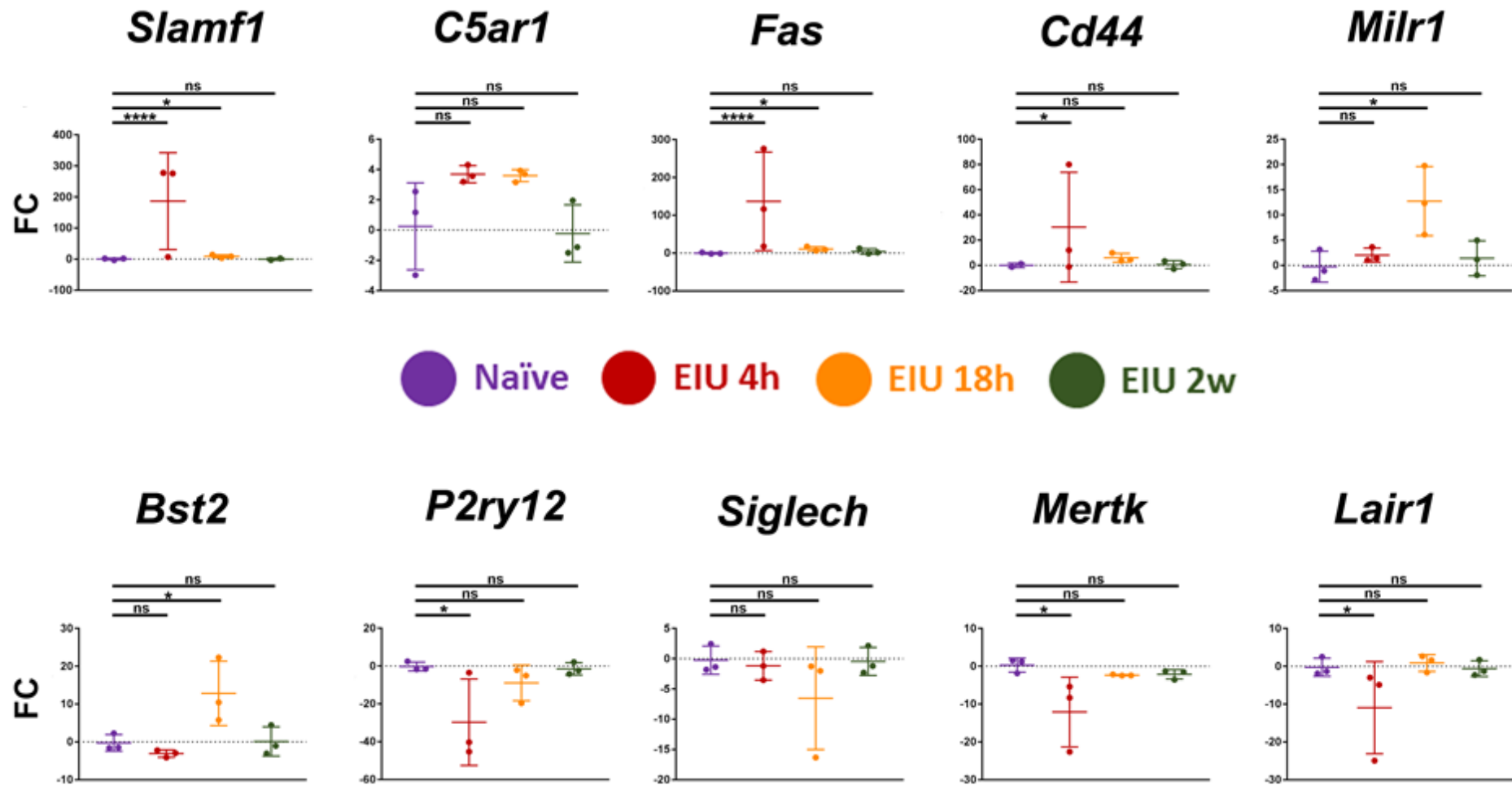


Figure 5.2.9. qPCR validates microglial transcriptomic changes, identified by mRNA-Seq, at the gene-level. Remaining cDNA from 600 microglia used for bulk mRNA-Seq was used for qPCR validation with Taqman probes. Fold-changes (FC) relative to the naïve baseline are shown for each of the 10 selected markers, demonstrating changes in expression during the course of EIU. For statistical analysis, One-way ANOVA with Tukey's post-hoc test was used. * = $p \leq 0.05$, **** = $p \leq 0.0001$, ns = not significant ($n = 3$).

With the transcripts validated at the gene-level, validation at the protein level was then required by utilising flow cytometric assessment. Increased expression of SLAMF1, MILR1, C5AR1, CD44, BST2, and LAIR1 was observed at 18 hours post-injection (Figure 5.2.10). Furthermore, differences in the proportion of marker-positive cells were evident, with C5AR1, CD44, and BST2 upregulated in the majority of microglia (>50%), in contrast to the other markers which were elevated in a smaller fraction (<20%) of cells. Whilst P2RY12 was highly expressed in naïve microglia (>80%), no change in expression in response to LPS was observed. Similarly, low-level SIGLECH, MERTK, and FAS expression in naïve populations remained unchanged and restricted to a small percentage of the microglia (<10%). The upregulation of CD44 was also confirmed in retinal flatmounts at 18 hours post-injection using fluorescence microscopy (Figure 5.2.11).

Expression of P2RY12 and SIGLECH was compared between microglia and CD45⁺ cells, as both of the former are previously suggested markers that differentiate microglial populations from other immune cells [308, 348]. Flow cytometric analysis clearly demonstrates that both markers are equally expressed on some CD45⁺ infiltrating cells and microglia, indicating these markers exhibit poor specificity for retinal microglia during the acute response (Figure 5.2.12).

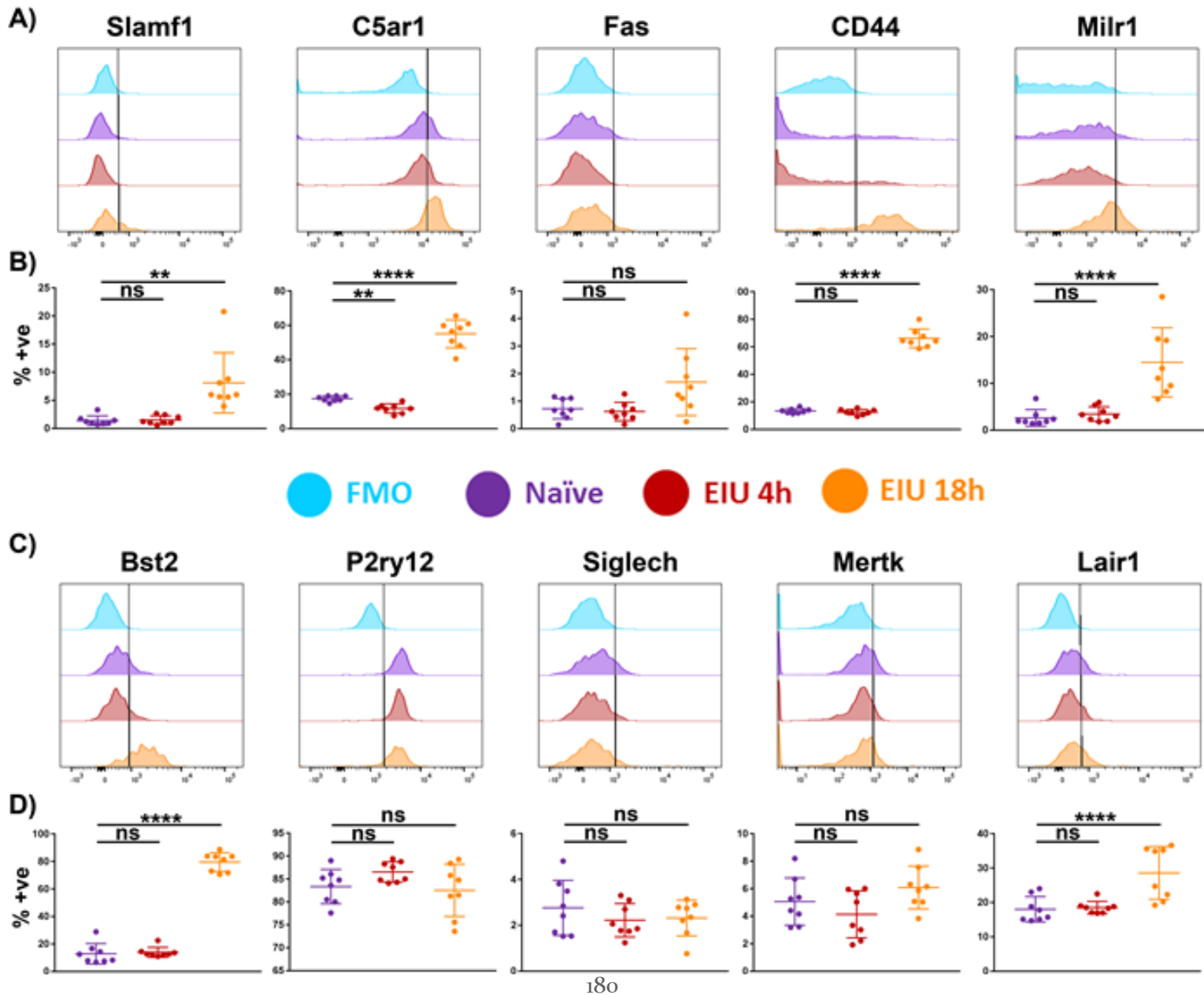


Figure 5.2.10. Changes in protein expression of selected markers in microglia, as determined using flow cytometry, over a time-course of EIU. A, C) A representative flow cytometric histogram is shown for the 10 selected markers B, D) in-line vertically with matching scatterplots of the aggregate flow cytometry data summarising the percentage of microglia positive for each marker at each timepoint. Gates were drawn with the assistance of fluorescence minus one (FMO) controls (light blue). For statistical analysis, One-way ANOVA with Tukey's post-hoc test was used. ** = $p \leq 0.01$, ** = $p \leq 0.0001$, ns = not significant ($n = 8$).**

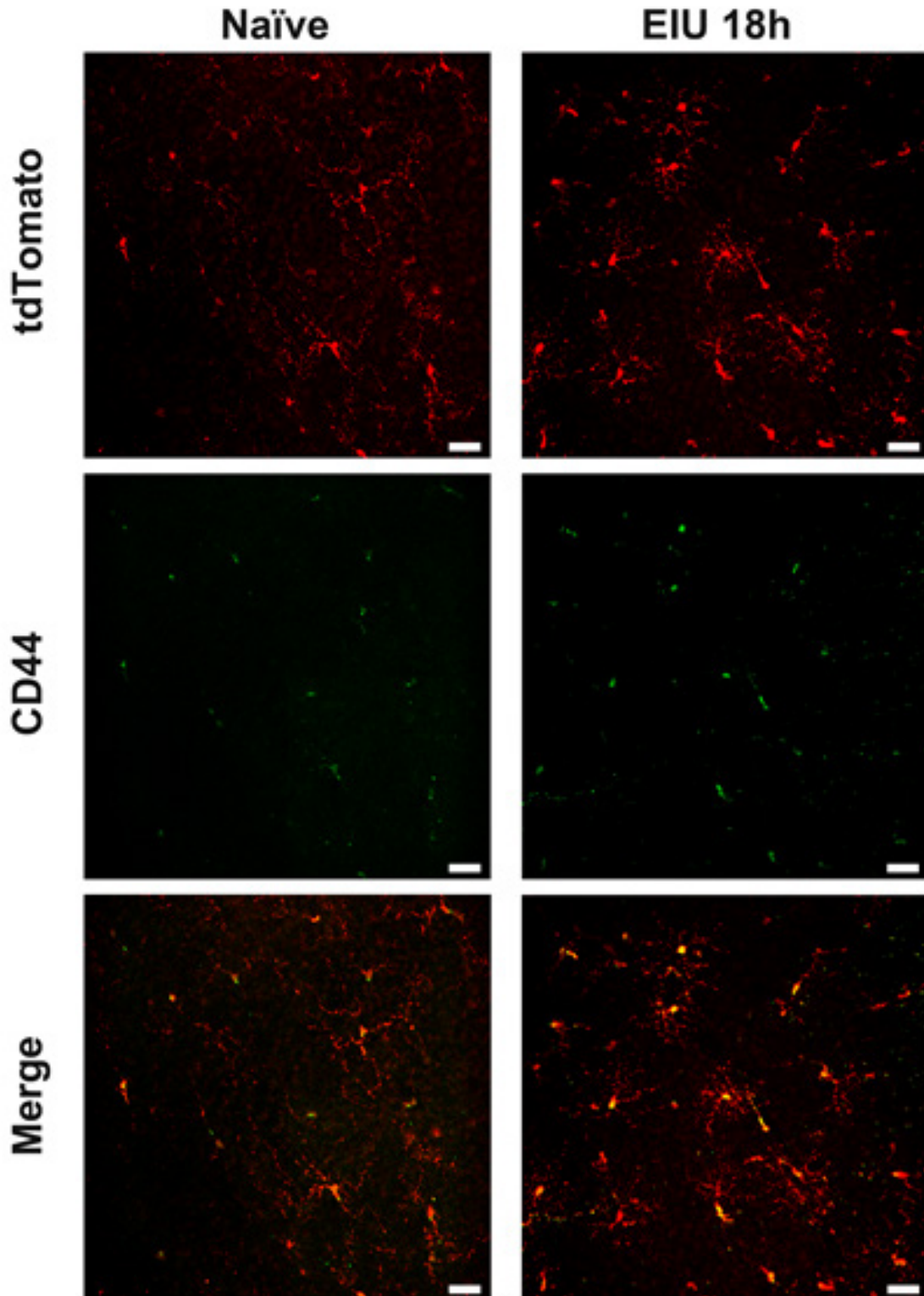


Figure 5.2.11. Confocal-laser scanning microscopy highlights upregulation of CD44 in microglia at peak EIU, compared to naïve controls. Separate channel images and a merge highlight the upregulation of CD44 and colocalisation with the tdTomato signals from microglia. Scale bars = 30 μ m.

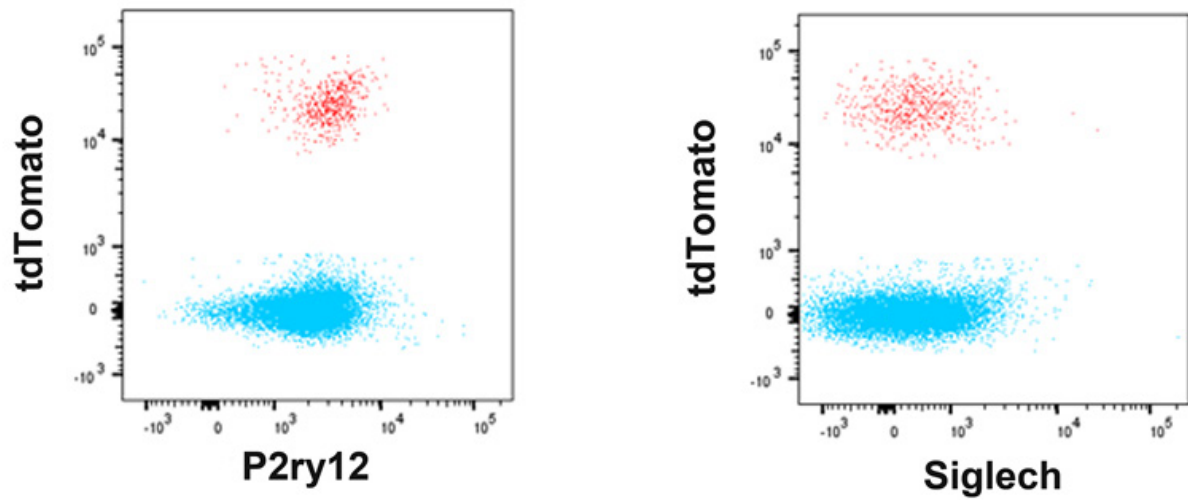


Figure 5.2.12. Flow cytometric analysis demonstrates *P2RY12* and *SIGLECH* expression on $CD45^+ tdTomato^-$ non-microglial immune cells (blue) and $CD45^{lo} tdTomato^+$ microglia (red) at 18 hours EIU. The gating strategy to generate these plots is as described previously (cells, singlets, live cells, $CD45^+$).

5.2.4 Stratifying Microglia using C5AR1 Identifies Both Generalised and Restricted Microglial Responses

Recent reports show that *C5ar1* was one of several markers that was enriched in a subset of brain microglia (identified by sc-mRNA-Seq data) responding to systemic LPS challenge *in vivo* [342]. Furthermore, mounting evidence from numerous reports identify heterogeneity in the microglial response during other pathological states [340, 341, 344, 586]. We therefore examined whether stratifying microglia based on C5AR1 expression would delineate differences in the markers selected for validation, highlighting specificity to this subset of C5AR1-expressing cells or generalised expression across the whole population of microglia.

Microglia were stratified into three main groups: C5AR1^{neg}, C5AR1^{lo}, and C5AR1^{hi}. The C5AR1-expressing microglia were sub-stratified based on whether the C5AR1 expression was equivalent to microglia observed within a naïve mouse (C5AR1^{lo}) or whether expression was elevated (C5AR1^{hi}; Figure 5.2.13a). C5AR1^{hi} expression correlated to the extent of immune cell (CD45⁺ tdTomato⁻) infiltrate within the retinas and represents a potential microglial marker for disease scoring (Figure 5.2.13b).

Flow cytometric analysis compared expression of the other surface markers in C5AR1^{neg} and C5AR1^{hi} subsets, as two distinctive populations, in naïve and peak EIU retinas. Delineating the two populations on this basis demonstrates elevation of several markers (SLAMF1, FAS, MILR1, and LAIR1) which are restricted to the C5AR1-expressing microglia, including a marker that previously did not achieve statistical significance (FAS). In contrast, CD44 and BST2 were enriched within the C5AR1-expressing population but also expressed by a large proportion of the C5AR1^{neg} microglia, thus representing more generalised markers of microglial perturbation (Figure 5.2.14).

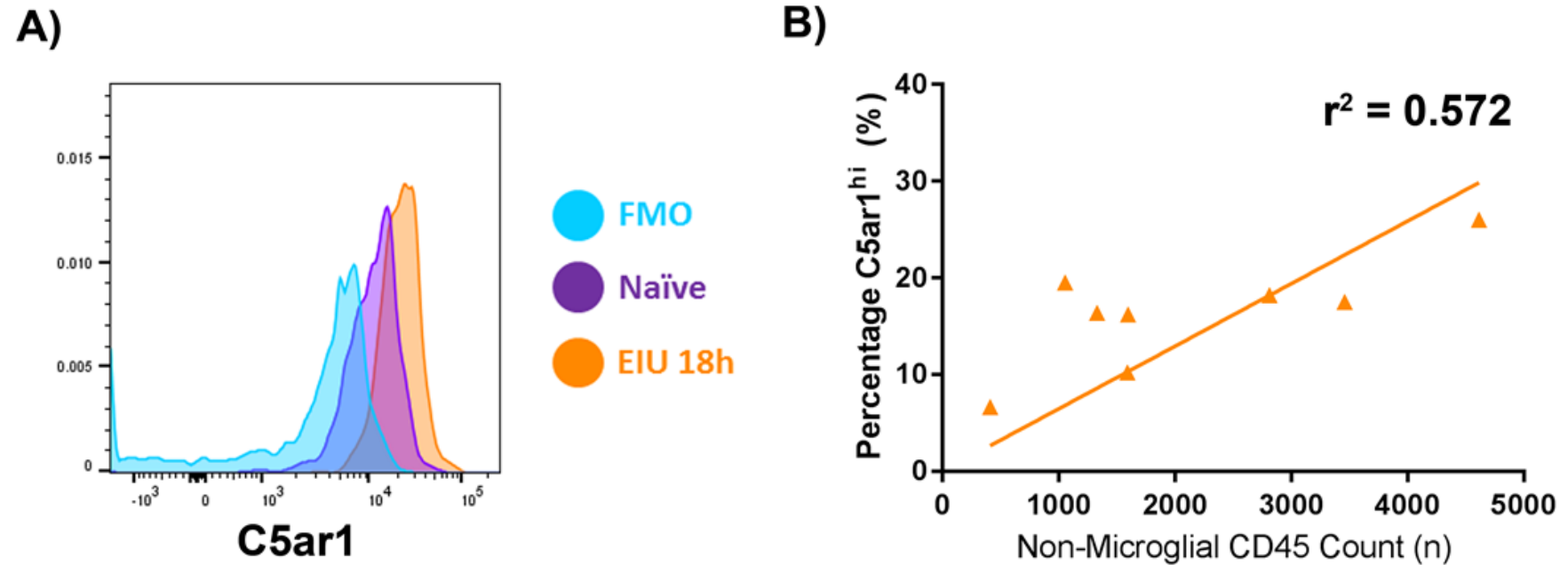


Figure 5.2.13. Microglia can be stratified based on *C5AR1* expression and this correlates with the amount of immune cell infiltrate. **A)** A histogram shows microglial *C5AR1* expression in a fluorescence minus one (FMO) control (blue), naïve retina (purple), and at 18 hours EIU (orange). Microglia can be subsequently classified on whether they are *C5AR1*⁻, *C5AR1*^{lo} (equivalent to positive populations in the naïve retina), or *C5AR1*^{hi} (expression above the baseline level observed in a naïve retina). **B)** Immune cell infiltrate correlates with *C5AR1*^{hi} expression in microglial populations ($p = 0.0298$). For statistical analysis, Pearson's test was used.

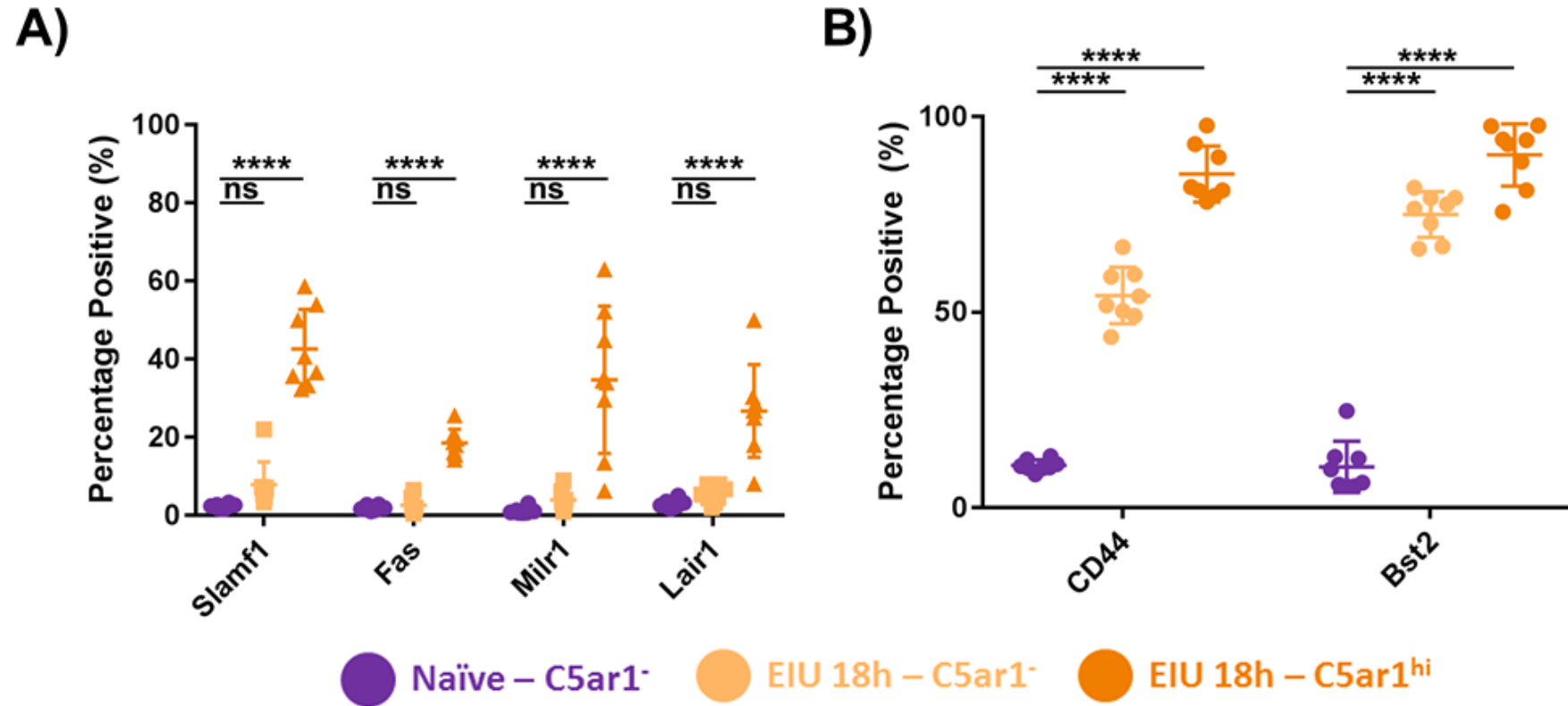


Figure 5.2.14. Stratifying microglia using C5AR1 expression identifies both exclusive and generalised responses to LPS in vivo. **A)** Stratifying microglia into C5AR1⁻ and C5AR1^{hi} identifies changes in cell-surface protein expression that are exclusive to C5AR1-expressing microglia, **B)** but also changes in proteins which are generalised microglial responses (not exclusive to, but somewhat enriched in, the C5AR1-expressing microglia). For statistical analysis, One-way ANOVA with Tukey's post-hoc test was used. **** = $p \leq 0.0001$, ns = not significant.

5.3 Discussion

Having confirmed the EIU kinetics as synonymous to prior work, it was then possible to investigate changes to the microglia using a variety of techniques. Confocal microscopy demonstrated an amoeboid-to-ramified transition in morphology which broadly corresponds (but is not exclusive) to an activated state. This then enabled investigation of the microglial transcriptome at different stages of their activation with LPS.

Single eye mRNA-Seq revealed inflammation-responsive transcriptional changes in retinal microglia following LPS stimulation which resolve within two weeks, confirming the potential for these cells to reset their homeostatic state. Hierarchical clustering of the 1,069 DEGs highlights a consensus group of downregulated genes at both 4- and 18 hours EIU (black box) but reveals a highly plastic transcriptome of upregulated genes (brown and yellow boxes, Figure 5.3). It calls into question the validity of curated lists of “microglia activation” genes as their expression may be time dependent in addition to stimulus dependent. This highlights a need for further stratification of gene groups based on the kinetics of microglial activation in addition to existing stratification measures (such as exact model/stimulus, or “acute/primed microglia” groups as determined by co-expressional meta-analyses). This is further evidenced by multiple examples of altered pathways at only 4- or 18 hours EIU, but not at both timepoints. Nonetheless, our data was also in agreement with curated lists for transcript-level data, whether these be microglial-specific lists (as published by other groups) or generalised pathways relating to changes in immune function or signalling (GO terms, KEGG pathways, and IPA canonical pathways).

As expected, due to the generally promiscuous role of many proteins (or even isoforms), some significant pathways were identified which do not necessarily translate perfectly into the microglial inflammatory context of our dataset (e.g. dendritic cell maturation, FAT10 cancer signaling, and osteoarthritis). However, most of these involve changes in immune cell function, which is what our data shows, and highlights why pathway analysis should always be interpreted with caution as a broad method of interrogating the data. In support of this, alterations to the TREM1 signaling pathway were observed, and published reports already indicate that microglia signal via the TREM2 pathway [599-601]; it is likely that overlap between the TREM pathways allowed for identification of enrichment of the TREM1 pathway (whereas no such pathway for TREM2 currently exists) – it is one example highlighting one of the most pertinent challenges surrounding pathway analysis.

Orthogonal validation by qPCR of the 10 markers, selected as they represent key and novel transcripts, confirmed the mRNA-Seq findings. However, altered expression of some of these membrane-associated markers did not translate to changes at the protein level as determined by flow cytometry. In part, this may reflect the presence of intracellular protein that our flow cytometric approach did not detect or represents genuine discrepancies between the transcriptome and proteome as these are not always in direct proportion [602-604]. Our results emphasise caution in reading out mRNA-Seq results alone as a true representation of the cell's activity and highlight the need for orthogonal validation. Despite this, the single eye mRNA-Seq approach identified key and novel transcriptional changes which informed subsequent testing on a smaller number of markers via low-throughput approaches. Ideally and for future work, use of integrated 'omics' (epigenetics, transcript, protein, and other data [e.g. phosphoproteomics]) would enable investigation of multiple different levels of cellular state, and for cross-comparison to identify key overlapping pathways or discrepancies where the use of low-throughput orthogonal approaches for further investigation could be warranted. Cutting-edge 'omics' techniques can currently couple two or three different assays in tandem, with some techniques incorporating single-cell resolution for the most powerful analysis [605-609]. Single-cell resolution with one or several of these 'omic' approaches would greatly enhance the understanding of cellular heterogeneity within the tissue. Despite this, 'omics' approaches currently have limited capacity to decipher information in the time dimension, and as existing assays are terminal it is not possible to follow the same cell or tissue across time with these techniques. Nonetheless, mRNA-Seq currently remains the most widely used high-throughput and sensitive approach used to decipher molecular changes occurring in cells and enables the sampling of vast amounts of information about the cellular phenotype.

Irrespective of when the transcript was perturbed, no significant changes were identified at the protein-level by 4 hours EIU. For example, multiple markers (SLAMF1, C5AR1, FAS, CD44, LAIR1) were changed at the transcript level by 4 hours EIU, but no change was observed using flow cytometry until 18 hours. This is likely explained by the delay between transcript generation and translation (and subsequent folding and transport to the plasma membrane).

Conflicting with previous reports investigating LPS-responses and EAE, we did not find significant down-regulation of P2RY12 upon microglial activation [342, 352]. In EAE, the microglia exhibit a chronic inflammatory state different to the acute LPS response, whilst the report investigating the LPS response used a systemic dose 400 times greater than our own local dose and had an endpoint 24 hours post-injection which could explain the discrepancy. We suggest microglial loss of P2RY12 as context-dependent, for example when subject to a

significant immune stimulus or persistent inflammation – it could be utilised as one of several markers to classify the severity/persistence of inflammation. P2RY₁₂ has been classified as important in microglial motility and response, so perhaps its downregulation is part of a negative feedback mechanism to help inhibit excess and/or persistent inflammation [610].

Our report conflicted with previous evidence that suggested MERTK was upregulated in microglia following LPS stimulation [597]. This study was performed in the BV-2 microglial cell line; it is generally well-recognised that immortalised cell lines are not necessarily representative of an *in vivo* environment because: 1) they have been modified as part of the immortalisation process and 2) they grow in culture conditions which are very different to an organ where multiple cells and the extracellular matrix (ECM) interact in a dynamic fashion as part of a complex microenvironment. Other transcriptomic studies have shown that freshly-isolated microglia and primary cultures are more similar to one another and that the BV-2 cell line, whilst useful, is not completely synonymous in responses to microglia or microglial primary cultures [611]; most strikingly, there is loss of TGF- β secretion in the BV-2 cells which has previously been characterised as critical to the microglial programme [308]. It should also be noted that the study involving BV-2 cultured the cells for 24 hours, as opposed to our timepoints of 4- and 18 hours, that BV-2 cells have been characterised as predisposed towards more activation generally, and that these factors may also explain the discrepancy [597, 611]. In macrophages, expression of MERTK was required for resolution of inflammation at 72 hours in a peritonitis model *in vivo*. MERTK expression was also observed *in vivo* in microglia but only by 3 days post-ischaemia; its blockade resulted in better clinical outcomes [612, 613]. Lastly, missense mutations in MERTK can cause a retinal degenerative disease called retinitis pigmentosa [614]; this may link to aberrant microglial regulation. Other recent work suggests MERTK is important for efferocytosis of dying cells and promoting immune tolerance. Blockade of MERTK results in STING activation (a pathway associated with autoinflammation) and IFN β secretion via a purine receptor-dependent process, suggesting an important role in negative regulation of an immune response [615]. Overall, this suggests that downregulation of MERTK enables greater microglial responses, and that its upregulation may occur at a later stage of inflammation (e.g. 3 days EIU) to assist in resolution. Short-term loss of MERTK has been shown to enhance neurogenesis [616], although it is evident (as exemplified by the missense mutations) that long-term loss is detrimental as MERTK represents an immune checkpoint.

The data shows that three previously suggested markers (P2RY₁₂, CD44, and SIGLECH) exhibit poor specificity for microglia. The studies suggesting P2RY₁₂ as microglial-specific did so based on bulk mRNA-Seq data, where different proportions of immune cells positive for P2RY₁₂ would

result in differential RPKM (or other normalised count) values. As only a proportion (~30%) of various immune cell types were observed as P2ry12⁺, compared to a large fraction (~80%) of microglia, this explains why it was previously identified and suggested as a microglia marker; transcript-level work will always identify it as an enriched marker, highlighting why protein-level validation is essential before it is confirmed as a specific marker. Furthermore, it has already been reported that loss of P2RY12 on the microglia can occur in some contexts, making it more suitable as a type of activation marker (severe and/or persistent inflammation), even if this loss was not observed in our study [342, 352].

For CD44, the poor specificity is because the microglia do not retain a CD44^{lo} signature, meaning that CD44^{lo} cells in the retina observed during inflammation (that were hypothesised as microglia in another report [558]) are infiltrating immune cells and not microglia.

In the case of SIGLECH, we did not find evidence of expression at the cell surface in more than a small proportion of microglia. This could be a reflection of possible intracellular protein not measured by our assay, or poor correlation between transcript and protein in this example. It could also represent poor binding by the antibody; for example, if the microglia express a different isoform to the receptor it was generated against or our positive control to test the antibody (spleen preparations containing SIGLECH⁺ dendritic cells).

Nonetheless, with the *Cx3cr1^{CreER}:R26-tdTomato* line, it remains possible to validate potential markers assuming the line retains specificity for microglia across disease contexts; the hunt continues.

Flow cytometric analysis confirmed and validated some of the transcriptional changes but also found that the differences were enhanced, and an additional marker (FAS) was identified as significantly different, when microglia were first stratified based on their C5AR1 expression as suggested via a transcripts-led report [342]. The percentage of C5AR1^{hi}-expressing microglia also had a moderate positive correlation with the number of infiltrating immune cells, representing a potential score for disease – with greater microglial activation comes greater inflammation and immune cell infiltration. Conversely, when microglia are depleted inflammation within the retina is considerably reduced if not completely prevented [390]. C5AR1 is a G protein-coupled receptor (GPCR) for C5a (generated as part of the complement cascade), that enables chemotaxis of myeloid cells towards an area of complement activation via one of the three pathways [617, 618]. C5AR1 expression is also controversial, with models of spinal cord injury showing an absence of C5AR1 resulting in clinical improvements in the early stages, but an ultimately worsened outcome later-on [619]; in contrast, C5AR1 loss resulted in clinical

improvements in AD models, showing how its expression and the role of microglia (and neuroinflammation) in different pathologies can be potentially beneficial, harmful, or both depending on context and timing [366].

Nonetheless, further work could be performed to validate changes in expression in addition to determining the cellular localisation of different proteins (using immunohistochemistry). Quantification of fluorescence (in addition to sampling of a greater volume and performing statistical analysis) would enhance the validity and robustness of the microscopy data. Furthermore, morphological analysis of microglia across EIU would provide insight; unfortunately, the tdTomato fluorescence was discontinuous within the microglia and this meant that pre-processing required for morphological analyses such as frac-lac and sholl analysis (e.g. skeletonisation) was unsuccessful. Without an alternative marker (such as IBA-1) it would not be possible to perform this type of analysis in a robust fashion.

With C5AR₁ stratification, markers which were exclusive to the C5AR₁-expressing microglia were identified (SLAMF₁, FAS, MILR₁, and LAIR₁) in addition to generalised markers which were slightly enriched but certainly not exclusive (CD44 and BST₂). Other reports suggest that C5AR₁ is needed for microglial polarisation to pro-inflammatory states, with its knock-out improving outcomes in an AD model [366]. Polymorphisms in complement components also associate with AMD in addition to evidence for complement association with drusen, potentially implicating microglia as key players in neuronal loss when homeostasis is perturbed [620]. Furthermore, microglial heterogeneity has already been reported in AD disease, light-damage models, EAE, and in response to LPS stimulation *in vivo* [340-342, 344, 586]. Understanding microglial heterogeneity, permitting identification of changes which are exclusive to subpopulations (which are yet to be fully realised), is critical for developing targeted therapies.

Further work to understand the differences between C5AR₁⁺ and C5AR₁⁻ microglia could potentially uncover therapeutic targets but also assist in understanding the mechanisms of microglial changes; ergo, whether they are responding to a stimulus or happen to be in the microenvironment.

Expressed by C5AR₁⁺ microglia, the protein SLAMF₁ plays a role in activation of lymphocytes. In contrast, MILR₁ and LAIR₁ act as inhibitory receptors for activation. This implies simultaneous activation alongside accumulating inhibitory factors which could act as part of a negative feedback loop to prevent persistent inflammation. Work in natural killer (NK) cells has shown that a lack of inhibitory receptors leads to hyporesponsiveness (to activating factors) as a possible mechanism to prevent or reduce auto-aggression/possible autoimmunity as these

cells lack an “off” switch [621]. Furthermore, inhibitory receptors co-localise with the activating receptors in the immunological synapse of NK cells [622]; it is plausible that the expression of inhibitory receptors by microglia and our observation of them on the cell surface enables greater activation of the microglia, akin to that of the NK cell. This could explain their presence during the inflammatory response (in addition to the possible negative feedback loop).

Furthermore, persistent FAS expression could lead to formation of a death-inducing signalling complex (DISC), inducing apoptosis in microglia. Contrastingly, other studies have identified FAS as important in the resolution of inflammation via apoptosis-independent pathways and that these immune cells are resistant to FAS-mediated apoptosis [623].

Taken together this suggests that the $C5AR_1^+$ microglia are actively engaging with infiltrating immune cells, acting as “responders” presumably through direct LPS stimulation to TLR4; this is supported by other reports which showed that $C5AR_1$ knock-out prevented lineage commitment of microglia to pro-inflammatory states in an AD model [366]. These are likely analogous to the DAM/AM observed in other disease states/models.

On the other hand, BST2 has functions involved in antiviral responses and is typically associated with activation through $IFN\alpha/\beta$ [624, 625]; $IFN\beta$ was upregulated by microglia during EIU, implying autocrine/paracrine signalling. There is no data from these experiments to distinguish whether the $C5ar_1^+$ or $C5ar_1^-$ microglia (or both) were secreting $IFN\beta$ and hence the exact signalling process and mechanisms are unclear.

CD44 is a receptor for hyaluronic acid, osteopontin, collagens (components of the ECM) and matrix metalloproteinases [626]; it is associated with lymphocyte activation and homing [627].

Therefore, the $C5AR_1^-$ microglia may represent “active bystanders” that aren’t directly engaged with LPS, but due to changes in the microenvironment (ergo paracrine signalling induced by the “responding [$C5AR_1^+$] microglia”) enhance their general immunological defence and surveillance programmes (e.g. through enhanced expression of antiviral proteins (BST2) and receptors involved in homing and interaction with the ECM [CD44]) to better detect further damage and respond more quickly as a mechanism of ultimately protecting the tissue. Unpublished adaptive optics imaging data from my Supervisor, Colin Chu, has shown that microglia within the tissue can interact with immune cells adhering to the endothelium of blood vessels. It is plausible that molecules such as CD44 permit microglial interaction with the vessels and enable them to assist in extravasation of peripheral immune cells into the tissue (but also to signal endothelium with much greater efficiency due to spatial proximity) and could at least

partially explain why there is considerable perivascular sheathing caused by microglia in models such as EAU (see Chapter VI). These are compatible with the notion that active inflammation or activation of a region of the retina would result in enhanced surveillance throughout the tissue (and possibly beyond) to allow for rapid elimination of infection.

In summary, the data demonstrates that the homeostatic threshold of retinal microglia is reset following an acute inflammatory insult and identifies potential markers for delineating the heterogeneity of microglia that may be used depending on the context of retinal perturbation.

Chapter VI: Final Discussion and Future Directions

Prior to the work presented in this thesis, it was known that microglia play a key role in the maintenance of homeostasis within the ocular compartment, that a fine balance exists between immune activation and regulation, and that new transgenic models had recently emerged which were proposed as sensitive and specific for microglial tagging to permit their investigation. However, comprehensive validation of the transgenic models and specific investigation into the microglial transcriptome *in vivo* during inflammatory states had not been performed comprehensively. Likewise, many proposed/hypothesised microglia markers had yet to be tested for validation (or invalidation) at the protein level. Critically, it was unclear whether homeostasis was permanently altered in response to autoimmune/inflammatory stimuli, or whether it can reset with time as proof-of-concept to reset immune states of uveitis or other patients with inflammatory disorders.

The data presented in this thesis demonstrates how development and optimisation of a low cell number mRNA-Seq platform, using FACS isolation, permits transcriptomic assessment of immune cells within the retina. Proof of concept validation using naïve microglia, and CD4⁺ T cells isolated during EAU, confirmed this approach could be applied to the sequencing of microglia isolated from single inflamed eyes (Chapter III).

To investigate microglia, use and validation of the latest transgenic models with temporal and conditional gene targeting for microglial specific tagging was required (the *Cx3cr1^{CreER}:R26-tdTomato* mouse strain). Furthermore, tamoxifen administration regimes for inducing recombination were compared and a shortened local (topical) approach was found to be superior, validating the sensitivity and specificity of this mouse strain for microglial identification during inflammation within the eye (Chapter IV).

With both the transcriptomic pipeline and microglial identification optimised, it was then possible to specifically interrogate the transcriptome of retinal microglia during inflammatory states. mRNA-Seq data acquired using the EIU model shows how LPS induces an acute and highly-plastic transcriptional response in microglia that resets by 2 weeks. A consistent set of downregulated homeostatic microglial genes, in agreement with the literature, was observed across the microglial activation stages. Furthermore, microglial subtypes could be stratified during the response via C5AR₁ expression (Chapter V).

In summary, the over-arching aim of ultimately determining the transcriptional changes occurring in microglia during intraocular inflammation was achieved, highlighting that during acute inflammation the microglial homeostatic state is restored post-inflammation.

6.1 Single-cell mRNA-Seq

Before a comprehensive analysis of the microglial transcriptome could be initiated, optimisation of a suitable mRNA-Seq pipeline was required. With approximately 1,500 microglia present in the mouse retina, and lower recovery when utilising FACS, a specialist pipeline that could process ultra-low inputs was required. To this end the SMART-Seq v4 Ultra Low Input RNA Kit by Clontech was selected. Several optimisations including cycling conditions, sequencing flow cell utilised, and staggered preparations were required to ensure a high success rate for sample preparation. Furthermore, as part of other experiments in the lab, the experimental pipeline has been scaled to even lower numbers of cells (<50).

Using various QC/QA metrics, the data highlights both a high accuracy in base calling by the sequencer but also quality input material as the results dependent on that (i.e. alignment rates) meet the gold standard as well. Furthering this, optimisation of the analytical pipeline and methods of data visualisation enabled key data to be displayed in a format more easily interpretable to others. Additionally, power analysis was required to inform the suggested number of biological replicates beyond the general considerations and suggestions presented in various technical papers, many of which were based on cell lines or other *in vitro* work. In all, optimisations were successful and have resulted in the generation of high-quality data and publication of our approach, both of which are available in public repositories.

Nonetheless, mRNA-Seq has the major limitation that it samples the average expression profile of the input material and cannot account for heterogeneity. Microglial heterogeneity in responses during disease states are becoming increasingly recognised [340-342], and the data presented in Chapter V on C5AR1 expression delineating microglia into what we term “Responders” and “Active Bystanders” also highlights this. Specific targeting of the microglial subsets responsible for disease or damage would be important to help restore tissue homeostasis. Two main technologies are used for the *in vivo* isolation of cells for sc-mRNA-Seq pipelines: 1) FACS and 2) specialised microfluidics devices (e.g. Drop-Seq, 10x chromium, and the Fluidigm C1) [628].

Systematic review of the published literature on scRNA-Seq protocols was performed to identify which protocol/s would be suitable for use with locally available equipment. Ultimately, three key criteria were used to determine which method to utilise: 1) low cost (utilisation of off-the-shelf reagents as opposed to kits where there is a large mark-up on price), 2) being FACS-ready (i.e. no requirement for the use of a specialist microfluidics device or other equipment currently unavailable locally), and 3) barcoding availability (to allow for pooling, which would greatly

reduce the time and cost implications of the experiment, allowing for much larger numbers of samples to be ran in parallel). Over 30 protocols were identified which allowed for low-level mRNA detection (ergo single-cell and ultra-low cell number mRNA-Seq) [629, 630].

Of the protocols identified, a number passed the latter two criteria, but many technical papers comparing methods highlighted three methodologies which clearly were of enhanced sensitivity and correlation (between technical replicates) than the others: cell expression by linear amplification and sequencing 2 (CEL-Seq2) [631], QUARTZ-Seq2 [632], and adapted versions of the Smart-Seq2 protocol (on which the SMART Seq v4 kit by Clontech, used for the mRNA-Seq data presented in this thesis, is based) [518] to include barcoding [633]. Whilst none of these were compared head-to-head, CEL-Seq2 was shown to be more sensitive (defined as the number of genes detected from single cells) than a non-barcoding version of Smart-Seq2 [631]. As they all appeared to (nonetheless) be reliable methods that were highly cited (or at the least the original versions of these protocols were), the main deciding factor for the protocol selected for use was cost. Using a Smart-Seq2 with barcoding or a QUARTZ-Seq2 approach was estimated to cost a total of £7,000 for a single run of a 384-well plate for single-cell sequencing (based on the best available estimators of cost and internal facility costings) whereas the CEL-Seq2 protocol was estimated at £3,100 per run. The primary reason for the discrepancy was the high cost of commercial library preparation kits (Illumina's Nextera XT kits) that the former two protocols used, whilst CEL-Seq2 used exclusively off-the-shelf reagents. For reference, use of the Illumina recommended pipeline for single-cell mRNA-Seq (utilising the Clontech SMART Seq v4 kits and Nextera XT DNA Library preparation kits) [516] was estimated at costing £61,000 for an equivalent experiment which was deemed unaffordable.

Additionally, the protocols had multiple pros and cons. The main considerations for CEL-Seq2 were that it possessed strand specificity (which few other protocols did), higher sensitivity, but importantly that it would only sequence the 3' fragment of the mRNA; the latter means that it would be unsuitable for sequencing of a poorly-annotated genome or for transcript/splicing analysis. The current mouse genome assembly, mm10, is well-refined and based on the C57BL/6 background meaning this limitation is not an obstacle to this continuing research. Furthermore, new technologies such as Nanopore [634] (which is available at the University of Bristol) are more suitable for transcript analysis because they provide long reads of direct mRNA molecules (as opposed to the short reads and subsequent alignment using Illumina sequencing). Therefore, experiments requiring transcript analysis would likely be performed using nanopore instead because of its improved validity.

Initial experiments wanted to confirm populations that would delineate nicely on a t-distributed stochastic neighbour embedding (t-SNE) plot as positive controls to validate the pipeline, in addition to generating interesting data on microglial heterogeneity. Barcoded 384-well plates were prepared, and CD4⁺ T cells isolated from spleen, naïve retinal microglia, retinal microglia 18 hours post-EIU, and GFP⁺ cells from the liver of a *Cx3cr1^{GFP}* heterozygote (the majority of these cells will be Kupffer cells, but a small proportion of T and other cells was anticipated based on previous flow cytometric characterisation of this organ) were sorted into single wells. It was hypothesised that the microglia and Kupffer cells would map to a similar 3D space (but nonetheless segregate), and the T cells would be located elsewhere but potentially further delineated by subset (e.g. naïve, effector, memory, etc). The samples were then barcoded, pooled, and then processed for mRNA-Seq. A library of lower than expected yield was generated in 1 of the 4 pools (each comprising 96 cells), which means that further optimisations are required before performing sequencing (Figure 6.1.1). Discussions are underway with the protocol Authors about possible modifications and improvements to improve the yield and success rate of the experimental pipeline (e.g. inclusion of a lysis reagent, such as nonyl phenoxyethoxyethanol-40 [NP-40], and an RNase inhibitor to the first mix cells are sorted into).

Further to sc-mRNA-Seq, as part of systematic review several protocols were identified which incorporate multi-omics approaches, such as transcriptomics with methylation (epigenetic) status and single-cell resolution [605-609]. It remains possible that once sc-mRNA-Seq is optimised that even more advanced techniques could be attempted to broaden the range of information on the cellular state that be acquired with single-cell resolution simultaneously.

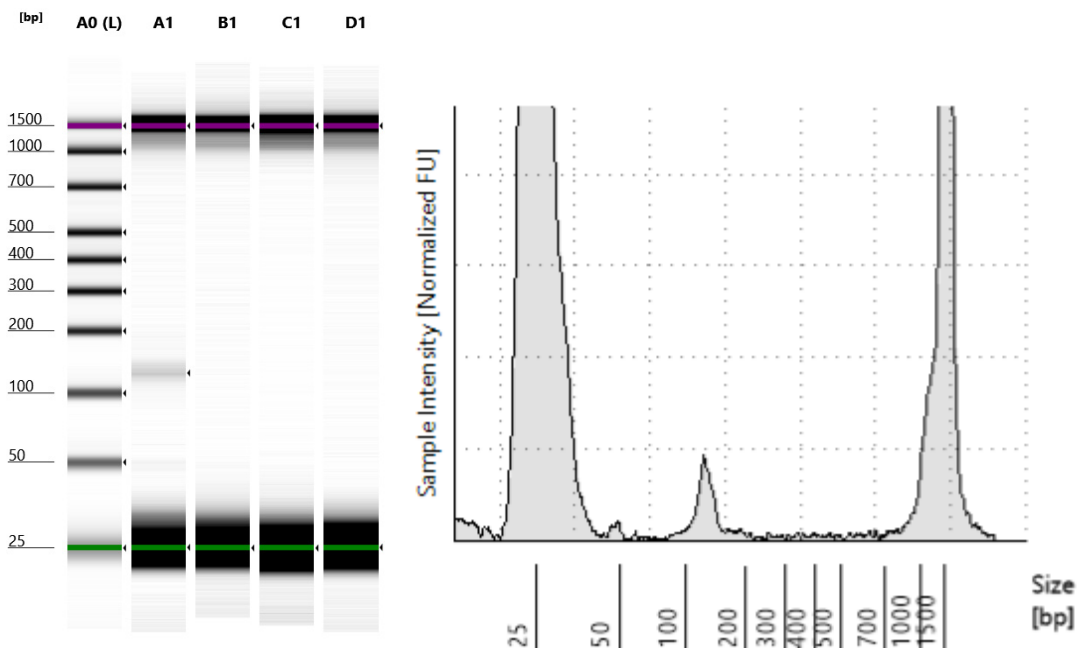


Figure 6.1.1. Agilent Bioanalyser output of libraries generated through the CEL-Seq2 protocol. Barcoded single cells, sorted into a 384-well, were pooled (96 cells per pool) into 4 samples for processing. Post-library generation and cleanup, these were then analysed on an Agilent 2100 Bioanalyser high-sensitivity DNA tapestation. (Left) electropherogram image with the ladder indicate a small positive peak around 130 bp (expected peak at 200-400 bp) for one of the four samples in the experiment. (Right) the gel trace for the positive sample indicates low yield. The ladders can clearly be observed at 25 and 1500 bp in green and purple, respectively.

We remain hopeful that this pipeline can generate novel and interesting datasets on retinal microglia. It will be especially interesting to observe how the two different niches of microglia [34] react during disease states, if it is differential due to their inherent differences, and to ultimately map the kinetics of microglial activation in uveitis models through pseudotime analysis. With reliable and robust models such as EIU, and sampling of microglia (from different mice) at different timepoints it may be possible to map the kinetics of microglial activation using real time and overcome some of the existing limitations that pseudotime analysis (of a sample at a single time-point) currently exhibits, albeit acknowledging that acquired cells from different timepoints were not from the same mouse. Furthermore, sc-mRNA-Seq of various myeloid cells, in addition to microglia, would help to highlight transcriptional differences between these groups and whether they are genuinely different or distinguishable (without fate-mapping or chimeras) during inflammation to identify possible microglial markers with more precision. Genome annotation to include tdTomato transcripts could act as a positive control for microglial identification in the context of these datasets.

6.2 Digital Cell Quantification and Demultiplexing of Cells and Cell Subsets

A novel analysis strategy, called digital cell quantification (DCQ), was recently described [635]. It involves using bulk mRNA-Seq data generated from known specific cell types and then applying it to mRNA-Seq data generated from a mixed population of cells. This then enables delineation of the gene expression values into an estimated representation of each cell type within a given sample. For example, in the original publication it utilises transcriptomic data generated by the ImmGen project for 213 different immune cells (grouped into stem cells, B cells, monocytes, macrophages, granulocytes, NK cells, T $\alpha\beta$ cells, NKT cells, T $\gamma\delta$ cells, and dendritic cells – they originated from a variety of tissues, stimulations, and time-points and were isolated using FACS [418]) to show and validate predicted changes in immune cell proportions within the lung during influenza infection. It was able to effectively predict changes in immune cell subsets that were already known to change but additionally provide novel insight into dendritic cell subtypes and their possible roles in the infection response.

This type of approach holds various advantages. For example, mRNA-Seq on immune cells isolated from patient blood could enable a better understanding of how specific immune cell subsets change over the course of treatment or disease, and it may assist in disease classification if certain subsets or gene expression profiles associate strongly with disease. A simple test of robustness could be to ask what cell populations are predicted in a sequenced sample of known cell type to observe how the algorithm performs as a form of positive control. In the case of the CD4⁺ T cell data (Chapter III), analysis highlights high predictive scores (on the raw data) for developing T cells, a large number of CD4⁺ T cells, and one CD8⁺ T cell signature (Figure 6.2.1). The over-representation of a CD8⁺ T cell signature, T $\gamma\delta$ signature, and developing T cell signatures is likely due to overlap in their expression signatures with CD4⁺ T cells. Nonetheless, this highlights the algorithm as accurate in identifying the data as derived from CD4⁺ T cells.

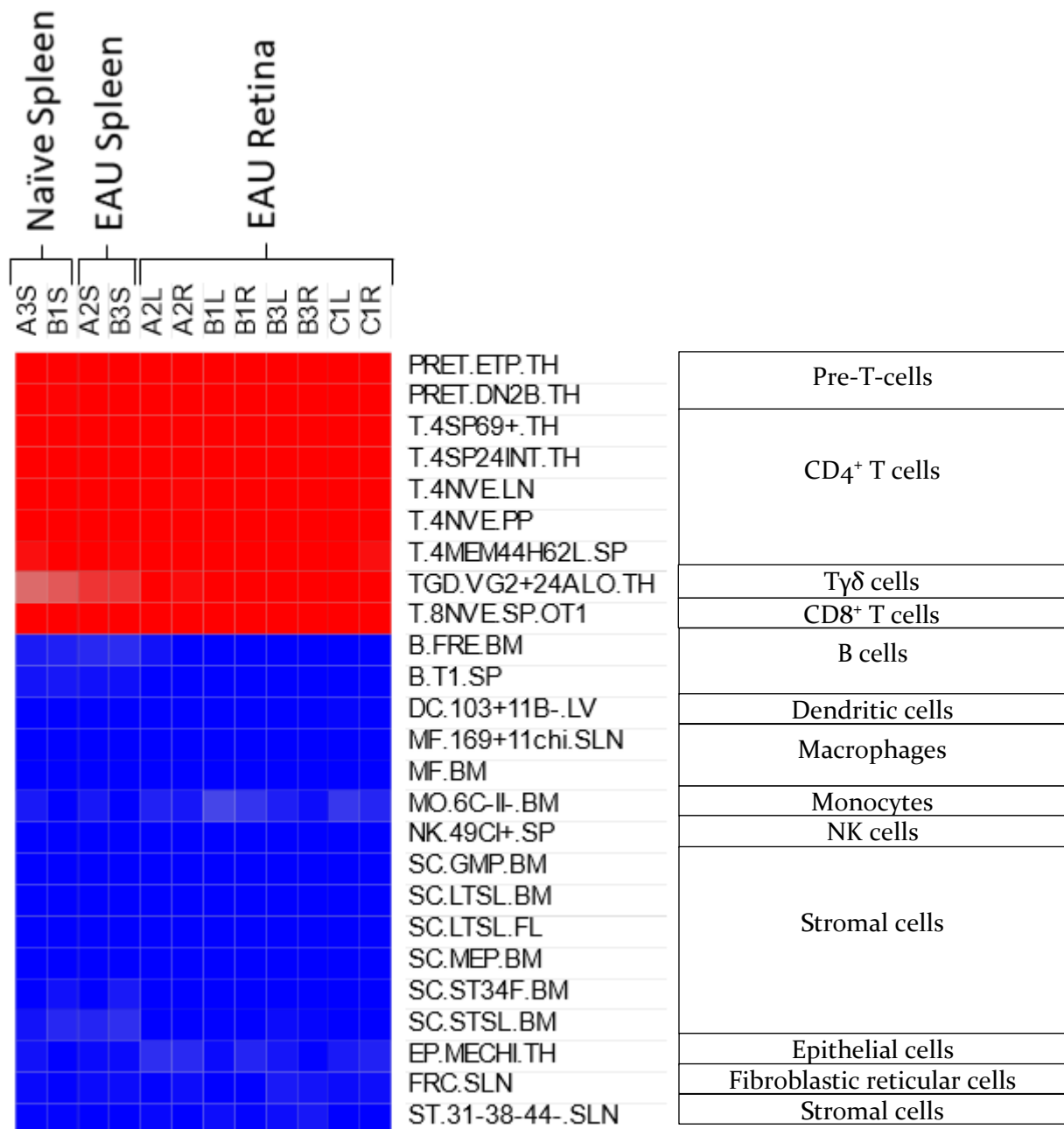


Figure 6.2.1. Digital Cell Quantification (DCQ) highlights an abundance of T cell signals in the CD4⁺ T cell dataset. The DCQ algorithm [635] was ran on the raw data obtained from 600 CD4⁺ T cells isolated from naïve spleens, and EAU peak disease (D25) spleens and retinas. Output values in red represent high predictive scores; blue represents low predictive score. An abundance of Pre-T cell, CD4⁺ T cell, and one Tyδ and CD8⁺ T cell signatures were observed. An absence of other signals (from major immune cell types and stromal cells) was observed. Output values which differ by ≥ 2 SDs (compared to the overall SD of all samples) are shown. Basic cell types are labelled to the right of the corresponding rows. Additional abbreviations: NVE – naïve, LN – lymph node, SP – spleen, BM – bone marrow, LV – liver. For a full explanation of the cell type labels, see the Immunological Genome Project data files and metadata [418] ($n = 2-8$).

When performing the same analysis but subtracting signals from the control samples (the recommended analysis strategy by the Authors; in this case, the naïve samples were the controls) this describes how the cells change from the baseline state in comparison to the cell types in the reference database. This is because our sample contains a known population of CD4⁺ cells, and not a mixture. Multiple NKT and CD8⁺ effector signals were overrepresented in the EAU retinas but not the EAU spleens (Figure 6.2.2). This suggests a transition within the population to NKT and CD4⁺ cytotoxic T cells (the CD8⁺ signatures, in what are known/sorted CD4⁺ T cells) – both of which are recognised as associated with autoimmune conditions [636-639]. It could also be that there is skewed representation of these cellular populations in the retinas, and that they for some reason are selectively retained or recruited to the eye during EAU and this accounts for the observation. NKT cells appear to be protective against autoimmunity in most, but not all, cases of autoimmune disease [640-642]. Additionally, somewhat conflicting results were obtained about B cell, dendritic cell, monocyte, and stromal cell signatures: some of the signatures appear enriched within EAU spleen samples, and others in EAU retinas, and both predictive enrichment and depletion of similar cell types can be observed in the same samples. It is unclear what this means but it highlights inherent variability and possible noise present within the system – and a lack of clarity about what is or is not significant. Nonetheless the DCQ algorithm was able to predict consistent changes to CD4⁺ T cell populations that are already known within the autoimmunity field.

Despite these strengths, the ImmGen reference dataset currently contains no information on microglia for analysis (a compendium bias) and it is coarse in identification because it has little ability for subtype discrimination. Additionally, it provides a single readout of representation of that given cell-type without any indication of deviation, and there is no clear cut-off for what constitutes a significantly different representation (in the dataset an arbitrary cut-off of ≥ 2 SDs from the overall dataset was used).

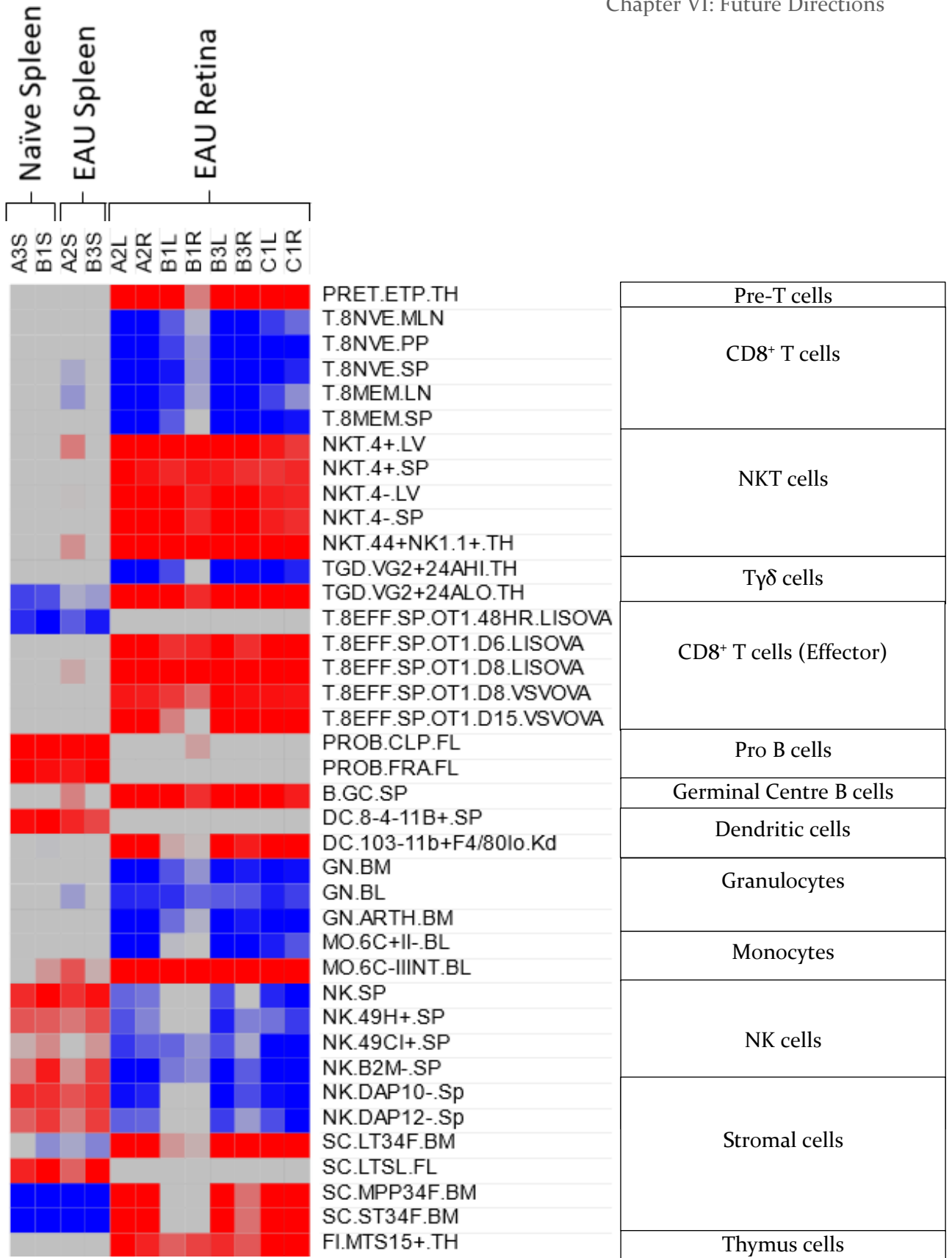


Figure 6.2.2. Digital Cell Quantification (DCQ) highlights over-representation of NKT and T effector cell signatures. The DCQ algorithm [635] was ran on the data processed (as per the recommended analytical strategy) obtained from 600 CD4⁺ T cells isolated from naïve spleens (A3S, B1S), and EAU peak disease (D25) spleens (A2S, B3S) and retinas (A2L-C1R). Output values in red represent high predictive scores; blue represents low predictive score. Output values which differ by ≥ 2 SDs (compared to the overall SD of all samples) are shown. Basic cell types are labelled to the right of the corresponding rows. Additional abbreviations: NVE – naïve, MEM – memory, LN – lymph node, SP – spleen, BM – bone marrow, LV – liver. Over-representation of multiple NKT and CD8⁺ effector cell signatures were observed, with a loss of multiple naïve CD8⁺ T cell signatures in EAU retinas. The naïve and EAU spleen signatures were found to be highly similar through this analysis. For a full explanation of the cell type labels, see the Immunological Genome Project data files and metadata [418] (n = 2–8).

Nonetheless, DCQ brings several other possible exciting prospects beyond the ImmGen data because it is modular and allows provision of your own reference dataset. This hypothetically enables quantification of any cell types or subsets present in the reference data provided. Unfortunately, there are no well-classified microglial subtypes currently (aside from the relatively poorly-fitting M1/M2 classification borrowed from macrophage field [158, 159]) let alone mRNA-Seq reference datasets of these hypothetical subtypes, and therefore analysis of them is currently not possible. However, CD4⁺ T cell subtypes are well-classified (primarily into Naïve, T_{h1}, T_{h2}, T_{h17}, and T_{reg} cells) and mRNA-Seq datasets on all these subtypes have already been generated [643]. Therefore, as the T_{h1}/T_{h17} axis is critical to the disease mechanisms of EAU [1, 644], delineating subsets using the CD4⁺ dataset could generate novel insight.

The results with DCQ were difficult to compare and contrast because of arbitrary cut-offs (determined by us) for what constitutes significance and an inability to perform robust statistical analyses, but it suggested over-representation of T_{h1}, T_{reg}, and T_{h17} signals in EAU retinas with a T_{h1}/T_{reg} signal in EAU spleens as compared to naïve (Figure 6.2.3). Optimisation of the number of input reference markers was required (<100 total reference genes worked best as a greater number of markers resulted in ceiling scores for many cell types. The markers were selected on the best enrichment for each specific group i.e. highest fold-change in favour of that subtype versus each of the other subtypes [10 per subtype in the case of the CD4⁺ subsets]). Due to the aforementioned limitations, comparing the data in a different manner to overcome these challenges could be helpful.

Therefore, the DEGs identified previously with the ANOVA model (Chapter III; naïve vs. EAU spleen, naïve vs. EAU retina, EAU spleen vs. EAU retina) were taken and classified by which subtype upregulated group (i.e. relative specificity to a single CD4⁺ subset, as identified in the original paper generating the CD4⁺ T cell subset dataset [643]) they associated with. It was then possible to use statistical analysis to observe if any subset was over-represented in the DEGs through use of Fisher's exact tests with FDR step-up p value correction (this mimics how pathway analysis is performed). The results of this approach generally agreed with the DCQ findings (Figure 6.2.4): that T_{h1}, T_{h17}, and T_{reg} signatures were over-represented in EAU retinas compared to naïve spleens. It also indicated (in a head-to-head comparison not possible with DCQ) that T_{h1} and T_{reg} were over-represented in EAU retinas compared to EAU spleens but not T_{h17}; the T_{h17} signal was similar between EAU spleens and retinas. As expected, the naïve signal was most prominent in the naïve spleen. A lack of enrichment was observed in EAU spleens to naïve retinas and this is likely due to poor statistical power rather than lack of genuine difference (n = 2 in both groups for comparison).

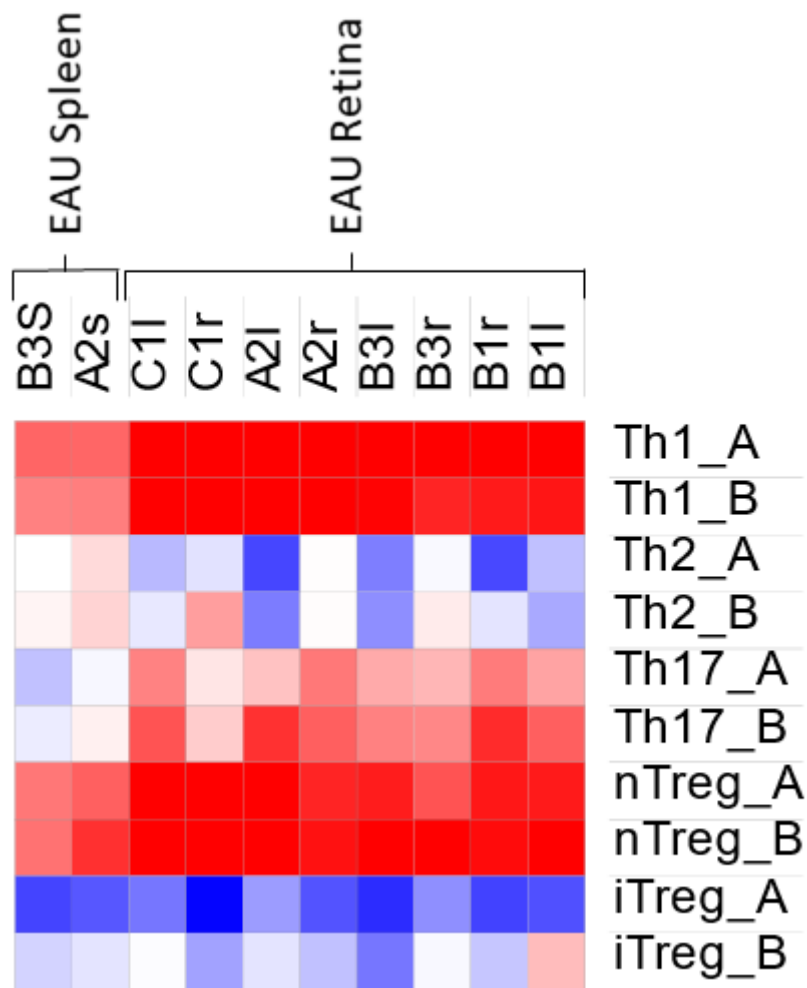


Figure 6.2.3. Digital Cell Quantification (DCQ) [635] identifies a prominent Th1/Th17 signatures in EAU retinas, in addition to a natural T_{reg} signature. EAU spleens and retinas were compared to naïve spleens in their expression signature for various $CD4^+$ T cells subtypes using a dataset generated by Stubbington et al. [643]. Output values in red represent high predictive scores; blue represents low predictive score. nT_{reg} cells were obtained from mice, whilst all other subtypes were derived from in vitro culturing conditions. The reference dataset includes replicates for each of the subtypes. Abbreviations: nT_{reg} – natural T_{reg} cell, iT_{reg} – induced T_{reg} cell.

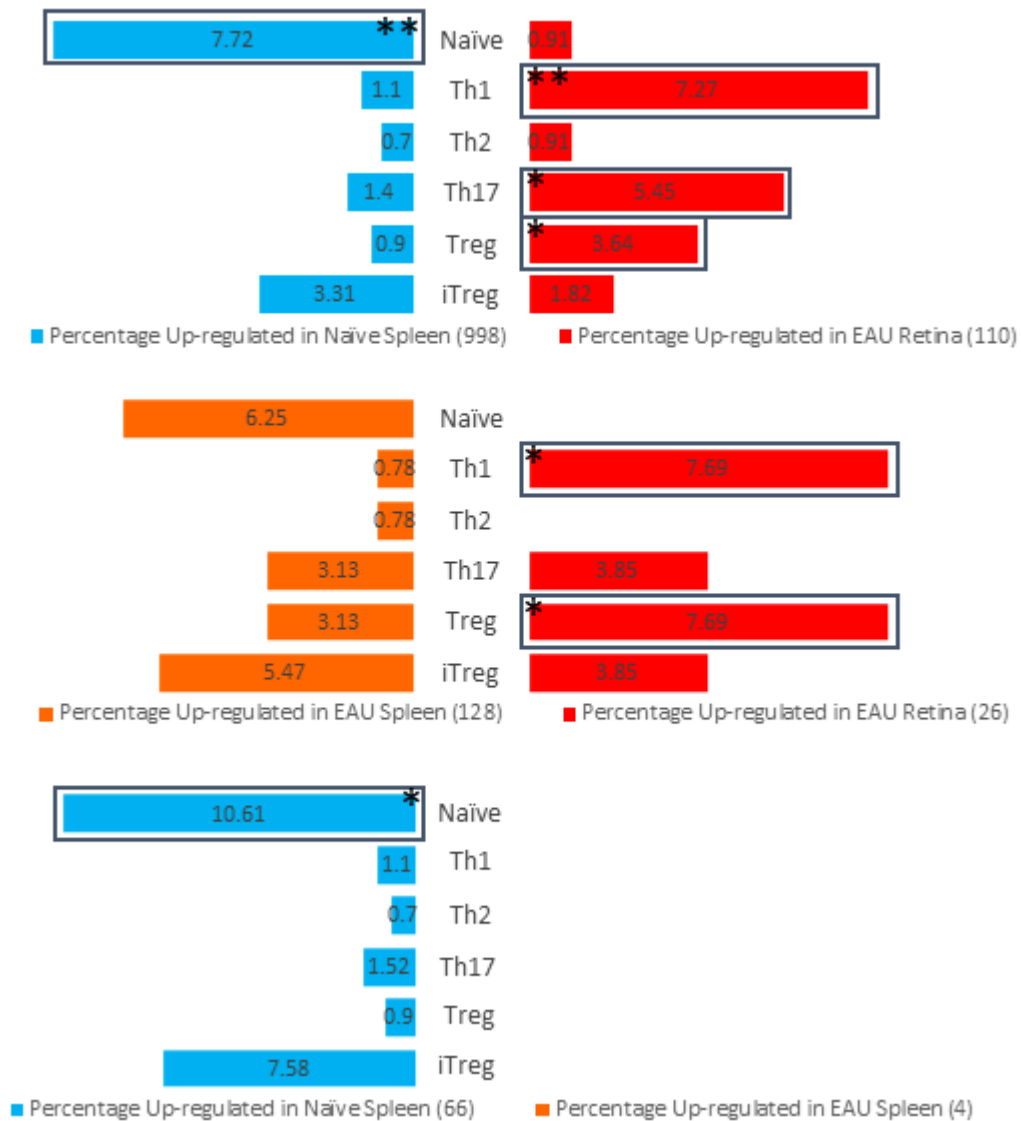


Figure 6.2.4. Differential gene expression analysis (DGEA) of “subtype upregulated” $CD4^+$ T Cell subset genes highlights general agreement with Digital Cell Quantification (DCQ) results. Head-to-head comparisons between naïve spleen, EAU spleen, and EAU retinas was performed. Total numbers of differentially-expressed genes (DEGs) between group comparisons are indicated in brackets (all genes), with the percentage overlap into subtype upregulated genes indicated on the bars ($n = 2-6$). * = $p \leq 0.05$, ** = $p \leq 0.01$.

As the spleen samples were prepared from eyes at peak EAU disease, it isn't possible to extrapolate whether these changes preclude infiltration of T cells into the retina, represent changes occurring from T cells that recirculated from the retina, or both. However, the data suggests that T cells shift from a more T_{h17} -like phenotype to a T_{h1} -like phenotype in the retina at the peak/late stages of disease. In agreement, other recent sc-mRNA-Seq data also suggests that T_{h1} cells dominate the response in a spontaneous EAU model [561]. Whether this is a response to the microenvironment, interactions with microglia, both, or other reasons is unclear. However, evidence suggests that T_{h1} cells could differentiate from other $CD4^+$ cell types (such as T_{h17}) by inducing IL-27 expression in microglia via IFN- γ (see "Retinal Microglia and Homeostasis" Chapter I which describes IL-27 preventing T_{h17} lineage commitment and the formation of ex- T_{h17} cells). Does commitment to a more T_{h1} -like phenotype help to drive or prevent further damage in the retina? As IL-27R knockout exaggerates autoimmune disease [410] this suggests that a more T_{h1} -like phenotype might cause reduced damage in comparison to a more T_{h17} -like phenotype. Most pertinently, is there a way to enhance the immunosuppressive environment? Further work could help to delineate the kinetics and changes across the stages of EAU, in addition to validation of the phenotypes using orthogonal approaches such as flow cytometry and immunohistochemistry (including iterative staining for an increased marker repertoire in stains).

If in the future microglial subsets are modelled and mRNA-Seq data produced on them, it would become possible for retrospective analysis of multiple existing datasets generated from microglia. New analysis strategies similar in function to DCQ have since been developed which can infer estimated cell proportions in bulk-mRNA-Seq from cell subsets identified using sc-mRNA-Seq data and may assist in bridging the gap between old and new [645, 646]. This could yield both rapid and novel insight into microglial lineage differentiation in various disease states and models because it could utilise a pool of readily-available data from mRNA-Seq repositories such as the NCBI's GEO. Ultimately this could result in rapid expansion of microglial knowledge and understanding and highlights why DCQ or other similar analyses represent a very powerful approach to probe/mine historic datasets for continued utility.

6.3 Further Investigation of Microglia in EIU

Prior to use of the *Cx3cr1^{CreER}:R26-tdTomato* mouse strain, it was important to validate this as both sensitive and specific for microglia. A reduced sensitivity would have meant fewer numbers of microglia tagged, resulting in a potentially less representative mRNA-Seq dataset generated. Additionally, downstream processing and testing of marker specificity would have been more difficult because the tdTomato⁺ fraction of cells would still include microglia. Lastly, lower numbers of microglia would have reduced the power and ability to validate changes using flow cytometric analysis because data such as percentage positivity would be more susceptible to skewing. Conversely, specificity also needed to be high so that cDNA was generated from a pure population of microglia and observed differences in the mRNA-Seq dataset were not due to infiltrating cells and changing proportions of cell types. Such confounding would have greatly reduced the validity of the datasets generated. Whilst validation in each disease context is recommended, it is evident that this approach of microglial identification is considerably superior to the conventional approaches and will enable more robust analysis of microglial changes during disease until a specific marker or set can be identified to reliably differentiate them from infiltrating myeloid cells.

With both the mRNA-Seq pipeline and *Cx3cr1^{CreER}:R26-tdTomato* mouse strain optimised and validated, it was then possible to begin investigation of retinal microglia during inflammatory states using the EIU model. After confirming unaltered kinetics to the WT C57BL/6 mouse, and that microglial morphological perturbation occurs by 4 hours post-injection, sorting and sequencing of microglia before, during, and after resolution of EIU identified a highly-plastic transcriptome over time in response to LPS. It also confirmed that the microglia did reset by 2 weeks and identifies the potential for immune state reset in diseases such as uveitis. Importantly, this series of experiments highlights the importance of orthogonal validation of both DEGs but also suggested microglial markers. Lastly, a key marker (C5AR1) that helps to delineate microglial subsets during the response was identified and validated.

With the work presented in Chapters III–V now published, there are still many unanswered questions and further lines of investigation into microglia during and after EIU: What potential treatments could be identified and tested through further bioinformatic analysis, what does the flow cytometric panel of validated markers and imaging show when treatments (both novel and existing) are administered, and what happens if the retinas are subject to a second LPS stimulus during or after the reset period, or how the anti-viral (e.g. TLR3-mediated) and anti-fungal (e.g. TLR-2 mediated) response compare to name a few.

To this end, work is already underway to test a variety of treatments: dexamethasone (as glucocorticoids represent a first-line treatment in uveitis and a treatment known to have efficacy – a positive control to observe how the microglia change with treatment), prostaglandin (PG) E₂ receptor (EP₂) agonists and antagonists Butaprost and AH6809 respectively [647] (as IPA identified PGE₂ as a key regulator), and searching for GPCRs expressed by microglia that signal through the G α q subunit (an IPA canonical pathway identified as greatly altered that could be modulated through agonists, antagonists, biased or inverse agonists). Based on an RPKM threshold of 5, the existing datasets indicate that only one combination of G α , G β , and G γ subunit isoforms are expressed by retinal microglia: α_{15} , β_1 , and γ_{13} . In contrast, three phospholipase C (PLC) isoforms are expressed: γ_2 , δ_3 , and δ_4 . However, due to the large numbers of subunit isoforms and downstream targets little is known about each combination could specifically interact and the functional and regulatory consequences this may have in a given cell type [648]. It is known however that the G α_{15} subunit can couple in a highly promiscuous fashion to multiple receptors and may explain why other α subunits are not expressed [649]. Key GPCRs expressed by microglia include C₅AR₁, P₂RY₁₂, and CX₃CR₁, which have roles in inflammatory state polarisation, neurone-coupling and responsiveness to injury, and neuronal interactions respectively, further highlighting the potential critical role this signalling pathway may have [366, 372, 610, 650, 651]. Assays utilising primary murine microglia and PLC isoform inhibition have already been described, and may be useful in delineating the roles of different signalling molecules expressed by the microglia as identified by mRNA-Seq [652]. Furthermore, generalised inactivation of the G α q subunit could be achieved by using a selective inhibitor such as YM-254890 [653, 654]. However, due to G α_{15} 's promiscuous nature, the critical receptors it couples to, and lack of alternate isoforms expressed by microglia for partial compensation this may have limited utility in experiments and unlikely to be useful as a therapeutic due to wide potential for side effects. It would however confirm if certain functions were mediated by a receptor (or receptors) coupling to that signalling pathway. Other avenues for possible therapeutics include targeting PLC γ_2 , a variant of which with a small hypermorphic effect on enzyme function associated with a protective effect in AD [655]. Receptor tyrosine kinases (such as TREM₂, Fc receptors, and CSF₁R), acting through the intermediate protein SYK, can interact with PLC γ variants and TREM₂ signalling/dysfunction has already been identified as important in AD [340, 356].

In addition to possible therapeutics, it is possible to investigate EIU and microglial responses from a more mechanistic viewpoint. Re-stimulation with LPS in other organs leads to a local refractory state and it would be interesting to observe and characterise whether the same

phenomenon occurs in the eye [656]. Research into different TLR agonists has already been performed in the retina, indicating that TLR3- and TLR2-mediated agonisation (e.g. using poly(I:C) and zymosan) can induce an immune response [92, 657]. Investigating whether microglia exhibit differential responses to simulated infection with different broad classes of pathogen would assist in delineating core response programmes and specialised responses to specific stimuli – opening the possibility of generalised inhibition of activation or targeted inhibition of a specialised response induced under specific circumstances.

6.4 Investigating Microglia in EAU

Beyond EIU, several other models and variants exist. For example, EAU (where CD4⁺ responses are driven against retinal antigens through immunisation) is a widely used model that simulates a variety of aspects of uveitis well. It is possible to investigate several variants of EAU including conventional peptide immunisation vs. AT and compare the microglial response between them. AT would be especially useful in removing the effects adjuvants (i.e. CFA and PTX) have on the disease phenotype, enabling delineation between adaptive immune system effects and innate immune influences [88, 658]. In short, AT involves conventional peptide immunisation of mice, harvesting of lymph nodes during disease, culturing of these for T_H17-inducing cytokines and peptide, and lastly intraperitoneal transfer into new recipient mice and is a model that has been previously optimised by a PhD student within the Ophthalmology group. With various allelic markers (such as CD45.1 and CD45.2) but also the arrival of CAG-eGFP mice (where all cells are labelled with GFP) to Bristol, it will permit investigation of various hypotheses and already has interesting implications such as repeatable *in vivo* imaging of the microglia and transferred cells and their interactions (Figure 6.4.1). The pinnacle version of this experiment would enable imaging of endogenous cells, microglia, and transferred cells all with different fluorescent markers and is possible using the right combination of transgenic lines: For example, tagging microglia with tdTomato in the *Cx3cxr1^{CreER}:R26-tdTomato* line, subsequently generating a chimera (HPI) with a mouse line expressing BFP (e.g. to the CD45 promoter) to label endogenous cells, and AT of CAG-EGFP cells would enable visualisation of how each cell group/type move and interact with one another *in vivo*. Furthermore, with new technologies such as adaptive optics (repeatable *in vivo* high resolution imaging) could be performed in the mouse and would synergise with this multi-fluorescent tagging approach [659-661].

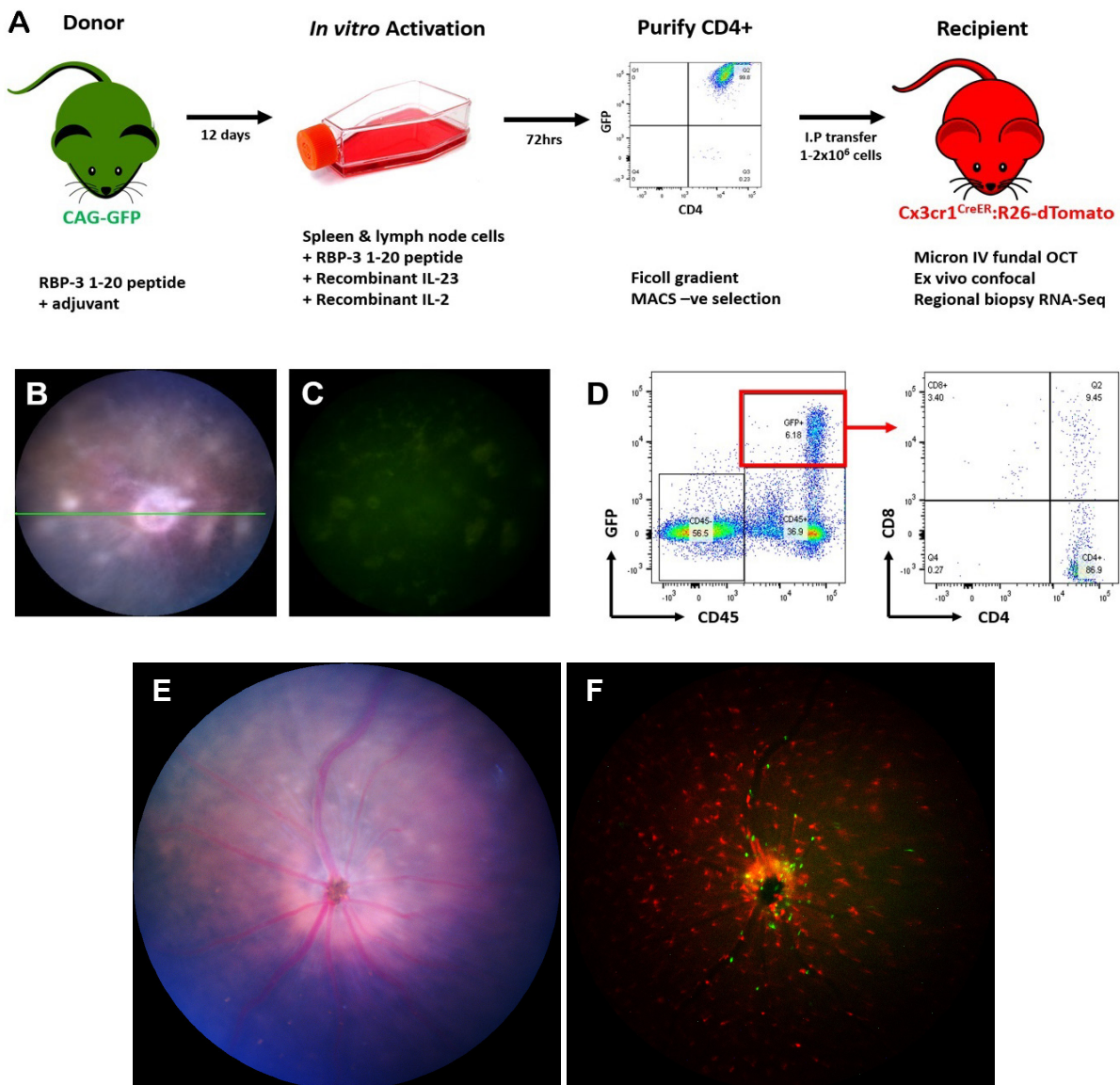


Figure 6.4.1. Inducing EAU by adoptive transfer of CD4⁺ T cells and initial assessment with imaging and flow cytometric platforms. *A)* The adoptive transfer model pipeline is summarised, showing how the antigen-specific T cells are generated, cultured, purified (90% purity by magnetic-activated cell sorting), and lastly administered to recipient mice by intraperitoneal injection. *B)* Disease is obtained in 80% of recipients by day 10 (a faster onset than conventional peptide immunisation). Tissue damage can be imaged in brightfield, *C)* whilst transferred cells can also be visualised using fluorescent filters. *D)* Flow cytometric analysis can be used to identify the GFP⁺ transfer cells and confirm them as high purity CD4⁺ T cells. *E)* Brightfield imaging at day 5 post-transfer shows very early signs of disease and *F)* fluorescent imaging highlights the presence of CD4⁺ T cells (green) in the retina alongside microglial (red) perturbations primarily adjacent to the optic disc. The data presented in this figure were generated by Dave Copland and Colin Chu.

Work is already underway for analysis of EAU in the *Cx3cr1^{CreER}:R26-tdTomato* line. Imaging of the conventional peptide EAU model shows simultaneous microglial association with both lesions and other regions that appear physiological (Figure 6.4.2). This is analogous to some of the highly diverse range of pathological appearances in uveitis. Clinically, inflammation can be restricted to different anatomical compartments and even within the same ocular tissue as the retina can have strikingly varied appearances [662]. Similarly, damage-associated microglia have been described in other disease models [340] and microglial heterogeneity is becoming increasingly recognised, with reports highlighting heterogeneity in AD, light-damage models, EAE and in response to LPS stimulation *in vivo* [340-342, 344, 586].

Additionally, long-term imaging highlights that EAU continues post-peak disease with “flare-ups” and activation of the microglia – whether this is by recirculation (into and from lymphoid tissues) and activation of CD4⁺ T cells that had already caused disease, or activation of new CD4⁺ T cells by peptide loading (or both) is unclear. What it does highlight is that conventional peptide EAU is a disease model which certainly does not resolve in the immediate aftermath from peak disease, or for up to 74 days post-immunisation (the latest time-point in imaging in these mice), with regards to microglial involvement and perturbation. This means that the model exhibits remission and lower-severity (compared to peak) regionality-specific relapse, the latter of which may not necessarily be completely representative of relapse in uveitis patients (Figure 6.4.2). Nonetheless it could be utilised to characterise changes to microglia after repeated activation versus peak disease, but also compared to repeated stimulation EIU experiments for both similarities and differences (i.e. a comparison between repeated innate stimuli and adaptive responses). Additionally, the tdTomato fluorescence intensity was raised considerably, although from the imaging data this is unclear whether it is due to microglial migration (e.g. from ON into retina), upregulation of tdTomato by microglia, proliferation of microglia, or a combination of these factors.

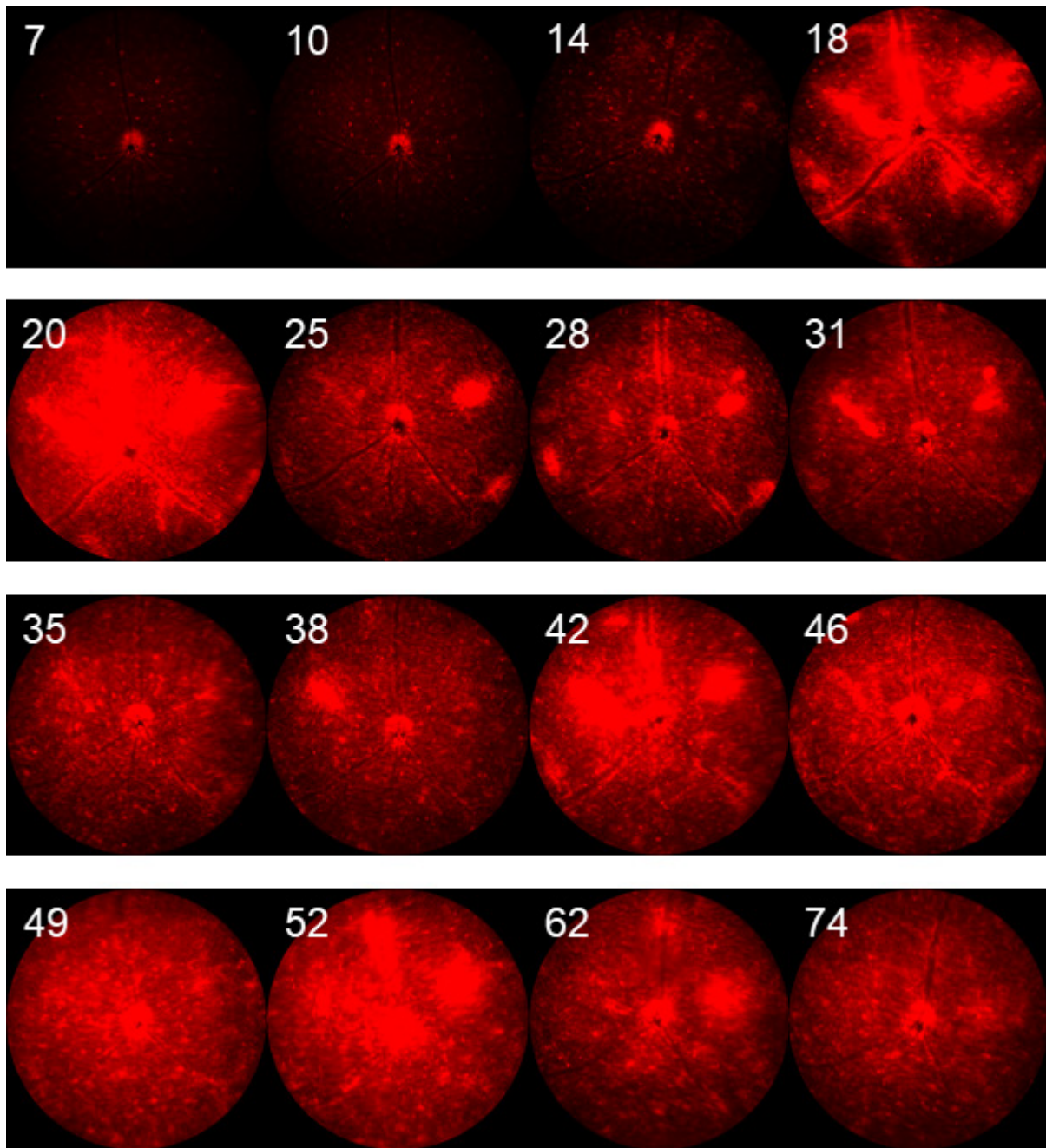


Figure 6.4.2. *tdTomato acquisition-normalised fluorescent fundal imaging time-course in a single mouse highlights continuing pathology and microglial association in the EAU model long-term.* The mouse was immunised for EAU using RBP-3 peptide 1–20 and both eyes imaged using the Micron IV. The day of imaging is indicated to the upper left of each image. The time-course shows changes occurring in the right eye over time. This particular mouse had a peak of disease around day 20, with evidence of some remission at day 25. Resurgence and worsening of disease severity is evident at day 28 (but most prominently at days 42 and 52), highlighting ongoing disease and changes in this model long-term. This mouse received a 3-day topical tamoxifen regime.

Flow cytometric analysis highlights a reduced specificity for microglia with a subcutaneous tamoxifen regime that negatively correlates with immune cell infiltrate (Figure 6.4.3a–b). These experiments were required as the severity and persistence of inflammation are different to EIU. This means it is possible that other immune cells may acquire the tdTomato tag through constitutive recombination if *Cx3cr1* expression was elevated, in addition to surviving long-term due to persistent inflammation or possible engraftment into the tissue. In a spontaneous uveitis model (*Aire*^{-/-}) there is evidence for the formation of tertiary lymphoid structures for example [561]. Ultimately, use of the same or a similar pipeline for microglial isolation and investigation will be critical to future experiments and necessitates confirmation of specificity in this context.

At peak EAU the microglial count is elevated roughly two-fold during EAU (Figure 6.4.3c), although it is currently unclear whether this is due to proliferation, migration of microglia from other regions to the retina, or both; it could even be due to engraftment, although this seems unlikely as it has already been shown that it takes several weeks to achieve high expression of tdTomato (Chapter IV). Research into microglia in other contexts highlights microglial proliferation as a feature of neuroinflammation, suggesting that proliferation in EAU (at least) is happening [663–665]. The fact that there are regions which appear quiescent during EAU suggest that microglia remain within their niche and that it is only microglia local to the damage that are proliferating, although this remains yet to be proven. Additionally, CD45 mean fluorescence intensity (MFI) was elevated in microglia (Figure 6.4.3d) in agreement with other work [415, 549, 550]. tdTomato expression was also elevated and this positively correlates with immune cell infiltrate in EAU (Figure 6.4.3e–f), representing another possible flow cytometric marker for scoring disease specific to the *Cx3cr1*^{CreER}:*R26-tdTomato* mouse line.

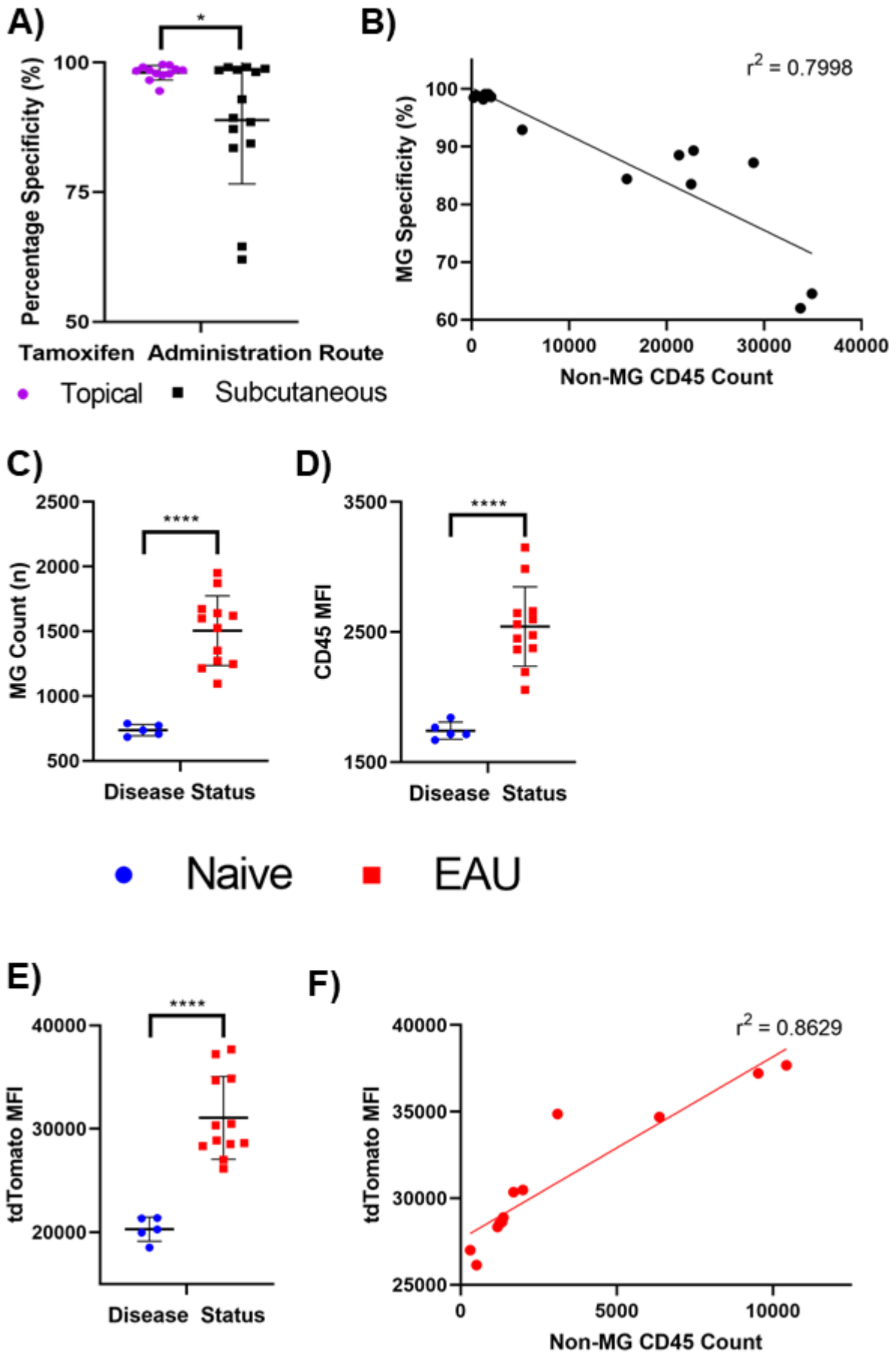


Figure 6.4.3. Preliminary flow cytometric analysis of microglia during EAU in the *Cx3cr1^{CreER}:R26-tdTomato* mouse strain. The mice were immunised for disease using RBP-3 peptide 1-20 and were taken for flow cytometric assessment at day 24 (peak disease). **A)** The specificity of microglial tagging in a topical vs. subcutaneous approach indicates a reduced specificity with subcutaneous tamoxifen (gating as per Figure 4.2.4). **B)** The percentage specificity correlates with immune cell infiltrate at peak disease in the EAU model of mice that received a subcutaneous tamoxifen regime, highlighting a reduced specificity as disease severity increases. Further analyses (C-E) utilised mice that had received a topical tamoxifen regime to overcome this possible confounding. **C)** Microglial count is elevated by roughly two-fold during EAU. **D)** In-line with published work [415, 549, 550], microglial CD45 expression was increased during inflammation. **E)** tdTomato expression is elevated during EAU. **F)** tdTomato MFI correlates with immune cell infiltrate in the EAU model (n = 5-17). For statistical analysis, both the T test (with FDR step-up correction) and Pearson's test were used. * = $p \leq 0.05$, **** = $p \leq 0.0001$.

Continuing the work beyond basic phenotyping and analysis of microglia in the EAU model (e.g. the panel of markers validated as differentially-expressed during EIU and stratification using C5AR1; Chapter V), it would be interesting to observe what effects LPS treatment, other treatments (such as potential therapeutic interventions), or even other variations of the EAU model (such as PMU, a more chronic disease model [85]) have on microglial activation, fundal appearance, and transcriptional status. The PMU model, for example, could be important in helping to investigate the role of the CD8-microglia interactions observed in the brain [394], and delineating that aspect of uveitis due to its chronicity. Ultimately, co-expressional meta-analysis of these transcriptomes during inflammation would be interesting to identify core sets of genes associated to inflammation/immune cell ingress, but also how they compare to microglia in other disease states. Ideally, stratifying microglial subtypes or regional damage during disease and improvements in disease severity classification will permit more powerful and meaningful bioinformatic analysis of the data generated.

6.5 Regional Biopsies of Retinas for Analysis of Intra-Tissue Heterogeneity

To address the challenge of heterogeneity in retinal tissue damage observed in EAU (Figure 6.5.1), my Supervisors (Colin Chu and Dave Copland) developed a regional biopsy technique whereby these heterogeneous regions can be visualised and excised using microscopy-guided dissection (Figure 6.5.2). Preliminary experiments aim to perfect the technique by performing regional biopsies on microglia obtained from different anatomical regions in the retina (e.g. ON, parenchyma, perivascular), but then progress onto controlled lesion formation through use of the laser-CNV model. Performing flow cytometry and mRNA-Seq on these regional biopsies is anticipated. By using regional biopsies from the same mouse, the general microenvironment could be controlled for and damage-associated signals could be enriched (compared to performing bulk mRNA-Seq on whole tissues) leading to better power and detection of transcriptional changes in this microglial subpopulation. It may even be possible to identify microglial subsets within the same biopsy using $C5AR_1$ stratification. Regional biopsies represent a novel and unique opportunity in eye research as part of the synthesis between available imaging technologies and their utility in informing other techniques.

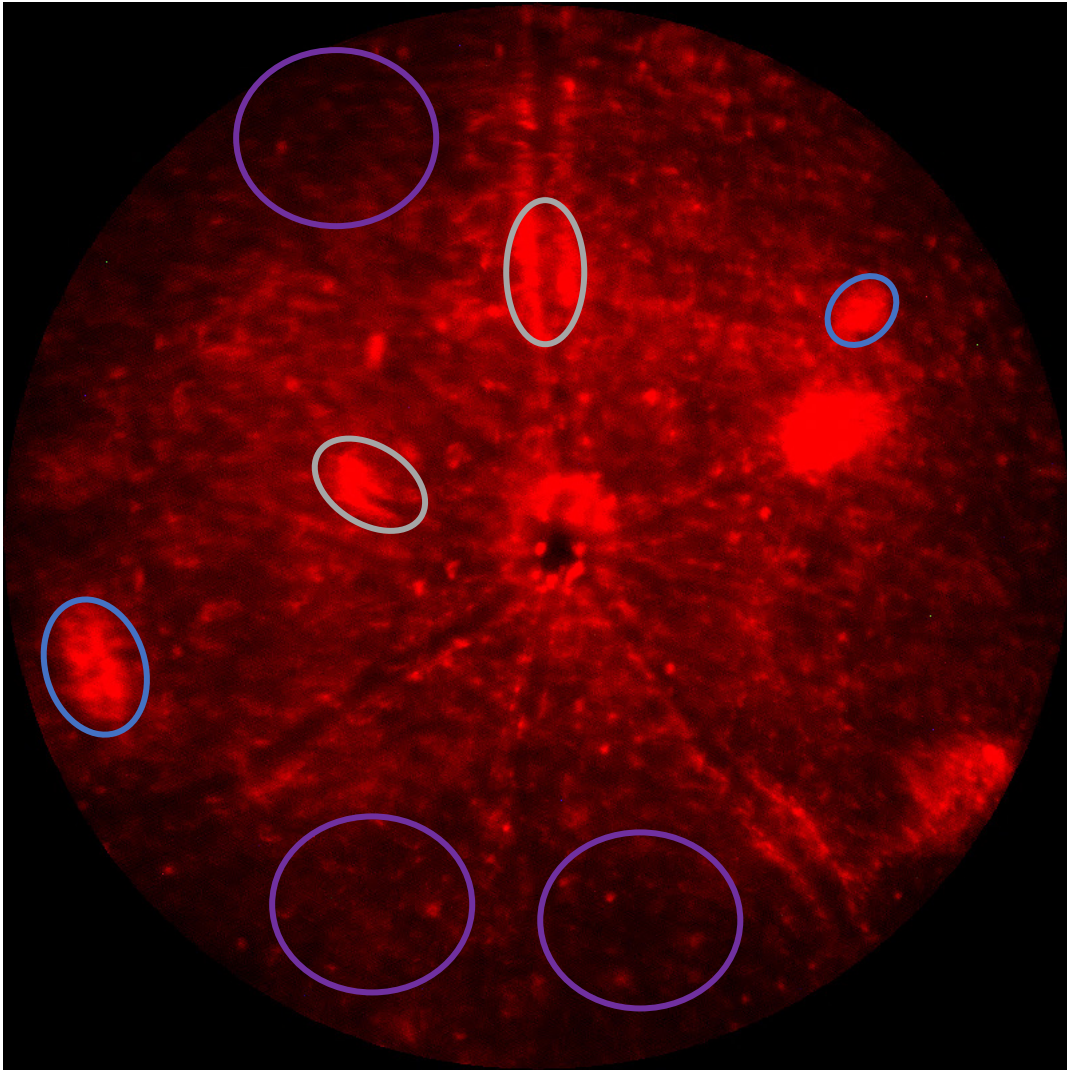


Figure 6.5.1. *Fluorescent fundal images of tdTomato (microglia) in the $Cx3cr1^{CreER};R26-tdTomato$ mouse line highlights heterogeneity in the microglial response during EAU. Regions of microglial activation in parenchymal (blue, circled) and perivascular (grey, circled) regions highlights focal points of activation. Other regions possess microglia which, in viewed in isolation, could be considered naïve or certainly appear more quiescent with regards to disease (purple, circled).*

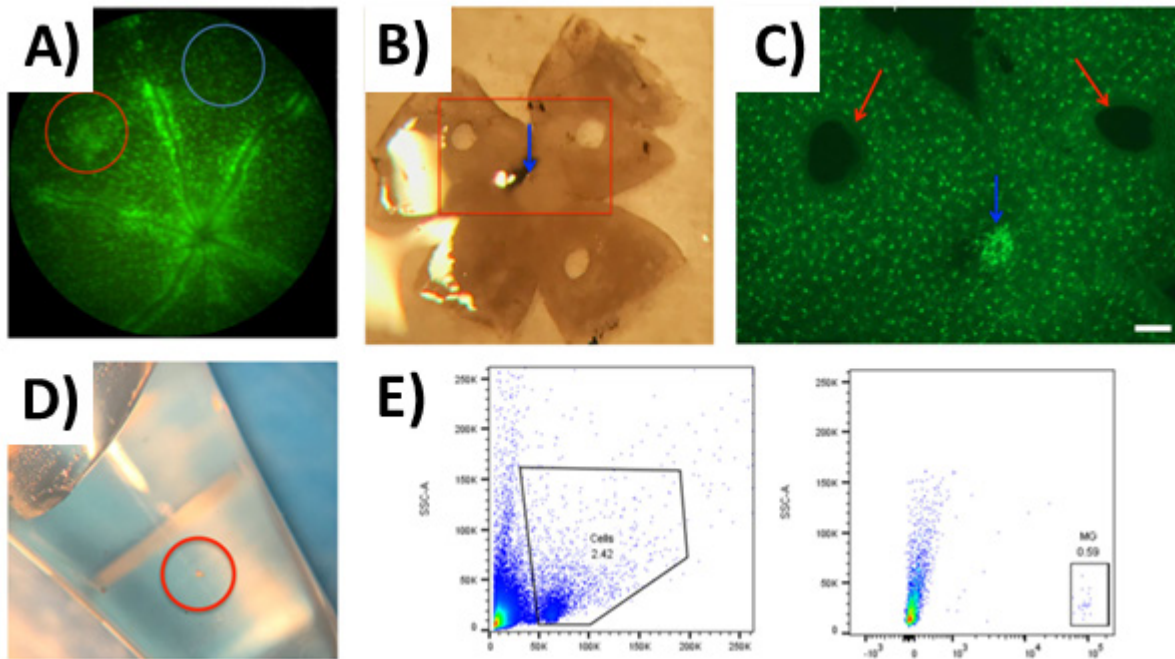


Figure 6.5.2. An overview of the regional biopsy technique. *A)* In agreement with images in the $Cx3cr1^{CreER}:R26-tdTomato$ mouse, heterogeneity in the microglia is also observed in the $Cx3cr1^{GFP}$ mouse line. *B)* Using a curved 21G lacrimal cannula, tissue punches of live full thickness retina can be obtained reliably (blue arrow highlights the optic nerve). *C)* Fluorescent imaging of the same retina shown in *B* (red box). *D)* Punches can be isolated (circled) and homogenised as per standard protocols. *E)* Flow cytometric analysis shows the presence of 25 GFP^+ microglia per punch in a naïve retina. The data for this figure, and figure itself, were prepared by Dave Copland and Colin Chu.

A potentially very powerful synthesis of techniques could be that of regional biopsies and sc-mRNA-Seq. Regional biopsies could be utilised to ensure representation of all tissue phenotypes in fewer cells than at a tissue level (where a rare population may be missed or under-represented unless the whole tissue was sequenced) which would permit a greater number of biological replicates to be assessed for improved validity and reproducibility (a lack of biological replicates is one major flaw of the sc-mRNA-Seq field currently). Additionally, the phenotype of the biopsies (identified by imaging pre-mortem) could be cross-correlated to the sc-mRNA-Seq data and enable the prediction of signal (and cell) localisation without the need for microscopy or techniques such as fluorescence *in situ* hybridisation (FISH) – but may inform where these techniques would be best-placed to validate the findings nonetheless. Furthermore, with imaging over a time-course it may be possible to retrospectively analyse early microglial changes and signals that preclude later changes, and ultimately guide targeted therapies.

6.6 Three-Dimensional OCT Disease Scoring

Research into the eye carries the advantage of *in vivo* imaging, a repeatable and non-terminal procedure. Disease models carry inherent variability and this decreases statistical power of analyses. However, in the eye it is possible to image and score/grade eyes for disease severity and then associate this to downstream assays – a major advantage of this field. With the mRNA-Seq data currently generated, one pertinent question which could be asked is: does disease severity correlate well to any expression patterns? This could serve as an approach of identifying novel biomarkers in addition to potential therapeutic targets by identifying those genes which are critical and robust in expression across samples which have been delineated based on disease severity/stage.

The currently available approaches for scoring disease (based on brightfield fundal imaging) are useful but have limitations [104]. For example, the measures are subjective and therefore subject to bias, they are unlikely to be linear (meaning use of more powerful parametric statistics is not possible), and are not particularly sensitive in grading scale. Other, conventional approaches for scoring (i.e. histology) prevent use of samples for other analyses.

However, a different method utilising OCT and measurement of particles in the VB was recently described [109]. In theory, this approach is linear, objective, and could be more sensitive than current approaches. Despite this, the method utilises a small sampling region (one or a few OCT line scans) and could be argued as less representative because of this. Nonetheless, with the OCT it is possible to sample larger regions of the retina by acquiring 512 B-scans adjacent to one another (each B-scan is 0.9 mm in length horizontally, scans have a spacing of $\sim 1.75 \mu\text{m}$, and a depth of ~ 1.3 mm leading to acquisition of a $0.9 \times 0.9 \times 1.3$ mm region of space; Figure 6.6.1a), termed a volume scan, that can be reconstructed into a three-dimensional render (Figure 6.6.1b–d). They can be acquired with the optic disc located centrally, ensuring the same mouse is sampled in the same location (i.e. posterior retina) at different time-points, but also that equivalent regions are sampled between different mice for better comparability.

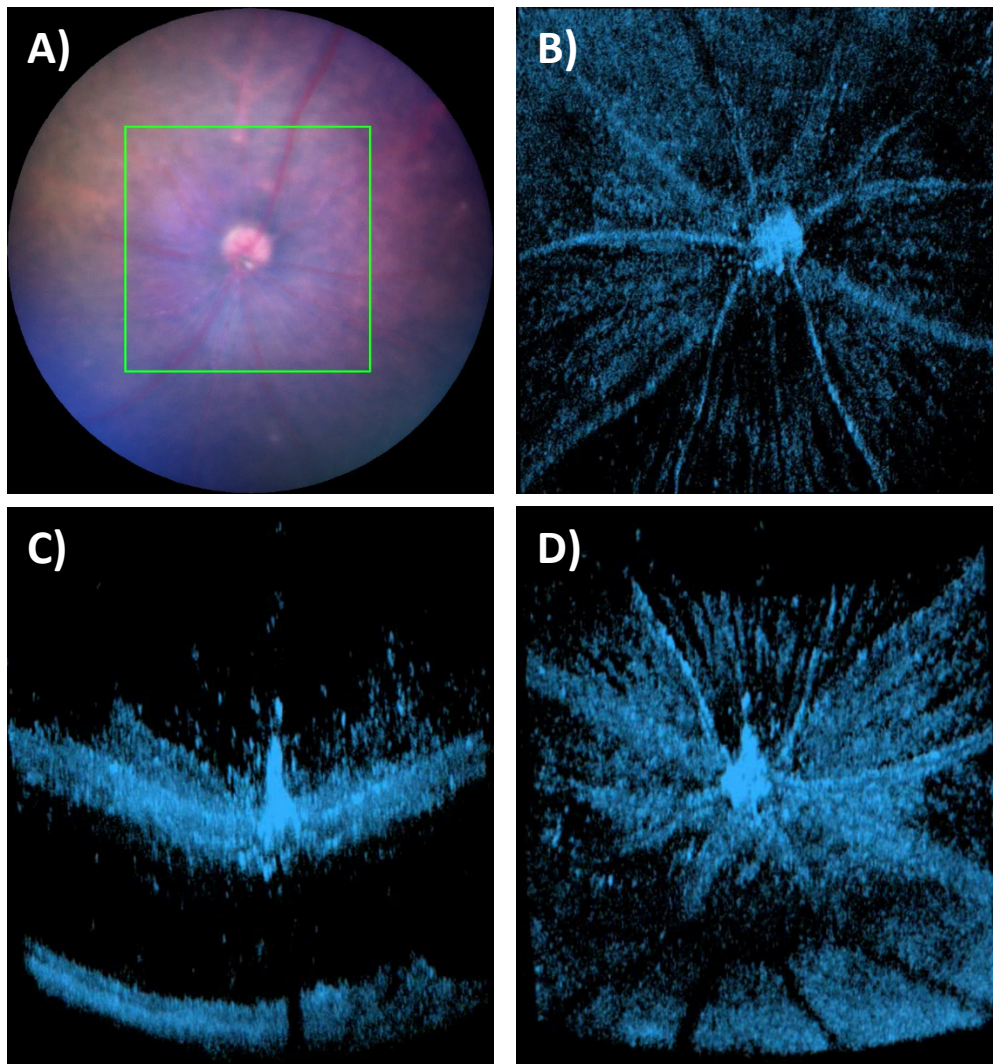


Figure 6.6.1. Three-dimensional projections of the retina using OCT. A) The OCT can rapidly acquire 512 horizontal b-scans running superiorly within the target box area (green) to enable sampling of the retina and vitreous in a larger, more representative region. These can then be used to create different projections, such as B) en-face, C) slices similar to those obtained with single line b-scan acquisition (with extended depth of view), and D) oblique images that help to visualise the three-dimensional space. Abbreviation: OCT – optical coherence tomography.

An analysis strategy that can quantify parameters from these volume scans was recently optimised using Imaris software (Bitplane, Belfast, UK). Manual boxes are drawn from the NFL/GCP/IP to the upper boundaries of the scan (this was usually within the VB) every 75 scans which can then be used to create a surface (similar to a layer in photo-editing programmes) of this region. This will capture the inner retinal regions (before the INL), which on the OCT appears as a continuous region of high intensity. Imaris can then automatically detect surfaces on absolute intensity, and size filters can be applied to remove the very small objects (noise) and the large objects (continuous inner retina and hypothetical corneal/lens artefacts). From here, the number of objects, their volume, and other parameters can be extracted for further analysis (Figure 6.6.2). With calibration, the voxel count can be attributed to exact size/volume of identified objects. It would also be possible to introduce a standardised metric, such as score per volume (to normalise for differences in the volume of space sampled), or measurement of a standardised volume size.

Whilst the Imaris protocol could represent a potential improvement over previously described approaches, it requires validation. Future work aims to score and characterise disease in retinas (running comparisons to both fundal image analysis and flow cytometric scoring approaches) of mice with EAU and/or EIU. It may be possible to intentionally induce differential disease severities in EIU through dosing with LPS or use of different TLR agonists, and this could represent a powerful way to validate this approach because you could predictively know the order of severity in the eyes measured. Once validated, it could then be correlated to mRNA-Seq data (either acquired post-validation or through retrospective analysis).

Nonetheless, this analytical approach is not without shortfalls. The approach is not fully automated, meaning that it could be labour-intensive to utilise. It might be only pragmatic to use on limited numbers of samples, such as mRNA-Seq datasets, rather than large experiments. Additionally, it utilises proprietary software for which the code running it is unavailable, which also limits customisation of analysis to the hardcoding in the application; these former points will limit its potential adoption and use by others. It also makes the underlying assumption that the disease course has linear kinetics that are equivalent in each mouse; existing data already indicates that the loss of P2RY12 is context-dependent and could be differential to the amount of cellular infiltrate for example (Chapter V). However, if the same disease model and induction approach were compared then results would be comparable as variability in cellular infiltrate due to disease model would be controlled. Additionally, in the early stages of disease there are very few changes in the VB, meaning this approach may be unable to quantify early disease scores unlike existing methods. Lastly, in a mouse with very severe disease (such as white-out),

it is likely that the number of objects (cells) in the eye would be too great for analysis – they may be in contact with the retina and each other, resulting in exclusion by the size filter. Conventional scoring is unable to score retinas with this severity of disease either, providing them with a ceiling score.

Work is already underway to potentially improve and optimise this approach. A PhD student has recently started in our group, and her project aims to design code which can extract these and other parameters in an automated fashion through the use of registration and other image-processing techniques in MATLAB. This would allow for customisation, faster processing, and freely available code which could be more widely adopted in the field. In summary, continuing developments in image analysis could provide further insights and novel findings, especially when correlated to other datasets including mRNA-Seq.

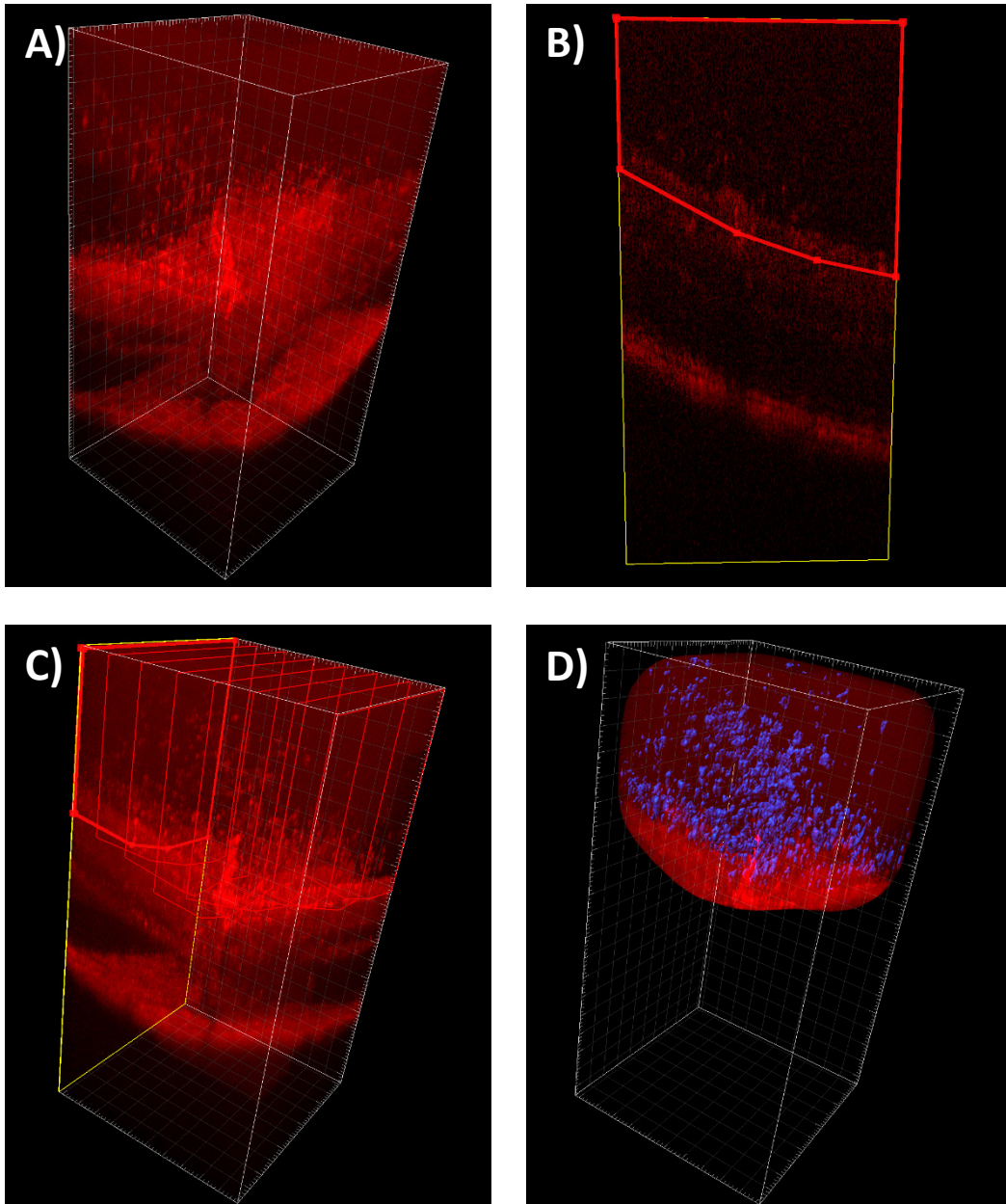


Figure 6.6.2. A series of images showing the key stages of analysis of OCT volume scans using the Imaris software. **A)** The series of 512 images are loaded and rendered. **B)** Manual segmentation of the vitreous and inner retinal layers in a single scan (NFL/GCP/IP). **C)** Summary of key locations where manual segmentation was performed (every 75 scans was the maximum spacing in which a reliable result was obtained). **D)** A blue box represents the mask created from the segments drawn in C, with red shapes highlighting identified objects that passed the size exclusion criterion (this removed the inner retina in this render).

6.7 Summary

The synthesis of imaging and image analysis, regional biopsies, AT with labelling of disease-inducing cells, and sc-mRNA-Seq using the *Cx3cr1^{CreER}:R26-tdTomato* mouse line has the potential to generate novel insight and understanding into both uveitis and the role of microglia far greater than what has been previously possible. It would enable us to begin answering many pertinent questions about microglia and uveitis on the quest for a “microglia marker” and novel targeted therapeutics, ideally one which could reset the microglial transcriptome – confirmed as possible by the work presented within this thesis.

Chapter VII: References

1. Forrester JV, Klaska IP, Yu T, Kuffova L. Uveitis in mouse and man. *Int Rev Immunol*. 2013;32(1):76-96. Epub 2013/01/31. doi: 10.3109/08830185.2012.747524. PubMed PMID: 23360160.
2. Cunningham ET, London NJS, Rathinam SR. Uveitis: a global view. *Expert Review of Ophthalmology*. 2010;5(2):113-4. doi: 10.1586/eop.10.14.
3. Acharya NR, Tham VM, Esterberg E, et al. Incidence and prevalence of uveitis: Results from the Pacific Ocular Inflammation Study. *JAMA Ophthalmology*. 2013;131(11):1405-12. doi: 10.1001/jamaophthalmol.2013.4237.
4. Jabs DA. Epidemiology of Uveitis. *Ophthalmic Epidemiology*. 2008;15(5):283-4. doi: 10.1080/09286580802478724.
5. Gritz DC, Wong IG. Incidence and prevalence of uveitis in Northern California. *Ophthalmology*. 111(3):491-500. doi: 10.1016/j.ophtha.2003.06.014.
6. Khairallah M, Attia S, Zaouali S, Yahia SB, Kahloun R, Messaoud R, et al. Pattern of childhood-onset uveitis in a referral center in Tunisia, North Africa. *Ocul Immunol Inflamm*. 2006;14(4):225-31. Epub 2006/08/17. doi: 10.1080/09273940600732372. PubMed PMID: 1691984.
7. Kitamei H, Kitaichi N, Namba K, Kotake S, Goda C, Kitamura M, et al. Clinical features of intraocular inflammation in Hokkaido, Japan. *Acta Ophthalmol*. 2009;87(4):424-8. Epub 2008/07/26. doi: 10.1111/j.1755-3768.2008.01282.x. PubMed PMID: 18652578.
8. Keino H, Nakashima C, Watanabe T, Taki W, Hayakawa R, Sugitani A, et al. Frequency and clinical features of intraocular inflammation in Tokyo. *Clinical & Experimental Ophthalmology*. 2009;37(6):595-601. doi: 10.1111/j.1442-9071.2009.02102.x.
9. Nussenblatt RB. The natural history of uveitis. *Int Ophthalmol*. 1990;14(5-6):303-8. Epub 1990/10/01. PubMed PMID: 2249907.
10. Weih LM, Hassell JB, Keeffe J. Assessment of the impact of vision impairment. *Invest Ophthalmol Vis Sci*. 2002;43(4):927-35. Epub 2002/03/30. PubMed PMID: 11923230.
11. Brown GC. Vision and quality-of-life. *Trans Am Ophthalmol Soc*. 1999;97:473-511. PubMed PMID: 10703139; PubMed Central PMCID: PMC1298275.
12. Taylor HR, McCarty CA, Nanjan MB. Vision impairment predicts five-year mortality. *Trans Am Ophthalmol Soc*. 2000;98:91-6; discussion 6-9. Epub 2001/02/24. PubMed PMID: 11190044; PubMed Central PMCID: PMC1298215.
13. Jabs DA, Nussenblatt RB, Rosenbaum JT. Standardization of uveitis nomenclature for reporting clinical data. Results of the First International Workshop. *Am J Ophthalmol*. 2005;140(3):509-16. Epub 2005/10/01. PubMed PMID: 16196117.
14. McGonagle D, McDermott MF. A proposed classification of the immunological diseases. *PLoS Med*. 2006;3(8):e297. Epub 2006/09/01. doi: 10.1371/journal.pmed.0030297. PubMed PMID: 16942393; PubMed Central PMCID: PMC1564298.
15. Molins B, Mesquida M, Lee RW, Llorens V, Pelegrin L, Adan A. Regulatory T cell levels and cytokine production in active non-infectious uveitis: in-vitro effects of pharmacological treatment. *Clin Exp Immunol*. 2015;179(3):529-38. Epub 2014/10/31. doi: 10.1111/cei.12479. PubMed PMID: 25354724; PubMed Central PMCID: PMC4337685.
16. Prete M, Dammacco R, Fatone MC, Racanelli V. Autoimmune uveitis: clinical, pathogenetic, and therapeutic features. *Clinical and Experimental Medicine*. 2016;16(2):125-36. doi: 10.1007/s10238-015-0345-6.
17. Barisani-Asenbauer T, Maca SM, Mejdoubi L, Emminger W, Machold K, Auer H. Uveitis- a rare disease often associated with systemic diseases and infections- a systematic review of 2619 patients. *Orphanet Journal of Rare Diseases*. 2012;7(1):57. doi: 10.1186/1750-1172-7-57.
18. Bodaghi B, Cassoux N, Wechsler B, Hannouche D, Fardeau C, Papo T, et al. Chronic Severe Uveitis: Etiology and Visual Outcome in 927 Patients from a Single Center. *Medicine*. 2001;80(4).
19. Chan NS, Chee SP, Caspers L, Bodaghi B. Clinical Features of CMV-Associated Anterior Uveitis. *Ocul Immunol Inflamm*. 2018;26(1):107-15. Epub 2017/11/28. doi: 10.1080/09273948.2017.1394471. PubMed PMID: 29172842.

20. Rotsos TG, Moschos MM. Cystoid macular edema. *Clin Ophthalmol.* 2008;2(4):919-30. Epub 2009/08/12. doi: 10.2147/opth.s4033. PubMed PMID: 19668445; PubMed Central PMCID: PMCPMC2699812.
21. Schewitz-Bowers LP, Lee RWJ, Dick AD. Immune mechanisms of intraocular inflammation. *Expert Review of Ophthalmology.* 2010;5(1):43-58. doi: 10.1586/eop.09.68.
22. NICE. Uveitis - NICE CKS 2014 [cited 2017 11/01/2017]. Available from: <https://cks.nice.org.uk/uveitis#!scenario>.
23. Dick AD, Rosenbaum JT, Al-Dhibi HA, Belfort R, Jr., Brezin AP, Chee SP, et al. Guidance on Noncorticosteroid Systemic Immunomodulatory Therapy in Noninfectious Uveitis: Fundamentals Of Care for UveitiS (FOCUS) Initiative. *Ophthalmology.* 2018;125(5):757-73. Epub 2018/01/10. doi: 10.1016/j.ophtha.2017.11.017. PubMed PMID: 29310963.
24. McCaa CS. The eye and visual nervous system: anatomy, physiology and toxicology. *Environ Health Perspect.* 1982;44:1-8. Epub 1982/04/01. doi: 10.1289/ehp.82441. PubMed PMID: 7084144; PubMed Central PMCID: PMCPMC1568971.
25. Schwab IR. The evolution of eyes: major steps. The Keeler lecture 2017: centenary of Keeler Ltd. *Eye (Lond).* 2018;32(2):302-13. Epub 2017/10/21. doi: 10.1038/eye.2017.226. PubMed PMID: 29052606; PubMed Central PMCID: PMCPMC5811732.
26. Forrester JV, Dick AD, McMenemy PG, Roberts F, Pearlman E. *The eye : basic sciences in practice.* 2016.
27. Willoughby CE, Ponzin D, Ferrari S, Lobo A, Landau K, Omid Y. Anatomy and physiology of the human eye: effects of mucopolysaccharidoses disease on structure and function – a review. *Clinical & Experimental Ophthalmology.* 2010;38(s1):2-11. doi: 10.1111/j.1442-9071.2010.02363.x.
28. DelMonte DW, Kim T. Anatomy and physiology of the cornea. *J Cataract Refract Surg.* 2011;37(3):588-98. Epub 2011/02/22. doi: 10.1016/j.jcrs.2010.12.037. PubMed PMID: 21333881.
29. Kung P, Kung J, Lu S-E. A Comparison of Pupillary Dilation Velocity Using Tropicamide 1% and Phenylephrine 2.5%. *Investigative Ophthalmology & Visual Science.* 2007;48(13):1217-.
30. Willermain F, Libert S, Motulsky E, Salik D, Caspers L, Perret J, et al. Origins and consequences of hyperosmolar stress in retinal pigmented epithelial cells. *Front Physiol.* 2014;5:199. Epub 2014/06/10. doi: 10.3389/fphys.2014.00199. PubMed PMID: 24910616; PubMed Central PMCID: PMCPMC4038854.
31. The Retina Reference. Normal Retinal Anatomy 2020 [05/06/2020]. Available from: <http://www.retinareference.com/anatomy/>.
32. A. Triviño RdH, B. Rojas, B.I. Gallego, A.I. Ramírez, J.J. Salazar, J.M. Ramírez. Effects of Hypercholesterolaemia in the Retina. *Ocular Diseases: IntechOpen;* 2012.
33. Berson DM. 1.25 - Retinal Ganglion Cell Types and Their Central Projections. In: Masland RH, Albright TD, Albright TD, Masland RH, Dallos P, Oertel D, et al., editors. *The Senses: A Comprehensive Reference.* New York: Academic Press; 2008. p. 491-519.
34. Omri S, Omri B, Savoldelli M, Jonet L, Thillaye-Goldenberg B, Thuret G, et al. The outer limiting membrane (OLM) revisited: clinical implications. *Clin Ophthalmol.* 2010;4:183-95. Epub 2010/05/14. doi: 10.2147/opth.s5901. PubMed PMID: 20463783; PubMed Central PMCID: PMCPMC2861922.
35. Goebel R, Muckli L, Kim D-S. CHAPTER 35 - Visual System. In: Paxinos G, Mai JK, editors. *The Human Nervous System (Second Edition).* San Diego: Academic Press; 2004. p. 1280-305.
36. Chen L, Miyamura N, Ninomiya Y, Handa JT. Distribution of the collagen IV isoforms in human Bruch's membrane. *The British journal of ophthalmology.* 2003;87(2):212-5. Epub 2003/01/25. doi: 10.1136/bjo.87.2.212. PubMed PMID: 12543754; PubMed Central PMCID: PMCPMC1771521.
37. Reichenbach A, Bringmann A. Glia of the human retina. *Glia.* 2020;68(4):768-96. Epub 2019/12/04. doi: 10.1002/glia.23727. PubMed PMID: 31793693.

38. Seyed-Razavi Y, Chinnery HR, McMenemy PG. A Novel Association Between Resident Tissue Macrophages and Nerves in the Peripheral Stroma of the Murine Cornea. *Investigative Ophthalmology & Visual Science*. 2014;55(3):1313-20. doi: 10.1167/iovs.13-12995.
39. Butler TL, McMenemy PG. Resident and infiltrating immune cells in the uveal tract in the early and late stages of experimental autoimmune uveoretinitis. *Invest Ophthalmol Vis Sci*. 1996;37(11):2195-210. Epub 1996/10/01. PubMed PMID: 8843906.
40. McMenemy PG. The distribution of immune cells in the uveal tract of the normal eye. *Eye (Lond)*. 1997;11 (Pt 2):183-93. Epub 1997/01/01. doi: 10.1038/eye.1997.49. PubMed PMID: 9349410.
41. Rashid K, Akhtar-Schaefer I, Langmann T. Microglia in Retinal Degeneration. *Front Immunol*. 2019;10:1975. Epub 2019/09/05. doi: 10.3389/fimmu.2019.01975. PubMed PMID: 31481963; PubMed Central PMCID: PMC6710350.
42. Simo R, Villarreal M, Corraliza L, Hernandez C, Garcia-Ramirez M. The retinal pigment epithelium: something more than a constituent of the blood-retinal barrier--implications for the pathogenesis of diabetic retinopathy. *J Biomed Biotechnol*. 2010;2010:190724. Epub 2010/02/26. doi: 10.1155/2010/190724. PubMed PMID: 20182540; PubMed Central PMCID: PMC2825554.
43. Bose T, Lee R, Hou A, Tong L, Chandy KG. Tissue resident memory T cells in the human conjunctiva and immune signatures in human dry eye disease. *Sci Rep*. 2017;7:45312. Epub 2017/03/28. doi: 10.1038/srep45312. PubMed PMID: 28345628; PubMed Central PMCID: PMC5366884.
44. Kielczewski JL, Horai R, Jittayasothorn Y, Chan CC, Caspi RR. Tertiary Lymphoid Tissue Forms in Retinas of Mice with Spontaneous Autoimmune Uveitis and Has Consequences on Visual Function. *J Immunol*. 2016;196(3):1013-25. Epub 2015/12/30. doi: 10.4049/jimmunol.1501570. PubMed PMID: 26712943; PubMed Central PMCID: PMC4783793.
45. Springer MS, Murphy WJ, Eizirik E, O'Brien SJ. Placental mammal diversification and the Cretaceous-Tertiary boundary. *Proc Natl Acad Sci U S A*. 2003;100(3):1056-61. Epub 2003/01/29. doi: 10.1073/pnas.0334222100. PubMed PMID: 12552136; PubMed Central PMCID: PMC298725.
46. Lucas BA, Lavi E, Shiue L, Cho H, Katzman S, Miyoshi K, et al. Evidence for convergent evolution of SINE-directed Staufen-mediated mRNA decay. *Proceedings of the National Academy of Sciences*. 2018;115(5):968-73. doi: 10.1073/pnas.1715531115.
47. Mestas J, Hughes CCW. Of Mice and Not Men: Differences between Mouse and Human Immunology. *The Journal of Immunology*. 2004;172(5):2731-8. doi: 10.4049/jimmunol.172.5.2731.
48. Veleri S, Lazar CH, Chang B, Sieving PA, Banin E, Swaroop A. Biology and therapy of inherited retinal degenerative disease: insights from mouse models. *Disease Models & Mechanisms*. 2015;8(2):109-29. doi: 10.1242/dmm.017913.
49. Sellers RS. Translating Mouse Models: Immune Variation and Efficacy Testing. *Toxicologic Pathology*. 2017;45(1):134-45. doi: 10.1177/0192623316675767. PubMed PMID: 27815489.
50. Tao L, Reese TA. Making Mouse Models That Reflect Human Immune Responses. *Trends Immunol*. 2017;38(3):181-93. Epub 2017/02/06. doi: 10.1016/j.it.2016.12.007. PubMed PMID: 28161189.
51. A Toxic Ocular Reaction. I New Property of Shwartzman Toxins. 1943;46(3):113-25.
52. Rosenbaum JT, McDevitt HO, Guss RB, Egbert PR. Endotoxin-induced uveitis in rats as a model for human disease. *Nature*. 1980;286(5773):611-3. Epub 1980/08/07. PubMed PMID: 7402339.
53. Forrester JV, Worgul BV, Merriam GR. Endotoxin-induced uveitis in the rat. *Albrecht von Graefes Archiv für klinische und experimentelle Ophthalmologie*. 1980;213(4):221-33. doi: 10.1007/BF00417543.

54. de Kozak Y, Sakai J, Thillaye B, Faure JP. S antigen-induced experimental autoimmune uveo-retinitis in rats. *Curr Eye Res.* 1981;1(6):327-37. Epub 1981/01/01. doi: 10.3109/02713688108998359. PubMed PMID: 6975701.
55. Klaska IP, Forrester JV. Mouse models of autoimmune uveitis. *Current pharmaceutical design.* 2015;21(18):2453-67. Epub 2015/03/18. doi: 10.2174/1381612821666150316122928. PubMed PMID: 25777760.
56. Chen J, Qian H, Horai R, Chan CC, Caspi RR. Mouse Models of Experimental Autoimmune Uveitis: Comparative Analysis of Adjuvant-Induced vs Spontaneous Models of Uveitis. *Curr Mol Med.* 2015;15(6):550-7. Epub 2015/08/05. doi: 10.2174/1566524015666150731100318. PubMed PMID: 26238369.
57. Bansal S, Barathi VA, Iwata D, Agrawal R. Experimental autoimmune uveitis and other animal models of uveitis: An update. *Indian J Ophthalmol.* 2015;63(3):211-8. Epub 2015/05/15. doi: 10.4103/0301-4738.156914. PubMed PMID: 25971165; PubMed Central PMCID: PMC4448233.
58. Caspi RR, Roberge FG, Chan CC, Wiggert B, Chader GJ, Rozenszajn LA, et al. A new model of autoimmune disease. Experimental autoimmune uveoretinitis induced in mice with two different retinal antigens. *Journal of Immunology.* 1988;140(5):1490.
59. Caspi RR, Silver PB, Luger D, Tang J, Cortes LM, Pennesi G, et al. Mouse Models of Experimental Autoimmune Uveitis. *Ophthalmic research.* 2008;40(3-4):169-74. doi: 10.1159/000119871. PubMed PMID: PMC2735820.
60. Chen WL, Sheu JR, Chen RJ, Hsiao SH, Hsiao CJ, Chou YC, et al. Mycobacterium tuberculosis Upregulates TNF-alpha Expression via TLR2/ERK Signaling and Induces MMP-1 and MMP-9 Production in Human Pleural Mesothelial Cells. *PLoS One.* 2015;10(9):e0137979. Epub 2015/09/15. doi: 10.1371/journal.pone.0137979. PubMed PMID: 26367274; PubMed Central PMCID: PMC4569295.
61. Su SB, Silver PB, Grajewski RS, Agarwal RK, Tang J, Chan CC, et al. Essential role of the MyD88 pathway, but nonessential roles of TLRs 2, 4, and 9, in the adjuvant effect promoting Th1-mediated autoimmunity. *J Immunol.* 2005;175(10):6303-10. Epub 2005/11/08. PubMed PMID: 16272281.
62. Fang J, Fang D, Silver PB, Wen F, Li B, Ren X, et al. The Role of TLR2, TLR3, TLR4, and TLR9 Signaling in the Pathogenesis of Autoimmune Disease in a Retinal Autoimmunity Model. *Invest Ophthalmol Vis Sci.* 2010;51(6):3092-9. doi: 10.1167/iovs.09-4754. PubMed PMID: 20107166; PubMed Central PMCID: PMC2891468.
63. Garlanda C, Dinarello CA, Mantovani A. The interleukin-1 family: back to the future. *Immunity.* 2013;39(6):1003-18. Epub 2013/12/18. doi: 10.1016/j.immuni.2013.11.010. PubMed PMID: 24332029; PubMed Central PMCID: PMC3933951.
64. Kugler S, Bocker K, Heusipp G, Greune L, Kim KS, Schmidt MA. Pertussis toxin transiently affects barrier integrity, organelle organization and transmigration of monocytes in a human brain microvascular endothelial cell barrier model. *Cell Microbiol.* 2007;9(3):619-32. Epub 2006/09/28. doi: 10.1111/j.1462-5822.2006.00813.x. PubMed PMID: 17002784.
65. Wong WS, Rosoff PM. Pharmacology of pertussis toxin B-oligomer. *Can J Physiol Pharmacol.* 1996;74(5):559-64. Epub 1996/05/01. PubMed PMID: 8884020.
66. Wang ZY, Yang D, Chen Q, Leifer CA, Segal DM, Su SB, et al. Induction of dendritic cell maturation by pertussis toxin and its B subunit differentially initiate Toll-like receptor 4-dependent signal transduction pathways. *Exp Hematol.* 2006;34(8):1115-24. Epub 2006/07/26. doi: 10.1016/j.exphem.2006.04.025. PubMed PMID: 16863919.
67. Fujimoto C, Shi G, Gery I. Microbial Products Trigger Autoimmune Ocular Inflammation. *Ophthalmic Res.* 2008;40(3-4):193-9. doi: 10.1159/000119875. PubMed PMID: 18421238; PubMed Central PMCID: PMC2755186.
68. Ryan M, McCarthy L, Rappuoli R, Mahon BP, Mills KH. Pertussis toxin potentiates Th1 and Th2 responses to co-injected antigen: adjuvant action is associated with enhanced

- regulatory cytokine production and expression of the co-stimulatory molecules B7-1, B7-2 and CD28. *Int Immunol.* 1998;10(5):651-62. Epub 1998/06/30. PubMed PMID: 9645613.
69. Chen X, Howard OM, Oppenheim JJ. Pertussis toxin by inducing IL-6 promotes the generation of IL-17-producing CD4 cells. *J Immunol.* 2007;178(10):6123-9. Epub 2007/05/04. PubMed PMID: 17475838.
70. Copland DA, Wertheim MS, Armitage WJ, Nicholson LB, Raveney BJ, Dick AD. The clinical time-course of experimental autoimmune uveoretinitis using topical endoscopic fundal imaging with histologic and cellular infiltrate correlation. *Invest Ophthalmol Vis Sci.* 2008;49(12):5458-65. Epub 2008/09/02. doi: 10.1167/iovs.08-2348. PubMed PMID: 18757507.
71. Boldison J, Khera TK, Copland DA, Stimpson ML, Crawford GL, Dick AD, et al. A novel pathogenic RBP-3 peptide reveals epitope spreading in persistent experimental autoimmune uveoretinitis. *Immunology.* 2015;146(2):301-11. Epub 2015/07/15. doi: 10.1111/imm.12503. PubMed PMID: 26152845; PubMed Central PMCID: PMC4582971.
72. Forrester JV, Kuffova L, Dick AD. Autoimmunity, Autoinflammation, and Infection in Uveitis. *American journal of ophthalmology.* 2018;189:77-85. doi: <https://doi.org/10.1016/j.ajo.2018.02.019>.
73. Pfister C, Chabre M, Plouet J, Tuyen VV, De Kozak Y, Faure JP, et al. Retinal S antigen identified as the 48K protein regulating light-dependent phosphodiesterase in rods. *Science.* 1985;228(4701):891-3. Epub 1985/05/17. doi: 10.1126/science.2988124. PubMed PMID: 2988124.
74. Borst DE, Redmond TM, Elser JE, Gonda MA, Wiggert B, Chader GJ, et al. Interphotoreceptor retinoid-binding protein. Gene characterization, protein repeat structure, and its evolution. *J Biol Chem.* 1989;264(2):1115-23. Epub 1989/01/15. PubMed PMID: 2910846.
75. Applebury ML, Hargrave PA. Molecular biology of the visual pigments. *Vision Res.* 1986;26(12):1881-95. Epub 1986/01/01. doi: 10.1016/0042-6989(86)90115-x. PubMed PMID: 3303660.
76. Chan CC, Caspi RR, Ni M, Leake WC, Wiggert B, Chader GJ, et al. Pathology of experimental autoimmune uveoretinitis in mice. *J Autoimmun.* 1990;3(3):247-55. Epub 1990/06/01. doi: 10.1016/0896-8411(90)90144-h. PubMed PMID: 2397018.
77. Gery I, Chanaud NP, 3rd, Anglade E. Recoverin is highly uveitogenic in Lewis rats. *Invest Ophthalmol Vis Sci.* 1994;35(8):3342-5. Epub 1994/07/01. PubMed PMID: 8045724.
78. Mochizuki M, Kuwabara T, McAllister C, Nussenblatt RB, Gery I. Adoptive transfer of experimental autoimmune uveoretinitis in rats. Immunopathogenic mechanisms and histologic features. *Invest Ophthalmol Vis Sci.* 1985;26(1):1-9. Epub 1985/01/01. PubMed PMID: 3967952.
79. Broekhuysse RM, Kuhlmann ED, Winkens HJ. Experimental autoimmune anterior uveitis (EAAU). II. Dose-dependent induction and adoptive transfer using a melanin-bound antigen of the retinal pigment epithelium. *Exp Eye Res.* 1992;55(3):401-11. Epub 1992/09/01. doi: 10.1016/0014-4835(92)90112-6. PubMed PMID: 1358666.
80. Broekhuysse RM, Kuhlmann ED, Winkens HJ. Experimental autoimmune anterior uveitis (EAAU). III. Induction by immunization with purified uveal and skin melanins. *Exp Eye Res.* 1993;56(5):575-83. Epub 1993/05/01. doi: 10.1006/exer.1993.1071. PubMed PMID: 8500566.
81. Pennesi G, Mattapallil MJ, Sun SH, Avichezer D, Silver PB, Karabekian Z, et al. A humanized model of experimental autoimmune uveitis in HLA class II transgenic mice. *J Clin Invest.* 2003;111(8):1171-80. Epub 2003/04/17. doi: 10.1172/JCI15155. PubMed PMID: 12697736; PubMed Central PMCID: PMC152930.
82. Szpak Y, Vieville JC, Tabary T, Naud MC, Chopin M, Edelson C, et al. Spontaneous retinopathy in HLA-A29 transgenic mice. *Proc Natl Acad Sci U S A.* 2001;98(5):2572-6. Epub 2001/02/28. doi: 10.1073/pnas.051595998. PubMed PMID: 11226280; PubMed Central PMCID: PMC30179.
83. Zucchiatti I, Miserocchi E, Sacconi R, Bandello F, Modorati G. HLA-A29-Positive Uveitis: Birdshot Chorioretinopathy, What Else? *Case Rep Ophthalmol.* 2013;4(3):287-93. Epub

- 2014/01/30. doi: 10.1159/000357276. PubMed PMID: 24474930; PubMed Central PMCID: PMC3901631.
84. DeVoss J, Hou Y, Johannes K, Lu W, Liou GI, Rinn J, et al. Spontaneous autoimmunity prevented by thymic expression of a single self-antigen. *J Exp Med*. 2006;203(12):2727-35. Epub 2006/11/23. doi: 10.1084/jem.20061864. PubMed PMID: 17116738; PubMed Central PMCID: PMC2118158.
85. Pepple KL, Rotkis L, Van Grol J, Wilson L, Sandt A, Lam DL, et al. Primed Mycobacterial Uveitis (PMU): Histologic and Cytokine Characterization of a Model of Uveitis in Rats. *Invest Ophthalmol Vis Sci*. 2015;56(13):8438-48. Epub 2016/01/10. doi: 10.1167/iovs.15-17523. PubMed PMID: 26747775; PubMed Central PMCID: PMC3469941.
86. Dix RD, Giedlin M, Cousins SW. Systemic cytokine immunotherapy for experimental cytomegalovirus retinitis in mice with retrovirus-induced immunodeficiency. *Invest Ophthalmol Vis Sci*. 1997;38(7):1411-7. Epub 1997/06/01. PubMed PMID: 9191604.
87. Chen J, Qian H, Horai R, Chan CC, Falick Y, Caspi RR. Comparative analysis of induced vs. spontaneous models of autoimmune uveitis targeting the interphotoreceptor retinoid binding protein. *PLoS One*. 2013;8(8):e72161. Epub 2013/09/10. doi: 10.1371/journal.pone.0072161. PubMed PMID: 24015215; PubMed Central PMCID: PMC3756070.
88. Agarwal RK, Silver PB, Caspi RR. Rodent models of experimental autoimmune uveitis. *Methods Mol Biol*. 2012;900:443-69. Epub 2012/08/31. doi: 10.1007/978-1-60761-720-4_22. PubMed PMID: 22933083; PubMed Central PMCID: PMC3810964.
89. Poltorak A, He X, Smirnova I, Liu MY, Van Huffel C, Du X, et al. Defective LPS signaling in C3H/HeJ and C57BL/10ScCr mice: mutations in Tlr4 gene. *Science*. 1998;282(5396):2085-8. Epub 1998/12/16. PubMed PMID: 9851930.
90. Kubota S, Kurihara T, Mochimaru H, Satofuka S, Noda K, Ozawa Y, et al. Prevention of ocular inflammation in endotoxin-induced uveitis with resveratrol by inhibiting oxidative damage and nuclear factor-kappaB activation. *Invest Ophthalmol Vis Sci*. 2009;50(7):3512-9. Epub 2009/03/13. doi: 10.1167/iovs.08-2666. PubMed PMID: 19279313.
91. Smith JR, Subbarao K, Franc DT, Haribabu B, Rosenbaum JT. Susceptibility to endotoxin induced uveitis is not reduced in mice deficient in BLT1, the high affinity leukotriene B4 receptor. *The British journal of ophthalmology*. 2004;88(2):273-5. Epub 2004/01/23. PubMed PMID: 14736790; PubMed Central PMCID: PMC1771988.
92. Allensworth JJ, Planck SR, Rosenbaum JT, Rosenzweig HL. Investigation of the differential potentials of TLR agonists to elicit uveitis in mice. *J Leukoc Biol*. 2011;90(6):1159-66. Epub 2011/09/22. doi: 10.1189/jlb.0511249. PubMed PMID: 21934069; PubMed Central PMCID: PMC3236551.
93. Rosenbaum JT, Woods A, Kezic J, Planck SR, Rosenzweig HL. Contrasting ocular effects of local versus systemic endotoxin. *Invest Ophthalmol Vis Sci*. 2011;52(9):6472-7. Epub 2011/07/16. doi: 10.1167/iovs.11-7742. PubMed PMID: 21757585; PubMed Central PMCID: PMC3176004.
94. National Centre for the Replacement, Reduction of Animals in R. The 3Rs | NC3Rs: @nc3rs; 2018 [cited 2018 14/11/2018]. Available from: <https://www.nc3rs.org.uk/the-3rs>.
95. Thompson BT. Greater Treatment Effect With Lower Disease Severity: VASST Insights. *Crit Care Med*. 2017;45(6):1094-5. Epub 2017/05/17. doi: 10.1097/CCM.0000000000002397. PubMed PMID: 28509731.
96. Wang Q, Niemi J, Tan CM, You L, West M. Image segmentation and dynamic lineage analysis in single-cell fluorescence microscopy. *Cytometry A*. 2010;77(1):101-10. Epub 2009/10/22. doi: 10.1002/cyto.a.20812. PubMed PMID: 19845017; PubMed Central PMCID: PMC2797831.
97. Chu CJ, Gardner PJ, Copland DA, Liyanage SE, Gonzalez-Cordero A, Kleine Holthaus SM, et al. Multimodal analysis of ocular inflammation using the endotoxin-induced uveitis mouse model. *Dis Model Mech*. 2016;9(4):473-81. Epub 2016/01/23. doi: 10.1242/dmm.022475. PubMed PMID: 26794131; PubMed Central PMCID: PMC4852501.

98. Lai JC, Lobanoff MC, Fukushima A, Wawrousek EF, Chan CC, Whitcup SM, et al. Uveitis Induced by Lymphocytes Sensitized against a Transgenically Expressed Lens Protein. *Investigative ophthalmology & visual science*. 1999;40(11):2735-9.
99. Horai R, Silver PB, Chen J, Agarwal RK, Chong WP, Jittayasothorn Y, et al. Breakdown of immune privilege and spontaneous autoimmunity in mice expressing a transgenic T cell receptor specific for a retinal autoantigen. *Journal of autoimmunity*. 2013;44:21-33. Epub 2013/06/28. doi: 10.1016/j.jaut.2013.06.003. PubMed PMID: 23810578.
100. Lambe T, Leung JC, Bouriez-Jones T, Silver K, Makinen K, Crockford TL, et al. CD4 T cell-dependent autoimmunity against a melanocyte neoantigen induces spontaneous vitiligo and depends upon Fas-Fas ligand interactions. *Journal of immunology (Baltimore, Md : 1950)*. 2006;177(5):3055-62. Epub 2006/08/22. doi: 10.4049/jimmunol.177.5.3055. PubMed PMID: 16920942.
101. Lambe T, Leung JC, Ferry H, Bouriez-Jones T, Makinen K, Crockford TL, et al. Limited peripheral T cell anergy predisposes to retinal autoimmunity. *Journal of immunology (Baltimore, Md : 1950)*. 2007;178(7):4276-83. Epub 2007/03/21. doi: 10.4049/jimmunol.178.7.4276. PubMed PMID: 17371984.
102. Qiu Y, Yu P, Lin R, Fu X, Hao B, Lei B. Genome-wide retinal transcriptome analysis of endotoxin-induced uveitis in mice with next-generation sequencing. *Mol Vis*. 2017;23:395-406. Epub 2017/07/15. PubMed PMID: 28706439; PubMed Central PMCID: PMC5501689.
103. Qiu Y, Shil PK, Zhu P, Yang H, Verma A, Lei B, et al. Angiotensin-converting enzyme 2 (ACE2) activator diminazene aceturate ameliorates endotoxin-induced uveitis in mice. *Investigative ophthalmology & visual science*. 2014;55(6):3809-18. Epub 2014/05/24. doi: 10.1167/iovs.14-13883. PubMed PMID: 24854854; PubMed Central PMCID: PMC4062403.
104. Xu H, Koch P, Chen M, Lau A, Reid DM, Forrester JV. A clinical grading system for retinal inflammation in the chronic model of experimental autoimmune uveoretinitis using digital fundus images. *Exp Eye Res*. 2008;87(4):319-26. Epub 2008/07/19. doi: 10.1016/j.exer.2008.06.012. PubMed PMID: 18634784.
105. Paques M, Guyomard JL, Simonutti M, Roux MJ, Picaud S, Legargasson JF, et al. Panretinal, high-resolution color photography of the mouse fundus. *Investigative ophthalmology & visual science*. 2007;48(6):2769-74. Epub 2007/05/26. doi: 10.1167/iovs.06-1099. PubMed PMID: 17525211.
106. Gong Y, Li J, Sun Y, Fu Z, Liu CH, Evans L, et al. Optimization of an Image-Guided Laser-Induced Choroidal Neovascularization Model in Mice. *PLoS One*. 2015;10(7):e0132643. Epub 2015/07/15. doi: 10.1371/journal.pone.0132643. PubMed PMID: 26161975; PubMed Central PMCID: PMC4498645.
107. Khalili H, Lee RW, Khaw PT, Brocchini S, Dick AD, Copland DA. An anti-TNF- α antibody mimetic to treat ocular inflammation. *Scientific reports*. 2016;6:36905-. doi: 10.1038/srep36905. PubMed PMID: 27874029.
108. Saltaji H, Armijo-Olivo S, Cummings GG, Amin M, da Costa BR, Flores-Mir C. Influence of blinding on treatment effect size estimate in randomized controlled trials of oral health interventions. *BMC Med Res Methodol*. 2018;18(1):42. Epub 2018/05/20. doi: 10.1186/s12874-018-0491-0. PubMed PMID: 29776394; PubMed Central PMCID: PMC5960173.
109. Chu CJ, Herrmann P, Carvalho LS, Liyanage SE, Bainbridge JW, Ali RR, et al. Assessment and in vivo scoring of murine experimental autoimmune uveoretinitis using optical coherence tomography. *PLoS One*. 2013;8(5):e63002. Epub 2013/05/22. doi: 10.1371/journal.pone.0063002. PubMed PMID: 23690973; PubMed Central PMCID: PMC3653962.
110. Read RW, Vogt SD, Barnum SR, Szalai AJ. Experimental autoimmune uveitis in the C57BL/6 mouse. *Exp Eye Res*. 2006;83(1):229-30; author reply 31. Epub 2006/03/10. doi: 10.1016/j.exer.2005.10.028. PubMed PMID: 16524572.

111. Coventry B, Ashdown M, Henneberg M, Davies P. The Immune System and Responses to Cancer: Coordinated Evolution. *F1000Research*. 2015;4(552). doi: 10.12688/f1000research.6718.1.
112. Wynn TA, Chawla A, Pollard JW. Macrophage biology in development, homeostasis and disease. *Nature*. 2013;496(7446):445-55. Epub 2013/04/27. doi: 10.1038/nature12034. PubMed PMID: 23619691; PubMed Central PMCID: PMC3725458.
113. Davies LC, Jenkins SJ, Allen JE, Taylor PR. Tissue-resident macrophages. *Nat Immunol*. 2013;14(10):986-95. Epub 2013/09/21. doi: 10.1038/ni.2705. PubMed PMID: 24048120; PubMed Central PMCID: PMC374045180.
114. Soares MP, Hamza I. Macrophages and Iron Metabolism. *Immunity*. 2016;44(3):492-504. Epub 2016/03/18. doi: 10.1016/j.immuni.2016.02.016. PubMed PMID: 26982356; PubMed Central PMCID: PMC4794998.
115. Sellgren CM, Gracias J, Watmuff B, Biag JD, Thanos JM, Whittredge PB, et al. Increased synapse elimination by microglia in schizophrenia patient-derived models of synaptic pruning. *Nat Neurosci*. 2019;22(3):374-85. Epub 2019/02/06. doi: 10.1038/s41593-018-0334-7. PubMed PMID: 30718903; PubMed Central PMCID: PMC6410571.
116. de Souza AWS, Mesquita Júnior D, Araújo JAP, Catelan TTT, Cruvinel WdM, Andrade LEC, et al. Immune system - part III. The delicate balance of the immune system between tolerance and autoimmunity. *Rev Bras Reumatol*. 2010;50:665-79.
117. Zhang G, Meredith TC, Kahne D. On the essentiality of lipopolysaccharide to Gram-negative bacteria. *Current opinion in microbiology*. 2013;16(6):779-85. Epub 2013/10/24. doi: 10.1016/j.mib.2013.09.007. PubMed PMID: 24148302; PubMed Central PMCID: PMC3974409.
118. Hoeksema MA, Scicluna BP, Boshuizen MC, van der Velden S, Neele AE, Van den Bossche J, et al. IFN- γ priming of macrophages represses a part of the inflammatory program and attenuates neutrophil recruitment. *Journal of immunology (Baltimore, Md : 1950)*. 2015;194(8):3909-16. Epub 2015/03/10. doi: 10.4049/jimmunol.1402077. PubMed PMID: 25750432.
119. Lau CM, Adams NM, Geary CD, Weizman O-E, Rapp M, Pritykin Y, et al. Epigenetic control of innate and adaptive immune memory. *Nature Immunology*. 2018;19(9):963-72. doi: 10.1038/s41590-018-0176-1.
120. Van Belleghem JD, Bollyky PL. Macrophages and innate immune memory against *Staphylococcus* skin infections. *Proceedings of the National Academy of Sciences*. 2018;115(47):11865-7. doi: 10.1073/pnas.1816935115.
121. Häggström M. Medical gallery of Mikael Häggström 2014 [Hematopoiesis (human) diagram.png]. *WikiJournal of Medicine*. 2014;1(2). doi: 10.15347/wjm/2014.008.
122. Gordon S, Plüddemann A. The Mononuclear Phagocytic System. Generation of Diversity. *Frontiers in Immunology*. 2019;10(1893). doi: 10.3389/fimmu.2019.01893.
123. Gordon S, Plüddemann A. Tissue macrophages: heterogeneity and functions. *BMC Biology*. 2017;15(1):53. doi: 10.1186/s12915-017-0392-4.
124. Amarante-Mendes GP, Adjemian S, Branco LM, Zanetti LC, Weinlich R, Bortoluci KR. Pattern Recognition Receptors and the Host Cell Death Molecular Machinery. *Frontiers in Immunology*. 2018;9(2379). doi: 10.3389/fimmu.2018.02379.
125. Kawai T, Akira S. The role of pattern-recognition receptors in innate immunity: update on Toll-like receptors. *Nature Immunology*. 2010;11(5):373-84. doi: 10.1038/ni.1863.
126. Kim YK, Shin JS, Nahm MH. NOD-Like Receptors in Infection, Immunity, and Diseases. *Yonsei Med J*. 2016;57(1):5-14. Epub 2015/12/04. doi: 10.3349/ymj.2016.57.1.5. PubMed PMID: 26632377; PubMed Central PMCID: PMC4696971.
127. Bermejo-Jambrina M, Eder J, Helgers LC, Hertoghs N, Nijmeijer BM, Stunnenberg M, et al. C-Type Lectin Receptors in Antiviral Immunity and Viral Escape. *Front Immunol*. 2018;9:590. Epub 2018/04/11. doi: 10.3389/fimmu.2018.00590. PubMed PMID: 29632536; PubMed Central PMCID: PMC5879224.

128. Kawai T, Akira S. The roles of TLRs, RLRs and NLRs in pathogen recognition. *International immunology*. 2009;21(4):317-37. Epub 2009/02/28. doi: 10.1093/intimm/dxp017. PubMed PMID: 19246554; PubMed Central PMCID: PMCPMC2721684.
129. Hoving JC, Wilson GJ, Brown GD. Signalling C-type lectin receptors, microbial recognition and immunity. *Cellular microbiology*. 2014;16(2):185-94. Epub 2013/12/18. doi: 10.1111/cmi.12249. PubMed PMID: 24330199; PubMed Central PMCID: PMCPMC4016756.
130. Blander JM, Sander LE. Beyond pattern recognition: five immune checkpoints for scaling the microbial threat. *Nature Reviews Immunology*. 2012;12(3):215-25. doi: 10.1038/nri3167.
131. Bayly-Jones C, Bubeck D, Dunstone MA. The mystery behind membrane insertion: a review of the complement membrane attack complex. *Philos Trans R Soc Lond B Biol Sci*. 2017;372(1726). Epub 2017/06/21. doi: 10.1098/rstb.2016.0221. PubMed PMID: 28630159; PubMed Central PMCID: PMCPMC5483522.
132. Merle NS, Church SE, Fremeaux-Bacchi V, Roumenina LT. Complement System Part I – Molecular Mechanisms of Activation and Regulation. *Frontiers in Immunology*. 2015;6(262). doi: 10.3389/fimmu.2015.00262.
133. Dunkelberger JR, Song W-C. Complement and its role in innate and adaptive immune responses. *Cell Research*. 2010;20(1):34-50. doi: 10.1038/cr.2009.139.
134. Trinchieri G, Sher A. Cooperation of Toll-like receptor signals in innate immune defence. *Nature Reviews Immunology*. 2007;7(3):179-90. doi: 10.1038/nri2038.
135. Kleczko EK, Kwak JW, Schenk EL, Nemenoff RA. Targeting the Complement Pathway as a Therapeutic Strategy in Lung Cancer. *Frontiers in Immunology*. 2019;10(954). doi: 10.3389/fimmu.2019.00954.
136. Hirayama D, Iida T, Nakase H. The Phagocytic Function of Macrophage-Enforcing Innate Immunity and Tissue Homeostasis. *Int J Mol Sci*. 2017;19(1). Epub 2017/12/30. doi: 10.3390/ijms19010092. PubMed PMID: 29286292; PubMed Central PMCID: PMCPMC5796042.
137. Freeman SA, Grinstein S. Phagocytosis: receptors, signal integration, and the cytoskeleton. *Immunological reviews*. 2014;262(1):193-215. Epub 2014/10/17. doi: 10.1111/imr.12212. PubMed PMID: 25319336.
138. Turner MD, Nedjai B, Hurst T, Pennington DJ. Cytokines and chemokines: At the crossroads of cell signalling and inflammatory disease. *Biochimica et Biophysica Acta (BBA) - Molecular Cell Research*. 2014;1843(11):2563-82. doi: <https://doi.org/10.1016/j.bbamcr.2014.05.014>.
139. Cameron M, Kelvin D. Cytokines, Chemokines and Their Receptors. Austin, Texas.: Landes Bioscience; 2000-2013 [26/09/20]. Available from: <https://www.ncbi.nlm.nih.gov/books/NBK6294/>.
140. Hughes CE, Nibbs RJB. A guide to chemokines and their receptors. *Febs j*. 2018;285(16):2944-71. Epub 2018/04/11. doi: 10.1111/febs.14466. PubMed PMID: 29637711; PubMed Central PMCID: PMCPMC6120486.
141. Crola Da Silva C, Lamerant-Fayel N, Paprocka M, Mitterrand M, Gosset D, Dus D, et al. Selective human endothelial cell activation by chemokines as a guide to cell homing. *Immunology*. 2009;126(3):394-404. Epub 2008/09/20. doi: 10.1111/j.1365-2567.2008.02906.x. PubMed PMID: 18800989; PubMed Central PMCID: PMCPMC2669820.
142. Vestweber D. How leukocytes cross the vascular endothelium. *Nature Reviews Immunology*. 2015;15(11):692-704. doi: 10.1038/nri3908.
143. Dominguez GA, Hammer DA. Effect of adhesion and chemokine presentation on T-lymphocyte haptokinesis. *Integr Biol (Camb)*. 2014;6(9):862-73. Epub 2014/07/12. doi: 10.1039/c4ib00094c. PubMed PMID: 25012074; PubMed Central PMCID: PMCPMC4746476.
144. Melchers F, Rolink AG, Schaniel C. The Role of Chemokines in Regulating Cell Migration during Humoral Immune Responses. *Cell*. 1999;99(4):351-4. doi: 10.1016/S0092-8674(00)81521-4.
145. Kunkel EJ, Butcher EC. Chemokines and the Tissue-Specific Migration of Lymphocytes. *Immunity*. 2002;16(1):1-4. doi: [https://doi.org/10.1016/S1074-7613\(01\)00261-8](https://doi.org/10.1016/S1074-7613(01)00261-8).

146. Kambayashi T, Laufer TM. Atypical MHC class II-expressing antigen-presenting cells: can anything replace a dendritic cell? *Nature Reviews Immunology*. 2014;14(11):719-30. doi: 10.1038/nri3754.
147. Abrahamsen G, Sundvold-Gjerstad V, Habtamu M, Bogen B, Spurkland A. Polarity of CD4+ T cells towards the antigen presenting cell is regulated by the Lck adapter TSA. *Scientific Reports*. 2018;8(1):13319. doi: 10.1038/s41598-018-31510-6.
148. Carbone FR, Belz GT, Heath WR. Transfer of antigen between migrating and lymph node-resident DCs in peripheral T-cell tolerance and immunity. *Trends Immunol*. 2004;25(12):655-8. Epub 2004/11/09. doi: 10.1016/j.it.2004.09.013. PubMed PMID: 15530835.
149. Hato T, Dagher PC. How the Innate Immune System Senses Trouble and Causes Trouble. *Clinical Journal of the American Society of Nephrology*. 2015;10(8):1459-69. doi: 10.2215/cjn.04680514.
150. Dominguez G. Effect of Substrate Ligand Presentation on the Motility of Human T-Lymphocytes. 2014.
151. Hong S, Zhang Z, Liu H, Tian M, Zhu X, Zhang Z, et al. B Cells Are the Dominant Antigen-Presenting Cells that Activate Naive CD4(+) T Cells upon Immunization with a Virus-Derived Nanoparticle Antigen. *Immunity*. 2018;49(4):695-708.e4. Epub 2018/10/07. doi: 10.1016/j.immuni.2018.08.012. PubMed PMID: 30291027.
152. Sampath P, Moideen K, Ranganathan UD, Bethunaickan R. Monocyte Subsets: Phenotypes and Function in Tuberculosis Infection. *Frontiers in Immunology*. 2018;9(1726). doi: 10.3389/fimmu.2018.01726.
153. Wolf AA, Yáñez A, Barman PK, Goodridge HS. The Ontogeny of Monocyte Subsets. *Frontiers in Immunology*. 2019;10(1642). doi: 10.3389/fimmu.2019.01642.
154. Shi C, Pamer EG. Monocyte recruitment during infection and inflammation. *Nat Rev Immunol*. 2011;11(11):762-74. Epub 2011/10/11. doi: 10.1038/nri3070. PubMed PMID: 21984070; PubMed Central PMCID: PMC3947780.
155. Qu C, Brinck-Jensen N-S, Zang M, Chen K. Monocyte-derived dendritic cells: targets as potent antigen-presenting cells for the design of vaccines against infectious diseases. *International Journal of Infectious Diseases*. 2014;19:1-5. doi: <https://doi.org/10.1016/j.ijid.2013.09.023>.
156. Murray PJ, Wynn TA. Protective and pathogenic functions of macrophage subsets. *Nat Rev Immunol*. 2011;11(11):723-37. Epub 2011/10/15. doi: 10.1038/nri3073. PubMed PMID: 21997792; PubMed Central PMCID: PMC3422549.
157. Patente TA, Pinho MP, Oliveira AA, Evangelista GCM, Bergami-Santos PC, Barbuto JAM. Human Dendritic Cells: Their Heterogeneity and Clinical Application Potential in Cancer Immunotherapy. *Frontiers in Immunology*. 2019;9(3176). doi: 10.3389/fimmu.2018.03176.
158. Holtman IR, Raj DD, Miller JA, Schaafsma W, Yin Z, Brouwer N, et al. Induction of a common microglia gene expression signature by aging and neurodegenerative conditions: a co-expression meta-analysis. *Acta Neuropathologica Communications*. 2015;3(1):31. doi: 10.1186/s40478-015-0203-5.
159. Ransohoff RM. A polarizing question: do M1 and M2 microglia exist? *Nat Neurosci*. 2016;19(8):987-91. Epub 2016/07/28. doi: 10.1038/nn.4338. PubMed PMID: 27459405.
160. Borges da Silva H, Fonseca R, Pereira RM, Cassado AdA, Álvarez JM, D'Império Lima MR. Splenic Macrophage Subsets and Their Function during Blood-Borne Infections. *Frontiers in Immunology*. 2015;6(480). doi: 10.3389/fimmu.2015.00480.
161. McArdle S, Buscher K, Ghosheh Y, Pramod AB, Miller J, Winkels H, et al. Migratory and Dancing Macrophage Subsets in Atherosclerotic Lesions. *Circulation research*. 2019;125(12):1038-51. doi: 10.1161/CIRCRESAHA.119.315175.
162. Chinetti-Gbaguidi G, Colin S, Staels B. Macrophage subsets in atherosclerosis. *Nature Reviews Cardiology*. 2015;12(1):10-7. doi: 10.1038/nrcardio.2014.173.

163. Chávez-Galán L, Olleros ML, Vesin D, Garcia I. Much More than M₁ and M₂ Macrophages, There are also CD169+ and TCR+ Macrophages. *Frontiers in Immunology*. 2015;6(263). doi: 10.3389/fimmu.2015.00263.
164. Ghosn EEB, Cassado AA, Govoni GR, Fukuhara T, Yang Y, Monack DM, et al. Two physically, functionally, and developmentally distinct peritoneal macrophage subsets. *Proceedings of the National Academy of Sciences*. 2010;107(6):2568-73. doi: 10.1073/pnas.0915000107.
165. Ong S-M, Teng K, Newell E, Chen H, Chen J, Loy T, et al. A Novel, Five-Marker Alternative to CD16-CD14 Gating to Identify the Three Human Monocyte Subsets. *Frontiers in Immunology*. 2019;10(1761). doi: 10.3389/fimmu.2019.01761.
166. Geissmann F, Jung S, Littman DR. Blood Monocytes Consist of Two Principal Subsets with Distinct Migratory Properties. *Immunity*. 2003;19(1):71-82. doi: [https://doi.org/10.1016/S1074-7613\(03\)00174-2](https://doi.org/10.1016/S1074-7613(03)00174-2).
167. Mildner A, Schönheit J, Giladi A, David E, Lara-Astiaso D, Lorenzo-Vivas E, et al. Genomic Characterization of Murine Monocytes Reveals C/EBP β Transcription Factor Dependence of Ly6C(-) Cells. *Immunity*. 2017;46(5):849-62.e7. Epub 2017/05/18. doi: 10.1016/j.immuni.2017.04.018. PubMed PMID: 28514690.
168. Sunderkötter C, Nikolic T, Dillon MJ, Van Rooijen N, Stehling M, Drevets DA, et al. Subpopulations of mouse blood monocytes differ in maturation stage and inflammatory response. *Journal of immunology (Baltimore, Md : 1950)*. 2004;172(7):4410-7. Epub 2004/03/23. doi: 10.4049/jimmunol.172.7.4410. PubMed PMID: 15034056.
169. Tacke F, Ginhoux F, Jakubzick C, van Rooijen N, Merad M, Randolph GJ. Immature monocytes acquire antigens from other cells in the bone marrow and present them to T cells after maturing in the periphery. *J Exp Med*. 2006;203(3):583-97. Epub 2006/02/24. doi: 10.1084/jem.20052119. PubMed PMID: 16492803; PubMed Central PMCID: PMC2118235.
170. Varol C, Landsman L, Fogg DK, Greenshtein L, Gildor B, Margalit R, et al. Monocytes give rise to mucosal, but not splenic, conventional dendritic cells. *J Exp Med*. 2007;204(1):171-80. Epub 2006/12/28. doi: 10.1084/jem.20061011. PubMed PMID: 17190836; PubMed Central PMCID: PMC2118434.
171. Anbazhagan K, Duroux-Richard I, Jorgensen C, Apparailly F. Transcriptomic network support distinct roles of classical and non-classical monocytes in human. *International reviews of immunology*. 2014;33(6):470-89. Epub 2014/04/16. doi: 10.3109/08830185.2014.902453. PubMed PMID: 24730730.
172. Zhao C, Zhang H, Wong W-C, Sem X, Han H, Ong S-M, et al. Identification of Novel Functional Differences in Monocyte Subsets Using Proteomic and Transcriptomic Methods. *Journal of Proteome Research*. 2009;8(8):4028-38. doi: 10.1021/pr900364p.
173. Villani A-C, Satija R, Reynolds G, Sarkizova S, Shekhar K, Fletcher J, et al. Single-cell RNA-seq reveals new types of human blood dendritic cells, monocytes, and progenitors. *Science*. 2017;356(6335):eaah4573. doi: 10.1126/science.aah4573.
174. Boyette LB, Macedo C, Hadi K, Elinoff BD, Walters JT, Ramaswami B, et al. Phenotype, function, and differentiation potential of human monocyte subsets. *PLoS One*. 2017;12(4):e0176460. Epub 2017/04/27. doi: 10.1371/journal.pone.0176460. PubMed PMID: 28445506; PubMed Central PMCID: PMC5406034.
175. Narasimhan PB, Marcovecchio P, Hamers AAJ, Hedrick CC. Nonclassical Monocytes in Health and Disease. *Annual review of immunology*. 2019;37(1):439-56. doi: 10.1146/annurev-immunol-042617-053119. PubMed PMID: 31026415.
176. Olingy CE, San Emeterio CL, Ogle ME, Krieger JR, Bruce AC, Pfau DD, et al. Non-classical monocytes are biased progenitors of wound healing macrophages during soft tissue injury. *Scientific Reports*. 2017;7(1):447. doi: 10.1038/s41598-017-00477-1.

177. Kapellos TS, Bonaguro L, Gemünd I, Reusch N, Saglam A, Hinkley ER, et al. Human Monocyte Subsets and Phenotypes in Major Chronic Inflammatory Diseases. *Frontiers in Immunology*. 2019;10(2035). doi: 10.3389/fimmu.2019.02035.
178. Karlmark KR, Tacke F, Dunay IR. Monocytes in health and disease - Minireview. *Eur J Microbiol Immunol (Bp)*. 2012;2(2):97-102. Epub 2012/06/01. doi: 10.1556/EuJMI.2.2012.2.1. PubMed PMID: 24672677; PubMed Central PMCID: PMC3956957.
179. Geissmann F, Manz MG, Jung S, Sieweke MH, Merad M, Ley K. Development of monocytes, macrophages, and dendritic cells. *Science (New York, NY)*. 2010;327(5966):656-61. doi: 10.1126/science.1178331. PubMed PMID: 20133564.
180. Haldar M, Murphy KM. Origin, development, and homeostasis of tissue-resident macrophages. *Immunological reviews*. 2014;262(1):25-35. doi: 10.1111/imr.12215. PubMed PMID: 25319325.
181. Varol C, Mildner A, Jung S. Macrophages: Development and Tissue Specialization. *Annual review of immunology*. 2015;33(1):643-75. doi: 10.1146/annurev-immunol-032414-112220.
182. Orecchioni M, Ghosheh Y, Pramod AB, Ley K. Macrophage Polarization: Different Gene Signatures in M1(LPS+) vs. Classically and M2(LPS-) vs. Alternatively Activated Macrophages. *Frontiers in Immunology*. 2019;10(1084). doi: 10.3389/fimmu.2019.01084.
183. Gerrick KY, Gerrick ER, Gupta A, Wheelan SJ, Yegnasubramanian S, Jaffee EM. Transcriptional profiling identifies novel regulators of macrophage polarization. *PloS one*. 2018;13(12):e0208602-e. doi: 10.1371/journal.pone.0208602. PubMed PMID: 30532146.
184. Konttinen YT, Pajarinen J, Takakubo Y, Gallo J, Nich C, Takagi M, et al. Macrophage polarization and activation in response to implant debris: influence by "particle disease" and "ion disease". *J Long Term Eff Med Implants*. 2014;24(4):267-81. doi: 10.1615/jlongtermeffmedimplants.2014011355. PubMed PMID: 25747030.
185. Dalton DK, Pitts-Meek S, Keshav S, Figari IS, Bradley A, Stewart TA. Multiple defects of immune cell function in mice with disrupted interferon-gamma genes. *Science*. 1993;259(5102):1739-42. Epub 1993/03/19. doi: 10.1126/science.8456300. PubMed PMID: 8456300.
186. Nahrendorf M, Swirski FK. Abandoning M1/M2 for a Network Model of Macrophage Function. *Circulation research*. 2016;119(3):414-7. doi: 10.1161/CIRCRESAHA.116.309194. PubMed PMID: 27458196.
187. Mosser DM, Edwards JP. Exploring the full spectrum of macrophage activation. *Nature reviews Immunology*. 2008;8(12):958-69. doi: 10.1038/nri2448. PubMed PMID: 19029990.
188. Murray PJ, Allen JE, Biswas SK, Fisher EA, Gilroy DW, Goerdt S, et al. Macrophage activation and polarization: nomenclature and experimental guidelines. *Immunity*. 2014;41(1):14-20. doi: 10.1016/j.immuni.2014.06.008. PubMed PMID: 25035950.
189. Gabrilovich DI. Myeloid-Derived Suppressor Cells. *Cancer immunology research*. 2017;5(1):3-8. doi: 10.1158/2326-6066.CIR-16-0297. PubMed PMID: 28052991.
190. Glass CK, Natoli G. Molecular control of activation and priming in macrophages. *Nature immunology*. 2016;17(1):26-33. doi: 10.1038/ni.3306. PubMed PMID: 26681459.
191. Cavillon JM, Annane D. Compartmentalization of the inflammatory response in sepsis and SIRS. *Journal of Endotoxin Research*. 2006;12(3):151-70. doi: 10.1179/096805106X102246.
192. Lavin Y, Winter D, Blecher-Gonen R, David E, Keren-Shaul H, Merad M, et al. Tissue-resident macrophage enhancer landscapes are shaped by the local microenvironment. *Cell*. 2014;159(6):1312-26. Epub 2014/12/07. doi: 10.1016/j.cell.2014.11.018. PubMed PMID: 25480296; PubMed Central PMCID: PMC3956957.
193. Gautier EL, Shay T, Miller J, Greter M, Jakubzick C, Ivanov S, et al. Gene-expression profiles and transcriptional regulatory pathways that underlie the identity and diversity of mouse tissue macrophages. *Nature immunology*. 2012;13(11):1118-28. Epub 2012/09/30. doi: 10.1038/ni.2419. PubMed PMID: 23023392.

194. Sims NA, Walsh NC. Intercellular cross-talk among bone cells: new factors and pathways. *Curr Osteoporos Rep.* 2012;10(2):109-17. Epub 2012/03/20. doi: 10.1007/s11914-012-0096-1. PubMed PMID: 22427140.
195. Chasis JA, Mohandas N. Erythroblastic islands: niches for erythropoiesis. *Blood.* 2008;112(3):470-8. Epub 2008/07/25. doi: 10.1182/blood-2008-03-077883. PubMed PMID: 18650462; PubMed Central PMCID: PMCPMC2481536.
196. Ganz T. Macrophages and systemic iron homeostasis. *J Innate Immun.* 2012;4(5-6):446-53. Epub 2012/03/24. doi: 10.1159/000336423. PubMed PMID: 22441209; PubMed Central PMCID: PMCPMC6741611.
197. Nguyen KD, Qiu Y, Cui X, Goh YP, Mwangi J, David T, et al. Alternatively activated macrophages produce catecholamines to sustain adaptive thermogenesis. *Nature.* 2011;480(7375):104-8. Epub 2011/11/22. doi: 10.1038/nature10653. PubMed PMID: 22101429; PubMed Central PMCID: PMCPMC3371761.
198. Hulsmans M, Clauss S, Xiao L, Aguirre AD, King KR, Hanley A, et al. Macrophages Facilitate Electrical Conduction in the Heart. *Cell.* 2017;169(3):510-22.e20. Epub 2017/04/22. doi: 10.1016/j.cell.2017.03.050. PubMed PMID: 28431249; PubMed Central PMCID: PMCPMC5474950.
199. Hussell T, Bell TJ. Alveolar macrophages: plasticity in a tissue-specific context. *Nat Rev Immunol.* 2014;14(2):81-93. Epub 2014/01/22. doi: 10.1038/nri3600. PubMed PMID: 24445666.
200. de Back DZ, Kostova EB, van Kraaij M, van den Berg TK, van Bruggen R. Of macrophages and red blood cells; a complex love story. *Front Physiol.* 2014;5:9. Epub 2014/02/14. doi: 10.3389/fphys.2014.00009. PubMed PMID: 24523696; PubMed Central PMCID: PMCPMC3906564.
201. Odegaard JI, Ricardo-Gonzalez RR, Goforth MH, Morel CR, Subramanian V, Mukundan L, et al. Macrophage-specific PPARgamma controls alternative activation and improves insulin resistance. *Nature.* 2007;447(7148):1116-20. Epub 2007/05/23. doi: 10.1038/nature05894. PubMed PMID: 17515919; PubMed Central PMCID: PMCPMC2587297.
202. Ocaña-Guzman R, Vázquez-Bolaños L, Sada-Ovalle I. Receptors That Inhibit Macrophage Activation: Mechanisms and Signals of Regulation and Tolerance. *Journal of Immunology Research.* 2018;2018:8695157. doi: 10.1155/2018/8695157.
203. Uderhardt S, Martins AJ, Tsang JS, Lämmermann T, Germain RN. Resident Macrophages Cloak Tissue Microlesions to Prevent Neutrophil-Driven Inflammatory Damage. *Cell.* 2019;177(3):541-55.e17. Epub 2019/04/09. doi: 10.1016/j.cell.2019.02.028. PubMed PMID: 30955887; PubMed Central PMCID: PMCPMC6474841.
204. Roberts AW, Lee BL, Deguine J, John S, Shlomchik MJ, Barton GM. Tissue-Resident Macrophages Are Locally Programmed for Silent Clearance of Apoptotic Cells. *Immunity.* 2017;47(5):913-27.e6. doi: <https://doi.org/10.1016/j.immuni.2017.10.006>.
205. Kaur M, Bell T, Salek-Ardakani S, Hussell T. Macrophage adaptation in airway inflammatory resolution. *Eur Respir Rev.* 2015;24(137):510-5. Epub 2015/09/02. doi: 10.1183/16000617.0030-2015. PubMed PMID: 26324813.
206. Goulding J, Godlee A, Vekaria S, Hilty M, Snelgrove R, Hussell T. Lowering the threshold of lung innate immune cell activation alters susceptibility to secondary bacterial superinfection. *The Journal of infectious diseases.* 2011;204(7):1086-94. doi: 10.1093/infdis/jir467. PubMed PMID: 21881124.
207. Snelgrove RJ, Goulding J, Didierlaurent AM, Lyonga D, Vekaria S, Edwards L, et al. A critical function for CD200 in lung immune homeostasis and the severity of influenza infection. *Nature Immunology.* 2008;9(9):1074-83. doi: 10.1038/ni.1637.
208. Smythies LE, Sellers M, Clements RH, Mosteller-Barnum M, Meng G, Benjamin WH, et al. Human intestinal macrophages display profound inflammatory anergy despite avid phagocytic and bacteriocidal activity. *J Clin Invest.* 2005;115(1):66-75. Epub 2005/01/05. doi: 10.1172/jci9229. PubMed PMID: 15630445; PubMed Central PMCID: PMCPMC539188.

209. Davies LC, Rice CM, Palmieri EM, Taylor PR, Kuhns DB, McVicar DW. Peritoneal tissue-resident macrophages are metabolically poised to engage microbes using tissue-niche fuels. *Nature Communications*. 2017;8(1):2074. doi: 10.1038/s41467-017-02092-0.
210. Zhang X, Jiang Z, Gu Y, Liu Y, Cao X, Han Y. Inflammation-induced CD69⁺ Kupffer cell feedback inhibits T cell proliferation via membrane-bound TGF- β 1. *Science China Life Sciences*. 2016;59(12):1259-69. doi: 10.1007/s11427-016-0357-1.
211. Ruddle NH, Akirav EM. Secondary lymphoid organs: responding to genetic and environmental cues in ontogeny and the immune response. *Journal of immunology (Baltimore, Md : 1950)*. 2009;183(4):2205-12. Epub 2009/08/08. doi: 10.4049/jimmunol.0804324. PubMed PMID: 19661265; PubMed Central PMCID: PMCPMC2766168.
212. Luckheeram RV, Zhou R, Verma AD, Xia B. CD4⁺T Cells: Differentiation and Functions. *Clinical and Developmental Immunology*. 2012;2012:925135. doi: 10.1155/2012/925135.
213. Kara EE, Comerford I, Fenix KA, Bastow CR, Gregor CE, McKenzie DR, et al. Tailored immune responses: novel effector helper T cell subsets in protective immunity. *PLoS pathogens*. 2014;10(2):e1003905. Epub 2014/03/04. doi: 10.1371/journal.ppat.1003905. PubMed PMID: 24586147; PubMed Central PMCID: PMCPMC3930558.
214. Nistala K, Adams S, Cambrook H, Ursu S, Olivito B, de Jager W, et al. Th17 plasticity in human autoimmune arthritis is driven by the inflammatory environment. *Proc Natl Acad Sci U S A*. 2010;107(33):14751-6. Epub 2010/08/04. doi: 10.1073/pnas.1003852107. PubMed PMID: 20679229; PubMed Central PMCID: PMCPMC2930428.
215. Meiraz A, Garber OG, Harari S, Hassin D, Berke G. Switch from perforin-expressing to perforin-deficient CD8⁺ T cells accounts for two distinct types of effector cytotoxic T lymphocytes in vivo. *Immunology*. 2009;128(1):69-82. Epub 2009/08/20. doi: 10.1111/j.1365-2567.2009.03072.x. PubMed PMID: 19689737; PubMed Central PMCID: PMCPMC2747140.
216. Brynjolfsson SF, Persson Berg L, Olsen Ekerhult T, Rimkute I, Wick M-J, Mårtensson I-L, et al. Long-Lived Plasma Cells in Mice and Men. *Frontiers in Immunology*. 2018;9(2673). doi: 10.3389/fimmu.2018.02673.
217. Ratajczak W, Niedźwiedzka-Rystwej P, Tokarz-Deptuła B, Deptuła W. Immunological memory cells. *Cent Eur J Immunol*. 2018;43(2):194-203. Epub 2018/08/24. doi: 10.5114/cej.2018.77390. PubMed PMID: 30135633; PubMed Central PMCID: PMCPMC6102609.
218. Chaudhary N, Wesemann DR. Analyzing Immunoglobulin Repertoires. *Frontiers in Immunology*. 2018;9(462). doi: 10.3389/fimmu.2018.00462.
219. Glass EJ. The molecular pathways underlying host resistance and tolerance to pathogens. *Front Genet*. 2012;3:263. Epub 2013/02/14. doi: 10.3389/fgene.2012.00263. PubMed PMID: 23403960; PubMed Central PMCID: PMCPMC3566117.
220. Amos SM, Duong CP, Westwood JA, Ritchie DS, Junghans RP, Darcy PK, et al. Autoimmunity associated with immunotherapy of cancer. *Blood*. 2011;118(3):499-509. Epub 2011/05/03. doi: 10.1182/blood-2011-01-325266. PubMed PMID: 21531979.
221. Young A, Quandt Z, Bluestone JA. The Balancing Act between Cancer Immunity and Autoimmunity in Response to Immunotherapy. *Cancer Immunology Research*. 2018;6(12):1445-52. doi: 10.1158/2326-6066.Cir-18-0487.
222. Schnell A, Bod L, Madi A, Kuchroo VK. The yin and yang of co-inhibitory receptors: toward anti-tumor immunity without autoimmunity. *Cell Research*. 2020. doi: 10.1038/s41422-020-0277-x.
223. Chaplin DD. Overview of the immune response. *J Allergy Clin Immunol*. 2010;125(2 Suppl 2):S3-23. Epub 2010/03/05. doi: 10.1016/j.jaci.2009.12.980. PubMed PMID: 20176265; PubMed Central PMCID: PMCPMC2923430.
224. Jackson SE, Redeker A, Arens R, van Baarle D, van den Berg SPH, Benedict CA, et al. CMV immune evasion and manipulation of the immune system with aging. *Geroscience*.

- 2017;39(3):273-91. Epub 2017/06/26. doi: 10.1007/s11357-017-9986-6. PubMed PMID: 28647908; PubMed Central PMCID: PMC5505894.
225. Griffiths DJ. Endogenous retroviruses in the human genome sequence. *Genome Biol.* 2001;2(6):REVIEWS1017. Epub 2001/06/26. doi: 10.1186/gb-2001-2-6-reviews1017. PubMed PMID: 11423012; PubMed Central PMCID: PMC138943.
226. Moyes D, Griffiths DJ, Venables PJ. Insertional polymorphisms: a new lease of life for endogenous retroviruses in human disease. *Trends Genet.* 2007;23(7):326-33. Epub 2007/05/26. doi: 10.1016/j.tig.2007.05.004. PubMed PMID: 17524519.
227. Chen J, Deng YM. Influenza virus antigenic variation, host antibody production and new approach to control epidemics. *Virology.* 2009;6:30. Epub 2009/03/17. doi: 10.1186/1743-422x-6-30. PubMed PMID: 19284639; PubMed Central PMCID: PMC2666653.
228. Alberts B, Johnson A, Lewis J, Raff M, Roberts K, Walter P. *Molecular Biology of the Cell.* 4th ed. New York: Garland Science; 2002.
229. Pelanda R, Torres RM. Central B-cell tolerance: where selection begins. *Cold Spring Harb Perspect Biol.* 2012;4(4):a007146. Epub 2012/03/02. doi: 10.1101/cshperspect.a007146. PubMed PMID: 22378602; PubMed Central PMCID: PMC3312675.
230. Sandel PC, Monroe JG. Negative selection of immature B cells by receptor editing or deletion is determined by site of antigen encounter. *Immunity.* 1999;10(3):289-99. Epub 1999/04/16. doi: 10.1016/s1074-7613(00)80029-1. PubMed PMID: 10204485.
231. Klein L, Kyewski B, Allen PM, Hogquist KA. Positive and negative selection of the T cell repertoire: what thymocytes see (and don't see). *Nat Rev Immunol.* 2014;14(6):377-91. Epub 2014/05/17. doi: 10.1038/nri3667. PubMed PMID: 24830344; PubMed Central PMCID: PMC4757912.
232. McGargill MA, Derbinski JM, Hogquist KA. Receptor editing in developing T cells. *Nat Immunol.* 2000;1(4):336-41. Epub 2001/03/23. doi: 10.1038/79790. PubMed PMID: 11017106.
233. Kreslavsky T, Kim HJ, Koralov SB, Ghitza D, Buch T, Cantor H, et al. Negative selection, not receptor editing, is a physiological response of autoreactive thymocytes. *J Exp Med.* 2013;210(10):1911-8. Epub 2013/08/28. doi: 10.1084/jem.20130876. PubMed PMID: 23980099; PubMed Central PMCID: PMC3782038.
234. Ramsey C, Winqvist O, Puhakka L, Halonen M, Moro A, Kampe O, et al. Aire deficient mice develop multiple features of APECED phenotype and show altered immune response. *Hum Mol Genet.* 2002;11(4):397-409. Epub 2002/02/21. doi: 10.1093/hmg/11.4.397. PubMed PMID: 11854172.
235. Mueller DL. Mechanisms maintaining peripheral tolerance. *Nature Immunology.* 2010;11(1):21-7. doi: 10.1038/ni.1817.
236. Nave KA, Lai C, Bloom FE, Milner RJ. Splice site selection in the proteolipid protein (PLP) gene transcript and primary structure of the DM-20 protein of central nervous system myelin. *Proc Natl Acad Sci U S A.* 1987;84(16):5665-9. Epub 1987/08/01. doi: 10.1073/pnas.84.16.5665. PubMed PMID: 2441390; PubMed Central PMCID: PMC298923.
237. Zehn D, Bevan MJ. T cells with low avidity for a tissue-restricted antigen routinely evade central and peripheral tolerance and cause autoimmunity. *Immunity.* 2006;25(2):261-70. Epub 2006/08/02. doi: 10.1016/j.immuni.2006.06.009. PubMed PMID: 16879996; PubMed Central PMCID: PMC2774714.
238. Mason D. A very high level of crossreactivity is an essential feature of the T-cell receptor. *Immunol Today.* 1998;19(9):395-404. Epub 1998/09/24. doi: 10.1016/s0167-5699(98)01299-7. PubMed PMID: 9745202.
239. Anderton SM, Wraith DC. Selection and fine-tuning of the autoimmune T-cell repertoire. *Nat Rev Immunol.* 2002;2(7):487-98. Epub 2002/07/03. doi: 10.1038/nri842. PubMed PMID: 12094223.

240. Harding FA, McArthur JG, Gross JA, Raulet DH, Allison JP. CD28-mediated signalling co-stimulates murine T cells and prevents induction of anergy in T-cell clones. *Nature*. 1992;356(6370):607-9. Epub 1992/04/16. doi: 10.1038/356607a0. PubMed PMID: 1313950.
241. Arakaki R, Yamada A, Kudo Y, Hayashi Y, Ishimaru N. Mechanism of activation-induced cell death of T cells and regulation of FasL expression. *Crit Rev Immunol*. 2014;34(4):301-14. Epub 2014/06/19. doi: 10.1615/critrevimmunol.2014009988. PubMed PMID: 24941158.
242. Yadav M, Stephan S, Bluestone JA. Peripherally induced tregs - role in immune homeostasis and autoimmunity. *Front Immunol*. 2013;4:232. Epub 2013/08/24. doi: 10.3389/fimmu.2013.00232. PubMed PMID: 23966994; PubMed Central PMCID: PMC3736167.
243. Schwartz RH. T cell anergy. *Annu Rev Immunol*. 2003;21:305-34. Epub 2002/12/10. doi: 10.1146/annurev.immunol.21.120601.141110. PubMed PMID: 12471050.
244. Elgueta R, Benson MJ, de Vries VC, Wasiuk A, Guo Y, Noelle RJ. Molecular mechanism and function of CD40/CD40L engagement in the immune system. *Immunol Rev*. 2009;229(1):152-72. Epub 2009/05/12. doi: 10.1111/j.1600-065X.2009.00782.x. PubMed PMID: 19426221; PubMed Central PMCID: PMC3826168.
245. Dempsey PW, Allison ME, Akkaraju S, Goodnow CC, Fearon DT. C3d of complement as a molecular adjuvant: bridging innate and acquired immunity. *Science*. 1996;271(5247):348-50. Epub 1996/01/19. doi: 10.1126/science.271.5247.348. PubMed PMID: 8553069.
246. O'Sullivan BJ, Thomas HE, Pai S, Santamaria P, Iwakura Y, Steptoe RJ, et al. IL-1 β Breaks Tolerance through Expansion of CD25⁺ Effector T Cells. *The Journal of Immunology*. 2006;176(12):7278-87. doi: 10.4049/jimmunol.176.12.7278.
247. Hong S, Van Kaer L. Immune privilege: keeping an eye on natural killer T cells. *J Exp Med*. 1999;190(9):1197-200. Epub 1999/11/02. doi: 10.1084/jem.190.9.1197. PubMed PMID: 10544192; PubMed Central PMCID: PMC2195673.
248. Matta B, Bora PS, Neuhauser AJ, Bora NS. Inhibitory role of transforming growth factor beta2 in experimental autoimmune anterior uveitis. *Graefes Arch Clin Exp Ophthalmol*. 2019;257(5):953-60. Epub 2019/02/06. doi: 10.1007/s00417-019-04255-9. PubMed PMID: 30719689.
249. Dowling MR, Kan A, Heinzl S, Marchingo JM, Hodgkin PD, Hawkins ED. Regulatory T Cells Suppress Effector T Cell Proliferation by Limiting Division Destiny. *Front Immunol*. 2018;9:2461. Epub 2018/11/15. doi: 10.3389/fimmu.2018.02461. PubMed PMID: 30425712; PubMed Central PMCID: PMC6218578.
250. Schmidt A, Oberle N, Krammer PH. Molecular mechanisms of treg-mediated T cell suppression. *Front Immunol*. 2012;3:51. Epub 2012/05/09. doi: 10.3389/fimmu.2012.00051. PubMed PMID: 22566933; PubMed Central PMCID: PMC3341960.
251. Arce-Sillas A, Álvarez-Luquín DD, Tamaya-Domínguez B, Gomez-Fuentes S, Trejo-García A, Melo-Salas M, et al. Regulatory T Cells: Molecular Actions on Effector Cells in Immune Regulation. *J Immunol Res*. 2016;2016:1720827. Epub 2016/06/15. doi: 10.1155/2016/1720827. PubMed PMID: 27298831; PubMed Central PMCID: PMC4889823.
252. Wakefield D, Chang JH, Amjadi S, Maconochie Z, el-Asrar AA, McCluskey P. What Is New HLA-B27 Acute Anterior Uveitis? *Ocular Immunology and Inflammation*. 2011;19(2):139-44. doi: 10.3109/09273948.2010.542269.
253. Murtaza A, Kuchroo VK, Freeman GJ. Changes in the strength of co-stimulation through the B7/CD28 pathway alter functional T cell responses to altered peptide ligands. *Int Immunol*. 1999;11(3):407-16. Epub 1999/04/30. doi: 10.1093/intimm/11.3.407. PubMed PMID: 10221652.
254. Hoyer FF, Naxerova K, Schloss MJ, Hulsmans M, Nair AV, Dutta P, et al. Tissue-Specific Macrophage Responses to Remote Injury Impact the Outcome of Subsequent Local Immune Challenge. *Immunity*. 2019;51(5):899-914 e7. Epub 2019/11/17. doi: 10.1016/j.immuni.2019.10.010. PubMed PMID: 31732166; PubMed Central PMCID: PMC6892583.

255. Nicholson LB. The immune system. *Essays Biochem.* 2016;60(3):275-301. Epub 2016/10/28. doi: 10.1042/ebc20160017. PubMed PMID: 27784777; PubMed Central PMCID: PMC5091071.
256. Papadimitraki ED, Bertias GK, Boumpas DT. Toll like receptors and autoimmunity: a critical appraisal. *J Autoimmun.* 2007;29(4):310-8. Epub 2007/10/26. doi: 10.1016/j.jaut.2007.09.001. PubMed PMID: 17959357.
257. Baccala R, Hoebe K, Kono DH, Beutler B, Theofilopoulos AN. TLR-dependent and TLR-independent pathways of type I interferon induction in systemic autoimmunity. *Nat Med.* 2007;13(5):543-51. Epub 2007/05/05. doi: 10.1038/nm1590. PubMed PMID: 17479100.
258. Lai J-J, Cruz FM, Rock KL. Immune Sensing of Cell Death through Recognition of Histone Sequences by C-Type Lectin-Receptor-2d Causes Inflammation and Tissue Injury. *Immunity.* 2020;52(1):123-35.e6. doi: <https://doi.org/10.1016/j.immuni.2019.11.013>.
259. Arevalo JF, Garcia RA, Al-Dhibi HA, Sanchez JG, Suarez-Tata L. Update on sympathetic ophthalmia. *Middle East Afr J Ophthalmol.* 2012;19(1):13-21. Epub 2012/02/22. doi: 10.4103/0974-9233.92111. PubMed PMID: 22346110; PubMed Central PMCID: PMC3277011.
260. Zaharia MA, Lamarche J, Laurin M. Sympathetic uveitis 66 years after injury. *Can J Ophthalmol.* 1984;19(5):240-3. Epub 1984/08/01. PubMed PMID: 6478310.
261. Goronzy JJ, Weyand CM. T-cell co-stimulatory pathways in autoimmunity. *Arthritis Res Ther.* 2008;10 Suppl 1(Suppl 1):S3. Epub 2008/11/26. doi: 10.1186/ar2414. PubMed PMID: 19007423; PubMed Central PMCID: PMC2582810.
262. Hu P, Pollard JD, Chan-Ling T. Breakdown of the blood-retinal barrier induced by activated T cells of nonneural specificity. *Am J Pathol.* 2000;156(4):1139-49. Epub 2000/04/07. doi: 10.1016/s0002-9440(10)64982-6. PubMed PMID: 10751337; PubMed Central PMCID: PMC1876898.
263. Cusick MF, Libbey JE, Fujinami RS. Molecular mimicry as a mechanism of autoimmune disease. *Clin Rev Allergy Immunol.* 2012;42(1):102-11. Epub 2011/11/19. doi: 10.1007/s12016-011-8294-7. PubMed PMID: 22095454; PubMed Central PMCID: PMC3266166.
264. Frauendorf E, von Goessel H, May E, Märker-Hermann E. HLA-B27-restricted T cells from patients with ankylosing spondylitis recognize peptides from B*2705 that are similar to bacteria-derived peptides. *Clin Exp Immunol.* 2003;134(2):351-9. Epub 2003/11/18. doi: 10.1046/j.1365-2249.2003.02289.x. PubMed PMID: 14616798; PubMed Central PMCID: PMC1808853.
265. Kivity S, Agmon-Levin N, Blank M, Shoenfeld Y. Infections and autoimmunity--friends or foes? *Trends Immunol.* 2009;30(8):409-14. Epub 2009/08/01. doi: 10.1016/j.it.2009.05.005. PubMed PMID: 19643667.
266. Vanderlugt CL, Miller SD. Epitope spreading in immune-mediated diseases: implications for immunotherapy. *Nature Reviews Immunology.* 2002;2(2):85-95. doi: 10.1038/nri724.
267. Agmon-Levin N, Ram M, Barzilai O, Porat-Katz BS, Parikman R, Selmi C, et al. Prevalence of hepatitis C serum antibody in autoimmune diseases. *J Autoimmun.* 2009;32(3-4):261-6. Epub 2009/04/10. doi: 10.1016/j.jaut.2009.02.017. PubMed PMID: 19356903.
268. Farh KK-H, Marson A, Zhu J, Kleinewietfeld M, Housley WJ, Beik S, et al. Genetic and epigenetic fine mapping of causal autoimmune disease variants. *Nature.* 2015;518(7539):337-43. doi: 10.1038/nature13835.
269. Doria A, Zen M, Bettio S, Gatto M, Bassi N, Nalotto L, et al. Autoinflammation and autoimmunity: bridging the divide. *Autoimmun Rev.* 2012;12(1):22-30. Epub 2012/08/11. doi: 10.1016/j.autrev.2012.07.018. PubMed PMID: 22878274.
270. Lachmann HJ, Quartier P, So A, Hawkins PN. The emerging role of interleukin-1beta in autoinflammatory diseases. *Arthritis Rheum.* 2011;63(2):314-24. Epub 2010/10/23. doi: 10.1002/art.30105. PubMed PMID: 20967858.

271. Ozen S. What's new in autoinflammation? *Pediatr Nephrol.* 2019;34(12):2449-56. Epub 2018/12/16. doi: 10.1007/s00467-018-4155-4. PubMed PMID: 30552566.
272. Kantar. Healthcare 2020: The 10 key influencers of global health and wellness 2019 [19/02/20]. Available from: https://www.kantarhealth.com/docs/reports/10-key-influencers-on-global-health-and-wellness.pdf?sfvrsn=8c32d3bo_2.
273. Boraschi D, Italiani P. Innate Immune Memory: Time for Adopting a Correct Terminology. *Frontiers in Immunology.* 2018;9(799). doi: 10.3389/fimmu.2018.00799.
274. Netea MG, Schlitzer A, Placek K, Joosten LAB, Schultze JL. Innate and Adaptive Immune Memory: an Evolutionary Continuum in the Host's Response to Pathogens. *Cell host & microbe.* 2019;25(1):13-26. doi: <https://doi.org/10.1016/j.chom.2018.12.006>.
275. Beeson PB. Development of tolerance to typhoid bacterial pyrogen and its abolition by reticulo-endothelial blockade. *Proc Soc Exp Biol Med.* 1946;61:248-50. Epub 1946/03/01. doi: 10.3181/00379727-61-15291p. PubMed PMID: 21024160.
276. Boraschi D, Meltzer MS. Defective tumoricidal capacity of macrophages from A/J mice. II. Comparison of the macrophage cytotoxic defect of A/J mice with that of lipid A-unresponsive C3H/HeJ mice. *Journal of immunology (Baltimore, Md : 1950).* 1979;122(4):1592-97. Epub 1979/04/01. PubMed PMID: 376721.
277. Dubos RJ, Schaedler RW. Reversible changes in the susceptibility of mice to bacterial infections. I. Changes brought about by injection of pertussis vaccine or of bacterial endotoxins. *The Journal of experimental medicine.* 1956;104(1):53-65. doi: 10.1084/jem.104.1.53. PubMed PMID: 13332180.
278. Biswas SK, Lopez-Collazo E. Endotoxin tolerance: new mechanisms, molecules and clinical significance. *Trends in Immunology.* 2009;30(10):475-87. doi: <https://doi.org/10.1016/j.it.2009.07.009>.
279. Seeley JJ, Ghosh S. Molecular mechanisms of innate memory and tolerance to LPS. *Journal of Leukocyte Biology.* 2017;101(1):107-19. doi: 10.1189/jlb.3MR0316-118RR.
280. van der Heijden CDCC, Noz MP, Joosten LAB, Netea MG, Riksen NP, Keating ST. Epigenetics and Trained Immunity. *Antioxid Redox Signal.* 2018;29(11):1023-40. Epub 2017/11/21. doi: 10.1089/ars.2017.7310. PubMed PMID: 28978221.
281. Patel AA, Zhang Y, Fullerton JN, Boelen L, Rongvaux A, Maini AA, et al. The fate and lifespan of human monocyte subsets in steady state and systemic inflammation. *The Journal of experimental medicine.* 2017;214(7):1913-23. Epub 2017/06/12. doi: 10.1084/jem.20170355. PubMed PMID: 28606987.
282. Mitroulis I, Ruppova K, Wang B, Chen L-S, Grzybek M, Grinenko T, et al. Modulation of Myelopoiesis Progenitors Is an Integral Component of Trained Immunity. *Cell.* 2018;172(1-2):147-61.e12. doi: 10.1016/j.cell.2017.11.034. PubMed PMID: 29328910.
283. Guo R-F, Riedemann NC, Sun L, Gao H, Shi KX, Reuben JS, et al. Divergent Signaling Pathways in Phagocytic Cells during Sepsis. *The Journal of Immunology.* 2006;177(2):1306-13. doi: 10.4049/jimmunol.177.2.1306.
284. Suzuki T, Shimizu T, Szalay L, Choudhry MA, Rue LW, Bland KI, et al. Androstenediol ameliorates alterations in immune cells cytokine production capacity in a two-hit model of trauma-hemorrhage and sepsis. *Cytokine.* 2006;34(1):76-84. doi: <https://doi.org/10.1016/j.cyto.2006.04.007>.
285. Peng H, Tian Z. Natural Killer Cell Memory: Progress and Implications. *Frontiers in immunology.* 2017;8:1143-. doi: 10.3389/fimmu.2017.01143. PubMed PMID: 28955346.
286. Medzhitov R. Origin and physiological roles of inflammation. *Nature.* 2008;454(7203):428-35. doi: 10.1038/nature07201.
287. Chen M, Xu H. Parainflammation, chronic inflammation, and age-related macular degeneration. *J Leukoc Biol.* 2015;98(5):713-25. Epub 2015/08/22. doi: 10.1189/jlb.3RI0615-239R. PubMed PMID: 26292978; PubMed Central PMCID: PMC4733662.

288. Kono H, Rock KL. How dying cells alert the immune system to danger. *Nature Reviews Immunology*. 2008;8(4):279-89. doi: 10.1038/nri2215.
289. Xu H, Chen M, Forrester JV. Para-inflammation in the aging retina. *Progress in Retinal and Eye Research*. 2009;28(5):348-68. doi: <https://doi.org/10.1016/j.preteyeres.2009.06.001>.
290. Terao A, Apte-Deshpande A, Dousman L, Morairty S, Eynon BP, Kilduff TS, et al. Immune response gene expression increases in the aging murine hippocampus. *Journal of Neuroimmunology*. 2002;132(1):99-112. doi: [https://doi.org/10.1016/S0165-5728\(02\)00317-X](https://doi.org/10.1016/S0165-5728(02)00317-X).
291. Rönnbäck C, Hansson E. The Importance and Control of Low-Grade Inflammation Due to Damage of Cellular Barrier Systems That May Lead to Systemic Inflammation. *Front Neurol*. 2019;10:533. Epub 2019/06/14. doi: 10.3389/fneur.2019.00533. PubMed PMID: 31191433; PubMed Central PMCID: PMC6549124.
292. Sonoda A, Sonoda Y, Muramatu R, Streilein JW, Usui M. ACAID Induced by Allogeneic Corneal Tissue Promotes Subsequent Survival of Orthotopic Corneal Grafts. *Investigative Ophthalmology & Visual Science*. 2000;41(3):790-8.
293. Dang Z, Kuffová L, Liu L, Forrester J. Soluble antigen traffics rapidly and selectively from the corneal surface to the eye draining lymph node and activates T cells when codelivered with CpG oligonucleotides. *Journal of leukocyte biology*. 2013;95. doi: 10.1189/jlb.0612294.
294. Streilein JW. Immune regulation and the eye: a dangerous compromise. *Faseb j*. 1987;1(3):199-208. Epub 1987/09/01. PubMed PMID: 2957263.
295. Yang H, Fang G, Huang X, Yu J, Hsieh C-L, Grossniklaus HE. In-vivo xenograft murine human uveal melanoma model develops hepatic micrometastases. *Melanoma Res*. 2008;18(2):95-103. doi: 10.1097/CMR.0b013e3282f628df. PubMed PMID: 18337645.
296. Caspi RR. Ocular autoimmunity: the price of privilege? *Immunological Reviews*. 2006;213(1):23-35. doi: <https://doi.org/10.1111/j.1600-065X.2006.00439.x>.
297. Paglinawan R, Malipiero U, Schlapbach R, Frei K, Reith W, Fontana A. TGFbeta directs gene expression of activated microglia to an anti-inflammatory phenotype strongly focusing on chemokine genes and cell migratory genes. *Glia*. 2003;44(3):219-31. Epub 2003/11/07. doi: 10.1002/glia.10286. PubMed PMID: 14603463.
298. Hubert KE, Davies MH, Stempel AJ, Griffith TS, Powers MR. TRAIL-deficient mice exhibit delayed regression of retinal neovascularization. *Am J Pathol*. 2009;175(6):2697-708. Epub 2009/11/05. doi: 10.2353/ajpath.2009.090099. PubMed PMID: 19893042.
299. Knisely TL, Bleicher PA, Vibbard CA, Granstein RD. Production of latent transforming growth factor-beta and other inhibitory factors by cultured murine iris and ciliary body cells. *Curr Eye Res*. 1991;10(8):761-71. Epub 1991/08/01. doi: 10.3109/02713689109013870. PubMed PMID: 1914508.
300. Liang KJ, Lee JE, Wang YD, Ma W, Fontainhas AM, Fariss RN, et al. Regulation of Dynamic Behavior of Retinal Microglia by CX₃CR₁ Signaling. *Investigative Ophthalmology & Visual Science*. 2009;50(9):4444-51. doi: 10.1167/iovs.08-3357.
301. Okunuki Y, Mukai R, Pearsall EA, Klokman G, Husain D, Park D-H, et al. Microglia inhibit photoreceptor cell death and regulate immune cell infiltration in response to retinal detachment. *Proceedings of the National Academy of Sciences*. 2018;115(27):E6264-E73. doi: 10.1073/pnas.1719601115.
302. Detrick B, Hooks JJ. Immune regulation in the retina. *Immunol Res*. 2010;47(1-3):153-61. Epub 2010/01/19. doi: 10.1007/s12026-009-8146-1. PubMed PMID: 20082152; PubMed Central PMCID: PMC6549130.
303. Al-Ubaidi MR, Naash MI, Conley SM. A perspective on the role of the extracellular matrix in progressive retinal degenerative disorders. *Investigative ophthalmology & visual science*. 2013;54(13):8119-24. doi: 10.1167/iovs.13-13536. PubMed PMID: 24346621.
304. Jha P, Bora PS, Bora NS. The role of complement system in ocular diseases including uveitis and macular degeneration. *Mol Immunol*. 2007;44(16):3901-8. doi: 10.1016/j.molimm.2007.06.145. PubMed PMID: 17768108.

305. Chen M, Luo C, Zhao J, Devarajan G, Xu H. Immune regulation in the aging retina. *Prog Retin Eye Res.* 2019;69:159-72. Epub 2018/10/20. doi: 10.1016/j.preteyeres.2018.10.003. PubMed PMID: 30352305.
306. Tan YL, Yuan Y, Tian L. Microglial regional heterogeneity and its role in the brain. *Mol Psychiatry.* 2020;25(2):351-67. Epub 2019/11/28. doi: 10.1038/s41380-019-0609-8. PubMed PMID: 31772305; PubMed Central PMCID: PMC6974435.
307. Tong CK, Vidyadaran S. Role of microglia in embryonic neurogenesis. *Exp Biol Med (Maywood).* 2016;241(15):1669-75. Epub 2016/08/25. doi: 10.1177/1535370216664430. PubMed PMID: 27555616; PubMed Central PMCID: PMC695495.
308. Butovsky O, Jedrychowski MP, Moore CS, Cialic R, Lanser AJ, Gabriely G, et al. Identification of a Unique TGF- β Dependent Molecular and Functional Signature in Microglia. *Nat Neurosci.* 2014;17(1):131-43. doi: 10.1038/nn.3599. PubMed PMID: 24316888; PubMed Central PMCID: PMC66672.
309. Zhao L, Zabel MK, Wang X, Ma W, Shah P, Fariss RN, et al. Microglial phagocytosis of living photoreceptors contributes to inherited retinal degeneration. *EMBO Mol Med.* 2015;7(9):1179-97. Epub 2015/07/04. doi: 10.15252/emmm.201505298. PubMed PMID: 26139610; PubMed Central PMCID: PMC68951.
310. Hong S, Dissing-Olesen L, Stevens B. New insights on the role of microglia in synaptic pruning in health and disease. *Curr Opin Neurobiol.* 2016;36:128-34. Epub 2016/01/09. doi: 10.1016/j.conb.2015.12.004. PubMed PMID: 26745839; PubMed Central PMCID: PMC68951.
311. Wang C, Yue H, Hu Z, Shen Y, Ma J, Li J, et al. Microglia mediate forgetting via complement-dependent synaptic elimination. *Science.* 2020;367(6478):688-94. doi: 10.1126/science.aaz2288.
312. Lee YS, Amadi-Obi A, Yu CR, Egwuagu CE. Retinal cells suppress intraocular inflammation (uveitis) through production of interleukin-27 and interleukin-10. *Immunology.* 2011;132(4):492-502. Epub 2011/02/08. doi: 10.1111/j.1365-2567.2010.03379.x. PubMed PMID: 21294722; PubMed Central PMCID: PMC68951.
313. Han J, Zhu K, Zhang X-M, Harris RA. Enforced microglial depletion and repopulation as a promising strategy for the treatment of neurological disorders. *Glia.* 2019;67(2):217-31. doi: 10.1002/glia.23529.
314. Dowding AJ, Maggs A, Scholes J. Diversity amongst the microglia in growing and regenerating fish CNS: immunohistochemical characterization using FL1, an anti-macrophage monoclonal antibody. *Glia.* 1991;4(4):345-64. Epub 1991/01/01. doi: 10.1002/glia.440040403. PubMed PMID: 1834558.
315. Magazine HI, Liu Y, Bilfinger TV, Fricchione GL, Stefano GB. Morphine-induced conformational changes in human monocytes, granulocytes, and endothelial cells and in invertebrate immunocytes and microglia are mediated by nitric oxide. *J Immunol.* 1996;156(12):4845-50. Epub 1996/06/15. PubMed PMID: 8648133.
316. Dobrenis K. Microglia in cell culture and in transplantation therapy for central nervous system disease. *Methods.* 1998;16(3):320-44. Epub 1999/03/10. doi: 10.1006/meth.1998.0688. PubMed PMID: 10071070.
317. Bernhardt RV, Nicholls JG. Transformation of leech microglial cell morphology and properties following co-culture with injured central nervous system tissue. *J Exp Biol.* 1999;202 (Pt 6):723-8. Epub 1999/02/18. PubMed PMID: 10021325.
318. Navascues J, Calvente R, Marin-Teva JL, Cuadros MA. Entry, dispersion and differentiation of microglia in the developing central nervous system. *An Acad Bras Cienc.* 2000;72(1):91-102. Epub 2000/08/10. doi: 10.1590/s0001-37652000000100013. PubMed PMID: 10932110.
319. Arab T, Raffo-Romero A, Van Camp C, Lemaire Q, Le Marrec-Croq F, Drago F, et al. Proteomic characterisation of leech microglia extracellular vesicles (EVs): comparison between

- differential ultracentrifugation and Optiprep™ density gradient isolation. *J Extracell Vesicles*. 2019;8(1):1603048. Epub 2019/05/10. doi: 10.1080/20013078.2019.1603048. PubMed PMID: 31069026; PubMed Central PMCID: PMC6493217.
320. Sonetti D, Ottaviani E, Bianchi F, Rodriguez M, Stefano ML, Scharrer B, et al. Microglia in invertebrate ganglia. *Proc Natl Acad Sci U S A*. 1994;91(19):9180-4. Epub 1994/09/13. doi: 10.1073/pnas.91.19.9180. PubMed PMID: 8090788; PubMed Central PMCID: PMC644771.
321. Peterson KJ, Cotton JA, Gehling JG, Pisani D. The Ediacaran emergence of bilaterians: congruence between the genetic and the geological fossil records. *Philos Trans R Soc Lond B Biol Sci*. 2008;363(1496):1435-43. Epub 2008/01/15. doi: 10.1098/rstb.2007.2233. PubMed PMID: 18192191; PubMed Central PMCID: PMC64224.
322. Cannon JT, Vellutini BC, Smith J, Ronquist F, Jondelius U, Hejnol A. Xenacoelomorpha is the sister group to Nephrozoa. *Nature*. 2016;530(7588):89-93. doi: 10.1038/nature16520.
323. Hartenstein V, Giangrande A. Connecting the nervous and the immune systems in evolution. *Communications Biology*. 2018;1(1):64. doi: 10.1038/s42003-018-0070-2.
324. Carniglia L, Ramirez D, Durand D, Saba J, Turati J, Caruso C, et al. Neuropeptides and Microglial Activation in Inflammation, Pain, and Neurodegenerative Diseases. *Mediators Inflamm*. 2017;2017:5048616. Epub 2017/02/06. doi: 10.1155/2017/5048616. PubMed PMID: 28154473; PubMed Central PMCID: PMC644030 publication of this paper.
325. Li Q, Dong C, Li W, Bu W, Wu J, Zhao W. Neuropeptide Y protects cerebral cortical neurons by regulating microglial immune function. *Neural Regen Res*. 2014;9(9):959-67. Epub 2014/09/11. doi: 10.4103/1673-5374.133140. PubMed PMID: 25206918; PubMed Central PMCID: PMC64146213.
326. Suk K. Microglial Signaling Regulation by Neuropeptides. In: Binder MD, Hirokawa N, Windhorst U, editors. *Encyclopedia of Neuroscience*. Berlin, Heidelberg: Springer Berlin Heidelberg; 2009. p. 2358-63.
327. Morara S, Colangelo AM, Provini L. Microglia-Induced Maladaptive Plasticity Can Be Modulated by Neuropeptides In Vivo. *Neural Plasticity*. 2015. doi: Artn 135342 10.1155/2015/135342. PubMed PMID: WOS:000359249500001.
328. Thiel D, Franz-Wachtel M, Aguilera F, Hejnol A. Xenacoelomorph Neuropeptidomes Reveal a Major Expansion of Neuropeptide Systems during Early Bilaterian Evolution. *Molecular Biology and Evolution*. 2018;35(10):2528-43. doi: 10.1093/molbev/msy160.
329. Hejnol A, Pang K. Xenacoelomorpha's significance for understanding bilaterian evolution. *Current Opinion in Genetics & Development*. 2016;39:48-54. doi: <https://doi.org/10.1016/j.gde.2016.05.019>.
330. Matcovitch-Natan O, Winter DR, Giladi A, Vargas Aguilar S, Spinrad A, Sarrazin S, et al. Microglia development follows a stepwise program to regulate brain homeostasis. *Science*. 2016;353(6301):aad8670. doi: 10.1126/science.aad8670.
331. Kumar A, Zhang J, Yu FS. Toll-like receptor 3 agonist poly(I:C)-induced antiviral response in human corneal epithelial cells. *Immunology*. 2006;117(1):11-21. Epub 2006/01/21. doi: 10.1111/j.1365-2567.2005.02258.x. PubMed PMID: 16423036; PubMed Central PMCID: PMC641782193.
332. Meyer U, Nyffeler M, Engler A, Urwyler A, Schedlowski M, Knuesel I, et al. The Time of Prenatal Immune Challenge Determines the Specificity of Inflammation-Mediated Brain and Behavioral Pathology. *The Journal of Neuroscience*. 2006;26(18):4752-62. doi: 10.1523/jneurosci.0099-06.2006.
333. Thion MS, Low D, Silvin A, Chen J, Grisel P, Schulte-Schrepping J, et al. Microbiome Influences Prenatal and Adult Microglia in a Sex-Specific Manner. *Cell*. 2018;172(3):500-16 e16. Epub 2017/12/26. doi: 10.1016/j.cell.2017.11.042. PubMed PMID: 29275859; PubMed Central PMCID: PMC645786503.
334. Erny D, Hrabé de Angelis AL, Jaitin D, Wieghofer P, Staszewski O, David E, et al. Host microbiota constantly control maturation and function of microglia in the CNS. *Nat Neurosci*.

- 2015;18(7):965-77. Epub 2015/06/02. doi: 10.1038/nn.4030. PubMed PMID: 26030851; PubMed Central PMCID: PMC528863.
335. Paolicelli RC, Ferretti MT. Function and Dysfunction of Microglia during Brain Development: Consequences for Synapses and Neural Circuits. *Front Synaptic Neurosci.* 2017;9:9. Epub 2017/05/26. doi: 10.3389/fnsyn.2017.00009. PubMed PMID: 28539882; PubMed Central PMCID: PMC5423952.
336. Geirsdottir L, David E, Keren-Shaul H, Weiner A, Bohlen SC, Neuber J, et al. Cross-Species Single-Cell Analysis Reveals Divergence of the Primate Microglia Program. *Cell.* 2019;179(7):1609-22.e16. doi: <https://doi.org/10.1016/j.cell.2019.11.010>.
337. Yanguas-Casás N. Physiological sex differences in microglia and their relevance in neurological disorders. *Neuroimmunology and Neuroinflammation.* 2020;7:13-22.
338. Kodama L, Gan L. Do Microglial Sex Differences Contribute to Sex Differences in Neurodegenerative Diseases? *Trends Mol Med.* 2019;25(9):741-9. Epub 2019/06/07. doi: 10.1016/j.molmed.2019.05.001. PubMed PMID: 31171460; PubMed Central PMCID: PMC7338035.
339. Norden DM, Muccigrosso MM, Godbout JP. Microglial priming and enhanced reactivity to secondary insult in aging, and traumatic CNS injury, and neurodegenerative disease. *Neuropharmacology.* 2015;96(Pt A):29-41. Epub 2014/12/03. doi: 10.1016/j.neuropharm.2014.10.028. PubMed PMID: 25445485; PubMed Central PMCID: PMC4430467.
340. Keren-Shaul H, Spinrad A, Weiner A, Matcovitch-Natan O, Dvir-Szternfeld R, Ulland TK, et al. A Unique Microglia Type Associated with Restricting Development of Alzheimer's Disease. *Cell.* 2017;169(7):1276-90.e17. Epub 2017/06/13. doi: 10.1016/j.cell.2017.05.018. PubMed PMID: 28602351.
341. O'Koren EG, Yu C, Klingeborn M, Wong AYW, Prigge CL, Mathew R, et al. Microglial Function Is Distinct in Different Anatomical Locations during Retinal Homeostasis and Degeneration. *Immunity.* 2019;50(3):723-37.e7. Epub 2019/03/10. doi: 10.1016/j.immuni.2019.02.007. PubMed PMID: 30850344; PubMed Central PMCID: PMC6592635.
342. Sousa C, Golebiewska A, Poovathingal SK, Kaoma T, Pires-Afonso Y, Martina S, et al. Single-cell transcriptomics reveals distinct inflammation-induced microglia signatures. *EMBO Rep.* 2018;19(11). Epub 2018/09/13. doi: 10.15252/embr.201846171. PubMed PMID: 30206190; PubMed Central PMCID: PMC6216255.
343. Tay TL, Sagar, Dautzenberg J, Grun D, Prinz M. Unique microglia recovery population revealed by single-cell RNAseq following neurodegeneration. *Acta Neuropathol Commun.* 2018;6(1):87. Epub 2018/09/07. doi: 10.1186/s40478-018-0584-3. PubMed PMID: 30185219; PubMed Central PMCID: PMC6123921.
344. Masuda T, Sankowski R, Staszewski O, Prinz M. Microglia Heterogeneity in the Single-Cell Era. *Cell Rep.* 2020;30(5):1271-81. Epub 2020/02/06. doi: 10.1016/j.celrep.2020.01.010. PubMed PMID: 32023447.
345. Cho CE, Damle SS, Wancewicz EV, Mukhopadhyay S, Hart CE, Mazur C, et al. A modular analysis of microglia gene expression, insights into the aged phenotype. *BMC Genomics.* 2019;20(1):164. doi: 10.1186/s12864-019-5549-9.
346. Zhang Y, Chen K, Sloan SA, Bennett ML, Scholze AR, O'Keeffe S, et al. An RNA-sequencing transcriptome and splicing database of glia, neurons, and vascular cells of the cerebral cortex. *J Neurosci.* 2014;34(36):11929-47. Epub 2014/09/05. doi: 10.1523/JNEUROSCI.1860-14.2014. PubMed PMID: 25186741; PubMed Central PMCID: PMC4152602.
347. Beutner C, Linnartz-Gerlach B, Schmidt SV, Beyer M, Mallmann MR, Staratschek-Jox A, et al. Unique transcriptome signature of mouse microglia. *Glia.* 2013;61(9):1429-42. Epub 2013/07/09. doi: 10.1002/glia.22524. PubMed PMID: 23832717.

348. Chiu IM, Morimoto ET, Goodarzi H, Liao JT, O'Keeffe S, Phatnani HP, et al. A neurodegeneration-specific gene-expression signature of acutely isolated microglia from an amyotrophic lateral sclerosis mouse model. *Cell Rep.* 2013;4(2):385-401. Epub 2013/07/16. doi: 10.1016/j.celrep.2013.06.018. PubMed PMID: 23850290; PubMed Central PMCID: PMC4272581.
349. Hickman SE, Kingery ND, Ohsumi TK, Borowsky ML, Wang LC, Means TK, et al. The microglial sensome revealed by direct RNA sequencing. *Nat Neurosci.* 2013;16(12):1896-905. Epub 2013/10/29. doi: 10.1038/nn.3554. PubMed PMID: 24162652; PubMed Central PMCID: PMC40123.
350. Zeisel A, Muñoz-Manchado AB, Codeluppi S, Lönnerberg P, La Manno G, Juréus A, et al. Cell types in the mouse cortex and hippocampus revealed by single-cell RNA-seq. *Science.* 2015;347(6226):1138-42. doi: 10.1126/science.aaa1934.
351. Haage V, Semtner M, Vidal RO, Hernandez DP, Pong WW, Chen Z, et al. Comprehensive gene expression meta-analysis identifies signature genes that distinguish microglia from peripheral monocytes/macrophages in health and glioma. *Acta Neuropathologica Communications.* 2019;7(1):20. doi: 10.1186/s40478-019-0665-y.
352. Zrzavy T, Hametner S, Wimmer I, Butovsky O, Weiner HL, Lassmann H. Loss of 'homeostatic' microglia and patterns of their activation in active multiple sclerosis. *Brain.* 2017;140(7):1900-13. Epub 2017/05/26. doi: 10.1093/brain/awx113. PubMed PMID: 28541408.
353. Krasemann S, Madore C, Cialic R, Baufeld C, Calcagno N, El Fatimy R, et al. The TREM2-APOE Pathway Drives the Transcriptional Phenotype of Dysfunctional Microglia in Neurodegenerative Diseases. *Immunity.* 2017;47(3):566-81.e9. Epub 2017/09/21. doi: 10.1016/j.immuni.2017.08.008. PubMed PMID: 28930663; PubMed Central PMCID: PMC5719893.
354. DePaula-Silva AB, Gorbea C, Doty DJ, Libbey JE, Sanchez JMS, Hanak TJ, et al. Differential transcriptional profiles identify microglial- and macrophage-specific gene markers expressed during virus-induced neuroinflammation. *Journal of Neuroinflammation.* 2019;16(1):152. doi: 10.1186/s12974-019-1545-x.
355. Reed-Geaghan EG, Croxford AL, Becher B, Landreth GE. Plaque-associated myeloid cells derive from resident microglia in an Alzheimer's disease model. *J Exp Med.* 2020;217(4). Epub 2020/01/23. doi: 10.1084/jem.20191374. PubMed PMID: 31967645.
356. Song W, Hooli B, Mullin K, Jin SC, Cella M, Ulland TK, et al. Alzheimer's disease-associated TREM2 variants exhibit either decreased or increased ligand-dependent activation. *Alzheimer's & Dementia.* 2017;13(4):381-7. doi: <https://doi.org/10.1016/j.jalz.2016.07.004>.
357. Mathys H, Adaiக்கan C, Gao F, Young JZ, Manet E, Hemberg M, et al. Temporal Tracking of Microglia Activation in Neurodegeneration at Single-Cell Resolution. *Cell Rep.* 2017;21(2):366-80. Epub 2017/10/12. doi: 10.1016/j.celrep.2017.09.039. PubMed PMID: 29020624; PubMed Central PMCID: PMC5642107.
358. Davis AA, Inman CE, Wargel ZM, Dube U, Freeberg BM, Galluppi A, et al. APOE genotype regulates pathology and disease progression in synucleinopathy. *Sci Transl Med.* 2020;12(529). Epub 2020/02/07. doi: 10.1126/scitranslmed.aay3069. PubMed PMID: 32024799.
359. Huynh TV, Davis AA, Ulrich JD, Holtzman DM. Apolipoprotein E and Alzheimer's disease: the influence of apolipoprotein E on amyloid-beta and other amyloidogenic proteins. *J Lipid Res.* 2017;58(5):824-36. Epub 2017/03/02. doi: 10.1194/jlr.R075481. PubMed PMID: 28246336; PubMed Central PMCID: PMC5408619.
360. Marschallinger J, Iram T, Zardeneta M, Lee SE, Lehallier B, Haney MS, et al. Lipid-droplet-accumulating microglia represent a dysfunctional and proinflammatory state in the aging brain. *Nature Neuroscience.* 2020. doi: 10.1038/s41593-019-0566-1.
361. Huang Y, Mahley RW. Apolipoprotein E: structure and function in lipid metabolism, neurobiology, and Alzheimer's diseases. *Neurobiol Dis.* 2014;72 Pt A:3-12. Epub 2014/09/01. doi:

- 10.1016/j.nbd.2014.08.025. PubMed PMID: 25173806; PubMed Central PMCID: PMCPMC4253862.
362. Guram K, Kim SS, Wu V, Sanders PD, Patel S, Schoenberger SP, et al. A Threshold Model for T-Cell Activation in the Era of Checkpoint Blockade Immunotherapy. *Front Immunol.* 2019;10:491. Epub 2019/04/03. doi: 10.3389/fimmu.2019.00491. PubMed PMID: 30936880; PubMed Central PMCID: PMCPMC6431643.
363. Perry VH, Teeling J. Microglia and macrophages of the central nervous system: the contribution of microglia priming and systemic inflammation to chronic neurodegeneration. *Semin Immunopathol.* 2013;35(5):601-12. Epub 2013/06/05. doi: 10.1007/s00281-013-0382-8. PubMed PMID: 23732506; PubMed Central PMCID: PMCPMC3742955.
364. Nugent AA, Lin K, van Lengerich B, Lianoglou S, Przybyla L, Davis SS, et al. TREM2 Regulates Microglial Cholesterol Metabolism upon Chronic Phagocytic Challenge. *Neuron.* 2019. Epub 2020/01/07. doi: 10.1016/j.neuron.2019.12.007. PubMed PMID: 31902528.
365. Roy ER, Wang B, Wan YW, Chiu GS, Cole AL, Yin Z, et al. Type I interferon response drives neuroinflammation and synapse loss in Alzheimer disease. *J Clin Invest.* 2020. Epub 2020/01/10. doi: 10.1172/jci133737. PubMed PMID: 31917687.
366. Hernandez MX, Jiang S, Cole TA, Chu SH, Fonseca MI, Fang MJ, et al. Prevention of C5aR1 signaling delays microglial inflammatory polarization, favors clearance pathways and suppresses cognitive loss. *Mol Neurodegener.* 2017;12(1):66. Epub 2017/09/20. doi: 10.1186/s13024-017-0210-z. PubMed PMID: 28923083; PubMed Central PMCID: PMCPMC5604420.
367. Geerlings MJ, de Jong EK, den Hollander AI. The complement system in age-related macular degeneration: A review of rare genetic variants and implications for personalized treatment. *Mol Immunol.* 2017;84:65-76. Epub 2016/12/13. doi: 10.1016/j.molimm.2016.11.016. PubMed PMID: 27939104; PubMed Central PMCID: PMCPMC5380947.
368. Huang Z, Zhou T, Sun X, Zheng Y, Cheng B, Li M, et al. Necroptosis in microglia contributes to neuroinflammation and retinal degeneration through TLR4 activation. *Cell death and differentiation.* 2018;25(1):180.
369. Zeng H-y, Zhu X-a, Zhang C, Yang L-P, Wu L-m, Tso MO. Identification of sequential events and factors associated with microglial activation, migration, and cytotoxicity in retinal degeneration in rd mice. *Investigative ophthalmology & visual science.* 2005;46(8):2992-9.
370. Hawes NL, Chang B, Hageman GS, Nusinowitz S, Nishina PM, Schneider BS, et al. Retinal degeneration 6 (rd6): a new mouse model for human retinitis punctata albescens. *Investigative ophthalmology & visual science.* 2000;41(10):3149-57.
371. Li T, Aredo B, Chen X, Zhang K, Ufret-Vincenty R. Change in the Distribution and Phenotype of Subretinal Microglia in C57BL/6J and RD8 Mutant Mice with Aging. *Investigative Ophthalmology & Visual Science.* 2014;55(13):81-.
372. Tuo J, Smith BC, Bojanowski CM, Meleth AD, Gery I, Csaky KG, et al. The involvement of sequence variation and expression of CX3CR1 in the pathogenesis of age-related macular degeneration. *The FASEB Journal.* 2004;18(11):1297-9.
373. Di Pierdomenico J, García-Ayuso D, Agudo-Barriuso M, Vidal-Sanz M, Villegas-Pérez MP. Role of microglial cells in photoreceptor degeneration. *Neural regeneration research.* 2019;14(7):1186.
374. Zeng H, Ding M, Chen X-X, Lu Q. Microglial NADPH oxidase activation mediates rod cell death in the retinal degeneration in rd mice. *Neuroscience.* 2014;275:54-61.
375. Appelbaum T, Santana E, Aguirre GD. Strong upregulation of inflammatory genes accompanies photoreceptor demise in canine models of retinal degeneration. *PLOS ONE.* 2017;12(5):e0177224. doi: 10.1371/journal.pone.0177224.
376. Goldmann T, Wieghofer P, Muller PF, Wolf Y, Varol D, Yona S, et al. A new type of microglia gene targeting shows TAK1 to be pivotal in CNS autoimmune inflammation. *Nat Neurosci.* 2013;16(11):1618-26. Epub 2013/10/01. doi: 10.1038/nn.3531. PubMed PMID: 24077561.

377. Mathew NR, Vinnakota JM, Apostolova P, Erny D, Hamarsheh S, Andrieux G, et al. Graft-versus-host disease of the CNS is mediated by TNF upregulation in microglia. *The Journal of Clinical Investigation*. 2020;130(3). doi: 10.1172/JCI130272.
378. Walker FR, Beynon SB, Jones KA, Zhao Z, Kongsui R, Cairns M, et al. Dynamic structural remodelling of microglia in health and disease: a review of the models, the signals and the mechanisms. *Brain Behav Immun*. 2014;37:1-14. Epub 2014/01/15. doi: 10.1016/j.bbi.2013.12.010. PubMed PMID: 24412599.
379. York EM, LeDue JM, Bernier LP, MacVicar BA. 3DMorph Automatic Analysis of Microglial Morphology in Three Dimensions from Ex Vivo and In Vivo Imaging. *eNeuro*. 2018;5(6). Epub 2019/01/11. doi: 10.1523/ENEURO.0266-18.2018. PubMed PMID: 30627639; PubMed Central PMCID: PMC6325541.
380. Davis BM, Salinas-Navarro M, Cordeiro MF, Moons L, De Groef L. Characterizing microglia activation: a spatial statistics approach to maximize information extraction. *Sci Rep*. 2017;7(1):1576. Epub 2017/05/10. doi: 10.1038/s41598-017-01747-8. PubMed PMID: 28484229; PubMed Central PMCID: PMC631479.
381. O'Neill K, Akum B, Dhawan S, Kwon M, Langhammer C, Firestein B. Assessing effects on dendritic arborization using novel Sholl analyses. *Frontiers in Cellular Neuroscience*. 2015;9(285). doi: 10.3389/fncel.2015.00285.
382. Plotnick RE, Gardner RH, O'Neill RV. Lacunarity indices as measures of landscape texture. *Landscape Ecology*. 1993;8(3):201-11. doi: 10.1007/BF00125351.
383. Landini G, Murray PI, Misson GP. Local connected fractal dimensions and lacunarity analyses of 60 degrees fluorescein angiograms. *Investigative ophthalmology & visual science*. 1995;36(13):2749-55.
384. Smith TG, Jr., Lange GD, Marks WB. Fractal methods and results in cellular morphology-dimensions, lacunarity and multifractals. *J Neurosci Methods*. 1996;69(2):123-36. Epub 1996/11/01. doi: 10.1016/s0165-0270(96)00080-5. PubMed PMID: 8946315.
385. Young K, Morrison H. Quantifying Microglia Morphology from Photomicrographs of Immunohistochemistry Prepared Tissue Using ImageJ. *J Vis Exp*. 2018;(136). Epub 2018/06/26. doi: 10.3791/57648. PubMed PMID: 29939190; PubMed Central PMCID: PMC6103256.
386. Morrison HW, Filosa JA. A quantitative spatiotemporal analysis of microglia morphology during ischemic stroke and reperfusion. *J Neuroinflammation*. 2013;10:4. Epub 2013/01/15. doi: 10.1186/1742-2094-10-4. PubMed PMID: 2331642; PubMed Central PMCID: PMC3570327.
387. Verdonk F, Roux P, Flamant P, Fiette L, Bozza FA, Simard S, et al. Phenotypic clustering: a novel method for microglial morphology analysis. *J Neuroinflammation*. 2016;13(1):153. Epub 2016/06/19. doi: 10.1186/s12974-016-0614-7. PubMed PMID: 27317566; PubMed Central PMCID: PMC4912769.
388. Heindl S, Gesierich B, Benakis C, Llovera G, Duering M, Liesz A. Automated Morphological Analysis of Microglia After Stroke. *Front Cell Neurosci*. 2018;12:106. Epub 2018/05/05. doi: 10.3389/fncel.2018.00106. PubMed PMID: 29725290; PubMed Central PMCID: PMC5917008.
389. Nakamichi Y, Udagawa N, Takahashi N. IL-34 and CSF-1: similarities and differences. *Journal of Bone and Mineral Metabolism*. 2013;31(5):486-95. doi: 10.1007/s00774-013-0476-3.
390. Okunuki Y, Mukai R, Nakao T, Tabor SJ, Butovsky O, Dana R, et al. Retinal microglia initiate neuroinflammation in ocular autoimmunity. *Proc Natl Acad Sci U S A*. 2019;116(20):9989-98. Epub 2019/04/27. doi: 10.1073/pnas.1820387116. PubMed PMID: 31023885; PubMed Central PMCID: PMC6525481.
391. Ip WKE, Hoshi N, Shouval DS, Snapper S, Medzhitov R. Anti-inflammatory effect of IL-10 mediated by metabolic reprogramming of macrophages. *Science*. 2017;356(6337):513-9. Epub 2017/05/06. doi: 10.1126/science.aal3535. PubMed PMID: 28473584; PubMed Central PMCID: PMC6260791.

392. Iyer SS, Cheng G. Role of interleukin 10 transcriptional regulation in inflammation and autoimmune disease. *Crit Rev Immunol*. 2012;32(1):23-63. Epub 2012/03/21. doi: 10.1615/critrevimmunol.v32.i1.30. PubMed PMID: 22428854; PubMed Central PMCID: PMCPMC3410706.
393. Silverman SM, Wong WT. Microglia in the Retina: Roles in Development, Maturity, and Disease. *Annual Review of Vision Science*. 2018;4(1):45-77. doi: 10.1146/annurev-vision-091517-034425. PubMed PMID: 29852094.
394. Mohebiany AN, Ramphal NS, Karram K, Di Liberto G, Novkovic T, Klein M, et al. Microglial A20 Protects the Brain from CD8 T-Cell-Mediated Immunopathology. *Cell Rep*. 2020;30(5):1585-97 e6. Epub 2020/02/06. doi: 10.1016/j.celrep.2019.12.097. PubMed PMID: 32023471.
395. Deczkowska A, Amit I, Schwartz M. Microglial immune checkpoint mechanisms. *Nat Neurosci*. 2018;21(6):779-86. Epub 2018/05/08. doi: 10.1038/s41593-018-0145-x. PubMed PMID: 29735982.
396. Montarolo F, Perga S, Tessarolo C, Spadaro M, Martire S, Bertolotto A. TNFAIP3 Deficiency Affects Monocytes, Monocytes-Derived Cells and Microglia in Mice. *Int J Mol Sci*. 2020;21(8). Epub 2020/04/25. doi: 10.3390/ijms21082830. PubMed PMID: 32325694; PubMed Central PMCID: PMCPMC7215837.
397. Dick AD, Ford AL, Forrester JV, Sedgwick JD. Flow cytometric identification of a minority population of MHC class II positive cells in the normal rat retina distinct from CD45^{low}CD11b/c+CD4^{low} parenchymal microglia. *Br J Ophthalmol*. 1995;79(9):834-40. PubMed PMID: 7488603; PubMed Central PMCID: PMCPMC505270.
398. Rao NA, Kimoto T, Zamir E, Giri R, Wang R, Ito S, et al. Pathogenic role of retinal microglia in experimental uveoretinitis. *Invest Ophthalmol Vis Sci*. 2003;44(1):22-31. Epub 2002/12/31. PubMed PMID: 12506051.
399. Saraswathy S, Rao NA. Photoreceptor mitochondrial oxidative stress in experimental autoimmune uveitis. *Ophthalmic Res*. 2008;40(3-4):160-4. Epub 2008/04/19. doi: 10.1159/000119869. PubMed PMID: 18421232.
400. Khera TK, Copland DA, Boldison J, Lait PJ, Szymkowski DE, Dick AD, et al. Tumour necrosis factor-mediated macrophage activation in the target organ is critical for clinical manifestation of uveitis. *Clin Exp Immunol*. 2012;168(2):165-77. Epub 2012/04/05. doi: 10.1111/j.1365-2249.2012.04567.x. PubMed PMID: 22471277; PubMed Central PMCID: PMCPMC3390517.
401. Fernandez-Arjona MDM, Grondona JM, Granados-Duran P, Fernandez-Llebrez P, Lopez-Avalos MD. Microglia Morphological Categorization in a Rat Model of Neuroinflammation by Hierarchical Cluster and Principal Components Analysis. *Front Cell Neurosci*. 2017;11:235. Epub 2017/08/30. doi: 10.3389/fncel.2017.00235. PubMed PMID: 28848398; PubMed Central PMCID: PMCPMC5550745.
402. Broderick C, Hoek RM, Forrester JV, Liversidge J, Sedgwick JD, Dick AD. Constitutive retinal CD200 expression regulates resident microglia and activation state of inflammatory cells during experimental autoimmune uveoretinitis. *Am J Pathol*. 2002;161(5):1669-77. Epub 2002/11/05. doi: 10.1016/S0002-9440(10)64444-6. PubMed PMID: 12414514; PubMed Central PMCID: PMCPMC1850781.
403. Raouf R, van der Vlist M, Willemsen HLDM, Prado J, Versteeg S, Vos M, et al. Macrophages transfer mitochondria to sensory neurons to resolve inflammatory pain. *bioRxiv*. 2020:2020.02.12.940445. doi: 10.1101/2020.02.12.940445.
404. Dagkalis A, Wallace C, Hing B, Liversidge J, Crane IJ. CX3CR1-deficiency is associated with increased severity of disease in experimental autoimmune uveitis. *Immunology*. 2009;128(1):25-33. Epub 2009/08/20. doi: 10.1111/j.1365-2567.2009.03046.x. PubMed PMID: 19689733; PubMed Central PMCID: PMCPMC2747136.

405. Diveu C, McGeachy MJ, Boniface K, Stumhofer JS, Sathe M, Joyce-Shaikh B, et al. IL-27 blocks ROR γ c expression to inhibit lineage commitment of Th17 cells. *J Immunol.* 2009;182(9):5748-56. Epub 2009/04/22. doi: 10.4049/jimmunol.0801162. PubMed PMID: 19380822.
406. Amadi-Obi A, Yu CR, Liu X, Mahdi RM, Clarke GL, Nussenblatt RB, et al. TH17 cells contribute to uveitis and scleritis and are expanded by IL-2 and inhibited by IL-27/STAT1. *Nat Med.* 2007;13(6):711-8. Epub 2007/05/15. doi: 10.1038/nm1585. PubMed PMID: 17496900.
407. Downs-Canner S, Berkey S, Delgoffe GM, Edwards RP, Curiel T, Odunsi K, et al. Suppressive IL-17A(+)Foxp3(+) and ex-Th17 IL-17A(neg)Foxp3(+) Treg cells are a source of tumour-associated Treg cells. *Nat Commun.* 2017;8:14649. Epub 2017/03/16. doi: 10.1038/ncomms14649. PubMed PMID: 28290453; PubMed Central PMCID: PMC5355894.
408. Zielinski CE, Mele F, Aschenbrenner D, Jarrossay D, Ronchi F, Gattorno M, et al. Pathogen-induced human TH17 cells produce IFN-gamma or IL-10 and are regulated by IL-1beta. *Nature.* 2012;484(7395):514-8. Epub 2012/04/03. doi: 10.1038/nature10957. PubMed PMID: 22466287.
409. Wan CK, He C, Sun L, Ekwuagu CE, Leonard WJ. Interleukin-1 Receptor Signaling is Critical for the Development of Autoimmune Uveitis. *J Immunol.* 2016;196(2):543-6. doi: 10.4049/jimmunol.1502080. PubMed PMID: 26643477; PubMed Central PMCID: PMC4707108.
410. Batten M, Li J, Yi S, Kljavin NM, Danilenko DM, Lucas S, et al. Interleukin 27 limits autoimmune encephalomyelitis by suppressing the development of interleukin 17-producing T cells. *Nat Immunol.* 2006;7(9):929-36. Epub 2006/08/15. doi: 10.1038/ni1375. PubMed PMID: 16906167.
411. Epps SJ, Coplin N, Luthert PJ, Dick AD, Coupland SE, Nicholson LB. Features of ectopic lymphoid-like structures in human uveitis. *Experimental eye research.* 2020;191:107901. Epub 2019/12/27. doi: 10.1016/j.exer.2019.107901. PubMed PMID: 31877281; PubMed Central PMCID: PMC7029346.
412. Kokona D, Ebnetter A, Escher P, Zinkernagel MS. Colony-stimulating factor 1 receptor inhibition prevents disruption of the blood-retina barrier during chronic inflammation. *J Neuroinflammation.* 2018;15(1):340. Epub 2018/12/14. doi: 10.1186/s12974-018-1373-4. PubMed PMID: 30541565; PubMed Central PMCID: PMC6292111.
413. McPherson SW, Heuss ND, Lehmann U, Roehrich H, Abedin M, Gregerson DS. The retinal environment induces microglia-like properties in recruited myeloid cells. *J Neuroinflammation.* 2019;16(1):151. Epub 2019/07/22. doi: 10.1186/s12974-019-1546-9. PubMed PMID: 31325968; PubMed Central PMCID: PMC6642741.
414. Gosselin D, Skola D, Coufal NG, Holtman IR, Schlachetzki JCM, Sajti E, et al. An environment-dependent transcriptional network specifies human microglia identity. *Science.* 2017;356(6344). Epub 2017/05/27. doi: 10.1126/science.aal3222. PubMed PMID: 28546318; PubMed Central PMCID: PMC5858585.
415. Muller A, Brandenburg S, Turkowski K, Muller S, Vajkoczy P. Resident microglia, and not peripheral macrophages, are the main source of brain tumor mononuclear cells. *Int J Cancer.* 2015;137(2):278-88. Epub 2014/12/06. doi: 10.1002/ijc.29379. PubMed PMID: 25477239.
416. Moravan MJ, Olschowka JA, Williams JP, O'Banion MK. Brain radiation injury leads to a dose- and time-dependent recruitment of peripheral myeloid cells that depends on CCR2 signaling. *J Neuroinflammation.* 2016;13:30. Epub 2016/02/05. doi: 10.1186/s12974-016-0496-8. PubMed PMID: 26842770; PubMed Central PMCID: PMC4738790.
417. Cronk JC, Filiano AJ, Louveau A, Marin I, Marsh R, Ji E, et al. Peripherally derived macrophages can engraft the brain independent of irradiation and maintain an identity distinct from microglia. *J Exp Med.* 2018;215(6):1627-47. Epub 2018/04/13. doi: 10.1084/jem.20180247. PubMed PMID: 29643186; PubMed Central PMCID: PMC5987928.

418. Benoist C, Lanier L, Merad M, Mathis D, Immunological Genome P. Consortium biology in immunology: the perspective from the Immunological Genome Project. *Nat Rev Immunol*. 2012;12(10):734-40. Epub 2012/09/08. doi: 10.1038/nri3300. PubMed PMID: 22955842.
419. Bruttger J, Karram K, Wortge S, Regen T, Marini F, Hoppmann N, et al. Genetic Cell Ablation Reveals Clusters of Local Self-Renewing Microglia in the Mammalian Central Nervous System. *Immunity*. 2015;43(1):92-106. Epub 2015/07/15. doi: 10.1016/j.immuni.2015.06.012. PubMed PMID: 26163371.
420. Elmore MRP, Najafi AR, Koike MA, Dagher NN, Spangenberg EE, Rice RA, et al. Colony-stimulating factor 1 receptor signaling is necessary for microglia viability, unmasking a microglia progenitor cell in the adult brain. *Neuron*. 2014;82(2):380-97. doi: 10.1016/j.neuron.2014.02.040. PubMed PMID: 24742461.
421. Murphy JR. Mechanism of diphtheria toxin catalytic domain delivery to the eukaryotic cell cytosol and the cellular factors that directly participate in the process. *Toxins (Basel)*. 2011;3(3):294-308. Epub 2011/11/10. doi: 10.3390/toxins3030294. PubMed PMID: 22069710; PubMed Central PMCID: PMC3202816.
422. Satoh J, Kino Y, Asahina N, Takitani M, Miyoshi J, Ishida T, et al. TMEM119 marks a subset of microglia in the human brain. *Neuropathology*. 2016;36(1):39-49. Epub 2015/08/08. doi: 10.1111/neup.12235. PubMed PMID: 26250788.
423. Paschalis EI, Lei F, Zhou C, Kapoulea V, Dana R, Chodosh J, et al. Permanent neuroglial remodeling of the retina following infiltration of CSF1R inhibition-resistant peripheral monocytes. *Proc Natl Acad Sci U S A*. 2018;115(48):E11359-E68. Epub 2018/11/18. doi: 10.1073/pnas.1807123115. PubMed PMID: 30442669; PubMed Central PMCID: PMC6275537.
424. Zhao L CVJ, Liao J, Wong WT., editor *Microglia Repopulation Ameliorates Aging Phenotypes in Retinal Microglia and Neurons*. Association for Research in Vision and Ophthalmology 2019 Annual Meeting; 2019 30/04/2019; Vancouver, Canada.
425. Willis EF, MacDonald KPA, Nguyen QH, Garrido AL, Gillespie ER, Harley SBR, et al. Repopulating Microglia Promote Brain Repair in an IL-6-Dependent Manner. *Cell*. 2020;180(5):833-46.e16. Epub 2020/03/07. doi: 10.1016/j.cell.2020.02.013. PubMed PMID: 32142677.
426. Bennett FC, Bennett ML, Yaqoob F, Mulinyawe SB, Grant GA, Hayden Gephart M, et al. A Combination of Ontogeny and CNS Environment Establishes Microglial Identity. *Neuron*. 2018;98(6):1170-83 e8. Epub 2018/06/05. doi: 10.1016/j.neuron.2018.05.014. PubMed PMID: 29861285; PubMed Central PMCID: PMC6023731.
427. Shemer A, Grozovski J, Tay TL, Tao J, Volaski A, Suss P, et al. Engrafted parenchymal brain macrophages differ from microglia in transcriptome, chromatin landscape and response to challenge. *Nat Commun*. 2018;9(1):5206. Epub 2018/12/13. doi: 10.1038/s41467-018-07548-5. PubMed PMID: 30523248; PubMed Central PMCID: PMC6284018.
428. Wang Z, Gerstein M, Snyder M. RNA-Seq: a revolutionary tool for transcriptomics. *Nat Rev Genet*. 2009;10(1):57-63. Epub 2008/11/19. doi: 10.1038/nrg2484. PubMed PMID: 19015660; PubMed Central PMCID: PMC2949280.
429. Jung S, Aliberti J, Graemmel P, Sunshine MJ, Kreutzberg GW, Sher A, et al. Analysis of fractalkine receptor CX₃CR₁ function by targeted deletion and green fluorescent protein reporter gene insertion. *Mol Cell Biol*. 2000;20(11):4106-14. Epub 2000/05/11. PubMed PMID: 10805752; PubMed Central PMCID: PMC685780.
430. Loven J, Orlando DA, Sigova AA, Lin CY, Rahl PB, Burge CB, et al. Revisiting global gene expression analysis. *Cell*. 2012;151(3):476-82. Epub 2012/10/30. doi: 10.1016/j.cell.2012.10.012. PubMed PMID: 23101621; PubMed Central PMCID: PMC350597.
431. Jung J, Jung H. Methods to analyze cell type-specific gene expression profiles from heterogeneous cell populations. *Animal Cells and Systems*. 2016;20(3):113-7. doi: 10.1080/19768354.2016.1191544.

432. Morrison JA, Box AC, McKinney MC, McLennan R, Kulesa PM. Quantitative single cell gene expression profiling in the avian embryo. *Dev Dyn.* 2015;244(6):774-84. Epub 2015/03/27. doi: 10.1002/dvdy.24274. PubMed PMID: 25809747.
433. Grutzkau A, Radbruch A. Small but mighty: how the MACS-technology based on nanosized superparamagnetic particles has helped to analyze the immune system within the last 20 years. *Cytometry A.* 2010;77(7):643-7. Epub 2010/06/29. doi: 10.1002/cyto.a.20918. PubMed PMID: 20583279.
434. Fong CY, Peh GS, Gauthaman K, Bongso A. Separation of SSEA-4 and TRA-1-60 labelled undifferentiated human embryonic stem cells from a heterogeneous cell population using magnetic-activated cell sorting (MACS) and fluorescence-activated cell sorting (FACS). *Stem Cell Rev Rep.* 2009;5(1):72-80. Epub 2009/02/03. doi: 10.1007/s12015-009-9054-4. PubMed PMID: 19184635.
435. Yan H, Ding CG, Tian PX, Ge GQ, Jin ZK, Jia LN, et al. Magnetic cell sorting and flow cytometry sorting methods for the isolation and function analysis of mouse CD4+ CD25+ Treg cells. *J Zhejiang Univ Sci B.* 2009;10(12):928-32. Epub 2009/12/01. doi: 10.1631/jzus.B0920205. PubMed PMID: 19946957; PubMed Central PMCID: PMCPMC2789528.
436. Zhao S, Zhang Y, Gamini R, Zhang B, von Schack D. Evaluation of two main RNA-seq approaches for gene quantification in clinical RNA sequencing: polyA+ selection versus rRNA depletion. *Scientific Reports.* 2018;8(1):4781. doi: 10.1038/s41598-018-23226-4.
437. Chauhan A, Sharma JN, Modgil M, Siddappa S. Comparison of various RNA extraction methods, cDNA preparation and isolation of calmodulin gene from a highly melanized isolate of apple leaf blotch fungus *Marssonina coronaria*. *J Microbiol Methods.* 2018;151:7-15. Epub 2018/06/02. doi: 10.1016/j.mimet.2018.05.023. PubMed PMID: 29857016.
438. Zhao W, He X, Hoadley KA, Parker JS, Hayes DN, Perou CM. Comparison of RNA-Seq by poly (A) capture, ribosomal RNA depletion, and DNA microarray for expression profiling. *BMC Genomics.* 2014;15(1):419. doi: 10.1186/1471-2164-15-419.
439. Costa C, Giménez-Capitán A, Karachaliou N, Rosell R. Comprehensive molecular screening: from the RT-PCR to the RNA-seq. *Transl Lung Cancer Res.* 2013;2(2):87-91. Epub 2013/04/01. doi: 10.3978/j.issn.2218-6751.2013.02.05. PubMed PMID: 25806219; PubMed Central PMCID: PMCPMC4369859.
440. Schroeder A, Mueller O, Stocker S, Salowsky R, Leiber M, Gassmann M, et al. The RIN: an RNA integrity number for assigning integrity values to RNA measurements. *BMC Molecular Biology.* 2006;7(1):3. doi: 10.1186/1471-2199-7-3.
441. Picelli S, Bjorklund AK, Faridani OR, Sagasser S, Winberg G, Sandberg R. Smart-seq2 for sensitive full-length transcriptome profiling in single cells. *Nat Methods.* 2013;10(11):1096-8. Epub 2013/09/24. doi: 10.1038/nmeth.2639. PubMed PMID: 24056875.
442. Hashimshony T, Wagner F, Sher N, Yanai I. CEL-Seq: single-cell RNA-Seq by multiplexed linear amplification. *Cell Rep.* 2012;2(3):666-73. Epub 2012/09/04. doi: 10.1016/j.celrep.2012.08.003. PubMed PMID: 22939981.
443. Robin JD, Ludlow AT, LaRanger R, Wright WE, Shay JW. Comparison of DNA Quantification Methods for Next Generation Sequencing. *Sci Rep.* 2016;6:24067. Epub 2016/04/07. doi: 10.1038/srep24067. PubMed PMID: 27048884; PubMed Central PMCID: PMCPMC4822169.
444. Lahens NF, Ricciotti E, Smirnova O, Toorens E, Kim EJ, Baruzzo G, et al. A comparison of Illumina and Ion Torrent sequencing platforms in the context of differential gene expression. *BMC Genomics.* 2017;18(1):602. doi: 10.1186/s12864-017-4011-0.
445. Conesa A, Madrigal P, Tarazona S, Gomez-Cabrero D, Cervera A, McPherson A, et al. A survey of best practices for RNA-seq data analysis. *Genome Biol.* 2016;17:13. Epub 2016/01/28. doi: 10.1186/s13059-016-0881-8. PubMed PMID: 26813401; PubMed Central PMCID: PMCPMC4728800.

446. Gentleman RC, Carey VJ, Bates DM, Bolstad B, Dettling M, Dudoit S, et al. Bioconductor: open software development for computational biology and bioinformatics. *Genome Biol.* 2004;5(10):R80. Epub 2004/10/06. doi: 10.1186/gb-2004-5-10-r80. PubMed PMID: 15461798; PubMed Central PMCID: PMCPMC545600.
447. Huber W, Carey VJ, Gentleman R, Anders S, Carlson M, Carvalho BS, et al. Orchestrating high-throughput genomic analysis with Bioconductor. *Nature Methods.* 2015;12(2):115-21. doi: 10.1038/nmeth.3252.
448. Babraham Institute Bioinformatics Group. Babraham Bioinformatics [10/01/2020]. Available from: <https://www.bioinformatics.babraham.ac.uk/index.html>.
449. The Broad Institute. Data, Software and Tools [10/01/2020]. Available from: <https://www.broadinstitute.org/data-software-and-tools>.
450. Rodriguez-Tomé P, Stoehr PJ, Cameron GN, Flores TP. The European Bioinformatics Institute (EBI) databases. *Nucleic Acids Research.* 1996;24(1):6-12. doi: 10.1093/nar/24.1.6.
451. The European Bioinformatics Institute. EMBL-EBI [10/01/2020]. Available from: <https://www.ebi.ac.uk/>.
452. Huang DW, Sherman BT, Tan Q, Collins JR, Alvord WG, Roayaei J, et al. The DAVID Gene Functional Classification Tool: a novel biological module-centric algorithm to functionally analyze large gene lists. *Genome Biol.* 2007;8(9):R183. Epub 2007/09/06. doi: 10.1186/gb-2007-8-9-r183. PubMed PMID: 17784955; PubMed Central PMCID: PMCPMC2375021.
453. Huang da W, Sherman BT, Lempicki RA. Systematic and integrative analysis of large gene lists using DAVID bioinformatics resources. *Nat Protoc.* 2009;4(1):44-57. Epub 2009/01/10. doi: 10.1038/nprot.2008.211. PubMed PMID: 19131956.
454. Coordinators NR. Database resources of the National Center for Biotechnology Information. *Nucleic Acids Research.* 2015;44(D1):D7-D19. doi: 10.1093/nar/gkv1290.
455. Bult CJ, Blake JA, Smith CL, Kadin JA, Richardson JE. Mouse Genome Database (MGD) 2019. *Nucleic Acids Res.* 2019;47(D1):D801-d6. Epub 2018/11/09. doi: 10.1093/nar/gky1056. PubMed PMID: 30407599; PubMed Central PMCID: PMCPMC6323923.
456. Smith CM, Hayamizu TF, Finger JH, Bello SM, McCright IJ, Xu J, et al. The mouse Gene Expression Database (GXD): 2019 update. *Nucleic Acids Res.* 2019;47(D1):D774-d9. Epub 2018/10/20. doi: 10.1093/nar/gky922. PubMed PMID: 30335138; PubMed Central PMCID: PMCPMC6324054.
457. Zerbino DR, Achuthan P, Akanni W, Amode M R, Barrell D, Bhai J, et al. Ensembl 2018. *Nucleic Acids Research.* 2017;46(D1):D754-D61. doi: 10.1093/nar/gkx1098.
458. Cornwell M, Vangala M, Taing L, Herbert Z, Köster J, Li B, et al. VIPER: Visualization Pipeline for RNA-seq, a Snakemake workflow for efficient and complete RNA-seq analysis. *BMC Bioinformatics.* 2018;19(1):135. doi: 10.1186/s12859-018-2139-9.
459. Wikipedia. List of RNA-Seq bioinformatics tools [10/01/2020]. Available from: https://en.wikipedia.org/wiki/List_of_RNA-Seq_bioinformatics_tools#Commercial_solutions.
460. Kidd BA, Peters LA, Schadt EE, Dudley JT. Unifying immunology with informatics and multiscale biology. *Nat Immunol.* 2014;15(2):118-27. Epub 2014/01/23. doi: 10.1038/ni.2787. PubMed PMID: 24448569; PubMed Central PMCID: PMCPMC4345400.
461. Ewing B, Green P. Base-calling of automated sequencer traces using phred. II. Error probabilities. *Genome Res.* 1998;8(3):186-94. Epub 1998/05/16. PubMed PMID: 9521922.
462. Simon Andrews PL, Brian Howard, Phil Ewels. FastQC: a quality control tool for high throughput sequence data 2015 [17/08/2019]. Available from: <http://www.bioinformatics.babraham.ac.uk/projects/fastqc/>.
463. Bolger AM, Lohse M, Usadel B. Trimmomatic: a flexible trimmer for Illumina sequence data. *Bioinformatics.* 2014;30(15):2114-20. Epub 2014/04/04. doi: 10.1093/bioinformatics/btu170. PubMed PMID: 24695404; PubMed Central PMCID: PMCPMC4103590.
464. Illumina. Illumina Adapter Sequences 2017 [cited 2018 09/01/18]. Available from: <https://support.illumina.com/content/dam/illumina->

- support/documents/documentation/chemistry_documentation/experiment-design/illumina-adapter-sequences-100000002694-03.pdf.
465. Jolliffe IT, Cadima J. Principal component analysis: a review and recent developments. *Philos Trans A Math Phys Eng Sci.* 2016;374(2065):20150202. Epub 2016/03/10. doi: 10.1098/rsta.2015.0202. PubMed PMID: 26953178; PubMed Central PMCID: PMC4792409.
466. Gierlinski M, Cole C, Schofield P, Schurch NJ, Sherstnev A, Singh V, et al. Statistical models for RNA-seq data derived from a two-condition 48-replicate experiment. *Bioinformatics.* 2015;31(22):3625-30. Epub 2015/07/25. doi: 10.1093/bioinformatics/btv425. PubMed PMID: 26206307; PubMed Central PMCID: PMC4754627.
467. Mortazavi A, Williams BA, McCue K, Schaeffer L, Wold B. Mapping and quantifying mammalian transcriptomes by RNA-Seq. *Nature Methods.* 2008;5(7):621-8. doi: 10.1038/nmeth.1226.
468. Trapnell C, Roberts A, Goff L, Pertea G, Kim D, Kelley DR, et al. Differential gene and transcript expression analysis of RNA-seq experiments with TopHat and Cufflinks. *Nature Protocols.* 2012;7(3):562-78. doi: 10.1038/nprot.2012.016.
469. Langmead B, Salzberg SL. Fast gapped-read alignment with Bowtie 2. *Nat Methods.* 2012;9(4):357-9. Epub 2012/03/06. doi: 10.1038/nmeth.1923. PubMed PMID: 22388286; PubMed Central PMCID: PMC3322381.
470. Li H, Durbin R. Fast and accurate short read alignment with Burrows-Wheeler transform. *Bioinformatics.* 2009;25(14):1754-60. Epub 2009/05/20. doi: 10.1093/bioinformatics/btp324. PubMed PMID: 19451168; PubMed Central PMCID: PMC2705234.
471. Li H, Durbin R. Fast and accurate long-read alignment with Burrows-Wheeler transform. *Bioinformatics.* 2010;26(5):589-95. Epub 2010/01/19. doi: 10.1093/bioinformatics/btp698. PubMed PMID: 20080505; PubMed Central PMCID: PMC2828108.
472. Wu TD, Nacu S. Fast and SNP-tolerant detection of complex variants and splicing in short reads. *Bioinformatics.* 2010;26(7):873-81. Epub 2010/02/12. doi: 10.1093/bioinformatics/btq057. PubMed PMID: 20147302; PubMed Central PMCID: PMC2844994.
473. Kim D, Langmead B, Salzberg SL. HISAT: a fast spliced aligner with low memory requirements. *Nat Methods.* 2015;12(4):357-60. Epub 2015/03/10. doi: 10.1038/nmeth.3317. PubMed PMID: 25751142; PubMed Central PMCID: PMC4655817.
474. Racz C, Petrovski R, Saunders CT, Chorny I, Kruglyak S, Margulies EH, et al. Isaac: ultra-fast whole-genome secondary analysis on Illumina sequencing platforms. *Bioinformatics.* 2013;29(16):2041-3. Epub 2013/06/06. doi: 10.1093/bioinformatics/btt314. PubMed PMID: 23736529.
475. Dobin A, Davis CA, Schlesinger F, Drenkow J, Zaleski C, Jha S, et al. STAR: ultrafast universal RNA-seq aligner. *Bioinformatics.* 2013;29(1):15-21. Epub 2012/10/30. doi: 10.1093/bioinformatics/bts635. PubMed PMID: 23104886; PubMed Central PMCID: PMC3530905.
476. Grant GR, Farkas MH, Pizarro AD, Lahens NF, Schug J, Brunk BP, et al. Comparative analysis of RNA-Seq alignment algorithms and the RNA-Seq unified mapper (RUM). *Bioinformatics.* 2011;27(18):2518-28. Epub 2011/07/22. doi: 10.1093/bioinformatics/btr427. PubMed PMID: 21775302; PubMed Central PMCID: PMC3167048.
477. Wang K, Singh D, Zeng Z, Coleman SJ, Huang Y, Savich GL, et al. MapSplice: accurate mapping of RNA-seq reads for splice junction discovery. *Nucleic Acids Res.* 2010;38(18):e178. Epub 2010/08/31. doi: 10.1093/nar/gkq622. PubMed PMID: 20802226; PubMed Central PMCID: PMC2952873.

478. Wang L, Wang S, Li W. RSeQC: quality control of RNA-seq experiments. *Bioinformatics*. 2012;28(16):2184-5. Epub 2012/06/30. doi: 10.1093/bioinformatics/bts356. PubMed PMID: 22743226.
479. Garcia-Alcalde F, Okonechnikov K, Carbonell J, Cruz LM, Gotz S, Tarazona S, et al. Qualimap: evaluating next-generation sequencing alignment data. *Bioinformatics*. 2012;28(20):2678-9. Epub 2012/08/24. doi: 10.1093/bioinformatics/bts503. PubMed PMID: 22914218.
480. Howe K, Clark MD, Torroja CF, Torrance J, Berthelot C, Muffato M, et al. The zebrafish reference genome sequence and its relationship to the human genome. *Nature*. 2013;496(7446):498-503. Epub 2013/04/19. doi: 10.1038/nature12111. PubMed PMID: 23594743; PubMed Central PMCID: PMC3703927.
481. White RJ, Collins JE, Sealy IM, Wali N, Dooley CM, Digby Z, et al. A high-resolution mRNA expression time course of embryonic development in zebrafish. *Elife*. 2017;6. Epub 2017/11/17. doi: 10.7554/eLife.30860. PubMed PMID: 29144233; PubMed Central PMCID: PMC5690287.
482. Ghosh S, Chan C. Analysis of RNA-Seq Data Using TopHat and Cufflinks. *Methods in Molecular Biology*. 2016;1374.
483. Tarazona S, Furio-Tari P, Turra D, Pietro AD, Nueda MJ, Ferrer A, et al. Data quality aware analysis of differential expression in RNA-seq with NOISeq R/Bioc package. *Nucleic Acids Res*. 2015;43(21):e140. Epub 2015/07/18. doi: 10.1093/nar/gkv711. PubMed PMID: 26184878; PubMed Central PMCID: PMC4666377.
484. Risso D, Schwartz K, Sherlock G, Dudoit S. GC-content normalization for RNA-Seq data. *BMC Bioinformatics*. 2011;12:480. Epub 2011/12/20. doi: 10.1186/1471-2105-12-480. PubMed PMID: 22177264; PubMed Central PMCID: PMC3315510.
485. Patro R, Mount SM, Kingsford C. Sailfish enables alignment-free isoform quantification from RNA-seq reads using lightweight algorithms. *Nature Biotechnology*. 2014;32(5):462-4. doi: 10.1038/nbt.2862.
486. Anders S, Pyl PT, Huber W. HTSeq--a Python framework to work with high-throughput sequencing data. *Bioinformatics*. 2015;31(2):166-9. Epub 2014/09/28. doi: 10.1093/bioinformatics/btu638. PubMed PMID: 25260700; PubMed Central PMCID: PMC4287950.
487. Robert C, Watson M. Errors in RNA-Seq quantification affect genes of relevance to human disease. *Genome Biol*. 2015;16:177. Epub 2015/09/04. doi: 10.1186/s13059-015-0734-x. PubMed PMID: 26335491; PubMed Central PMCID: PMC4558956.
488. Hoffmann R, Seidl T, Dugas M. Profound effect of normalization on detection of differentially expressed genes in oligonucleotide microarray data analysis. *Genome Biol*. 2002;3(7):Research0033. Epub 2002/08/20. doi: 10.1186/gb-2002-3-7-research0033. PubMed PMID: 12184807; PubMed Central PMCID: PMC126238.
489. Trapnell C, Williams BA, Pertea G, Mortazavi A, Kwan G, van Baren MJ, et al. Transcript assembly and quantification by RNA-Seq reveals unannotated transcripts and isoform switching during cell differentiation. *Nat Biotechnol*. 2010;28(5):511-5. Epub 2010/05/04. doi: 10.1038/nbt.1621. PubMed PMID: 20436464; PubMed Central PMCID: PMC3146043.
490. Vera Alvarez R, Pongor LS, Mariño-Ramírez L, Landsman D. TPMCalculator: one-step software to quantify mRNA abundance of genomic features. *Bioinformatics*. 2018;35(11):1960-2. doi: 10.1093/bioinformatics/bty896.
491. Wagner GP, Kin K, Lynch VJ. Measurement of mRNA abundance using RNA-seq data: RPKM measure is inconsistent among samples. *Theory Biosci*. 2012;131(4):281-5. Epub 2012/08/09. doi: 10.1007/s12064-012-0162-3. PubMed PMID: 22872506.
492. Robinson MD, Oshlack A. A scaling normalization method for differential expression analysis of RNA-seq data. *Genome Biol*. 2010;11(3):R25. Epub 2010/03/04. doi: 10.1186/gb-2010-11-3-r25. PubMed PMID: 20196867; PubMed Central PMCID: PMC2864565.

493. Li J, Witten DM, Johnstone IM, Tibshirani R. Normalization, testing, and false discovery rate estimation for RNA-sequencing data. *Biostatistics*. 2012;13(3):523-38. Epub 2011/10/18. doi: 10.1093/biostatistics/kxr031. PubMed PMID: 22003245; PubMed Central PMCID: PMC3372940.
494. Jiang L, Schlesinger F, Davis CA, Zhang Y, Li R, Salit M, et al. Synthetic spike-in standards for RNA-seq experiments. *Genome Res*. 2011;21(9):1543-51. Epub 2011/08/06. doi: 10.1101/gr.121095.111. PubMed PMID: 21816910; PubMed Central PMCID: PMC3166838.
495. Li B, Dewey CN. RSEM: accurate transcript quantification from RNA-Seq data with or without a reference genome. *BMC Bioinformatics*. 2011;12:323. Epub 2011/08/06. doi: 10.1186/1471-2105-12-323. PubMed PMID: 21816040; PubMed Central PMCID: PMC3163565.
496. Roberts A, Pachter L. Streaming fragment assignment for real-time analysis of sequencing experiments. *Nat Methods*. 2013;10(1):71-3. Epub 2012/11/20. doi: 10.1038/nmeth.2251. PubMed PMID: 23160280; PubMed Central PMCID: PMC3880119.
497. Eisenberg E, Levanon EY. Human housekeeping genes, revisited. *Trends Genet*. 2013;29(10):569-74. Epub 2013/07/03. doi: 10.1016/j.tig.2013.05.010. PubMed PMID: 23810203.
498. Schurch NJ, Schofield P, Gierlinski M, Cole C, Sherstnev A, Singh V, et al. How many biological replicates are needed in an RNA-seq experiment and which differential expression tool should you use? *RNA*. 2016;22(6):839-51. Epub 2016/03/30. doi: 10.1261/rna.053959.115. PubMed PMID: 27022035; PubMed Central PMCID: PMC4878611.
499. Love MI, Huber W, Anders S. Moderated estimation of fold change and dispersion for RNA-seq data with DESeq2. *Genome Biol*. 2014;15(12):550. Epub 2014/12/18. doi: 10.1186/s13059-014-0550-8. PubMed PMID: 25516281; PubMed Central PMCID: PMC4302049.
500. Robinson MD, McCarthy DJ, Smyth GK. edgeR: a Bioconductor package for differential expression analysis of digital gene expression data. *Bioinformatics*. 2010;26(1):139-40. Epub 2009/11/17. doi: 10.1093/bioinformatics/btp616. PubMed PMID: 19910308; PubMed Central PMCID: PMC2796818.
501. Bell O, Copland D, Ward A, Nicholson L, Lange C, Chu C, et al. Single Eye mRNA-Seq Reveals Normalisation of the Retinal Microglial Transcriptome Following Acute Inflammation. *Frontiers in Immunology*. 2020;10(3033). doi: 10.3389/fimmu.2019.03033.
502. Rajkumar AP, Qvist P, Lazarus R, Lescai F, Ju J, Nyegaard M, et al. Experimental validation of methods for differential gene expression analysis and sample pooling in RNA-seq. *BMC Genomics*. 2015;16(1):548. doi: 10.1186/s12864-015-1767-y.
503. Garcia-Campos MA, Espinal-Enriquez J, Hernandez-Lemus E. Pathway Analysis: State of the Art. *Front Physiol*. 2015;6:383. Epub 2016/01/07. doi: 10.3389/fphys.2015.00383. PubMed PMID: 26733877; PubMed Central PMCID: PMC4681784.
504. Kanehisa M, Goto S. KEGG: kyoto encyclopedia of genes and genomes. *Nucleic Acids Res*. 2000;28(1):27-30. Epub 1999/12/11. doi: 10.1093/nar/28.1.27. PubMed PMID: 10592173; PubMed Central PMCID: PMC102409.
505. Ashburner M, Ball CA, Blake JA, Botstein D, Butler H, Cherry JM, et al. Gene ontology: tool for the unification of biology. The Gene Ontology Consortium. *Nat Genet*. 2000;25(1):25-9. Epub 2000/05/10. doi: 10.1038/75556. PubMed PMID: 10802651; PubMed Central PMCID: PMC3037419.
506. Hill DP, Smith B, McAndrews-Hill MS, Blake JA. Gene Ontology annotations: what they mean and where they come from. *BMC Bioinformatics*. 2008;9(5):S2. doi: 10.1186/1471-2105-9-S5-S2.
507. Subramanian A, Tamayo P, Mootha VK, Mukherjee S, Ebert BL, Gillette MA, et al. Gene set enrichment analysis: A knowledge-based approach for interpreting genome-wide expression profiles. *Proceedings of the National Academy of Sciences*. 2005;102(43):15545-50. doi: 10.1073/pnas.0506580102.
508. Langfelder P, Horvath S. WGCNA: an R package for weighted correlation network analysis. *BMC Bioinformatics*. 2008;9(1):559. doi: 10.1186/1471-2105-9-559.

509. Mattapallil MJ, Wawrousek EF, Chan CC, Zhao H, Roychoudhury J, Ferguson TA, et al. The Rd8 mutation of the *Crb1* gene is present in vendor lines of C57BL/6N mice and embryonic stem cells, and confounds ocular induced mutant phenotypes. *Invest Ophthalmol Vis Sci*. 2012;53(6):2921-7. Epub 2012/03/27. doi: 10.1167/iovs.12-9662. PubMed PMID: 22447858; PubMed Central PMCID: PMC3376073.
510. Boneva SK, Gross TR, Schlecht A, Schmitt SI, Sippl C, Jagle H, et al. Cre recombinase expression or topical tamoxifen treatment do not affect retinal structure and function, neuronal vulnerability or glial reactivity in the mouse eye. *Neuroscience*. 2016;325:188-201. Epub 2016/03/31. doi: 10.1016/j.neuroscience.2016.03.050. PubMed PMID: 27026593.
511. Rothstein EC, Nauman M, Chesnick S, Balaban RS. Multi-photon excitation microscopy in intact animals. *J Microsc*. 2006;222(Pt 1):58-64. Epub 2006/06/01. doi: 10.1111/j.1365-2818.2006.01570.x. PubMed PMID: 16734715; PubMed Central PMCID: PMC31473170.
512. Chen E. Refractive indices of the rat retinal layers. *Ophthalmic Res*. 1993;25(1):65-8. Epub 1993/01/01. doi: 10.1159/000267223. PubMed PMID: 8446370.
513. Schindelin J, Arganda-Carreras I, Frise E, Kaynig V, Longair M, Pietzsch T, et al. Fiji: an open-source platform for biological-image analysis. *Nat Methods*. 2012;9(7):676-82. Epub 2012/06/30. doi: 10.1038/nmeth.2019. PubMed PMID: 22743772; PubMed Central PMCID: PMC3855844.
514. Kokona D, Schneider N, Giannakaki-Zimmermann H, Jovanovic J, Ebnetter A, Zinkernagel M. Noninvasive Quantification of Retinal Microglia Using Widefield Autofluorescence Imaging. *Invest Ophthalmol Vis Sci*. 2017;58(4):2160-5. Epub 2017/04/11. doi: 10.1167/iovs.16-20916. PubMed PMID: 28395300.
515. Orfao A, Ruiz-Argüelles A. General concepts about cell sorting techniques. *Clinical Biochemistry*. 1996;29(1):5-9. doi: [https://doi.org/10.1016/0009-9120\(95\)02017-9](https://doi.org/10.1016/0009-9120(95)02017-9).
516. Illumina. Low-Input & Single-Cell RNA-Seq | Single-cell sequencing benefits 2019 [19/03/2019]. Available from: <https://emea.illumina.com/techniques/sequencing/rna-sequencing/ultra-low-input-single-cell-rna-seq.html>.
517. Ramskold D, Luo S, Wang YC, Li R, Deng Q, Faridani OR, et al. Full-length mRNA-Seq from single-cell levels of RNA and individual circulating tumor cells. *Nat Biotechnol*. 2012;30(8):777-82. Epub 2012/07/24. doi: 10.1038/nbt.2282. PubMed PMID: 22820318; PubMed Central PMCID: PMC3467340.
518. Picelli S, Faridani OR, Bjorklund AK, Winberg G, Sagasser S, Sandberg R. Full-length RNA-seq from single cells using Smart-seq2. *Nat Protoc*. 2014;9(1):171-81. Epub 2014/01/05. doi: 10.1038/nprot.2014.006. PubMed PMID: 24385147.
519. Baran-Gale J, Chandra T, Kirschner K. Experimental design for single-cell RNA sequencing. *Brief Funct Genomics*. 2018;17(4):233-9. Epub 2017/11/11. doi: 10.1093/bfpg/elx035. PubMed PMID: 29126257; PubMed Central PMCID: PMC6063265.
520. Baker M. 1,500 scientists lift the lid on reproducibility. *Nature News*. 2016;533(7604):452. doi: 10.1038/533452a.
521. Fisher R. *The Design of Experiments*. 8th ed. New York: Hafner Publishing Company; 1966.
522. ENCODE. ENCODE Guidelines and Best Practices for RNA-Seq. 2016.
523. Auer PL, Doerge RW. Statistical design and analysis of RNA sequencing data. *Genetics*. 2010;185(2):405-16. Epub 2010/05/05. doi: 10.1534/genetics.110.114983. PubMed PMID: 20439781; PubMed Central PMCID: PMC2881125.
524. Leek JT, Scharpf RB, Bravo HC, Simcha D, Langmead B, Johnson WE, et al. Tackling the widespread and critical impact of batch effects in high-throughput data. *Nat Rev Genet*. 2010;11(10):733-9. Epub 2010/09/15. doi: 10.1038/nrg2825. PubMed PMID: 20838408; PubMed Central PMCID: PMC3880143.
525. Churchill GA. Fundamentals of experimental design for cDNA microarrays. *Nat Genet*. 2002;32 Suppl:490-5. Epub 2002/11/28. doi: 10.1038/ng1031. PubMed PMID: 12454643.

526. Wang Q, Armenia J, Zhang C, Penson AV, Reznik E, Zhang L, et al. Unifying cancer and normal RNA sequencing data from different sources. *Scientific Data*. 2018;5(1):180061. doi: 10.1038/sdata.2018.61.
527. Laukens D, Brinkman BM, Raes J, De Vos M, Vandenabeele P. Heterogeneity of the gut microbiome in mice: guidelines for optimizing experimental design. *FEMS Microbiol Rev*. 2016;40(1):117-32. Epub 2015/09/02. doi: 10.1093/femsre/fuv036. PubMed PMID: 26323480; PubMed Central PMCID: PMC4703068.
528. Johnson WE, Li C, Rabinovic A. Adjusting batch effects in microarray expression data using empirical Bayes methods. *Biostatistics*. 2007;8(1):118-27. Epub 2006/04/25. doi: 10.1093/biostatistics/kxj037. PubMed PMID: 16632515.
529. Leek JT, Storey JD. Capturing heterogeneity in gene expression studies by surrogate variable analysis. *PLoS Genet*. 2007;3(9):1724-35. Epub 2007/10/03. doi: 10.1371/journal.pgen.0030161. PubMed PMID: 17907809; PubMed Central PMCID: PMC1994707.
530. Leek JT. svaseq: removing batch effects and other unwanted noise from sequencing data. *Nucleic Acids Res*. 2014;42(21). Epub 2014/10/09. doi: 10.1093/nar/gku864. PubMed PMID: 25294822; PubMed Central PMCID: PMC4245966.
531. Espin-Perez A, Portier C, Chadeau-Hyam M, van Veldhoven K, Kleinjans JCS, de Kok T. Comparison of statistical methods and the use of quality control samples for batch effect correction in human transcriptome data. *PLoS One*. 2018;13(8):e0202947. Epub 2018/08/31. doi: 10.1371/journal.pone.0202947. PubMed PMID: 30161168; PubMed Central PMCID: PMC6117018.
532. Luo J, Schumacher M, Scherer A, Sanoudou D, Megherbi D, Davison T, et al. A comparison of batch effect removal methods for enhancement of prediction performance using MAQC-II microarray gene expression data. *Pharmacogenomics J*. 2010;10(4):278-91. Epub 2010/08/03. doi: 10.1038/tpj.2010.57. PubMed PMID: 20676067; PubMed Central PMCID: PMC2920074.
533. Nygaard V, Rødland EA, Hovig E. Methods that remove batch effects while retaining group differences may lead to exaggerated confidence in downstream analyses. *Biostatistics*. 2015;17(1):29-39. doi: 10.1093/biostatistics/kxv027.
534. Wang Y, Ghaffari N, Johnson CD, Braga-Neto UM, Wang H, Chen R, et al. Evaluation of the coverage and depth of transcriptome by RNA-Seq in chickens. *BMC Bioinformatics*. 2011;12 Suppl 10:S5. Epub 2011/12/23. doi: 10.1186/1471-2105-12-S10-S5. PubMed PMID: 22165852; PubMed Central PMCID: PMC3236848.
535. Ramskold D, Kavak E, Sandberg R. How to analyze gene expression using RNA-sequencing data. *Methods Mol Biol*. 2012;802:259-74. Epub 2011/12/02. doi: 10.1007/978-1-61779-400-1_17. PubMed PMID: 22130886.
536. de Jong LC, Cree S, Lattimore V, Wiggins GAR, Spurdle AB, kConFab I, et al. Nanopore sequencing of full-length BRCA1 mRNA transcripts reveals co-occurrence of known exon skipping events. *Breast Cancer Res*. 2017;19(1):127. Epub 2017/12/01. doi: 10.1186/s13058-017-0919-1. PubMed PMID: 29183387; PubMed Central PMCID: PMC5706335.
537. Sonesson C, Delorenzi M. A comparison of methods for differential expression analysis of RNA-seq data. *BMC Bioinformatics*. 2013;14:91. Epub 2013/03/19. doi: 10.1186/1471-2105-14-91. PubMed PMID: 23497356; PubMed Central PMCID: PMC3608160.
538. Burden CJ, Qureshi SE, Wilson SR. Error estimates for the analysis of differential expression from RNA-seq count data. *PeerJ*. 2014;2:e576. Epub 2014/10/23. doi: 10.7717/peerj.576. PubMed PMID: 25337456; PubMed Central PMCID: PMC4179614.
539. Liu Y, Zhou J, White KP. RNA-seq differential expression studies: more sequence or more replication? *Bioinformatics*. 2014;30(3):301-4. Epub 2013/12/10. doi: 10.1093/bioinformatics/btt688. PubMed PMID: 24319002; PubMed Central PMCID: PMC3904521.

540. Yona S, Kim KW, Wolf Y, Mildner A, Varol D, Breker M, et al. Fate mapping reveals origins and dynamics of monocytes and tissue macrophages under homeostasis. *Immunity*. 2013;38(1):79-91. Epub 2013/01/01. doi: 10.1016/j.immuni.2012.12.001. PubMed PMID: 23273845; PubMed Central PMCID: PMC3908543.
541. Epps SJ, Boldison J, Stimpson ML, Khera TK, Lait PJP, Copland DA, et al. Re-programming immunosurveillance in persistent non-infectious ocular inflammation. *Prog Retin Eye Res*. 2018;65:93-106. Epub 2018/03/14. doi: 10.1016/j.preteyeres.2018.03.001. PubMed PMID: 29530739; PubMed Central PMCID: PMC6563519.
542. Kerr EC, Copland DA, Dick AD, Nicholson LB. The dynamics of leukocyte infiltration in experimental autoimmune uveoretinitis. *Prog Retin Eye Res*. 2008;27(5):527-35. Epub 2008/08/30. doi: 10.1016/j.preteyeres.2008.07.001. PubMed PMID: 18723108.
543. Takeuchi M, Higashino A, Takeuchi K, Hori Y, Koshiba-Takeuchi K, Makino H, et al. Transcriptional Dynamics of Immortalized Human Mesenchymal Stem Cells during Transformation. *PLoS One*. 2015;10(5):e0126562. Epub 2015/05/16. doi: 10.1371/journal.pone.0126562. PubMed PMID: 25978455; PubMed Central PMCID: PMC4433180.
544. Lin CY, Loven J, Rahl PB, Paranal RM, Burge CB, Bradner JE, et al. Transcriptional amplification in tumor cells with elevated c-Myc. *Cell*. 2012;151(1):56-67. Epub 2012/10/02. doi: 10.1016/j.cell.2012.08.026. PubMed PMID: 23021215; PubMed Central PMCID: PMC3462372.
545. Courey AJ, Jia S. Transcriptional repression: the long and the short of it. *Genes Dev*. 2001;15(21):2786-96. Epub 2001/11/03. doi: 10.1101/gad.939601. PubMed PMID: 11691830.
546. Keren-Shaul H, Kenigsberg E, Jaitin DA, David E, Paul F, Tanay A, et al. MARS-seq2.0: an experimental and analytical pipeline for indexed sorting combined with single-cell RNA sequencing. *Nat Protoc*. 2019;14(6):1841-62. Epub 2019/05/19. doi: 10.1038/s41596-019-0164-4. PubMed PMID: 31101904.
547. Rojas B, Gallego BI, Ramirez AI, Salazar JJ, de Hoz R, Valiente-Soriano FJ, et al. Microglia in mouse retina contralateral to experimental glaucoma exhibit multiple signs of activation in all retinal layers. *J Neuroinflammation*. 2014;11:133. Epub 2014/07/30. doi: 10.1186/1742-2094-11-133. PubMed PMID: 25064005; PubMed Central PMCID: PMC4128533.
548. Jabs DA, Busingye J. Approach to the diagnosis of the uveitides. *Am J Ophthalmol*. 2013;156(2):228-36. Epub 2013/05/15. doi: 10.1016/j.ajo.2013.03.027. PubMed PMID: 23668682; PubMed Central PMCID: PMC3720682.
549. Cosenza-Nashat MA, Kim MO, Zhao ML, Suh HS, Lee SC. CD45 Isoform Expression in Microglia and Inflammatory Cells in HIV-1 Encephalitis. *Brain Pathol*. 2006;16(4):256-65. doi: 10.1111/j.1750-3639.2006.00027.x. PubMed PMID: 17107594; PubMed Central PMCID: PMC1804203.
550. Sedgwick JD, Ford AL, Foulcher E, Airriess R. Central nervous system microglial cell activation and proliferation follows direct interaction with tissue-infiltrating T cell blasts. *J Immunol*. 1998;160(11):5320-30. Epub 1998/05/30. PubMed PMID: 9605131.
551. Remington LT, Babcock AA, Zehntner SP, Owens T. Microglial Recruitment, Activation, and Proliferation in Response to Primary Demyelination. *Am J Pathol*. 2007;170(5):1713-24. doi: 10.2353/ajpath.2007.060783. PubMed PMID: 17456776; PubMed Central PMCID: PMC1854965.
552. Sedgwick JD, Schwender S, Imrich H, Dörries R, Butcher GW, ter Meulen V. Isolation and direct characterization of resident microglial cells from the normal and inflamed central nervous system. *Proc Natl Acad Sci U S A*. 1991;88(16):7438-42. PubMed PMID: 1651506; PubMed Central PMCID: PMC52311.
553. Renno T, Krakowski M, Piccirillo C, Lin JY, Owens T. TNF-alpha expression by resident microglia and infiltrating leukocytes in the central nervous system of mice with experimental allergic encephalomyelitis. Regulation by Th1 cytokines. *J Immunol*. 1995;154(2):944-53. Epub 1995/01/15. PubMed PMID: 7814894.

554. Djukic M, Mildner A, Schmidt H, Czesnik D, Bruck W, Priller J, et al. Circulating monocytes engraft in the brain, differentiate into microglia and contribute to the pathology following meningitis in mice. *Brain*. 2006;129(Pt 9):2394-403. Epub 2006/08/08. doi: 10.1093/brain/awl206. PubMed PMID: 16891321.
555. De Martinis M, Modesti M, Ginaldi L. Phenotypic and functional changes of circulating monocytes and polymorphonuclear leucocytes from elderly persons. *Immunol Cell Biol*. 2004;82(4):415-20. Epub 2004/07/31. doi: 10.1111/j.0818-9641.2004.01242.x. PubMed PMID: 15283852.
556. Erdoes G, Balmer ML, Slack E, Kocsis I, Lehmann LE, Eberle B, et al. CD62L (L-selectin) shedding for assessment of perioperative immune sensitivity in patients undergoing cardiac surgery with cardiopulmonary bypass. *PLoS One*. 2013;8(1):e53045. Epub 2013/01/10. doi: 10.1371/journal.pone.0053045. PubMed PMID: 23301018; PubMed Central PMCID: PMC3536798.
557. London A, Benhar I, Mattapallil MJ, Mack M, Caspi RR, Schwartz M. Functional macrophage heterogeneity in a mouse model of autoimmune central nervous system pathology. *J Immunol*. 2013;190(7):3570-8. Epub 2013/03/01. doi: 10.4049/jimmunol.1202076. PubMed PMID: 23447691; PubMed Central PMCID: PMC3626074.
558. Lewis ND, Hill JD, Juchem KW, Stefanopoulos DE, Modis LK. RNA sequencing of microglia and monocyte-derived macrophages from mice with experimental autoimmune encephalomyelitis illustrates a changing phenotype with disease course. *J Neuroimmunol*. 2014;277(1-2):26-38. Epub 2014/10/02. doi: 10.1016/j.jneuroim.2014.09.014. PubMed PMID: 25270668.
559. Kim JY, Sohn HJ, Seo JH, Lee EY. CD44 Expression in Microglia of the Retina and Cerebellum of Developing and Adult Chicken. *Korean J Phys Anthropol*. 2017;30(1):29-38.
560. Bennett ML, Bennett FC, Liddel SA, Ajami B, Zamanian JL, Fernhoff NB, et al. New tools for studying microglia in the mouse and human CNS. *Proc Natl Acad Sci U S A*. 2016;113(12):E1738-46. Epub 2016/02/18. doi: 10.1073/pnas.1525528113. PubMed PMID: 26884166; PubMed Central PMCID: PMC4812770.
561. Heng JS, Hackett SF, Stein-O'Brien GL, Winer BL, Williams J, Goff LA, et al. Comprehensive analysis of a mouse model of spontaneous uveoretinitis using single-cell RNA sequencing. *Proceedings of the National Academy of Sciences*. 2019;201915571. doi: 10.1073/pnas.1915571116.
562. Grainge I, Jayaram M. The integrase family of recombinase: organization and function of the active site. *Mol Microbiol*. 1999;33(3):449-56. Epub 1999/11/30. PubMed PMID: 10577069.
563. Feil R, Wagner J, Metzger D, Chambon P. Regulation of Cre recombinase activity by mutated estrogen receptor ligand-binding domains. *Biochem Biophys Res Commun*. 1997;237(3):752-7. Epub 1997/08/28. doi: 10.1006/bbrc.1997.7124. PubMed PMID: 9299439.
564. Kristianto J, Johnson MG, Zastrow RK, Radcliff AB, Blank RD. Spontaneous recombinase activity of Cre-ERT2 in vivo. *Transgenic Res*. 2017;26(3):411-7. Epub 2017/04/15. doi: 10.1007/s11248-017-0018-1. PubMed PMID: 28409408.
565. Liu Y, Suckale J, Masjkur J, Magro MG, Steffen A, Anastassiadis K, et al. Tamoxifen-independent recombination in the RIP-CreER mouse. *PLoS One*. 2010;5(10):e13533. Epub 2010/11/11. doi: 10.1371/journal.pone.0013533. PubMed PMID: 21063464; PubMed Central PMCID: PMC2965077.
566. Soriano P. Generalized lacZ expression with the ROSA26 Cre reporter strain. *Nat Genet*. 1999;21(1):70-1. Epub 1999/01/23. doi: 10.1038/5007. PubMed PMID: 9916792.
567. Feil S, Valtcheva N, Feil R. Inducible Cre mice. *Methods Mol Biol*. 2009;530:343-63. Epub 2009/03/07. doi: 10.1007/978-1-59745-471-1_18. PubMed PMID: 19266339.
568. Madisen L, Zwingman TA, Sunkin SM, Oh SW, Zariwala HA, Gu H, et al. A robust and high-throughput Cre reporting and characterization system for the whole mouse brain. *Nat*

- Neurosci. 2010;13(1):133-40. Epub 2009/12/22. doi: 10.1038/nn.2467. PubMed PMID: 20023653; PubMed Central PMCID: PMCPMC2840225.
569. The Jackson Laboratory. 007914 - B6.Cg-Gt(ROSA)26Sor 2019 [30/07/2019]. Available from: <https://www.jax.org/strain/007914>.
570. Albin TA, Wang RC, Reiser B, Zamir E, Wu GS, Rao NA. Microglial stability and repopulation in the retina. *Br J Ophthalmol*. 2005;89(7):901-3. Epub 2005/06/21. doi: 10.1136/bjo.2004.060293. PubMed PMID: 15965175; PubMed Central PMCID: PMCPMC1772746.
571. Kaneko H, Nishiguchi KM, Nakamura M, Kachi S, Terasaki H. Characteristics of bone marrow-derived microglia in the normal and injured retina. *Invest Ophthalmol Vis Sci*. 2008;49(9):4162-8. Epub 2008/05/20. doi: 10.1167/iovs.08-1738. PubMed PMID: 18487364.
572. Hines DJ, Hines RM, Mulligan SJ, Macvicar BA. Microglia processes block the spread of damage in the brain and require functional chloride channels. *Glia*. 2009;57(15):1610-8. Epub 2009/04/22. doi: 10.1002/glia.20874. PubMed PMID: 19382211.
573. Higashi AY, Ikawa T, Muramatsu M, Economides AN, Niwa A, Okuda T, et al. Direct hematological toxicity and illegitimate chromosomal recombination caused by the systemic activation of CreERT2. *J Immunol*. 2009;182(9):5633-40. Epub 2009/04/22. doi: 10.4049/jimmunol.0802413. PubMed PMID: 19380810.
574. Ansari AM, Ahmed AK, Matsangos AE, Lay F, Born LJ, Marti G, et al. Cellular GFP Toxicity and Immunogenicity: Potential Confounders in in Vivo Cell Tracking Experiments. *Stem Cell Rev Rep*. 2016;12(5):553-9. Epub 2016/07/21. doi: 10.1007/s12015-016-9670-8. PubMed PMID: 27435468; PubMed Central PMCID: PMCPMC5050239.
575. Shaner NC, Steinbach PA, Tsien RY. A guide to choosing fluorescent proteins. *Nat Methods*. 2005;2(12):905-9. Epub 2005/11/22. doi: 10.1038/nmeth819. PubMed PMID: 16299475.
576. Siegel AP, Baird MA, Davidson MW, Day RN. Strengths and weaknesses of recently engineered red fluorescent proteins evaluated in live cells using fluorescence correlation spectroscopy. *Int J Mol Sci*. 2013;14(10):20340-58. Epub 2013/10/17. doi: 10.3390/ijms141020340. PubMed PMID: 24129172; PubMed Central PMCID: PMCPMC3821618.
577. Shaner NC, Campbell RE, Steinbach PA, Giepmans BN, Palmer AE, Tsien RY. Improved monomeric red, orange and yellow fluorescent proteins derived from *Discosoma* sp. red fluorescent protein. *Nat Biotechnol*. 2004;22(12):1567-72. Epub 2004/11/24. doi: 10.1038/nbt1037. PubMed PMID: 15558047.
578. Ango F, Prezeau L, Muller T, Tu JC, Xiao B, Worley PF, et al. Agonist-independent activation of metabotropic glutamate receptors by the intracellular protein Homer. *Nature*. 2001;411(6840):962-5. Epub 2001/06/22. doi: 10.1038/35082096. PubMed PMID: 11418862.
579. Lee M, Lee Y, Song J, Lee J, Chang SY. Tissue-specific Role of CX₃CR₁ Expressing Immune Cells and Their Relationships with Human Disease. *Immune Netw*. 2018;18(1):e5. Epub 2018/03/06. doi: 10.4110/in.2018.18.e5. PubMed PMID: 29503738; PubMed Central PMCID: PMCPMC5833124.
580. Dudakov JA, Mertelsmann AM, O'Connor MH, Jenq RR, Velardi E, Young LF, et al. Loss of thymic innate lymphoid cells leads to impaired thymopoiesis in experimental graft-versus-host disease. *Blood*. 2017;130(7):933-42. Epub 2017/06/14. doi: 10.1182/blood-2017-01-762658. PubMed PMID: 28607133; PubMed Central PMCID: PMCPMC5561900.
581. Kobayashi T, Okamoto S, Iwakami Y, Nakazawa A, Hisamatsu T, Chinen H, et al. Exclusive increase of CX₃CR₁+CD28-CD4+ T cells in inflammatory bowel disease and their recruitment as intraepithelial lymphocytes. *Inflamm Bowel Dis*. 2007;13(7):837-46. Epub 2007/02/08. doi: 10.1002/ibd.20113. PubMed PMID: 17285595.
582. Ducimetière L, Vermeer M, Tugues S. The Interplay Between Innate Lymphoid Cells and the Tumor Microenvironment. *Frontiers in Immunology*. 2019;10(2895). doi: 10.3389/fimmu.2019.02895.
583. O'Koren EG, Mathew R, Saban DR. Fate mapping reveals that microglia and recruited monocyte-derived macrophages are definitively distinguishable by phenotype in the retina. *Sci*

- Rep. 2016;6:20636. Epub 2016/02/10. doi: 10.1038/srep20636. PubMed PMID: 26856416; PubMed Central PMCID: PMC4746646.
584. Smith JR, Hart PH, Williams KA. Basic pathogenic mechanisms operating in experimental models of acute anterior uveitis. *Immunol Cell Biol.* 1998;76(6):497-512. Epub 1999/01/20. doi: 10.1046/j.1440-1711.1998.00783.x. PubMed PMID: 9893027.
585. Calippe B, Augustin S, Beguier F, Charles-Messance H, Poupel L, Conart JB, et al. Complement Factor H Inhibits CD47-Mediated Resolution of Inflammation. *Immunity.* 2017;46(2):261-72. Epub 2017/02/24. doi: 10.1016/j.immuni.2017.01.006. PubMed PMID: 28228282.
586. Ronning KE, Karlen SJ, Miller EB, Burns ME. Molecular profiling of resident and infiltrating mononuclear phagocytes during rapid adult retinal degeneration using single-cell RNA sequencing. *Scientific Reports.* 2019;9(1):4858. doi: 10.1038/s41598-019-41141-0.
587. Nilsson R, Bajic VB, Suzuki H, di Bernardo D, Bjorkegren J, Katayama S, et al. Transcriptional network dynamics in macrophage activation. *Genomics.* 2006;88(2):133-42. Epub 2006/05/16. doi: 10.1016/j.ygeno.2006.03.022. PubMed PMID: 16698233.
588. Dubbelaar ML, Kracht L, Eggen BJJ, Boddeke E. The Kaleidoscope of Microglial Phenotypes. *Front Immunol.* 2018;9:1753. Epub 2018/08/16. doi: 10.3389/fimmu.2018.01753. PubMed PMID: 30108586; PubMed Central PMCID: PMC6079257.
589. Parapatics K, Huber M, Lehmann D, Knoll C, Superti-Furga G, Bennett KL, et al. Proteomic analysis of low quantities of cellular material in the range obtainable from scarce patient samples. *Journal of Integrated OMICS.* 2015;5:30-43. doi: 10.5584/jiomics.v4i2.172.
590. Zhu Y, Piehowski PD, Zhao R, Chen J, Shen Y, Moore RJ, et al. Nanodroplet processing platform for deep and quantitative proteome profiling of 10-100 mammalian cells. *Nat Commun.* 2018;9(1):882. Epub 2018/03/02. doi: 10.1038/s41467-018-03367-w. PubMed PMID: 29491378; PubMed Central PMCID: PMC5830451.
591. Mirzaei M, Gupta VB, Chick JM, Greco TM, Wu Y, Chitranshi N, et al. Age-related neurodegenerative disease associated pathways identified in retinal and vitreous proteome from human glaucoma eyes. *Scientific Reports.* 2017;7(1):12685. doi: 10.1038/s41598-017-12858-7.
592. Rangaraju S, Dammer EB, Raza SA, Rathakrishnan P, Xiao H, Gao T, et al. Identification and therapeutic modulation of a pro-inflammatory subset of disease-associated-microglia in Alzheimer's disease. *Mol Neurodegener.* 2018;13(1):24. Epub 2018/05/23. doi: 10.1186/s13024-018-0254-8. PubMed PMID: 29784049; PubMed Central PMCID: PMC5963076.
593. Vogt M, Bauer MK, Ferrari D, Schulze-Osthoff K. Oxidative stress and hypoxia/reoxygenation trigger CD95 (APO-1/Fas) ligand expression in microglial cells. *FEBS Lett.* 1998;429(1):67-72. Epub 1998/07/10. doi: 10.1016/s0014-5793(98)00562-6. PubMed PMID: 9657385.
594. Das A, Chai JC, Kim SH, Park KS, Lee YS, Jung KH, et al. Dual RNA sequencing reveals the expression of unique transcriptomic signatures in lipopolysaccharide-induced BV-2 microglial cells. *PLoS One.* 2015;10(3):e0121117. Epub 2015/03/27. doi: 10.1371/journal.pone.0121117. PubMed PMID: 25811458; PubMed Central PMCID: PMC4374676.
595. Izzy S, Liu Q, Fang Z, Lule S, Wu L, Chung JY, et al. Time-Dependent Changes in Microglia Transcriptional Networks Following Traumatic Brain Injury. *Front Cell Neurosci.* 2019;13:307. Epub 2019/08/24. doi: 10.3389/fncel.2019.00307. PubMed PMID: 31440141; PubMed Central PMCID: PMC6694299.
596. Haslund-Vinding J, McBean G, Jaquet V, Vilhardt F. NADPH oxidases in oxidant production by microglia: activating receptors, pharmacology and association with disease. *Br J Pharmacol.* 2017;174(12):1733-49. Epub 2016/01/12. doi: 10.1111/bph.13425. PubMed PMID: 26750203; PubMed Central PMCID: PMC5446574.
597. Nomura K, Vilalta A, Allendorf DH, Hornik TC, Brown GC. Activated Microglia Desialylate and Phagocytose Cells via Neuraminidase, Galectin-3, and Mer Tyrosine Kinase. *J Immunol.* 2017;198(12):4792-801. Epub 2017/05/14. doi: 10.4049/jimmunol.1502532. PubMed PMID: 28500071; PubMed Central PMCID: PMC5458330.

598. Moher D, Liberati A, Tetzlaff J, Altman DG, Group P. Preferred reporting items for systematic reviews and meta-analyses: the PRISMA statement. *PLoS Med.* 2009;6(7):e1000097. Epub 2009/07/22. doi: 10.1371/journal.pmed.1000097. PubMed PMID: 19621072; PubMed Central PMCID: PMCPMC2707599.
599. Ulland TK, Colonna M. TREM2 - a key player in microglial biology and Alzheimer disease. *Nat Rev Neurol.* 2018;14(11):667-75. Epub 2018/09/30. doi: 10.1038/s41582-018-0072-1. PubMed PMID: 30266932.
600. Zhou Y, Ulland TK, Colonna M. TREM2-Dependent Effects on Microglia in Alzheimer's Disease. *Front Aging Neurosci.* 2018;10:202. Epub 2018/07/25. doi: 10.3389/fnagi.2018.00202. PubMed PMID: 30038567; PubMed Central PMCID: PMCPMC6046445.
601. Konishi H, Kiyama H. Microglial TREM2/DAP12 Signaling: A Double-Edged Sword in Neural Diseases. *Front Cell Neurosci.* 2018;12:206. Epub 2018/08/22. doi: 10.3389/fncel.2018.00206. PubMed PMID: 30127720; PubMed Central PMCID: PMCPMC6087757.
602. Lemee JM, Clavreul A, Aubry M, Com E, de Tairac M, Mosser J, et al. Integration of transcriptome and proteome profiles in glioblastoma: looking for the missing link. *BMC Mol Biol.* 2018;19(1):13. Epub 2018/11/23. doi: 10.1186/s12867-018-0115-6. PubMed PMID: 30463513; PubMed Central PMCID: PMCPMC6249855.
603. Bai Y, Wang S, Zhong H, Yang Q, Zhang F, Zhuang Z, et al. Integrative analyses reveal transcriptome-proteome correlation in biological pathways and secondary metabolism clusters in *A. flavus* in response to temperature. *Sci Rep.* 2015;5:14582. Epub 2015/09/30. doi: 10.1038/srep14582. PubMed PMID: 26416011; PubMed Central PMCID: PMCPMC4586720.
604. Wang D, Eraslan B, Wieland T, Hallstrom B, Hopf T, Zolg DP, et al. A deep proteome and transcriptome abundance atlas of 29 healthy human tissues. *Mol Syst Biol.* 2019;15(2):e8503. Epub 2019/02/20. doi: 10.15252/msb.20188503. PubMed PMID: 30777892; PubMed Central PMCID: PMCPMC6379049.
605. Macaulay IC, Haerty W, Kumar P, Li YI, Hu TX, Teng MJ, et al. G&T-seq: parallel sequencing of single-cell genomes and transcriptomes. *Nat Methods.* 2015;12(6):519-22. Epub 2015/04/29. doi: 10.1038/nmeth.3370. PubMed PMID: 25915121.
606. Angermueller C, Clark SJ, Lee HJ, Macaulay IC, Teng MJ, Hu TX, et al. Parallel single-cell sequencing links transcriptional and epigenetic heterogeneity. *Nat Methods.* 2016;13(3):229-32. Epub 2016/01/12. doi: 10.1038/nmeth.3728. PubMed PMID: 26752769; PubMed Central PMCID: PMCPMC4770512.
607. Ruggiero E, Nicolay JP, Fronza R, Arens A, Paruzynski A, Nowrouzi A, et al. High-resolution analysis of the human T-cell receptor repertoire. *Nat Commun.* 2015;6:8081. Epub 2015/09/02. doi: 10.1038/ncomms9081. PubMed PMID: 26324409; PubMed Central PMCID: PMCPMC4569693.
608. Turchaninova MA, Britanova OV, Bolotin DA, Shugay M, Putintseva EV, Staroverov DB, et al. Pairing of T-cell receptor chains via emulsion PCR. *Eur J Immunol.* 2013;43(9):2507-15. Epub 2013/05/23. doi: 10.1002/eji.201343453. PubMed PMID: 23696157.
609. Grigaityte K, Carter JA, Goldfless SJ, Jeffery EW, Hause RJ, Jiang Y, et al. Single-cell sequencing reveals $\alpha\beta$ chain pairing shapes the T cell repertoire. *bioRxiv.* 2017:213462. doi: 10.1101/213462.
610. Lou N, Takano T, Pei Y, Xavier AL, Goldman SA, Nedergaard M. Purinergic receptor P2RY12-dependent microglial closure of the injured blood-brain barrier. *Proc Natl Acad Sci U S A.* 2016;113(4):1074-9. Epub 2016/01/13. doi: 10.1073/pnas.1520398113. PubMed PMID: 26755608; PubMed Central PMCID: PMCPMC4743790.
611. He Y, Yao X, Taylor N, Bai Y, Lovenberg T, Bhattacharya A. RNA sequencing analysis reveals quiescent microglia isolation methods from postnatal mouse brains and limitations of BV2 cells. *J Neuroinflammation.* 2018;15(1):153. Epub 2018/05/24. doi: 10.1186/s12974-018-1195-4. PubMed PMID: 29788964; PubMed Central PMCID: PMCPMC5964710.

612. Cai B, Kasikara C, Doran AC, Ramakrishnan R, Birge RB, Tabas I. MerTK signaling in macrophages promotes the synthesis of inflammation resolution mediators by suppressing CaMKII activity. *Sci Signal*. 2018;11(549). Epub 2018/09/27. doi: 10.1126/scisignal.aar3721. PubMed PMID: 30254055; PubMed Central PMCID: PMC6171110.
613. Neher JJ, Emmrich JV, Fricker M, Mander PK, Thery C, Brown GC. Phagocytosis executes delayed neuronal death after focal brain ischemia. *Proc Natl Acad Sci U S A*. 2013;110(43):E4098-107. Epub 2013/10/09. doi: 10.1073/pnas.1308679110. PubMed PMID: 24101459; PubMed Central PMCID: PMC3808587.
614. Al-Kharsan H, Shah KP, Jung SC, Rodriguez A, Madduri RK, Grassi MA. A novel MERTK mutation causing retinitis pigmentosa. *Graefes Arch Clin Exp Ophthalmol*. 2017;255(8):1613-9. Epub 2017/05/04. doi: 10.1007/s00417-017-3679-9. PubMed PMID: 28462455; PubMed Central PMCID: PMC5542860.
615. Zhou Y, Fei M, Zhang G, Liang WC, Lin W, Wu Y, et al. Blockade of the Phagocytic Receptor MerTK on Tumor-Associated Macrophages Enhances P2X7R-Dependent STING Activation by Tumor-Derived cGAMP. *Immunity*. 2020. Epub 2020/02/13. doi: 10.1016/j.immuni.2020.01.014. PubMed PMID: 32049051.
616. Diaz-Aparicio I, Paris I, Sierra-Torre V, Plaza-Zabala A, Rodríguez-Iglesias N, Márquez-Ropero M, et al. Microglia Actively Remodel Adult Hippocampal Neurogenesis through the Phagocytosis Secretome. *The Journal of Neuroscience*. 2020;40(7):1453-82. doi: 10.1523/jneurosci.0993-19.2019.
617. Monk PN, Scola AM, Madala P, Fairlie DP. Function, structure and therapeutic potential of complement C5a receptors. *Br J Pharmacol*. 2007;152(4):429-48. Epub 2007/07/03. doi: 10.1038/sj.bjp.0707332. PubMed PMID: 17603557; PubMed Central PMCID: PMC2050825.
618. Klos A, Wende E, Wareham KJ, Monk PN. International Union of Basic and Clinical Pharmacology. [corrected]. LXXXVII. Complement peptide C5a, C4a, and C3a receptors. *Pharmacol Rev*. 2013;65(1):500-43. Epub 2013/02/07. PubMed PMID: 23383423.
619. Brennan FH, Gordon R, Lao HW, Biggins PJ, Taylor SM, Franklin RJ, et al. The Complement Receptor C5aR Controls Acute Inflammation and Astroglialosis following Spinal Cord Injury. *J Neurosci*. 2015;35(16):6517-31. Epub 2015/04/24. doi: 10.1523/JNEUROSCI.5218-14.2015. PubMed PMID: 25904802; PubMed Central PMCID: PMC6605214.
620. Wu J, Sun X. Complement system and age-related macular degeneration: drugs and challenges. *Drug Des Devel Ther*. 2019;13:2413-25. Epub 2019/08/15. doi: 10.2147/dddt.S206355. PubMed PMID: 31409975; PubMed Central PMCID: PMC6650090.
621. Orr MT, Murphy WJ, Lanier LL. 'Unlicensed' natural killer cells dominate the response to cytomegalovirus infection. *Nat Immunol*. 2010;11(4):321-7. Epub 2010/03/02. doi: 10.1038/ni.1849. PubMed PMID: 20190757; PubMed Central PMCID: PMC2842453.
622. Treanor B, Lanigan PM, Kumar S, Dunsby C, Munro I, Auksorius E, et al. Microclusters of inhibitory killer immunoglobulin-like receptor signaling at natural killer cell immunological synapses. *J Cell Biol*. 2006;174(1):153-61. Epub 2006/06/28. doi: 10.1083/jcb.200601108. PubMed PMID: 16801390; PubMed Central PMCID: PMC2064172.
623. Williams JW, Ferreira CM, Blaine KM, Rayon C, Velazquez F, Tong J, et al. Non-apoptotic Fas (CD95) Signaling on T Cells Regulates the Resolution of Th2-Mediated Inflammation. *Front Immunol*. 2018;9:2521. Epub 2018/11/18. doi: 10.3389/fimmu.2018.02521. PubMed PMID: 30443253; PubMed Central PMCID: PMC6221963.
624. Evans DT, Serra-Moreno R, Singh RK, Guatelli JC. BST-2/tetherin: a new component of the innate immune response to enveloped viruses. *Trends Microbiol*. 2010;18(9):388-96. Epub 2010/08/07. doi: 10.1016/j.tim.2010.06.010. PubMed PMID: 20688520; PubMed Central PMCID: PMC2956607.
625. Royer DJ, Carr DJ. A STING-dependent innate-sensing pathway mediates resistance to corneal HSV-1 infection via upregulation of the antiviral effector tetherin. *Mucosal Immunol*.

- 2016;9(4):1065-75. Epub 2015/12/03. doi: 10.1038/mi.2015.124. PubMed PMID: 26627457; PubMed Central PMCID: PMC4889566.
626. Williams K, Motiani K, Giridhar PV, Kasper S. CD44 integrates signaling in normal stem cell, cancer stem cell and (pre)metastatic niches. *Exp Biol Med (Maywood)*. 2013;238(3):324-38. Epub 2013/04/20. doi: 10.1177/1535370213480714. PubMed PMID: 23598979.
627. Senbanjo LT, Chellaiah MA. CD44: A Multifunctional Cell Surface Adhesion Receptor Is a Regulator of Progression and Metastasis of Cancer Cells. *Front Cell Dev Biol*. 2017;5:18. Epub 2017/03/23. doi: 10.3389/fcell.2017.00018. PubMed PMID: 28326306; PubMed Central PMCID: PMC5339222.
628. Hu P, Zhang W, Xin H, Deng G. Single Cell Isolation and Analysis. *Front Cell Dev Biol*. 2016;4:116. Epub 2016/11/09. doi: 10.3389/fcell.2016.00116. PubMed PMID: 27826548; PubMed Central PMCID: PMC485078503.
629. Hadfield J. *Enseqlpedia 2019* [19/03/2019]. Available from: <http://enseqlpedia.com/>.
630. Hadfield J, Retief J. A profusion of confusion in NGS methods naming. *Nat Methods*. 2018;15(1):7-8. Epub 2018/01/04. doi: 10.1038/nmeth.4558. PubMed PMID: 29298293.
631. Hashimshony T, Senderovich N, Avital G, Klochendler A, de Leeuw Y, Anavy L, et al. CEL-Seq2: sensitive highly-multiplexed single-cell RNA-Seq. *Genome Biol*. 2016;17:77. Epub 2016/04/29. doi: 10.1186/s13059-016-0938-8. PubMed PMID: 27121950; PubMed Central PMCID: PMC4848782.
632. Sasagawa Y, Danno H, Takada H, Ebisawa M, Tanaka K, Hayashi T, et al. Quartz-Seq2: a high-throughput single-cell RNA-sequencing method that effectively uses limited sequence reads. *Genome Biol*. 2018;19(1):29. Epub 2018/03/11. doi: 10.1186/s13059-018-1407-3. PubMed PMID: 29523163; PubMed Central PMCID: PMC5845169.
633. Trombetta JJ, Gennert D, Lu D, Satija R, Shalek AK, Regev A. Preparation of Single-Cell RNA-Seq Libraries for Next Generation Sequencing. *Curr Protoc Mol Biol*. 2014;107:4 22 1-17. Epub 2014/07/06. doi: 10.1002/0471142727.mbo422s107. PubMed PMID: 24984854; PubMed Central PMCID: PMC4338574.
634. Oxford Nanopore Technologies. *Nanopore Sequencing 2019* [20/05/2019]. Available from: <https://nanoporetech.com/>.
635. Altboum Z, Steuerma Y, David E, Barnett-Itzhaki Z, Valadarsky L, Keren-Shaul H, et al. Digital cell quantification identifies global immune cell dynamics during influenza infection. *Mol Syst Biol*. 2014;10:720. Epub 2014/03/04. doi: 10.1002/msb.134947. PubMed PMID: 24586061; PubMed Central PMCID: PMC4023392.
636. Dittel BN. CD4 T cells: Balancing the coming and going of autoimmune-mediated inflammation in the CNS. *Brain Behav Immun*. 2008;22(4):421-30. Epub 2008/01/22. doi: 10.1016/j.bbi.2007.11.010. PubMed PMID: 18207698; PubMed Central PMCID: PMC2376206.
637. Bano A, Pera A, Almoukayed A, Clarke THS, Kirmani S, Davies KA, et al. CD28 (null) CD4 T-cell expansions in autoimmune disease suggest a link with cytomegalovirus infection. *Fl000Res*. 2019;8. Epub 2019/04/16. doi: 10.12688/fl000research.17119.1. PubMed PMID: 30984377; PubMed Central PMCID: PMC6436193.
638. Wu L, Van Kaer L. Natural killer T cells and autoimmune disease. *Curr Mol Med*. 2009;9(1):4-14. Epub 2009/02/10. doi: 10.2174/156652409787314534. PubMed PMID: 19199937.
639. Subleski JJ, Jiang Q, Weiss JM, Wiltrout RH. The split personality of NKT cells in malignancy, autoimmune and allergic disorders. *Immunotherapy*. 2011;3(10):1167-84. Epub 2011/10/15. doi: 10.2217/imt.11.117. PubMed PMID: 21995570; PubMed Central PMCID: PMC3230042.
640. Mars LT, Gautron A-S, Novak J, Beaudoin L, Diana J, Liblau RS, et al. Invariant NKT Cells Regulate Experimental Autoimmune Encephalomyelitis and Infiltrate the Central Nervous System in a CD1d-Independent Manner. *The Journal of Immunology*. 2008;181(4):2321-9. doi: 10.4049/jimmunol.181.4.2321.

641. Mattner J, Savage PB, Leung P, Oertelt SS, Wang V, Trivedi O, et al. Liver autoimmunity triggered by microbial activation of natural killer T cells. *Cell Host Microbe*. 2008;3(5):304-15. Epub 2008/05/14. doi: 10.1016/j.chom.2008.03.009. PubMed PMID: 18474357; PubMed Central PMCID: PMC2453520.
642. Mars LT, Novak J, Liblau RS, Lehuen A. Therapeutic manipulation of iNKT cells in autoimmunity: modes of action and potential risks. *Trends in Immunology*. 2004;25(9):471-6. doi: <https://doi.org/10.1016/j.it.2004.07.001>.
643. Stubbington MJ, Mahata B, Svensson V, Deonaraine A, Nissen JK, Betz AG, et al. An atlas of mouse CD4(+) T cell transcriptomes. *Biol Direct*. 2015;10:14. Epub 2015/04/19. doi: 10.1186/s13062-015-0045-x. PubMed PMID: 25886751; PubMed Central PMCID: PMC4384382.
644. Damsker JM, Hansen AM, Caspi RR. Th1 and Th17 cells: adversaries and collaborators. *Ann NY Acad Sci*. 2010;1183:211-21. Epub 2010/02/12. doi: 10.1111/j.1749-6632.2009.05133.x. PubMed PMID: 20146717; PubMed Central PMCID: PMC2914500.
645. Dong M, Thennavan A, Urrutia E, Li Y, Perou CM, Zou F, et al. SCDC: bulk gene expression deconvolution by multiple single-cell RNA sequencing references. *Briefings in Bioinformatics*. 2020. doi: 10.1093/bib/bbz166.
646. Sun X, Sun S, Yang S. An Efficient and Flexible Method for Deconvoluting Bulk RNA-Seq Data with Single-Cell RNA-Seq Data. *Cells*. 2019;8(10). Epub 2019/10/02. doi: 10.3390/cells8101161. PubMed PMID: 31569701; PubMed Central PMCID: PMC6830085.
647. Wang M, Wang Y, Xie T, Zhan P, Zou J, Nie X, et al. Prostaglandin E2/EP2 receptor signalling pathway promotes diabetic retinopathy in a rat model of diabetes. *Diabetologia*. 2019;62(2):335-48. Epub 2018/11/10. doi: 10.1007/s00125-018-4755-3. PubMed PMID: 30411254.
648. Hillenbrand M, Schori C, Schöppe J, Plückthun A. Comprehensive analysis of heterotrimeric G-protein complex diversity and their interactions with GPCRs in solution. *Proceedings of the National Academy of Sciences*. 2015;112(11):E1181-E90. doi: 10.1073/pnas.1417573112.
649. Offermanns S, Simon MI. G alpha 15 and G alpha 16 couple a wide variety of receptors to phospholipase C. *J Biol Chem*. 1995;270(25):15175-80. Epub 1995/06/23. doi: 10.1074/jbc.270.25.15175. PubMed PMID: 7797501.
650. Cserép C, Pósfai B, Lénárt N, Fekete R, László ZI, Lele Z, et al. Microglia monitor and protect neuronal function via specialized somatic purinergic junctions. *Science*. 2019;eaax6752. doi: 10.1126/science.aax6752.
651. Blume ZI, Lambert JM, Lovel AG, Mitchell DM. Microglia in the developing retina couple phagocytosis with the progression of apoptosis via P2RY12 signaling. *Developmental Dynamics*. 2020;249(6):723-40. doi: 10.1002/dvdy.163.
652. Merighi S, Bencivenni S, Vincenzi F, Varani K, Borea PA, Gessi S. A(2B) adenosine receptors stimulate IL-6 production in primary murine microglia through p38 MAPK kinase pathway. *Pharmacol Res*. 2017;117:9-19. Epub 2016/12/16. doi: 10.1016/j.phrs.2016.11.024. PubMed PMID: 27974241.
653. Takasaki J, Saito T, Taniguchi M, Kawasaki T, Moritani Y, Hayashi K, et al. A novel Galphaq/11-selective inhibitor. *The Journal of biological chemistry*. 2004;279(46):47438-45. Epub 2004/09/02. doi: 10.1074/jbc.M408846200. PubMed PMID: 15339913.
654. Mizuno N, Itoh H. Functions and regulatory mechanisms of Gq-signaling pathways. *Neurosignals*. 2009;17(1):42-54. Epub 2009/02/13. doi: 10.1159/000186689. PubMed PMID: 19212139.
655. Magno L, Lessard CB, Martins M, Lang V, Cruz P, Asi Y, et al. Alzheimer's disease phospholipase C-gamma-2 (PLCG2) protective variant is a functional hypermorph. *Alzheimer's Research & Therapy*. 2019;11(1):16. doi: 10.1186/s13195-019-0469-0.
656. Natarajan S, Kim J, Remick DG. Acute pulmonary lipopolysaccharide tolerance decreases TNF-alpha without reducing neutrophil recruitment. *J Immunol*. 2008;181(12):8402-8.

- Epub 2008/12/04. doi: 10.4049/jimmunol.181.12.8402. PubMed PMID: 19050257; PubMed Central PMCID: PMCPMC3672419.
657. Sohn JH, Kaplan HJ, Suk HJ, Bora PS, Bora NS. Chronic low level complement activation within the eye is controlled by intraocular complement regulatory proteins. *Invest Ophthalmol Vis Sci.* 2000;41(11):3492-502. Epub 2000/09/28. PubMed PMID: 11006244; PubMed Central PMCID: PMCPMC1851917.
658. Caspi RR. A look at autoimmunity and inflammation in the eye. *J Clin Invest.* 2010;120(9):3073-83. Epub 2010/09/03. doi: 10.1172/jci42440. PubMed PMID: 20811163; PubMed Central PMCID: PMCPMC2929721.
659. Geng Y, Dubra A, Yin L, Merigan WH, Sharma R, Libby RT, et al. Adaptive optics retinal imaging in the living mouse eye. *Biomedical Optics Express.* 2012;3(4):715-34. doi: 10.1364/BOE.3.000715.
660. Biss DP, Sumorok D, Burns SA, Webb RH, Zhou Y, Bifano TG, et al. In vivo fluorescent imaging of the mouse retina using adaptive optics. *Opt Lett.* 2007;32(6):659-61. Epub 2007/02/20. doi: 10.1364/ol.32.000659. PubMed PMID: 17308593; PubMed Central PMCID: PMCPMC2808135.
661. Feeks JA, Hunter JJ. Adaptive optics two-photon excited fluorescence lifetime imaging ophthalmoscopy of exogenous fluorophores in mice. *Biomed Opt Express.* 2017;8(5):2483-95. Epub 2017/07/01. doi: 10.1364/boe.8.002483. PubMed PMID: 28663886; PubMed Central PMCID: PMCPMC5480493.
662. Trusko B, Thorne J, Jabs D, Belfort R, Dick A, Gangaputra S, et al. The Standardization of Uveitis Nomenclature (SUN) Project. Development of a clinical evidence base utilizing informatics tools and techniques. *Methods Inf Med.* 2013;52(3):259-65, S1-6. Epub 2013/02/09. doi: 10.3414/ME12-01-0063. PubMed PMID: 23392263.
663. Zeiss CJ, Johnson EA. Proliferation of microglia, but not photoreceptors, in the outer nuclear layer of the rd-1 mouse. *Invest Ophthalmol Vis Sci.* 2004;45(3):971-6. Epub 2004/02/27. doi: 10.1167/iovs.03-0301. PubMed PMID: 14985319.
664. Pepe G, De Maglie M, Minoli L, Villa A, Maggi A, Vegeto E. Selective proliferative response of microglia to alternative polarization signals. *J Neuroinflammation.* 2017;14(1):236. Epub 2017/12/06. doi: 10.1186/s12974-017-1011-6. PubMed PMID: 29202771; PubMed Central PMCID: PMCPMC5715534.
665. Gerber YN, Saint-Martin GP, Bringuier CM, Bartolami S, Goze-Bac C, Noristani HN, et al. CSF1R Inhibition Reduces Microglia Proliferation, Promotes Tissue Preservation and Improves Motor Recovery After Spinal Cord Injury. *Front Cell Neurosci.* 2018;12:368. Epub 2018/11/06. doi: 10.3389/fncel.2018.00368. PubMed PMID: 30386212; PubMed Central PMCID: PMCPMC6198221.
666. Ohtsubo Y, Nagata Y, Tsuda M. Efficient N-tailing of blunt DNA ends by Moloney murine leukemia virus reverse transcriptase. *Sci Rep.* 2017;7:41769. Epub 2017/02/06. doi: 10.1038/srep41769. PubMed PMID: 28150748; PubMed Central PMCID: PMCPMC5288710.
667. Mikheikin A, Olsen A, Picco L, Payton O, Mishra B, Gimzewski JK, et al. High-Speed Atomic Force Microscopy Revealing Contamination in DNA Purification Systems. *Anal Chem.* 2016;88(5):2527-32. Epub 2016/02/16. doi: 10.1021/acs.analchem.5b04023. PubMed PMID: 26878668.
668. Burrell A, Foy C, Burns M. Applicability of three alternative instruments for food authenticity analysis: GMO identification. *Biotechnol Res Int.* 2011;2011:838232. Epub 2011/04/30. doi: 10.4061/2011/838232. PubMed PMID: 21527985; PubMed Central PMCID: PMCPMC3065168.
669. Picelli S, Bjorklund AK, Reinius B, Sagasser S, Winberg G, Sandberg R. Tn5 transposase and tagmentation procedures for massively scaled sequencing projects. *Genome Res.* 2014;24(12):2033-40. Epub 2014/08/01. doi: 10.1101/gr.177881.114. PubMed PMID: 25079858; PubMed Central PMCID: PMCPMC4248319.

670. Caruccio N. Preparation of next-generation sequencing libraries using Nextera technology: simultaneous DNA fragmentation and adaptor tagging by in vitro transposition. *Methods Mol Biol.* 2011;733:241-55. Epub 2011/03/25. doi: 10.1007/978-1-61779-089-8_17. PubMed PMID: 21431775.
671. Inc SL, Yir-Shyuan W, Kevin G, John AM, inventors; Illumina, assignee. Patterned flow-cells useful for nucleic acid analysis. patent US 8778848B2. 2012 Dec 13.
672. Mercier JF, Slater GW, Mayer P. Solid phase DNA amplification: a simple Monte Carlo Lattice model. *Biophys J.* 2003;85(4):2075-86. Epub 2003/09/26. doi: 10.1016/S0006-3495(03)74636-0. PubMed PMID: 14507676; PubMed Central PMCID: PMC1303437.
673. Milton J, Xiaolin W, Mark S, Joseph B, Colin B, Xiaohai L, et al., inventors; Illumina Cambridge, assignee. Modified nucleotides patent US 7541444B2. 2009 June 2.
674. Earnshaw GPS, David Mark Dunstan B, Raquel Maria S, Harold S, David J, inventors; Illumina Cambridge, assignee. Modified polymerases for improved incorporation of nucleotide analogues. patent US 8460910B2. 2013 June 11.

Chapter VIII: Research Outputs

8.1 Publications – Thesis-Related

Bell OH, Copland DA, Ward A, Chu CJ, Lange CAK, Dick AD. Single eye mRNA-Seq Reveals Normalisation of the Retinal Microglial Transcriptome following Acute Inflammation. *Frontiers in Immunology*. 2019;10;3033.

8.2 Presentations – Thesis-Related

Oral Presentations

Bell OH, Copland DA, Ward A, Chu CJ, Lange C, Dick AD. RNA-Seq Reveals Alterations in Homeostatic Microglial Function during Inflammation and Resolution. *Association of Research in Vision and Ophthalmology Annual Meeting*, 28th April–2nd May 2019, Vancouver, British Columbia, Canada.

Poster Presentations

Bell OH, Copland DA, Ward A, Nicholson LB, Lange C, Chu CJ, Dick AD. mRNA-Seq Identifies Heterogeneity in the Retinal Microglial Function during Acute Inflammation. *BSI Congress 2019*, 2nd–5th December 2019, Liverpool, United Kingdom.

Bell OH, Ward A, Copland DA, Chu CJ, Dick AD. Optimisation of Tamoxifen Administration Routes in Cre Mice. *3Rs Symposium 2019*, 4th April 2019, Bristol, United Kingdom.

Bell OH, Scott LM, Ward A, Liu J, Copland DA, Chu CJ, Nicholson LB, Dick AD. Investigating Inflammatory Eye Disease. *3Rs Symposium 2018*, 12th April 2018, Bristol, United Kingdom.

Bell OH, Scott LM, Ward A, Copland DA, Nicholson LB. Enhancing Ocular Research using Photography. *3Rs Symposium 2017*, 27th April 2017, Bristol, United Kingdom.

8.3 Grant Awards

SAC043 (Dave Copland), National Eye Research Centre (NERC), £57,961, 1 year, Profiling Immune Cells during Regional Ocular Inflammation, Research Associate.

RES011 (Andrew Dick and Dave Copland), NERC, £50,000, 3 years, Using transcriptomics to define uveitis-specific gene signatures.

BR1018 (Lindsay Nicholson), NERC, £10,000, 2 years, The tissue specific signature of immune cells in persistent uveitis.

Travel Grant Recipient, British Society for Immunology (BSI), BSI Congress 2019, Liverpool United Kingdom.

Travel Grant Recipient, National Eye Research Centre (NERC), BSI Congress 2019, Liverpool, United Kingdom.

Travel Grant Recipient, NERC, ARVO Annual Meeting 2019, Vancouver, Canada.

8.4 Publications – Other

Bell OH, Carreño E, Williams EL, Wu J, Copland DA, Fruttiger M, Sim DA, Lee RWJ, Dick AD, Chu CJ. Intravenous Indocyanine Green Dye is Insufficient for Robust Human Immune Cell Labelling in the Retina. *PLoS One* 15 (2): e0226311; 2020.

Wu J, Bell OH, Copland DA, Young A, Pooley J, Maswood R, Evans R, Khaw PT, Ali RR, Dick AD, Chu CJ. Gene therapy for Glaucoma by Ciliary Body Aquaporin 1 disruption using CRISPR-Cas9. *Molecular Therapy*; 2020.

Tian X, Zheng R, Chu CJ, Bell OH, Nicholson LB, Achim A. Multimodal Retinal Image Registration and Fusion Based on Sparse Regularization via a Generalized Minimax-concave Penalty. In 2019 IEEE International Conference on Acoustics, Speech, and Signal Processing, ICASSP 2019 - Proceedings. Institute of Electrical and Electronics Engineers (IEEE). 2019. p. 1010-1014. 8683010. (ICASSP, IEEE International Conference on Acoustics, Speech and Signal Processing - Proceedings); 2019.

Appendix I: mRNA-Sequencing using SMART-Seq and Illumina – Technical Overview

Appendix I covers more detailed aspects of the mRNA-Seq pipeline utilised to generate data as part of this thesis. For an overview and rationale behind this pipeline, see Chapter III.

Cell Isolation and cDNA Generation

Initially, cells are isolated by sorting or direct harvesting (if cultured). The cells are lysed and the first-strand of cDNA is generated using oligonucleotide and Moloney murine leukaemia virus RT (MMLV-RT). The oligonucleotides (the “Oligo-dT primer”) contains a 30-length T sequence, two terminal 3’ nucleotides, and a 5’ 25 bp terminal sequence (containing a primer site). The T sequence ensures anchoring to the polyA tail, whilst the two terminal 3’ nucleotides ensure specific annealing at the beginning of the polyA tail. This means that cDNA generated using this pipeline will not include very long sequences of the polyA tail and waste reads, instead enriching the associated mRNA sequence upstream. The terminal sequence (5’ end) is used for amplification in later steps [518]. When the end of the mRNA strand is reached, addition of nucleotides beyond the original transcript’s 5’ end occurs via template-switching (a property of MMLV-RT [666]). Template-switching uses a template-switching oligonucleotide (TSO) that has a 3’ terminal sequence of rGrG+G (where rG represents ribosomal guanylate and +g represents a locked nucleic acid) which enhances the thermal stability to the DNA strand and therefore yield [441]. The TSO (in this pipeline) also contains a primer site, allowing for replication independent of the nucleotide composition of the strand sequence, thus eliminating GC bias often observed in mRNA-Seq datasets. Once the initial cDNA strand is generated, LD-PCR is performed (using the newly-incorporated primers that flank the mRNA strand) to increase the yield – the hallmark feature of this technology which enables use of low input amounts. A summary, highlighting template-switching to generate processed cDNA strands, is shown in Figure A1.1.

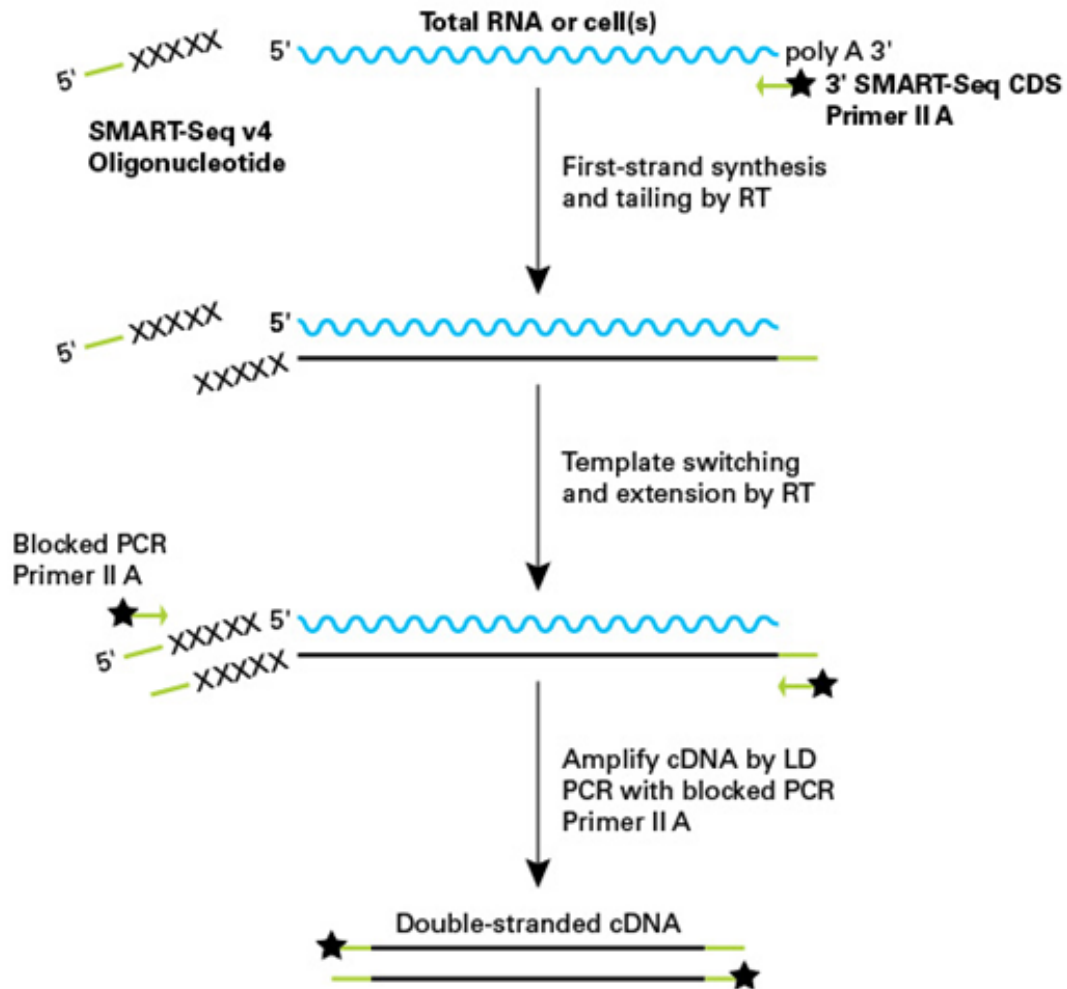


Figure A1.1. The initial cDNA generation using reverse transcriptase and template-switching, as utilised in the SMART-Seq v4 ultra low RNA input kit. First, oligo(dT) primers (labelled 3' SMART-Seq CDS Primer II A) anneal to the 3' poly(A) tail of the mRNA transcript and is copied utilising reverse transcriptase (RT). These primers also incorporate a primer binding site downstream of the transcript (highlighted in light green). Secondly, RT utilised adds additional nucleotides to the 5' end of the transcript which can anneal with the SMART-Seq v4 Oligonucleotide. RT can then switch templates and copy the remaining sequence present on the Oligonucleotide, integrating it into the cDNA strand. Thirdly, primers specific to the newly-incorporated regions enable the amplification of the full-length transcript by long-distance polymerase chain reaction (LD-PCR) to generate double-stranded cDNA at increased yield. Taken from Takarabio Inc.'s website.

cDNA Purification and Quantification

Once the cDNA has been generated, it requires purification from the remaining reaction components and subsequent quantification so that input amounts between samples can be normalised for library preparation and sequencing. Provided that the input number of cells is known, this also allows for an estimation of the average amount of mRNA per cell (with some underlying assumptions such as 100% reaction efficiency of the LD-PCR, and that the cell viability and mRNA content between samples remains constant – meaning that observed differences could represent genuine transcriptional amplification or repression).

Isolation of cDNA is performed using the Agencourt AMPure XP DNA beads, which are the gold-standard in nucleotide isolation for maximal recovery and minimal contamination [667]. It involves the use of paramagnetic beads to selectively bind nucleic acids by type and size (≥ 100 bp). The beads initially bind to the cDNA, are separated from the solution using a magnet, and retained (by the magnet) whilst the solution is aspirated. After wash steps, the cDNA is then eluted from the beads and aspirated whilst the beads are held by the magnet. The workflow for this stage is summarised in Figure A1.2.

Once the cDNA has been isolated and purified, it is ready for downstream applications such as mRNA-Seq (but also other applications including qPCR). However, normalisation of input cDNA amount is required and therefore requires quantification of the cDNA output. This step is performed using the Agilent TapeStation system, which represents a very precise method of quantification [668]. Nucleic acids are separated using electrophoresis and quantified under UV light (similarly to many other DNA applications) using especially sensitive equipment and reagents; they are stained using a highly sensitive fluorescent stain called “SYBR Gold”. The system is very sensitive at quantifying both the abundance (detects as low as 100 pg/uL peaks) and size (25-10,000 bp with an accuracy of $\pm 10\%$) of nucleic acids, whilst using considerably reduced input volumes compared to conventional methods such as detecting ethidium bromide intercalation using a UV transilluminator. In synthesis, it allows for the quantification of the low outputs expected from the ultra-low input RNA kit and uses minimal volume to retain as much sample as possible for downstream steps. Representative figures of output gels produced by the Agilent Bioanalyzer are presented within the results section Chapter III.

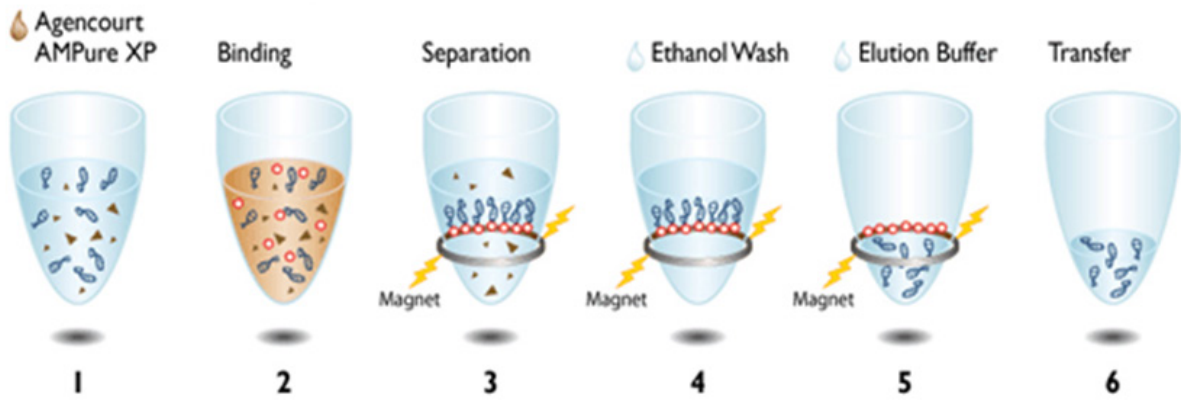


Figure A1.2. The workflow steps required for successful pure isolation of cDNA using the Agencourt AMPure XP beads. The beads are incubated with the cDNA (1) to enable binding (2). Then the beads (containing the bound cDNA) are separated from the solution using a magnet (3). They are washed (4), and then the cDNA is eluted from the beads (5) before transfer to a new tube as a purified preparation (6). Taken from the Agencourt AMPURE XP beads manual.

Tagmentation and Library Preparation

After purification removal of the original primer sites, in addition to insertion of new primer binding sites (for sequencing on the flow cell), an index (to enable multiplexing of samples on the flow cell), and a complementary region to the flow cell (for annealing) is required. For cleavage of the double-stranded cDNA and insertion of primer binding sites, a hyperactive and nonspecific variant of the Tn5 transposase is used [669, 670].

However, this inevitably results in the insertion of the primer binding sequences to all cDNA fragments generated. This includes terminal regions which contain artefacts such as the original primer binding sites, but also undesirable regions such as the polyA tail. PCR cycling (low number) using the new inserts will result in exponential replication of all fragments containing a primer binding site, including the artefacts/undesirable cDNA. The primers used for the cycling contain an index and a region complementary to the flow cell upstream of the primer binding site, which enables their integration into the cDNA fragments. Whilst undesirable regions will be amplified, because they contain only one region complementary to the flow cell (terminal regions would receive only one insert) they will be unable to generate clusters (see later). The end result (of desired regions) is a cDNA fragment containing a portion of the original mRNA strand (excluding artefact or undesirable segments, and assuming a 0% error rate of DNA polymerase) with the required indices (unique to each sample), primer binding sites, and both complementary regions to the flow cell required for cluster generation and subsequent sequencing (Figure A1.3).

From here, the libraries are cleaned using the Agencourt AMPure XP beads (Figure A1.2), with quantification on the Agilent Bioanalyser, as described earlier. Lastly, the libraries are normalised using beads to ensure they all have the same concentration prior to sequencing on the flow cell. This helps to ensure similar number of clusters are generated (and therefore reads) by each sample.

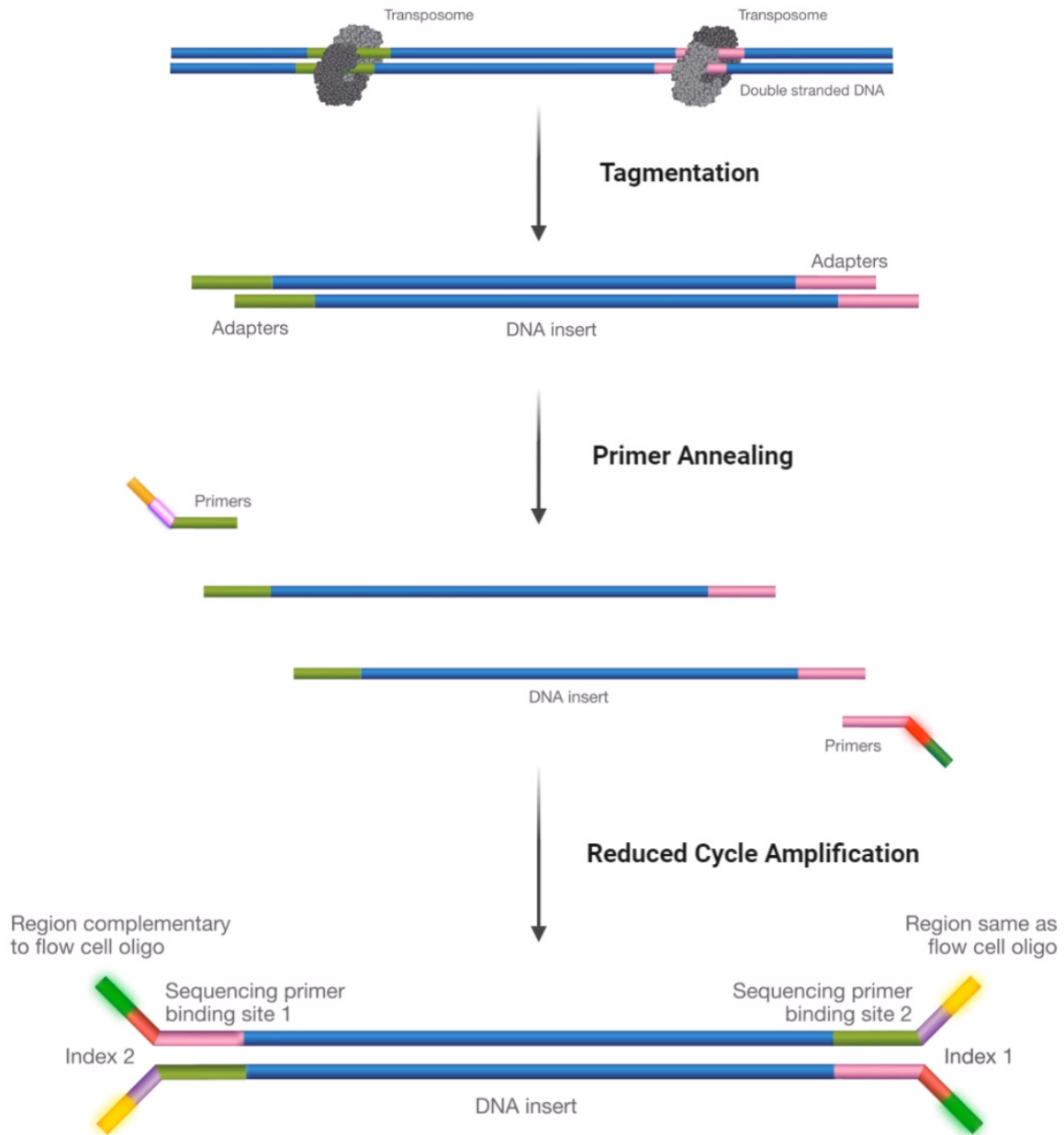


Figure A1.3. An overview of the mRNA-Seq library preparation steps utilised in the SMART-Seq v4 pipeline. Firstly, transposase is used to cleave dsDNA whilst incorporating novel primer binding sites (adapters). These can then be utilised for polymerase chain reaction (PCR) with a low number of cycles required. New sequences that are complementary to the flow cell (for sequencing) and an index are introduced upstream of each primer and are integrated with cycling. This results in the production of a DNA insert containing the original mRNA sequence and other sequences required for successful annealing to the flow cell, successful identification of sample source (i.e. index utilised for demultiplexing post-acquisition), and successful amplification as part of sequencing. This figure was made utilising parts of a video on the Illumina website that describe the mRNA-Seq process.

Sequencing (Illumina)

Sequencing is performed without modifications to the usual Illumina protocols; the library is treated as a small genome library for the purposes of processing. It is performed on a flow cell, which contains millions (or billions) of covalently-attached forward and reverse oligonucleotides (universal and complementary to the libraries generated); more recent versions of flow cells (patterned flow cells) contain nanowells etched into a glass substrate coated with a metal or metal compound. The nanowells are between 1 nm^2 and 1 mm^2 in size with spacing of between 0.5 and $100 \text{ }\mu\text{m}$; the former depends somewhat on the size of the transcript, and the latter depends on the density (how many reads) a flow cell might contain [671]. All flow cells possess a continuous gel layer (such as agarose, gelatin, or polyacrylamide covering all regions of the flow cell) and a glass top. The cDNA is amplified by solid-phase amplification (PCR with the use of surface-bound primers [672]) which enables clonal expansion of the cDNA fragments containing both complementary regions (and hence both primer binding sites) to generate clusters of up to 1,000 identical copies of an original strand. This ensures that fluorescent signals generated from the cDNA strand during sequencing are greatly enhanced so they can be detected much more easily and have improved signal-to-noise ratios. Different clusters are randomly spaced but spatially separated (for patterned flow cells they are found within the nanowells and therefore clusters will be both at a specified size and interval), being up to $1 \text{ }\mu\text{m}$ in diameter. The spacing between clusters is generally determined by how the libraries were loaded and their concentration and is optimised per individual machine and type of flow cell used. An overview of cluster generation is shown in Figure A1.4. Furthermore, most flow cells will contain between 4–10 segmented regions known as lanes. They contain discrete boundaries and assist in controlling cluster generation. As each lane (relative to others) may be susceptible to technical bias, they will typically contain clusters generated from every sample being ran on the flow cell.

After cluster generation, the flow cell is ready for sequencing. This is performed by repeated cycles of polymerase-directed single base extension through the use of reversible terminators (3'-O-azidomethyl 2'-deoxynucleoside triphosphates), each labelled with a different removable fluorophore [673]. To improve the efficiency of phosphodiester bond formation between the nucleotide analogues, the polymerase also has modifications to its active site [674]. This approach enables simultaneous incorporation of any base to limit the potential for non-specific or competitive binding (if different bases were added in different steps) but also enhance the speed of sequencing. It also enables control of extension base-by-base, which enables imaging

of the conjugated fluorophores a single nucleotide at a time, with fluorophore dissociation and exposure of the 3' on the pentose sugar for further extension (repeat of the prior steps) post-imaging until a new image is ready for acquisition. As the fluorophores are different for each of the four bases (A, T, C, G), this enables base-calling for every cluster on the flow cell in a simultaneous fashion and registration back to the specific location of the signal to generate a read (Figure A1.5). The extension reaction, imaging, and dissociation can be repeated to determine the base sequence for short reads (typically between 75 and 300 bp).

The index (a 3 base code unique to the biological sample – one for the forward read, and one for reverse read where applicable) is also sequenced which enables association of a particular read (cluster) to an original sample; use of paired indices like this enables multiplexing of up to a large number of samples on a single flow cell (typically ≥ 96) which is highly beneficial for many applications, through greatly enhancing the cost-efficiency, where the full depth (number) of reads isn't required for a single sample (e.g. mRNA-Seq). It would also block for any technical artefact caused by the flow cell or lane.

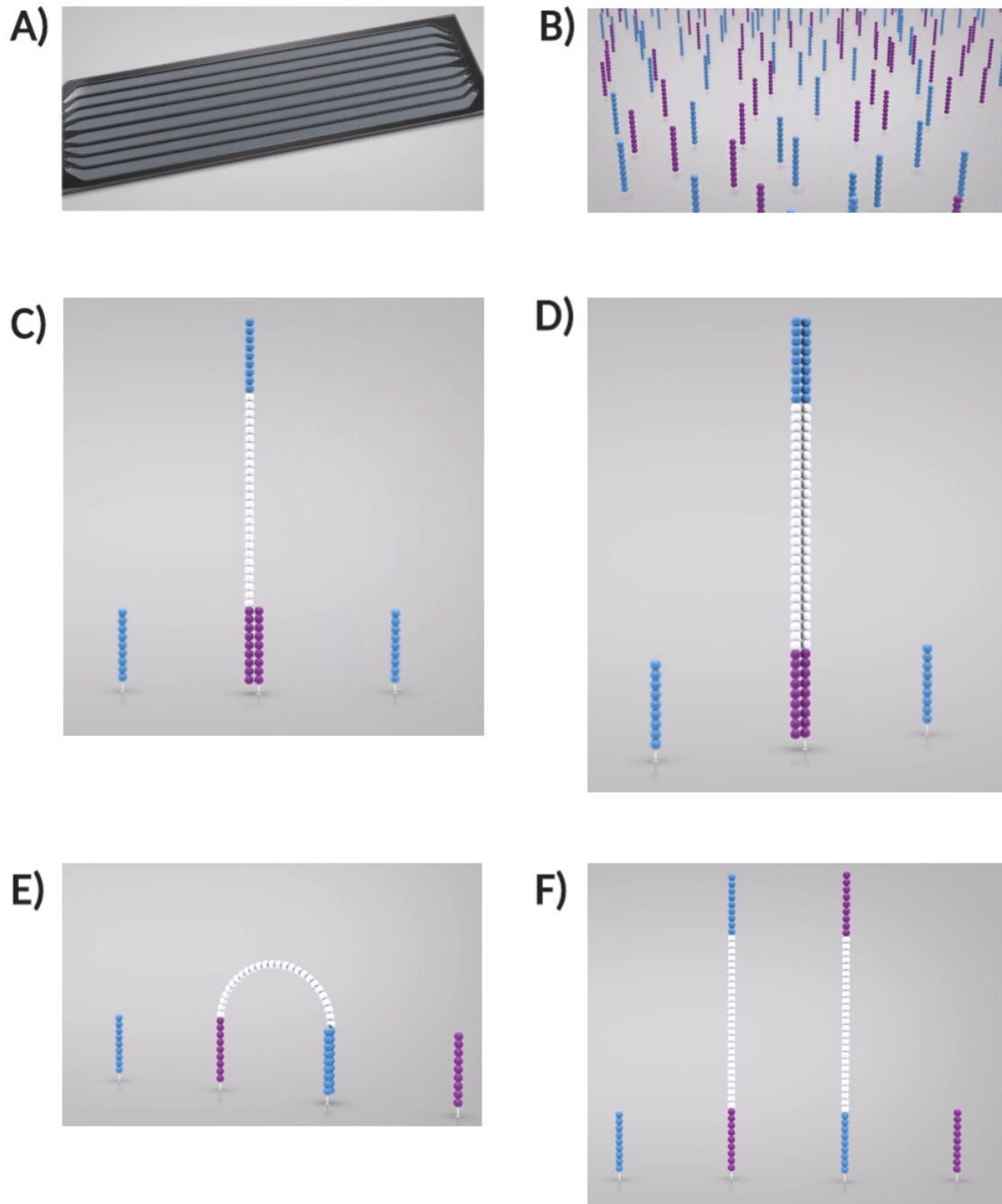


Figure A1.4. Cluster generation on Illumina flow cells. *A) A flow cell typically contains 4–10 segmented regions termed lanes. B) Within the flow cell are millions or billions of covalently-attached oligonucleotides (one of two sequences) complementary to a region on the cDNA in the libraries. C) The libraries can anneal to the oligos, and D) be copied by DNA polymerase to create a strand complementary to the original that is immobilised on the flow cell. The signal from a single strand is too weak to be easily imaged, and therefore E) the other terminal section of the strand can anneal to and F) be copied onto a different oligo, enabling clonal expansion (i.e. cluster generation) to greatly enhance the signal produced when sequencing. This figure was made utilising parts of a video on the Illumina website that describes the mRNA-Seq process.*

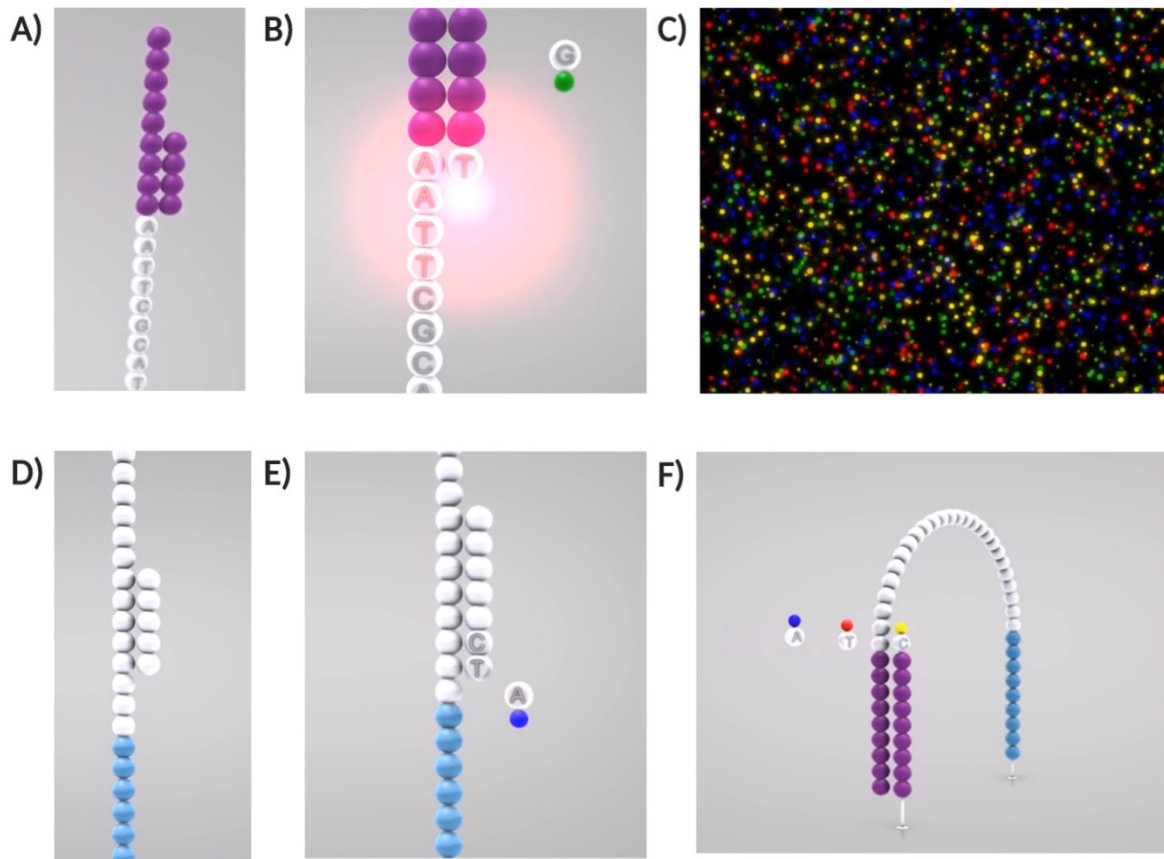


Figure A1.5. Illumina sequencing overview highlights how it is possible to sequence millions of reads in parallel with accuracy. **A)** Primers complementary to terminal regions of cDNA enable copying of strands. **B)** Immediately succeeding this is the 3-nucleotide index code that enables demultiplexing in analysis. Bases are added in a stepwise fashion using reversible terminators with tags. **C)** The tags can be visualised and registered to specific locations on the flow cell which correspond to the different clusters present. This enables construction of sequence reads in a parallel fashion. **D)** Once the read is complete (typically 75 or 150 bp), a primer is annealed near to the terminus which **E)** enables sequencing of the second 3-nucleotide index. Pairing indices like this allows for exponentially more samples to be ran in parallel. Lastly, after denaturation of the copied strand, it is possible to **F)** anneal the original strand terminus to the flow cell. This allows the process to repeat, generating a sequence from the other end of the mRNA transcript to generate paired reads. This figure was made utilising parts of a video on the Illumina website that describes the mRNA-Seq process.

Measurement Error within Illumina Sequencing

Measurement error refers to errors or artefacts introduced as part of obtaining reads when sequencing. It is well-recognised that differences can occur between flow cells but even lanes on the same flow cell. A balanced study design ideally multiplexes samples across all lanes of a flow cell to mitigate this (i.e. technical sequencing replicates) and, if using multiple flow cells, balances samples of the different experimental groups across them (or in an extremely complicated fashion balance all samples equally across all flow cells) [523]. An experimental concept schematic is shown in Figure A1.6 and highlights the differences between good and bad practice in this context. Illumina provide comprehensive instructions for sequencing that help to minimise measurement error: these include multiplexing samples across lanes, controlling the concentration of libraries added to the flow cell (this is machine-specific but is often determined when initially using the sequencer), and many more as part of their supplied protocols and standard operating procedures.

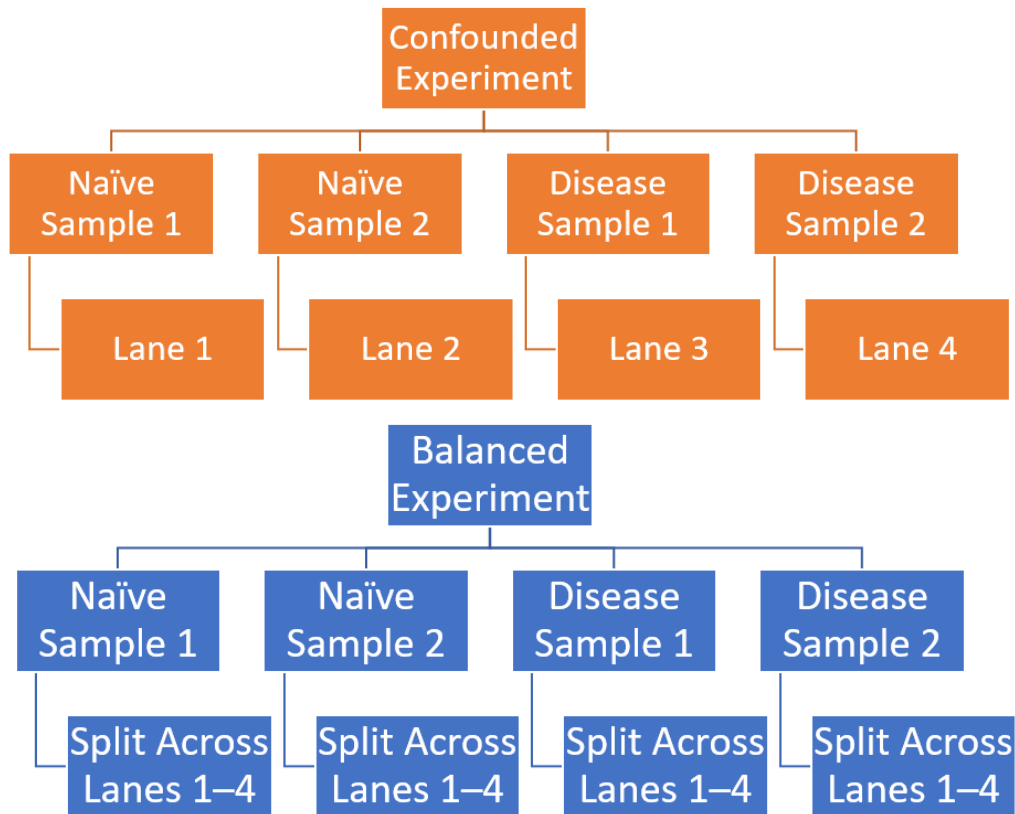


Figure A1.6. Examples of good and poor experimental design with regards to sequencing flow cells and lane allocation. In the confounded design, each sample is sequenced on a different lane of the flow cell. When performing analysis, differences between lanes could confound the results. In the balanced design, all samples are split and allocated across each lane (as technical replicates) to mitigate this potential effect.